Electrical-Field Activated Sintering and Forming of Micro-Components

Muhammad Bin Zulkipli

Glasgow, 2017

Electrical-Field Activated Sintering and Forming of Micro-Components

Muhammad Bin Zulkipli

This thesis is submitted to the Department of

Design, Manufacture and Engineering Management,

University of Strathclyde

for the degree of Doctor of Philosophy

Glasgow, 2017

Dedication

The author wished to dedicate the thesis to his wife Ilyana Janis and families.

Acknowledgement

Abstract

As the demand for miniature products has increased significantly, so also has the need for these products to be produced in a rapid, flexible and cost efficient manner. The application of electroplasticity shows significant potential to produce the components by using powder materials. Nevertheless, previous research has shown that there are still significant challenges to be met in order to achieve increased relative densification of product samples and simplification of the processes. The process concept in this study comprises the combination of electrical-field activated sintering and forming processes. Therefore, the aims of the research were to develop the process concept for the manufacture of micro-components and to design the die sets along with other tooling for machine setup to enable the forming of micro-components from powder materials. A comprehensive literature review on micro-manufacturing, size effects, powder metallurgy and the electroplasticity process has been conducted. The development of the die sets for the process has been described, followed by a series of experiments. The FE thermal-electrical analysis was also carried out to study the heating flows of the die sets development during the process. In this research, titanium (Ti) and titanium tin alloy (90Ti10Sn) have been selected for the main powder materials tested for both vacuum and open-air process environment by using a Gleeble® 3800 testing system and Projection Welding machine respectively. Meanwhile, for the additional experiment, copper (Cu) has been selected to be tested in the open-air process environment by using a Projection Welding machine with die sets prepared by the Micro-FAST project. Based on the data collected, this efficient process has the potential to produce components with a high relative density of around 98%. Changes of the particles concerning deformation and breaking are crucial in the course of achieving the densification which differs from a conventional sintering process.

Published Research Papers and Posters

a) Research Papers:

1. **Muhammad Bin Zulkipli**, Yi Qin, Kunlan Huang, Hasan Hazma Hijji, Yihui Zhao and Jie Zhao (6th to 9th August 2015), *"Forming of titanium and titanium alloy miniature-cylinder by electrical- field activated powder sintering and forming"*. 4th International Conference on New Forming Technology (ICNFT2015) – Glasgow, Scotland, United Kingdom. (http://dx.doi.org/10.1051/matecconf/20152110006).

2. Jie Zhao, Yi Qin, Kunlan Huang, **Muhammad Bin Zulkipli** and Hasan Hazma Hijji (6th to 9th August 2015), *"Forming of micro-components by electrical-field activated sintering"*. 4th International Conference on New Forming Technology (ICNFT2015) – Glasgow, Scotland, United Kingdom. (http://dx.doi.org/10.1051/matecconf/20152110001).

3. Kunlan Huang, Yi Qin, Jie Zhao, **Muhammad Bin Zulkipli** and Hasan Hazma Hijji (6th to 9th August 2015), *"Fabrication of NiTi shape memory alloy by Micro-FAST"*. 4th International Conference on New Forming Technology (ICNFT2015) – Glasgow, Scotland, United Kingdom. (http://dx.doi.org/10.1051/matecconf/20152110003).

4. Hasan Hijji, Yi Qin, Kunlan Huang, **Muhammad Bin Zulkipli,** Song Yang and Jie Zhao (6th to 8th September 2016), *"Forming Alumina (Al_2O_3) by Micro-FAST"*. 14th International Conference on Manufacturing Research (ICMR2016) – Loughborough, England, United Kingdom. (http://ebooks.iospress.nl/volumearticle/44320).

5. Hasan Hijji, Yi Qin, Kunlan Huang, Song Yang, **Muhammad Bin Zulkipli** and Jie Zhao (6th to 8th September 2016), *"Fabrication of micro components with MSZ material using electrical-field activated powder sintering technology"*. 14th International Conference on Manufacturing Research (ICMR2016) – Loughborough, England, United Kingdom. (http://ebooks.iospress.nl/volumearticle/44319).

b) Research Posters:

1. **Muhammad Bin Zulkipli** & Yi Qin (27th June 2013) *"Development of a New Process for the Forming of Micro-Components"*. Poster presentation. Faculty Engineering Research Presentation Day (RPD 2013) – University of Strathclyde Glasgow, Scotland, United Kingdom. **(2nd Prize for Best Poster Presentation).**

2. **Muhammad Bin Zulkipli** & Yi Qin (20th and 25th June 2014) *"Development of a New Process for the Forming of Micro-Components"*. Poster presentation. Department Design, Manufacture & Engineering Management Poster Critique 2014 and Faculty Engineering Research Presentation Day (RPD 2014) – University of Strathclyde Glasgow, Scotland, United Kingdom.

3. Hasan Hazma Hijji, **Muhammad Bin Zulkipli** & Yi Qin (31st January 2014), *"Development of a New Process for the Manufacture of Micro Parts by Using a Combination of Micro Forming and Fast Technology"*. Poster presentation. 8th Saudi Student Conference – Imperial College London, United Kingdom.

4. **Muhammad Bin Zulkipli** & Yi Qin (17th and 24th June 2015) *"Development of a New Process for the Forming of Micro-Components"*. Poster presentation. Department Design, Manufacture & Engineering Management Poster Critique 2015 – University of Strathclyde Glasgow, Scotland, United Kingdom.

5. **Muhammad Bin Zulkipli** & Yi Qin (31th March 2016) *"Electrical-Field Activated Forming and Sintering of Micro-Components with Titanium and Titanium Alloy"*. Poster presentation. Department Design, Manufacture & Engineering Management Poster Critique 2016 – University of Strathclyde Glasgow, Scotland, United Kingdom.

Contents

List of Tables

List of Figures

Chapter 1: Introduction

1.1. Research Background

In general demands for micro-electromechanical systems (MEMS) and micro-products have significantly increased due to the fast growth that can be seen in the field of biomedicine, telecommunications and automotive engineering. For example, the global industry association Semiconductor Equipment and Materials International (SEMI) has released the sales forecast for semiconductor equipment which had a market value of $37 billion in 2015 to approximately $38 billion in 2016 and enjoys an active growth in the global market of 1.4% [1]. Besides typical MEMS manufacturing methods, significant efforts have been made recently either to scale down traditional processes or to develop the new ones for the manufacture of micro- and nano-products [2]–[5]. For instance, the production of micro-gears which are significant actuating and transmission components used widely in MEMS and micro-mechanical-systems (MMS), is often enabled through ultra-precision machining or lithographic techniques especially LIGA processes [6], [7]. Micro-forming also plays important roles for manufacturers of millions of micro screws through upsetting and rolling every year [8]–[10]. In addition to that, micro-extrusion has been well investigated where it is capable of extruding copper pins in the laboratory with a shaft diameter of 0.5 to 0.8 mm and a wall thickness of 50 to 125 μm [11], [12]. Therefore, based on the previous research and experiment results there is no doubt that micro-products with high precision and accuracy can be produced, nevertheless concerning cycle time and cost for high production, there are still improvements to be made.

In micro-forming, the limits of the process are influenced largely by the workpiece's dimension. This phenomenon is being commonly referred as the size effects. The size effects that exist in metallic materials can be described as grain and feature/specimen size effects. According to Armstrong [13], grain size effect can be represented by the Hall-Petch law which states that the material strengthens as the grain size decreases. Meanwhile for feature/specimen size effects observed when the miniaturisation of the part occurs resulting in the decline of the flow stress. In this feature/specimen size effect, the workpiece cannot be considered as an isotropic continuum due to the huge share of the volume occupied by individual grains with different orientations if the microstructure, surface topology and tools of the workpiece used in the process remain unchanged [12], [14]. It was found that by

decreasing the workpiece dimensions this could lead to an increase of friction factor by 20 times, when performing extrusion experiments on the CuZn15 brass alloy [14].

Moreover, micro-forming needs tools with overall sizes in a range of tens of microns. Electrical discharge machining (EDM) is often used as the main process of fabricating the micro-tooling. The advantage of the micro-wire EDM process is its capability to provide excellent results for producing a micro-tooling with a high accuracy of shape and good surface quality, but the process is lacking in geometrical flexibility [15]. Other technologies for micro-tooling such as die-sinking, drilling, grinding and milling were used for making tools for stamping, embossing and coining processes [16]. Overall, micro-tooling is expensive process to be made. The development of micro-forming technology renders challenges to micro-tooling. Besides the cost issue, tool life is one of the key factors that need to be considered. The fragile tool often needs to meet a high forming force requirement and tool wear at the micro-scale is often quicker than at the macro-scale due to the size effect issues and difficulties to fabricate the micro-components with intricate design. This was particularly the case when a high strength material was used in the micro-forming process.

Therefore, to overcome the problem that has been stated above, the development of new high volume production and low-cost manufacturing capabilities are needed. The concept of this research comprises the combinations of electrical-field activated sintering and forming processes. It has a potential to address the existing problems and meet market needs especially for shortening the process chain, improving control of the shape of the part formed, reducing the forming pressure requirements, providing options to use different metal powders and combinations, improving the practicality of forming micro-components with high strength materials and reducing the influences of size effects. Among popular electroplasticity application, the spark plasma sintering (SPS) process has been claims for successfully formed components by many types of materials. Nevertheless, based on previous research, there are still significant challenges to meet the requirements of achieving high relative densification of samples and simplification of the processes [17]. In addition to that, Lange [18] stated that the densification process using the conventional powder sintering method involves a coarsening or neck growth, which is a critical mechanism needed to achieve densification caused by surface diffusion or evaporation/condensation. Thus, it is the reason why conventional powder

sintering takes a long time to be completed. Meanwhile, by using the electrical-field activated sintering and forming process, the densification can be achieved more quickly, by deformation and breakage of the powder particles. It is not dependent on a spark discharge to create the heating as in the SPS process where it requires gaps for the spark to ignite, which as a result the application of pressure cannot be too high to prevent the spark from disappearing [19]. However, by using electrical-field activated sintering and forming process, the application of high pressurisation can be applied where it helps breakage and increase plastic deformation of material particles between interfaces. Based on this finding, it is essential for the particle breakage and deformation process to be present to achieve adequate and quick densification of micro-parts.

1.2. Aims and Objectives

The aims of this research were to develop the process configurations to produce micro-components with high densification from powder materials and design the die sets along with other tooling for machine setup, enabling a high-efficiency process. The concept of the process comprises combinations of electrical-field activated sintering and forming. The specific objectives of the research were:

a)   Established of a fundamental understanding of the densification mechanism for electrical-field activated sintering and forming process.

b)   Developed the optimum process parameters, die sets and other tooling for experiments setup with the Gleeble® 3800 (vacuum) and Projection Welding (open-air) machines.

c)   Conducted experiments by using titanium (Ti) and titanium tin alloy (90Ti10Sn) powder to produce high relative density cylindrical samples with the Gleeble® 3800 and a Projection Welding machine.

d)   Conducted the experiments by using copper (Cu) powder with Micro-FAST die sets to successfully form domed hollow cylinder and turbine samples with the Projection Welding machine.

1.3. Research Methodology

A series of fundamental studies have been undertaken which consist of process concept evolution, a design of forming tools and process configurations for the experiments to achieve the aims and objectives as stated above. It started with a comprehensive literature review in the subject areas such as micro-manufacturing, size effects in micro-forming, powder metallurgy and the electroplasticity application in the sintering process. During the literature review, key development issues were identified, and solutions for technology advances proposed in detail.

These were followed by the development of process parameter configurations, die sets and other tooling for use in a series of experiments by using Ti and 90Ti10Sn powder materials. The experiment was conducted by using a Gleeble® 3800 machine from Dynamic Systems Inc., USA with the collaboration of Imperial College London and a Projection Welding machine from British Federal, UK for the vacuum and open-air environment process respectively. Meanwhile, for the additional experiment, copper (Cu) was been selected to be tested in the open-air process environment by using the Projection Welding machine with die sets prepared by the Micro-FAST project. The coupled FE thermal-electrical analysis also has been done to show the heating characteristics of the die sets used in the experiment. The information collected from the FE simulation is useful to understand how the heating distribution occurs to the die sets employed in the experiments of the electrical-field activated sintering process.

After the experiments were conducted, the effects of input parameters of the experiments such as heating temperature, heating rate, holding time, pressure and used die sets were discussed relative to the densification, microstructures and surface hardness of the formed samples. The comparison of higher sample densification with a previous electroplasticity sintering process was made. Based on this discussion if the samples were not achieving excellent results, improvements of the experimental process parameters and tool design were performed to increase high process efficiency and excellent product quality.

Finally, a general design and a manufacturing methodology by using electrical-field activated sintering and forming to produce micro-components from powder materials were established. **Figure 1.3-1** shows the flow chart which illustrates the experiment design process and how the research was performed.
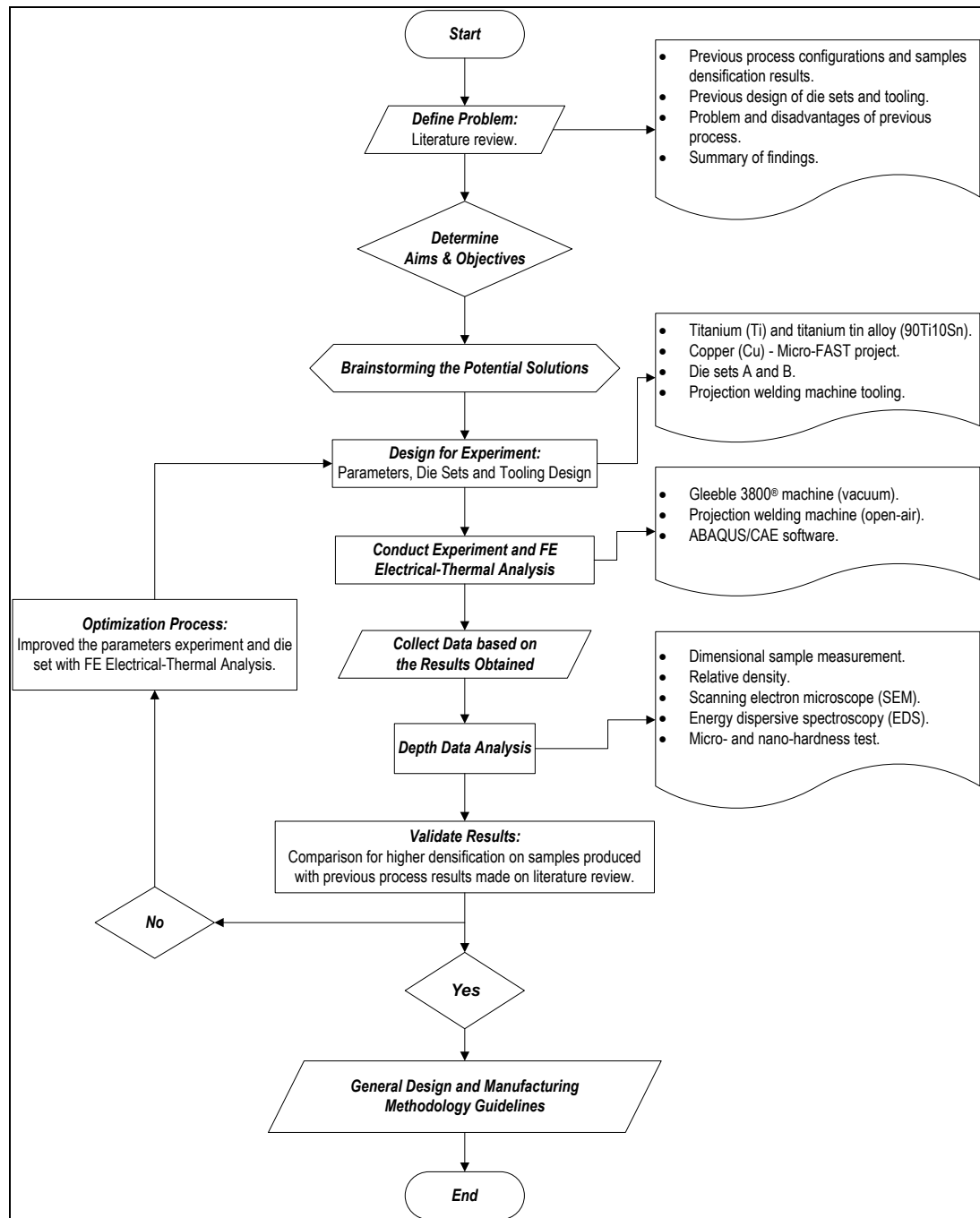
Figure 1.3-1: Experimental design process.

1.4. Thesis Structure

The thesis consists of eight chapters:

a)   Chapter 1: Introduction

The first chapter consists of a description of the background of the project and the aims along with the objectives which this research intended to achieve. This was followed by detailed discussion of the project methodology to be employed to complete the research. The structure of the thesis for all the development works carried out was shown in this chapter.

b)   Chapter 2: Literature Review

The second chapter provides an overview of the micro-manufacturing process and an introduction of the key problem with development issues being faced today. The review then concentrates on the micro-forming process with more discussion on the size effects issues. One of the contributions of this research project was to eliminate the size effects problems in the manufacturing process by producing net shape samples which can offer a higher production rate and save the cost. The literature review then focused on an overview of the powder metallurgy (PM) process. The previous electroplasticity in the sintering process also has been done with a focus on titanium, titanium alloy and copper. The key issues were identified for improvement and as guidelines to develop the experiment parameters along with the die sets design. The chapter ends with the summary of the findings obtained from the reviews.

c)   Chapter 3: Process Concept of Electrical-Field Activated Sintering and Forming

This chapter explains the densification mechanism of electrical-field activated sintering and forming process which mainly consists of four stages. In addition to that, the comparisons between this process and SPS have been made which shows the differentiation regarding mechanism densification of the part formed and common parameters used.

d)   Chapter 4: Die Sets Development

The development works on the die sets used in the Gleeble® 3800 and Projection Welding machine have been made. The discussion on consideration of tool geometric feature design and selection of the material for the die sets has been done.

e)   Chapter 5: Coupled FE Thermal-Electrical Analysis

By using ABAQUS/CAE software as a tool for coupled FE thermal-electrical analysis, the effect of heating distributions applied to the die sets during the electrical-field activated sintering and forming processes were obtained. Results and discussion from each die sets have been analysed in detail.

f)   Chapter 6: Process Investigation with a Gleeble® 3800 Machine

This chapter explains the experimental study on the electrical-field activated sintering and forming process. All the information regarding the equipment, powder materials, parameters and procedures employed in the experiment and analysis has been stated. The samples obtained from the experiments were analysed and discussed in detail to provide conclusive results and findings of reliability of the overall process. Also the die sets produced excellent quality micro-components with a high process efficiency.

g)   Chapter 7: Open-Air Sintering with a Projection Welding Machine

The focus of this chapter was to investigate the open-air electrical-field activated sintering and forming process with the application of the Projection Welding machine. The idea of adopting this machine was to deliver the same capabilities as the Gleeble® 3800 machine. The Projection Welding machine could be used more practically in the factories, whereas the Gleeble® 3800 machine is more suitable for experimental work in the laboratory. In addition to that, it was a further comparison study for the vacuum environment which used the Gleeble® 3800 machine. Besides the cylinder shape of the 90Ti10Sn micro-components, there were two

other samples shapes made by Cu powder that have been produced using the Micro-FAST project die sets which were named as the domed hollow cylinder and the turbine samples.

h)   Chapter 8: Conclusions and Recommendations for Future Work

This chapter draws the conclusions from the whole of the development work conducted. Considerations for future work that may assist in further development of the research topic were also given.

Chapter 2: Literature Review

2.1. Micro-Manufacturing

The definition of manufacturing in general terms can be referred as an industrial production that has been designed for specific applications. It is a process for making an excellent output concerning quantity with the maximum possible utilisation of raw materials. The manufacturing process can produce either discrete or continuous products. Discrete product means individual parts such as a nail, gear, engine block and steel ball. Meanwhile, an example of a continuous product is like wire, hose, metal sheet, tube and pipe. The continuous product can also be cut to be served as discrete products. Changes to the manufacturing industry have emerged in the past twenty years covering the output of products, methods of production and how it was managed. It was affected not only by the increase in demand for the manufacture of common or new products but also caused by social, economic and political changes [4], [20]. Manufacturing is essential for industrial activities that contribute to economic growth of a particular country where it can be presumed that the higher the level of manufacturing activities, the better will be the population's standard of living.
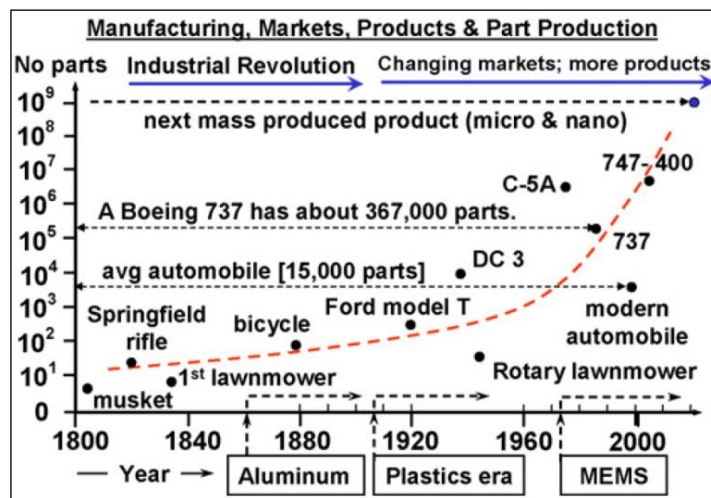
Figure 2.1-1: The revolutionary of industrial towards productions of complex parts [21], [22].

The continuous manufacturing development can be observed in the production of micro-products as applied in mechanical, MEMS and medical industries. It has been popularly used in vehicles, aircraft, household appliances, telecommunications devices and information technology facilities as illustrated in **Figure 2.1-1**. The trend towards miniaturisation of

11

products has led to some challenges where the industries aim to produce new products that integrate with a variety of functions and expand the application area without increasing the weight or the overall size of the product.[23]. Hence, micro-manufacturing has focused more on processes and tool technologies used in the production of components that have at least two dimensions in sub-millimetres. The emphasis on micro-manufacturing varies from different sources where it depends on the combined function of the product and its mode of operation. Accordingly, various methods and strategies can be used to produce micro-products.

Figure 2.1-2: Sample micro-extruded parts [24].

Manufacturing techniques such as extrusion, embossing, stamping and forging which are encapsulated in the fabrication of micro-forming were considered for further research because they have a potential to produce a large amount of components cost-effectively with enhance product performance [24]–[26]. **Figure 2.1-2** shows the example of micro-extruded parts produced by using the micro-forming process. It can generate products in near-net shape requiring less finishing operations. But there are also difficulties in regards to size and frictional effects in forming material. For the components in the range of 0.1 to 5 mm, the surface area per volume ratio is large and surface forces play a major role [12], [27]. When the ratio of the grain and feature size becomes larger, deformation characteristics change abruptly with significant variations in the response of the material [14]. Thus further research is needed to improve the weaknesses in the micro-forming process.

2.1.1. Challenges to Manufacture Micro-Products

High volume and low-cost production are not only essential for efficient micro-manufacturing systems, but the challenges with the design of micro-products need to be taken into full consideration. The primary difficulties that relate to the manufacture of micro-products are negligible when the work is done conventionally. Traditional macro-scale manufacturing has a limit as to how far it can be scaled down, and factors that were insignificant at the macro-scale become more important in influencing the manufacturing process for a micro-product. The example factors that are irrelevant in the conventional machining but become essential in micro-manufacturing are vibration, chip removal, tool-offset, temperature and the rigidity of the tools [28], [29]. In addition to that, some of the biggest problems encountered in the handling of micro-parts is a precise positioning [30]. An example such as electrostatic, adhesion influence, and Van Der Waals effect are the unwanted external forces involved in physical contact that need to be eliminated [31]–[35]. Another common issue to be addressed at the design stage of micro-manufacturing is the significant characteristic of volume production. It is different from prototyping in a lab scale compared to products that are manufactured in the production. The selection of the materials for manufacturing and design of the component with their features will have an influence on achievable production yield, which is mainly relevant by the capability of machinery, tools, processes and auxiliary equipment. It can be seen that the micro-process technology is time-consuming and only suitable for low yield rates and does not yet have the potential of conventional processes due to manual adjustments that need to be done in every aspect of the process [28].

The tooling dimension also plays a challenge when dealing with the production of micro-manufacturing. The development of the micro-tooling was started a decade ago, but there is still a limitation on the applicability of tooling [36], [37]. For example in the drilling process, the acceptable aspect ratio which is the tool diameter to the drilling depth is from five to ten which can even be lower than five, but deeper plunging and drilling can cause tooling breakage [38]. The usage of a proper tooling used in the micro-manufacturing also deals with the commercial sensors dimension. The problems regarding sensor use in production are mainly related to the bulky size which will affect the performance because the sensor has to be placed accurately on a small workspace. It was not feasible for micro-parts application which requires at least

sub-micron precision. Moreover, calibration precisions are more demanding for current machines [29]. In addition to that, grade tolerance and surface quality specification for micro-products are not as straightforward to obtain compared to the design of a macro-product that can usually be determined from handbooks of the processes [4]. It requires the trial and error method to get the specific data that can be employed for a particular process, tools, and materials.

The limitation on the shape of micro-products that need to be produced is also one of the difficulties faced by the manufacturer. Standard rules that applied on the shaping capability of manufacturing before this was not applicable. This phenomenon due to the size effect factor and limitation to the tool shape [12]–[14]. For example, most of the processes only dealt with 2D/2.5D compare 3D shape, because to generate 3D shapes needs significant efforts such as new processes development and expensive equipment [4]. The material capability also plays a major role in the micro-manufacturing process. It can be seen in the previous research that usually used brass, copper and aluminium as test materials due to the flexible and soft characteristics with low strength properties which made them easy to deform a under low applied force. Based on the results only a simple micro-feature was successfully created [39]–[41]. Therefore, further development of the process in micro-manufacturing still needs to be done to produce more products that have a high strength capability with more intricate micro-feature design [28].

2.1.2. Classification of Micro-Manufacturing Processes

There are several processes that have been applied which can be categorised as conventional, non-conventional and hybrid micro-manufacturing as illustrated in **Figure 2.1-3**. A conventional process involves changing the shape of the workpiece using a device made from the harder material. Meanwhile, for non-conventional machining the other forms of energy are utilised which are not associated with sharp cutting tools as is needed for the conventional process. Hybrid manufacturing instead uses the combination of two or more processes to manufacture the micro-products. Due to the increasing demand of time and energy that can lead to the increasing of cost when using the conventional manufacturing methods, it is not feasible for the process to be applied in the mass production of micro-

products. Depending on what type of energy that the manufacturing processes deployed, it can be categorised into mechanical, thermal, chemical and electrical. General production processes also can be classified according to the way in which the micro-products are to be made such as subtractive, additive, deforming, joining and hybrid processes as shown in **Table 2.1-1** [4], [29], [42].
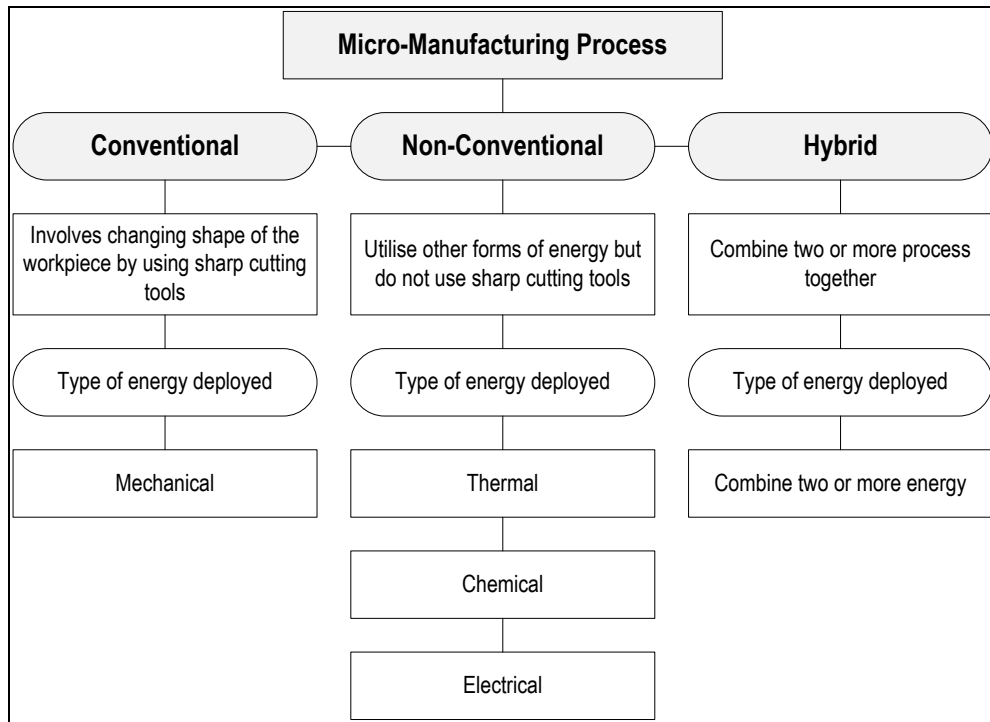
Figure 2.1-3: Classification of micro-manufacturing methods and processes.

Table 2.1-1: General processes of micro-manufacturing [4], [29], [42].

Processes	**Subtractive**	Micro-mechanical cutting (milling, turning, grinding and polishing), micro-EDM, micro-ECM, laser beam machining, electro-beam machining and photo-chemical-machining.
	Additive	Surface coating (CVD and PVD), direct writing (ink-jet and laser-guided), micro-casting, micro-injection moulding, sintering, photo-electro-forming, chemical deposition, polymer deposition and stereolithography.
	Deforming	Micro-forming (stamping, extrusion, forging, bending, deep drawing, incremental forming, superplastic forming and hydro-forming), hot-embossing and micro/nano-imprinting.
	Joining	Micro-mechanical-assembly, laser-welding, resistance, laser, vacuum soldering, bonding and glueing.
	Hybrid	Micro-laser-ECM, LIGA combined with laser-machining, micro-EDM and laser assembly, shape deposition and laser machining, laser-assisted-micro-forming, micro assembly injection moulding and combined micro-machining with casting.

It is not usual to manufacture the micro-products with a single process. Process chains are needed to complete the micro-manufacturing processes to achieve a better quality and efficiency of the production as shown in the examples of **Table 2.1-2**. The hybrid micro-manufacturing can be used to achieve high efficiency, reduced manufacturing errors and elimination of additional handling or transport of micro-components. This process takes the merits of the particular micro-manufacturing process while some of the inherited disadvantages may be reduced or eliminated. By using hybrid micro-manufacturing, various forms of energy may be combined and used at the same time as illustrated in **Figure 2.1-4** to shorten the process chain [43].

Table 2.1-2: Examples of hybrid micro-manufacturing processes.

Combined Processes	Purpose	Reviews
Lithographic tooling and injection moulding [44].	Enable mass production.	It could enable mass production of micro-components with a various of material such as polymers, metals and ceramics.
LIGA process and direct femtosecond laser [45].	Fabricating micro-moulds.	An approach leads to practical and cost-effective 3-D MEMS with various materials.
Ultra-precision micro-machining and sacrificial/structural multilayer [46].	Produce self-assembled, 3-D microsystems and associated meso-scale interfaces.	A new class of micro-systems could be developed that is highly three-dimensional, precisely machined and automatically assembled from the variety of materials for MEMS applications.
Laser micro-machining and replication via photo-moulding [47].	Fabrication of micro-components.	Fabrication of micro-components which dealt with materials such as polymers and composites.
Micro-EDM and laser assembly [48].	Fabricate 3D metal microstructures.	The system increases the number of patterns, higher aspect ratios and joint strength of the microstructures. It eliminates the post assembly which involves various efforts in handling and high-precision positioning.
Laser transmission welding and photolithographic mask techniques [49].	Enables assembly of plastic microfluidic devices and micro-arrays.	Allowed a quick welding of plastic parts with high reproducibility and excellent welding quality. Excellent positioning and welding accuracy in the micrometre range can be achieved.
Thermally assisted micro-moulding and micro-drawing [50].	Manufacture grade surgical knife from the bulk metallic glass.	Capable of producing bulk metallic glass grade surgical knife with an edge radius less than 50 nm. It is also possible to go further for radius at or below 100 nm.
Nano-particle deposition system (NPDS) and focused ion beam (FIB) [51].	Minimise limitations on manufacturing precision, product geometry or processing condition.	It can fabricate a nanoscale 3D structure with no thermal and unwanted chemical reactions using various materials and short processing time.
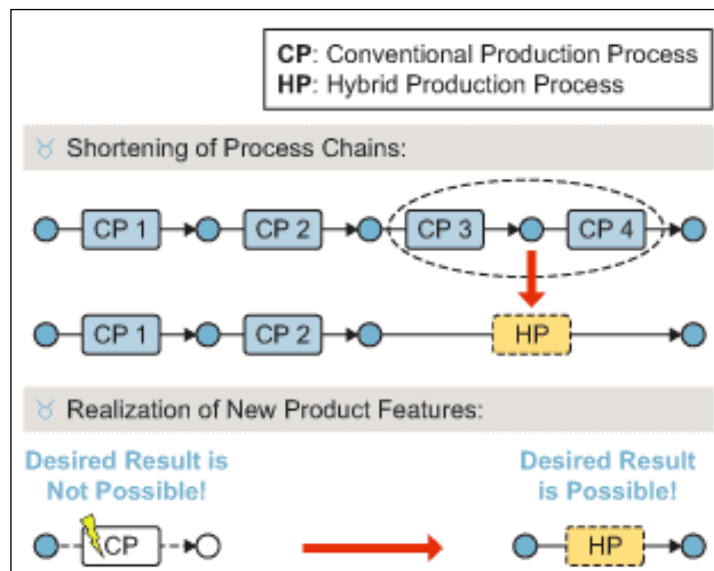
Figure 2.1-4: Hybrid production processes [43].

2.1.3. Developments of Multi Processes Equipment

As has been described earlier, the implementation of various process chains within the integrated platforms is an ideal solution for the reduction of possible accumulation of manufacturing errors and reducing the amount of component handling. By taking advantage of the hybrid micro-manufacturing process, research and development of multi processes equipment has been done by several universities as discussed in **Table 2.1-3**.

Table 2.1-3: Examples of development of multi processes equipment.

Developers	Developments	Capable Processes
Harbin Institute of Technology, China [52].	Multifunctional micro-machining system.	Micro-electro-discharge machining (EDM), micro-electrochemical machining (ECM), micro-ultrasonic machining (USM) and as well as their combination.
Ibaraki University of Japan [53].	Multifunctional micro-machining system.	Micro-milling, micro-turning, micro-grinding, micro-buffing, micro-polishing, micro-EDM, micro-ECM, micro-laser machining and their combination.
National Taiwan University [54].	Multifunctional high precision table top CNC machine.	Micro-high-speed milling and micro-EDM (die-sinking and wire EDM). The system also equipped with an in-process workpiece/features geometrical measurement system.
National University of Singapore [55].	Multi-process miniature machine tools.	Micro-EDM, micro-ECM, micro-turning, micro-drilling and micro-milling as well as electrolytic in-process dressing (ELID) grinding and single point diamond tool cutting.

Another example of an interesting concept that targeted low-cost equipment despite the fact it does not involve multiple processes can be seen in the research of five-axis milling machining. By using this machine, it is capable of machining micro-walls, micro-columns and micro-blades [56].

2.1.4. Size Effects in Micro-Forming Processes

The issues related to the size effects happen when the sizes/features are reduced from a conventional process to the micro-scale. It causes the ratio between the dimensions of the part such as width, height, length and thickness together with the microstructure of grain size to change [12]. Due to this, size effects alter almost all aspects of the forming process such as the material behaviour, heat transfer, friction and handling of the part. Therefore, methods of metal-forming technology meant for a macro-scale cannot be simply applied to micro-scale processes [25]. A few conventional forming machine designs using micro-tools that have been scaled down for micro-forming needs have been used. However, considerations incorporated with machine design have to meet the process requirements of higher quality and efficiency towards positional precision and handling of micro-parts/materials [57]–[59].
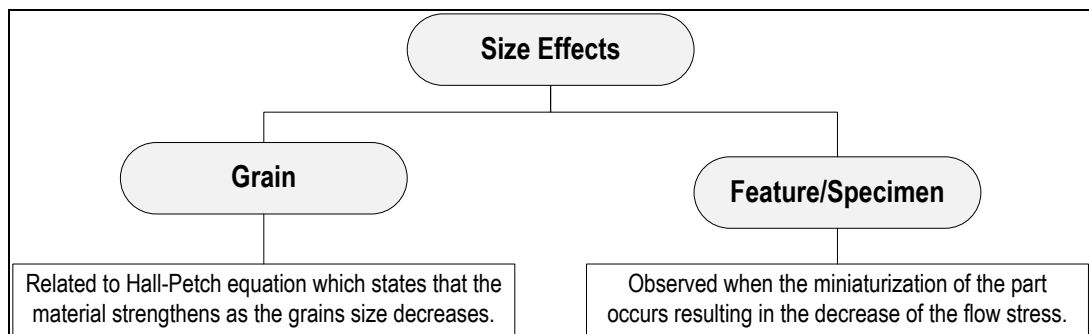
Figure 2.1-5: Classification of sizes effects in micro-forming processes.

There are two size effects existing in metallic materials which are grain and feature/specimen size effect as represented in **Figure 2.1-5**. According to Armstrong [13], the grain size effect is represented by the Hall-Petch law, which states that the material strengthens as the grain size decreases. Grain size effect is purely dependent on the average size of the grains which dominate the material response at the macro-levels. Meanwhile for a feature/specimen size effect observed when the miniaturisation of the part occurs results in

the decline of the flow stress [13], [25], [60]–[62]. **Figure 2.1-6** shows microstructures grain and feature/specimen size effects.
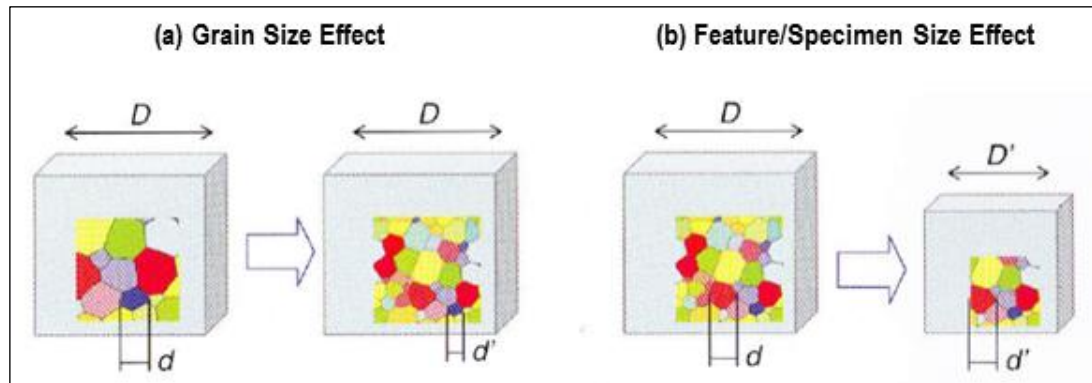
Figure 2.1-6: Illustration of microstructures **(a)** grain and **(b)** feature/specimen size effects [25].

As shown in **Figure 2.1-7**, the feature/specimen size effect also could be divided into two distinctive effects which are feature size effect and the specimen size effect depending on the material testing methods or metal forming processes. Feature size effect can be referred to as the smallest feature on the components such as channels, radius or protrusions which will be formed. Meanwhile, specimen size effect can be referred to as the diameter of a rod or the thickness of the blank sheet to be tested. Below in **Table 2.1-4** there are shown several processes used as an example to define and differentiate between feature and specimen size [25].
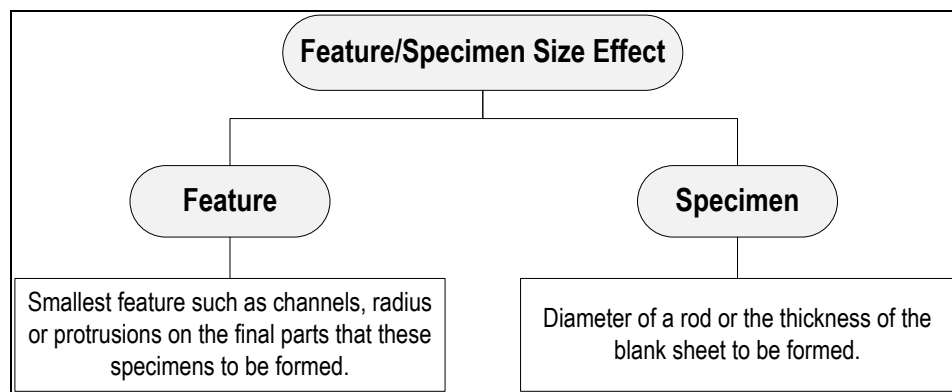
Figure 2.1-7: Classification of featured/specimen size effect.

Table 2.1-4: Examples of classification of feature sizes and specimen sizes on several processes.

Example Processes	Feature Size	Specimen Size
Extrusion process of micro-pins.	Diameter of the reduced section.	Initial diameter of the rod
Micro-channels formed on an initially flat thin sheet blank.	Micro-channel with their dimensions.	Thickness of the blank.
Bulge test of thin sheet blank.	Bulge diameter.	Thickness of the blank.

According to the Koç and Mahabunphachai [25], [63], as the grain, specimen and feature size get even smaller into micro-scales, their effects are coupled and therefore should be considered together even though these size effects have been distinguished based on the previous discussion as shown in **Figure 2.1-7**. They proposed the use of two characteristic parameters N and M to pair which represent the interactive effects. N can be defined as the ratio between the specimen to the grain sizes. Meanwhile M can be defined as the ratio between the feature to the specimen sizes. By defining N and M, all combinations of the interactive effects can be represented and qualified using $N \times M$ (feature to grain size) as presented in **Table 2.1-5**.

Table 2.1-5: Types of size effects and characteristic parameters [63].

Processes Description	Size Effects		
	Grain Size	Feature Size	Specimen Size
Tensile Test	d		t_o, D_o
Bulge Test	d	D_c	t_o
Stamping Process	d	D_c	t_o
Extrusion Process	d	D_c	D_o
Characteristic Parameter	$N = t_o/d$ **or** D_o/d		
	$M = D_c/t_o$ **or** D_c/D_o		
	$N \times M = D_c/d$		

Symbols in Table 2.1-5:

d - Material grain size.
t_o - Specimen thickness.
D_o - Specimen diameter.

D_c - Die cavity.
N - Ratio between the specimen and grain sizes.
M - Ratio between the feature and the specimen sizes.

Materials such as aluminium [64], [65], CuNi18Zn20, CuZn36 [66], CuZn15 [67] and CuAl alloy [68] were observed on the material flow curve by various testing conditions as shown in **Figure 2.1-8** to measure the material response on specimen size. From all the tests that have been done, it has been demonstrated that the trend of decreasing flow stress with a declining of N value was rather consistent. Meanwhile the grain size effect shows a strong influence on the material response at all scales until the N value is around 10 to 15 when the specimen size effect starts to affect the material response [60], [64], [69] as shown in **Figure 2.1-9**.
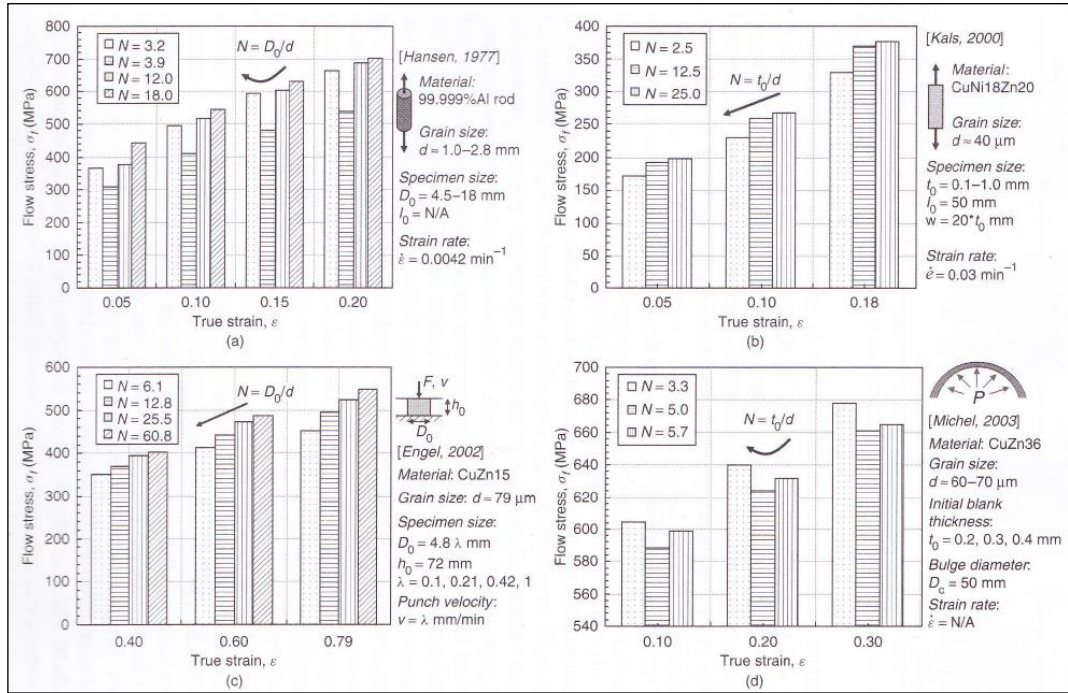
Figure 2.1-8: Effect of N on material flow stress under different testing conditions [25].
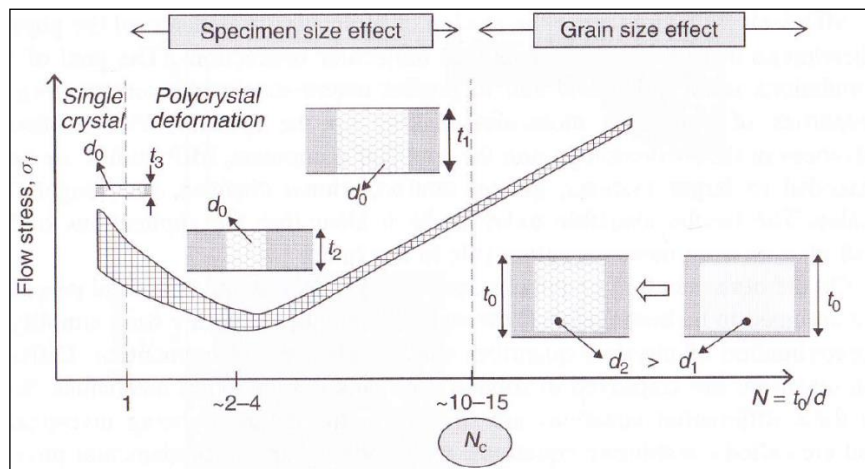
Figure 2.1-9: Grain and specimen size effect as function on N against the flow stress of the components [25].

However, based on the testing reported an increment in flow stress N was decreased close to the range of five to three. As an example, Hansen [64] has conducted a tensile test of 99.999% Al rods, and the results showed an increase in flow stress as N increased from 3.2 to 3.9 as illustrated in **Figure 2.1-8 (a)**. Meanwhile, a hydraulic bulge testing of thin CuZn36 blanks also showed similar results, where there was an increase in flow stress as N value increased from 3.3 to 5.0 as illustrate in **Figure 2.1-8 (d)** [66]. The observation of the increasing flow stress continued to occur as N was reduced close to one (single crystal deformation) as reported in the resulting test of CuZn15 [67] and Al (99.0 to 99.5%) [65]. **Figure 2.1-9** visualises the summary of the effect of N against the flow stress of the components tested.

Meanwhile, the feature size effect was still lacking a comprehensive understanding because only a few studies have been done. As an example, by Michel and Picart [66], using thin blanks of CuZn36 with the initial thickness of 0.25 mm were bulged by using two different diameters of 20 and 50 mm. As the result when using a bulge diameter of 20 mm the value for M was recorded as 80, while using 50 mm bulge the value for M was equal to 200. From the observation that has been made, there was a decrease in the material flow stress when a smaller bulge diameter was used. This showed the effect of the featured size on the material response. Nevertheless, there was no discussion provided regarding the feature size effect.
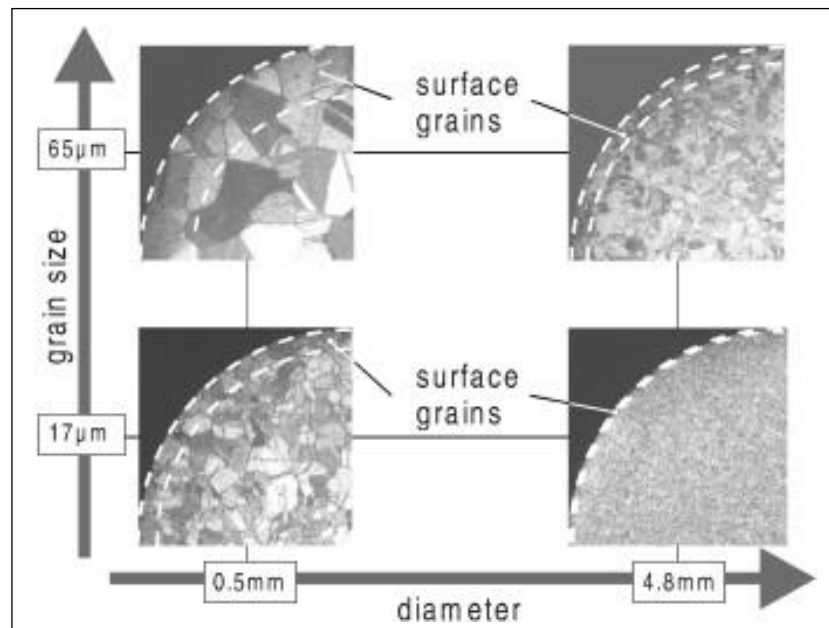
Figure 2.1-10: Surface layer model in bulk metal [12].

22

The explanation of variations in the material flow curve due to the size effects can be explained by using a surface layer model as shown in **Figure 2.1-10**. The dislocation movements in the grains located at the surface are less restricted than grains inside the material. Therefore, these surface grains show less hardening [11], [12], [24], [67], [68]. By referring to **Figure 2.1-10** when the diameter of the components become smaller, but the grain size is the same, the surface grain's area becomes larger. Hence, the movements of grains located at the surface are more active compared to the inside of the material and show less hardening. As a result, the flow stress will be decreased. Meanwhile, when the size of the grain become smaller but the diameter of the components remains the same, the surface grains area become smaller. Thus, the movements of grains located at the surface are more limited compared to the inside of the material and show more hardening. As a result, the flow stress will be increased.

2.2. Powder Metallurgy

Powder metallurgy can be categorised as a combination of processing consolidation to make a solid metal from fine particles. The main advantages of powder metallurgy over the other methods lie on efficient usage of powder material and greater shape flexibility. In the early stage of the powder metallurgy industry, the core objective was to concentrate on a cost reduction while mechanical properties came as a secondary role [70], [71]. Powder metallurgy shows a potential that can be utilised for a development process to produced micro-components. By using a powder metallurgy improvement process, complex shapes of designs with a hard material typically require necessary machining as a post-process can be made. As an example, based on the observation in **Table 2.2-1**, excellent characteristics are shown in powder metallurgy forging which determines it could cope with a production quantity of more than 10,000 units and have the density properties which equal wrought parts [72]. Fundamentally, powder metallurgy major processing steps are divided into mixing, pressing and sintering as seen in **Figure 2.2-1**. The explanations on each process in the powder metallurgy have been described.

Table 2.2-1: Comparison of four powder processing methods of the conventional press and sinter, metal injection moulding (MIM), hot-isostatic pressing (HIP) and powder metallurgy forging [72].

Characteristic	Conventional Press and Sinter	Metal Injection Moulding (MIM)	Hot-Isostatic Pressing (HIP)	Powder Metallurgy Forging
Size of Workpiece	Intermediate: <5 pounds	Smallest: <1/4 pounds	Largest: 1-1000 pounds	Intermediate: <5 pounds
Shape Complexity	Good	Excellent	Very good	Good
Production Rate	Excellent	Good	Poor	Excellent
Production Quantity	>5000	>5000	1-1000	>10,000
Dimensional Precision	Excellent: ±0.001 in./in	Good: ±0.003 in./in	Poor: ±0.020 in./in.	Very good: ±0.0015 in/in.
Density Mechanical Properties	Fair: 80–90% of wrought	Very good: 90-95% of wrought	Excellent: Better than wrought	Excellent: Equal to wrought
Cost	Low: $0.50-5.00/lb	Intermediate: $1.00-10.00/lb	High: >$100.00/lb	Intermediate: $1.00-5.00/lb
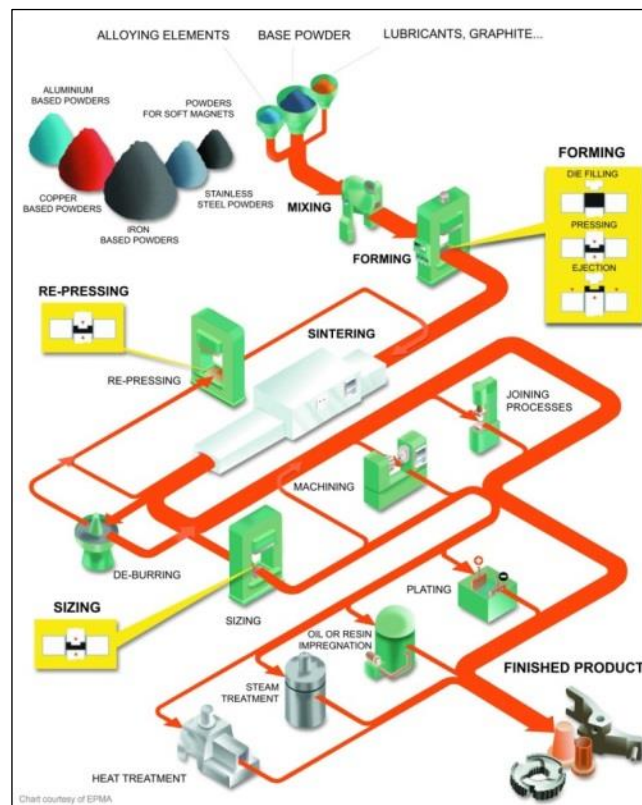
Figure 2.2-1: Illustration of traditional powder metallurgy which consists of three major steps of mixing, pressing and sintering [73].

2.2.1. Mixing

During the mixing process, metal powders are thoroughly mixed with a lubricant before the pressure is applied. This step provides a homogeneous mixture which helps to combine the used powder material. The most common lubricants being used are metallic stearates (zinc stearate), stearic acid, stearin and organic compounds of a waxy nature [73]. Other purposes of lubricant usage in this process were to reduce the friction between the surfaces of tools and the powder mass. Reduction of friction plays a significant role during the ejection process as it helps to ease the part extraction from the die sets and reduces the chances of cracking [70]. In addition to that, the powder material should be evaluated based on its suitability for further processing. The factors that need to be taken into consideration are the flow rate for feeding and distributing the powder materials into the die, the apparent density which is associated with the ability to fill the available space without external pressure, the effective compressibility of applied pressure and green strength of the pressed powder after compacting but before the sintering [71].

2.2.2. Pressing

After the process of mixing has been done, the mixed powder is inserted into the die made from rigid steel or carbide. Then the die set is pressed by using pressure as shown in **Table 2.2-2** [74]. During this forming process, the compacts maintain their shape by a cold forming of powder grains within the mass. It is crucial for the compact to last the ejection process and handled safely to the next stage which is the sintering process.

Table 2.2-2: Common compacting pressure for various applications in powder metallurgy process [74].

Application	Compaction Pressures (MPa)
Porous metals and filters.	40 to 70
Refractory metals and carbides.	70 to 200
Porous bearings.	146 to 350
Machine parts (medium density iron & steels).	275 to 690
High-density copper and aluminium parts.	250 to 275
High-density iron and steel parts.	690 to1650

2.2.3. Sintering

In the sintering process, powder particles are welded together in a protective atmosphere usually in a continuous belt vacuum furnace. This process operates at the temperature around but not exceeding the melting point of the used material component as described in **Table 2.2-3**. The reason why it must not exceed the melting point because the liquid phase must be restricted during the heating period in order the part to sustain its shape. In certain cases, pressing and sintering is done together at an elevated temperature to make sure the part did not change its condition into liquid phase, weld together and confer a sufficient strength for the intended purpose [75]. Lange [18] stated that the densification process using the conventional powder sintering method involves a coarsening or neck growth, which is a critical mechanism needed to achieve densification caused by surface diffusion or evaporation/condensation as illustrated in **Figure 2.2-3**. Thus, it is the reason why conventional powder sintering takes a long time to be completed. The sintering operation involves three stages as illustrated in **Figure 2.2-2** which is the preheat or burn off, high-temperature and cooling period. The purpose of the first stage was to combust any air and remove lubricants that would interfere with good bonding. Then, during the high-temperature period, solid-state diffusion and bonding between powder particles from mechanical to metallurgical bonding occurs. Finally, during the last period, gradual cooling in a controlled atmosphere happens to prevent oxidation and possible thermal shock. Additional processing in the sintered part was also needed such as hot isostatic pressing, forging, plating, impregnation, heat treatment, coating, and de-burring to ensure the high quality of the final part produced. [70], [71].

Table 2.2-3: Common sintering temperature for some common metals [75].

Metals	Sintering Temperature (˚C)
Titanium	600 to 1300
Copper	750 to 1000
Iron/Steel	1100 to1300
Aluminium alloys	590 to 620
Brass	850 to 950
Bronze	740 to 780
Hard metals	1200 to 1600
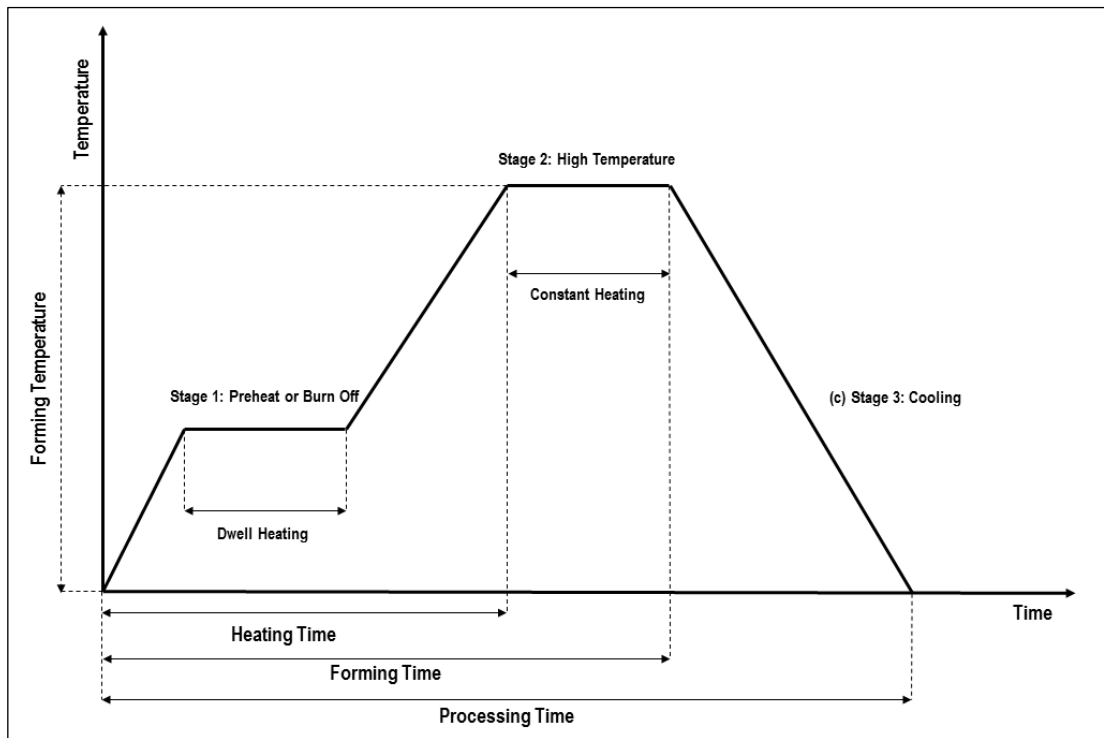
Figure 2.2-2: Sequence of the sintering process consist of preheat or burn off, high-temperature and cooling stage.
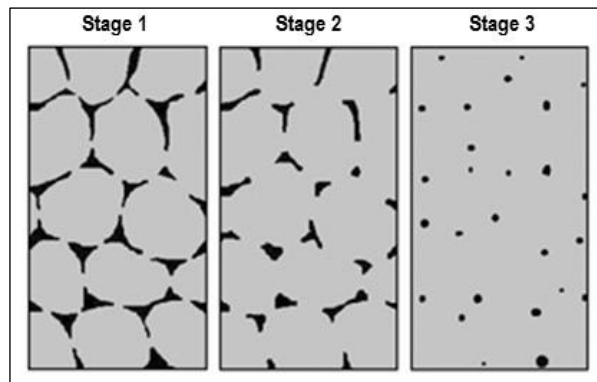
Figure 2.2-3: Solid-state sintering based on preheat or burn off (stage one), high-temperature (stage two) and cooling (stage three) [73].

2.3. Electroplasticity

The electroplasticity can be referred as a phenomenon which involves passing high electric current density pulses through the workpiece during the forming process. By applying current pulses or electric field to the metals, ceramics, superconductors and powder metallurgy products has shown significant improvements in the material plasticity [76]–[78].

27

Therefore, it is suitable to be applying to materials or product that require special shapes to be formed or less formable metal. Also, according to Tang et al. [77], by using electroplasticity the annealing and the acid-pickling processing in the traditional processing methods can be eliminated. It also can improve the surface quality and decrease the number of defects on the components being formed.

Before this, the hot forming process is a traditional method that has been used to decrease the flow stress. However, due to the limitations of the hot forming process, it is not suitable for the micro-forming process. It is because, in the hot forming, it has a complex and bigger apparatus as an overall machine due to the additional heating and heat insulating are needed. As a result, it has low efficiency and high energy consumption. In addition to that, when using the hot forming process at the elevated temperature, it would cause oxidation and poor surface quality of the workpiece. Moreover, it also takes some time to soften the workpiece. Therefore, the electroplasticity process was more appropriate for selection because it provides more reduction in the flow stress and the electroplasticity effect happens immediately when the current flows through the workpiece [79], [80].

The electroplasticity process is efficient for materials with more dislocation barriers where during the plastic deformation, dislocations are generated due to applied stress and interaction with the impurity particles. During deformation, dislocations move through the lattice structure until their motion is hindered by grain boundaries or impurity [81], [82]. When cold work was applied to the material in the compaction process, the dislocation density increases and as a result enhances the strength of the material. Therefore, when the electrical current is applied, a higher dislocation density will be gained, and this gives the most significant reduction in flow stress. This is because the current increases the energy in the lattice, thus causing the metal atoms to raise their vibration which acts as an external force on the dislocation and accelerates their movement [81], [83], [84]. Due to this, the internal friction resistance can be reduced in the course of deforming and the plasticity of the metal can be improved to ease the forming process.

2.3.1. Research Based on Electroplasticity for Bulk Materials Forming

In recent years the mechanism and engineering applications of electroplasticity have been explored. As early as in 1963, Troitskii et al. [85] conducted the experiments by deformation of zinc single crystals in the brittle state with the effect of electron-beam and α-irradiation. As a result, a decrease in the flow stress was observed. An extension of the research was done in 1969 also by Troitskii [76] concerning the influence of electric current pulses on plastic deformation of metals. From the findings, it shows that by using high-density current pulses through metals the flow stress decreased significantly compared to that caused by Joule heat. The findings were also supported by Conrad [86] who conducted research about the influence of electrical-field and corresponding current on the deformation of metals. It was found that the effect of the current was to decrease the thermal component of flow stress. It also showed that an electric current not only accelerates the recrystallization rate of copper and controls the speed of grain growth but also retards phase transformations in metals as well.

The study concerning electroplasticity was continued by Tang et al. [87] who conducted research on cold-drawing of wires with impulse current. It has been stated that the drawing stress is decreased about 20 to 50% compare to without impulse current. The research on electroplasticity and mechanical testing continues with tension tests done by Ross et al. [88] with a series of materials such as copper, brass, aluminium and steel. The results show that when the heavy flow of the conductive electrons applies in the plastic forming, the dislocation was assisted which causes the flow stress to decrease and also improves the quality of plastic forming. Therefore, this supports the theory of the electroplastic effect where it is induced by the massive drifting motion of conductive electrons. The investigation continued by Perkin et al. [83] using a compression test with the effect of electroplasticity for materials of steel alloys, aluminium alloys, Ti-6Al-4V and C110. It has shown that the yield and flow stresses have been reduced with the addition of electrical energy and this allows larger strains to be achieved before fracturing. In addition to that, the elastic recovery was also shown to be reduced which enhanced the final parts quality and accuracy. Meanwhile, based on the investigation by Andrawes et al. [89] using material AlMg1SiCu with the tensile test, it was shown that the mechanical behaviour of aluminium tends to change when the application of

current has been used which was similar to those that occur when the material was annealed. In addition to that the yield and fracture, ductility and toughness of the workpiece decrease to 13, 37 and 75% respectively. It was supported by Roth et al. [90], by using Al5754 showed that the workpiece did not induce the grain growth compared to the elevated temperature used in the hot forming where the microstructural changes and grain growth are common.

Moreover, based on Stolyarov [91] who has conducted a test using cold rolling with the influence of electric current pulse on the ultrafine-grained TiNi alloy it was shown that an enhancement on fracture strain occurs. The research related to the size effect of the workpiece with the influence of electrical pulse also has been conducted by Siopis and Kinsey [92]. The research used annealed copper on the axisymmetric compression test and as a result from the experiment, showed that the flow stress lessened as the grain size decrease. Besides that, Lu et al. [93] has been fabricating superconducting tapes on a rolling process with the applications of high-density current which shows the rolling force can be reduced and deformation can be improve homogeneity. Meanwhile, for micro-component fabrication, the production of the micro-channel on a metal workpiece by embossing and a high-density current process has been done by Mai et al. [80]. The results show that the stress in the workpiece was reduced and depth of the fabricated channel feature was increased.

Therefore, from the overview of previous research, it can be concluded that the application of electroplasticity processing can be considered as a promising new forming technique with high efficiency and low consumption of energy. This method, especially used in the resistance heating (RS) [94]–[100], was suitable for the process due to increasing the formability and decreasing the elastic recovery of materials without the adverse effects which are usually associated with forming at the elevated temperature such as microstructural changes, grain growth and significant deviations in the mechanical properties. Furthermore, by applying electroplasticity during the forming process with fine grain metals, it would ease the process by lower force requirement and hence, extending the tool life.

2.3.2. Application of Electrical-Field Activated on Sintering

The application of electrical-field activated can be seen applied in the sintering technology which shows significant potential to produce the micro-component by using powder as a raw material. Nevertheless, there are still major challenges to the manufacturing of micro-components to meet the requirements of the process which is associated with long processing times to achieve high densification of micro-components. In this review, it has focused more on titanium, titanium alloys and copper samples that have been conducted by the previous electroplasticity sintering processes. Based on the review that has been made below, experiments on electrical-field activated sintering on titanium, titanium alloys and copper shows there are still significant challenges to the manufacturing of miniature and micro-components to meet the requirements of short production times with higher densification of formed samples. Even though several researchers have made a development using mainly the SPS process with titanium, the total time to achieve densification above 90% was approximately in the range of 20 to 60 minutes [101], [102]. In addition to that, some of the operations used in the titanium alloy need to have the annealing process done to the sample about 24 to 40 hours at 1000 °C and 750 °C temperature respectively before or after the sintering process [103], [104]. Graphite was used as a common material for the die set during the experiments, and the samples size was in the range of five to 42 mm in diameter and five to 15 mm in thickness [101], [103], [105]–[109]. Therefore, it would be beneficial to have improvement of the proposed process to reduce cycle time and improve the quality densification of the sample. **Table 2.3-1** to **Table 2.3-3** show a summary of parameters of previous research using the electroplasticity sintering process on titanium, titanium alloy and copper powder.

2.3.2.1. Titanium

Based on research conducted by Liu and Kao [110] with titanium powder of purity more than 99.5%, -200 and -325 mesh by using resistance heating process, the investigation of microstructural and mechanical properties of the formed sample has been done. The preparation of 304 stainless steel die, a set of Cu-Cr alloy punches and mica insulation for die set components has been made. Meanwhile, 200 MPa of pressure with a low voltage of

maximum 5 volts, high ampere of maximum 2,500 A, alternating current power supply and specific energy input of two to three kJ/g was been used in the research which was performed in the ambient atmosphere. As a result, 96% of the relative density of sample with a dimension of length 60 mm, width 10 mm and depth of 4 mm have been achieved with two hours of annealing at 800 °C and two seconds of the sintering process. It was found that the obtained sintered titanium samples show relatively higher yield stress and ultimate tensile strength as compared to similar products obtained by other powder metallurgy techniques. Nevertheless, it is still considered as a long process due to the annealing procedure even though the samples produced an excellent relative densification.

Meanwhile by using the SPS process done by Asaoka and Kon [103], titanium with purity of 99.7%, -250/+150, -150/+45 and -45 μm of particle size have been sintered as a porous advanced biomaterial used for dental and medical implants. The input for current density and voltage parameter employed in this research are 750 A and 2.5 to 3.5 V respectively. Temporarily, the pressure and temperature used are 20 MPa and 560 to 570 °C correspondingly with the sintering time of 6 minutes to 20 minutes. The samples were compressed in a carbon die set of five-millimetre internal diameter and ten-millimetre height with the vacuum pressure in the range of three to four pascal. The sintered samples were annealed at 1,000 °C for 24 hours in an evacuated furnace which caused the compressive strength of the samples produced to be increased. The relative densification for the titanium sample was in the range of 68 to 73%.

Again using the SPS process, Eriksson et al. [101] used titanium containing 0.2 wt-% oxygen with an average of 45 μm for the experiment. The parameters employed are a pressure of 10 to 100 MPa, a temperature of 950 °C, a sintering time of 20 minutes and a heating rate of 25 to 200 °C/min to produce the sample that has the relative density of 99%. Also, the SPS samples were deformed in compression either in the same SPS apparatus or a hot pressing furnace to evaluate the final contribution to densification of spark discharging or anisotropic heating. The obtained results showed that none of them played a role in densification. The dimension of the sample in this research was indicated of 20 mm in diameter and five millimetres in thickness. The die set used graphite for the body of the die with a wall thickness of 15 mm and 10 mm.

A higher temperature range of the sintering also has been used in the research conducted by Zadra et al. [111] using the SPS process. The temperature has been set in the range of 700 to 1150 °C with the pressure of 60 MPa using titanium powder with particle size less than 45 μm. The experiment has been done in a vacuum atmosphere at two Pascals with the sintering time of five minutes. As a result, 90% relative densification of the sample has been achieved. Based on the findings, it shows that by using temperature in the range of 900 °C in the sintering process, the sample that has been produced could have a good microstructural chemical and mechanical property.

Besides that, the three-step process also has been proposed by Chaudhari and Bauri [102] which made a comparison with the single-step in the SPS process by using commercial titanium powder of -325 mesh (ASTM Grade-2) and average particle size of 45 μm. In this research 50 MPa pressure, 600 to 1300 °C heating temperature, 25 to 100 °C/min heating rate and 30 minutes for one-step to 60 minutes for three-step of sintering time has been used. The dwell time used in this experiment during the sintering temperature was 10 min for continues cycles. The vacuum atmosphere of about six Pascals was employed during the experiment with a graphite die set. As a result, the sample from the experiment shows a relative density of 99% with the average hardness value for the sample of 325 $HV_{0.3}$ can be obtained especially in the three-step process.

Table 2.3-1: Parameter of previous research using electroplasticity sintering process on titanium powder.

Ref.	Process	Annealing		Pressure	Sintering		Heating Rate	Relative Density
		Temp.	Time		Temp.	Time		
		(°C)	(min)	(MPa)	(°C)	(min)	(°C/min)	(%)
[110]	RS	800	120	200		0.0333		96
[103]	SPS	1,000	1,440	20	560 to 570	6 to 20		68 to 73
[101]	SPS			10 to 100	950	20	25 to 200	99
[111]	SPS			60	700 to 1150			90
[102]	SPS			50	600 to 1300	30 to 60	25 to 100	99

2.3.2.2. Titanium Alloys

The preparation of Ti-Pt samples by using the SPS process has been done by Onagawa et al. [104]. The Ti powder with a maximum particle diameter of 150 µm and a purity of 99.6% with Pt powder with a maximum particle diameter of 2 µm and a purity of 99.9% were used to be mixed for ten minutes in a mixer at a speed of 1 rotation per second. Meanwhile, the parameters that have been used during the experiments are 40 MPa in applied pressure and 800 °C for sintering temperature for the duration of ten minutes. The pulse voltage of 4,000 A per five volts in Ar gas atmosphere has been used. In addition to that, the annealing process has been done at temperature 800 °C for 40 hours for the sintered samples. The results show that the samples consisted of a Ti matrix with dispersed Pt and some Ti-Pt intermetallic in particular Ti_3Pt, which are responsible for the high corrosion resistance exhibited by the material.

By using the SPS process done by Asaoka and Kon [103], Ti-6Al-4V alloy powder with grain size of -150/+46 µm and composition of Ti-6.5Al-4.26V have been sintered as a porous advanced biomaterial used for dental and medical implants. The input for current density and voltage parameter employed in this research are 1,000 A and 2 to 3 V respectively. Temporarily, the pressure and temperature used are 30 MPa and 700 °C correspondingly with the sintering time of three minutes. The samples were compressed in a carbon die of five-millimetre internal diameter and ten-millimetre height with the vacuum pressure in the range of three to four pascal. The sintered samples were annealed at 1,000 °C for 24 hours in an evacuated furnace which caused the compressive strength of the samples produced to be increased. The relative densification for Ti-6Al-4V sample was in the range of 68 to 69%.

Table 2.3-2: Parameter of previous research using electroplasticity sintering process on titanium alloys powder.

Ref.	Process	Annealing		Pressure	Sintering		Heating Rate	Relative Density
		Temp.	Time		Temp.	Time		
		(°C)	(min)	(MPa)	(°C)	(min)	(°C/min)	(%)
[104]	SPS	750	2,400	40	800	10		
[103]	SPS	1,000	1,440	30	700	3		68 to 69
[105]	SPS			30	1,100	30	20	83

Yang et al. [105] have used Ti-6Al-4V powder with the purity of 99.5%, the particle size of 48 to 75 μm and 0.19 w/o O in the SPS process with a graphite die set of 42 mm in internal diameter and 15 mm in wall thickness. This is a different approach compared with previous research as stated before where a thin graphite foil was placed between the powder and graphite die inner surface to eliminate welding and enhance the uniformity of current flow. The process has been made in a vacuum atmosphere at less than four Pascals. Other than that, 30 MPa of pressure, 1100 °C of heating temperature, 20 °C/min of heating rate and 30 minutes of heating rate has been set which as a result made the relative density of the sample achieved 83%.

2.3.2.3. Copper

Fine grain (two to three μm) copper powder material has been sintered by using a plasma activated sintering (PAS) process [106]. It was divided into two stages. In the first stage, a pulse current of 400 A was applied for zero to 30 s. Meanwhile, during the second stage, a direct current used was varied from 300 to 800 A for 300 to 330 s, and a uniaxial pressure of 12.6 to 25.2 MPa was employed. The graphite die set of 20 mm in diameter was used and insulated by using a BN coating to allow the current pass only through the punches and Cu powder compact. As a result, based on the parameters stated above, a larger direct current caused a higher heating rate and correspondingly a higher densification rate. In contrast, when the current was maintained constant with higher mechanical pressure, it led to lower heating and densification rates.

Srivatsan et al. [107] made a solidification of Cu powder with a particle size of 13 μm with plasma pressure compaction (P^2C) using processing parameters of 40 MPa applied pressure and 880 to 900 °C of sintering heating for three to five minutes. The compaction process was initiated by applying a pulsed direct current of 3 V maximum and 2000 A average current to the powder compact. The used die set was made from graphite and the samples produced were measured 25 mm in diameter and 15 mm in thickness. From the result of the experiment, it was found that by using pressure assisted with plasma to densify the sample would produce a higher micro-hardness value and densification can be achieved in the range of 95 to 98%.

Srivatsan et al. [108] also continued the investigation by using the same P^{2}C process with high current density of approximately 1140 A/cm^2 to densified Cu powder with a particle size of 100 nm as a comparison to the previous experiment. In this experiment, 40 MPa of applied pressure, 880 °C of sintering heating for durations about three minutes and 500 °C/min of heating rate was used to produce the samples of 13 mm in thickness and 25 mm in diameter with 99% of relative densification. The die set also used graphite as its material. As a result, on the micro-hardness test, it showed that the sample with nano-size particles was four times the hardness of micro-size particle samples. Meanwhile, in the nano-hardness test, the nano-size particle sample was twice the hardness of micro-size particle samples.

The RS process was used to fabricate W-Cu composite containing five to 80% of Cu by Zhou and Kwon [109]. Cu powder with particle size of -200 mesh and purity of over 99% along W powder with particle size of 1 μm and purity over 99.5% was used. The sample assembly was encapsulated in a pyrophyllite sleeve which acted as heat/electric insulator. Graphite and steel platelets were used as sealing and pressure transfer components as well as electric conductors. The samples with the dimension of 20 mm in diameter and thickness of 5 mm were obtained. The pressure that has been applied was increased to the range of 6 or 8 GPa for three minutes for the first stage. Then, alternating current with the input power of 18 to 23 kW was passed through the sample and hold for 50 s. Finally, after increasing the current, the pressure was kept for 25 s and then depressurized. As a result, the final density of the sample recorded was in the range of 90.43 to 98.40%. The densification of the samples was raised as the W particle size increased from 0.5 to 7 μm.

Table 2.3-3: Parameter of previous research using electroplasticity sintering process on copper powder.

| Ref. | Process | Pressure | Sintering | | Heating Rate | Relative Density |
| | | | Temp. | Time | | |
		(MPa)	(°C)	(min)	(°C/min)	(%)
[106]	PAS	12.6 to 25.2		5.50 to 6.00		
[107]	P^{2}C	40.0	880 to 900	3.00 to 5.00		95.00 to 98.00
[108]	P^{2}C	40.0	880	3.00	500	99.00
[109]	RS	6.0 to 8.0 × 10^3		4.25		90.43 to 98.40

2.4. Summary of the Findings

Based on the literature review conducted in this chapter, it has been conclusively proved that micro-manufacturing has received proper attention regarding its manufacturing processes. Micro-forming is one of the popular processes known that can satisfy the demands of mass production including the enhancement of product performance with minimal waste. This has the aim to satisfy the constant demand by customers as well as manufacturers that are relying more on smaller products with various applications. Some of the micro-machining processes, such as chemical, soft lithography and laser beam machining are capable of producing high-grade micro-component, however concern regarding the manufacturing cost and material losses could be a significant matter in the mass production situation.

Considering the advantages of the micro-forming process mention above, they drive the micro-components manufacturers to attempt to produce parts and components with intricate geometries and features that are suitable to replace many of the costly conventional micro-manufacturing processes. Nonetheless, it was not an easy task to achieve the desired shape of a product using conventional process itself. This was because intricate details of some products require the use of the specific processes to obtain the accuracy in shape and dimensions of the final product. Other than that, the issues and challenges for manufacturing micro-products need to be handled such as tolerance and surface quality capability, overall dimension of parts, tooling dimension and unwanted external force. The details regarding the challenges in the production of micro-components have been discussed in section **2.1.1 Challenges to Manufacture Micro-Products.** It can be summarised that the manufacture of a micro-product still a challenging task which needs some improvement to be made due to lack of sufficient standards, design/manufacturing rules and understanding of the manufacturing processes itself. Based on competitive conventional micro-manufacturing processes stated in **Table 2.1-1**, no single process could be dominant to fulfil the requirements needed in the production of micro-components while maintaining low manufacturing cost.

Therefore, from the overview of the previous research, as stated in section **2.3.1 Research Based on Electroplasticity**, it shows that the application of the electroplasticity

processing can be considered as a promising new forming technique with high efficiency and low consumption of energy. This technique was suitable for the materials that are hard to be formed or less formable metal, especially for the bulk-form of micro-components. This phenomenon was due to the grain size effect as the Hall-Petch law stated that the finer the grains of the material, the higher the strength of the material would be. The details regarding the subject were shown in section **2.1.4 Size Effects in Micro-Forming Processes**. Moreover, by using electroplasticity, the microstructure of the material and its plastic flow could be controlled more efficiently which as a result improves surface quality, reduces the number of defects compared to conventional micro-forming processes and extends tools life due to lower forming forces.

The application of electroplasticity can be seen in the sintering technology which shows a significant potential to produce micro-components by using powder as a raw material. Based on the research review as stated in **2.3.2 Application of Electrical-Field Activated on** Sintering it has shown that there are still significant challenges to manufacturing micro-components to fulfil the requirement of the process which can be handled in the short time and achieve a higher relative densification of the product. The reviews showed that even though several researchers have made developments using mainly the SPS process with titanium materials, the total time to achieve samples densification above 90% was approximately in the range of 20 to 60 minutes. In addition to that, some of the operations used in the titanium alloy materials needed to have the annealing process done to the samples about 24 to 40 hours at 1,000 °C and 750 °C temperature respectively before or after the sintering process. Most of the components that have been produced had overall sizes in the range of 5 to 42 mm in diameter and 5 to 15 mm in thickness. It would be beneficial to have improvements of the reviewed processes for the manufacture of micro-components through reduced cycle times and improved densification quality.

Therefore, the electrical-field activated sintering and forming process has been developed to save time compared to the conventional process where it was directly feeding the loose powders into the die set without the need to prepare a green compact and hence small size components could be made based on the design of the die set. In addition to that, directly forming the component without using lubricants decreases the impact on the

environment. Besides that, the process make it easy to manage the microstructure of the part formed which could reduce the application of forming pressure requirements, and it could also increase the tooling life. This is due to the induced heating from the high-efficiency of the alternating current. It is also feasible to form micro-components with high strength materials through reducing the influence of the grain size effect in the micro-forming process. Additionally there is also the option to use different powder material combinations.

Chapter 3: Process Concept of Electrical-Field Activated Sintering and Forming

3.1. Introduction

The electrical-field activated sintering and forming process is an improvement from a combination of traditional electroplasticity sintering and a forming process which has been developed to manufacture micro-components from a variety of powder material systems. It is also efficient where the entire process can be completed in a few minutes and has potential to produce samples with a high relative densification. The parameters of the process such as sintering temperature, heating rate and pressure applied to the samples have significant effects on the densification of the samples. Furthermore, by the help of continued high pressure used during the short forming time no coarsening of grains during the densification process. According to Lange [18], the densification process using the conventional powder sintering method involves a coarsening or neck growth, which was a critical mechanism needed to achieve densification. It was caused by surface diffusion or evaporation/condensation. Thus, it is the reason why conventional powder sintering takes a long time to become completed. By using the Joule heating as the main heat source during the electrical-field activated sintering process as shown in **Figure 3.1-1**, densification can be achieved more quickly, through plastic deformation, breakage and fluid flow of the powder particles. Based on this finding, it was essential for the particle changing process to be present to achieve adequate and quick densification of micro-components.
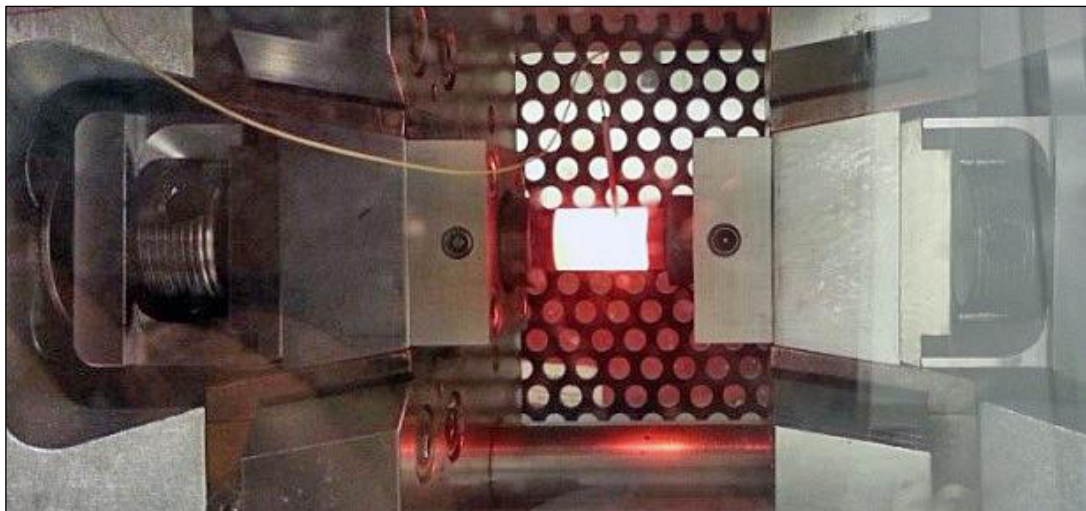
Figure 3.1-1: Die set with powder material during the experiment using Gleeble® 3800 machine.

During the process, the powders are sintered under the simultaneous influence of the high temperature produced by current flow through the die set and the forming pressure applied as presented in the schematic drawing of **Figure 3.1-2**. In this process the loose powder is being placed directly into a small die and the punch assembly is sandwiched between two electrodes. The heating was produced by passing an alternating current through the die to generate the necessary temperature within the die sets and powder inside. Then pressure was applied onto the powder concurrently to facilitate the consolidation and plastic deformation of the powder which made a significant contribution in forming a component with complex geometries. The electrical-field that has been used in the Gleeble® 3800 machine has a low voltage (three to ten volt), high current (3,000 to 30,000 A), large current density (200 to 400 kA/cm^2) and has been done in a vacuum atmosphere (4.6 × 10^{-1} Torr).
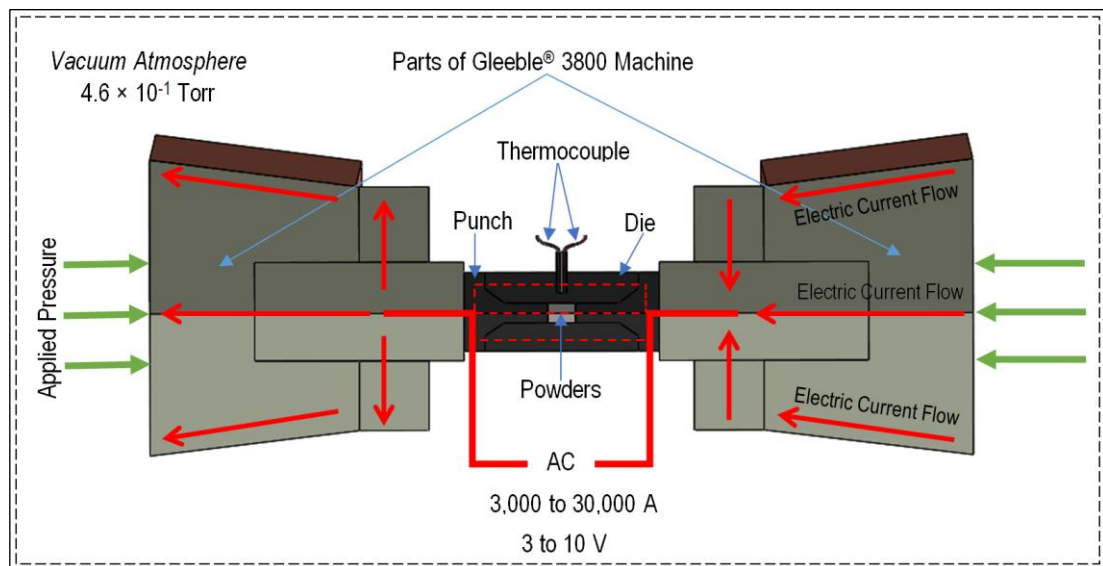
Figure 3.1-2: Schematic drawing of the Gleeble® 3800 machine tooling and current flows (red arrows) during the electrical-field activated sintering and forming process.

3.2. Comparison with Spark Plasma Sintering

By using the electrical-field activated sintering and forming process, it is better at achieving the densification of samples compared to spark plasma sintering. This is due to the larger pressure applied by the upper and lower punches assisting the mechanical plastic deformation and breakage of the powder particles which are located inside the die during the process. It was not dependant on spark discharge to create the heating as used in spark

42

plasma sintering, instead Joule heat was used to make the particle interface melt due to the high temperature created which helps induce the plasticity. In addition to that, no plasma occurred in the powder system by using electrical-field activated sintering process. This was due to the low voltage applied and rapid contacts established by the high pressure which it would not be possible to simulate electrodischarge during the rapidly compacted powder system. Meanwhile, in spark plasma sintering, it needs the gaps between particles in order to simulate the spark discharge that has been made by the pulse current. Due to this, the pressure that needs to be applied in the spark plasma sintering process cannot be too high which would close the gap of the particle. If the application of pressure were higher, the sparks would disappear [19].

In addition to that by using the parameters of the process such as low sintering temperature and short sintering time this can also effectively detain the grain growth and permit the preparation of materials with density and fine crystalline structure [112]–[114]. Therefore, using much higher heating rates during the electrical-field activated sintering process is an important feature as it helps to speed up the process to a few minutes to be completed. It was different in the spark plasma sintering process where the heating rate was found to have no influence on the final density of sintered part [115], [116]. According to the reviews on the application of electroplasticity on the sintering process it shows that even though several researchers have made a development of the process using spark plasma sintering with titanium, the total time to achieve densification above 90% was approximately in the range of 20 to 60 minutes [101], [102].

3.3. Densification Mechanism

In the conventional powder sintering method, neck and grain growth are the critical mechanisms needed to achieve densification. Grain growth was caused coarsening which is associated with surface diffusion or evaporation/condensation [18]. Thus, it is the reason why conventional powder sintering takes a long time to become completed which is caused by the requirement of high temperature and longer time processing needed which leads to unwanted grain growth in the sintered body [117]. Meanwhile, by using electrical-field activated sintering and forming process, there was no coarsening or neck growth with a short sintering process.

Instead, the densification can be achieved more quickly by deformation and breakage of the powder particles. The increase and then disappearance of the interface area between particles were the results of the densification of the part being formed. Based on this finding, it was critical for the particle changing process to be present under multi-fields which are pressure and electrical-field activation to achieve satisfactory and quick densification of micro-parts which is different from conventional powder sintering processes [118]. By using Joule heat which is generated by contact resistance between powders and resistance of powder itself, the temperature will rise quickly when a large current passes through the powders. Based on the Joule-Lenz's law, the heat can be produced by the current passing through the compact which can be represented as equation **(3.3-1)**. The densification mechanism of electrical-field activated sintering and forming process can be described as a fourth stage process as illustrated by **Figure 3.3-1** below.
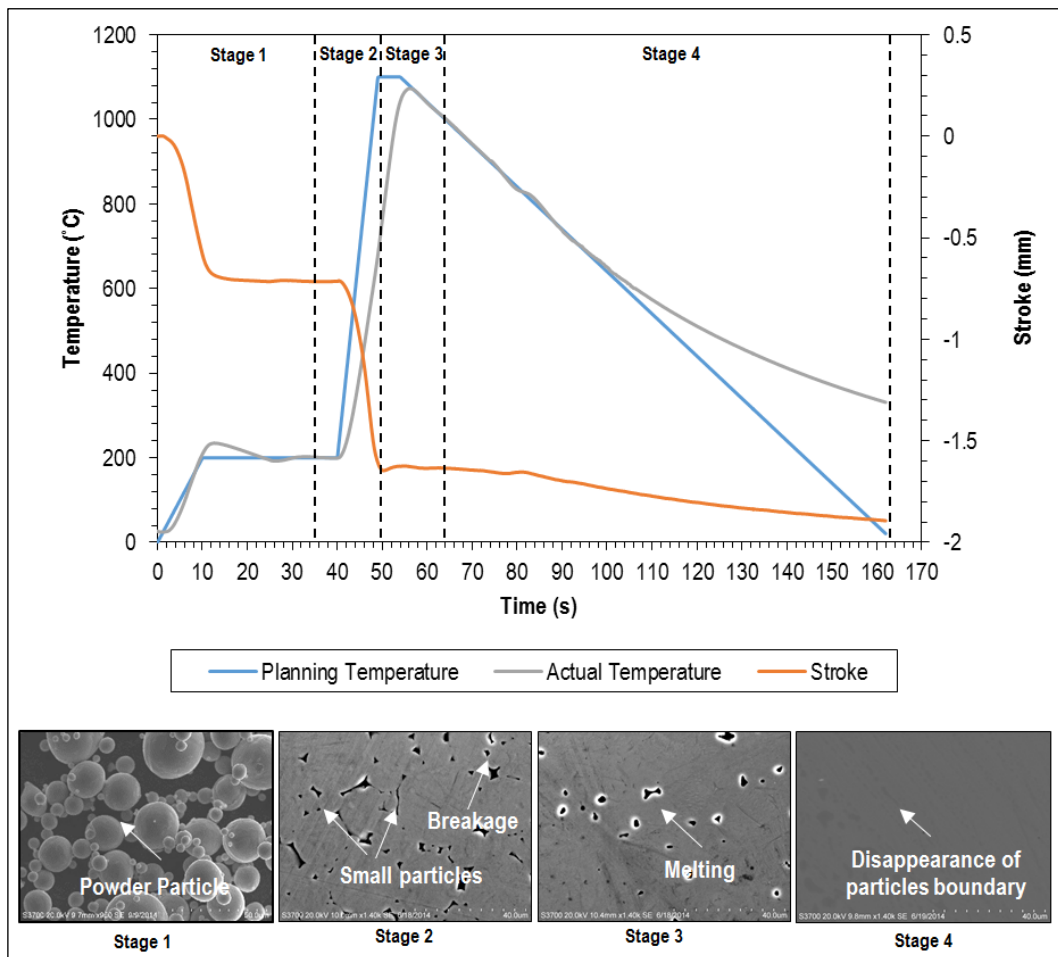
Figure 3.3-1: Illustration of stage level for electrical-field activated sintering and forming process.

44

$$Q = I^2 R t \tag{3.3-1}$$

Symbols in equation (3.3-1):

Q -   Heat generated by current passing through the compact.

I -   Current.

R -   Resistance of the particle or contact resistance.

t -   Time.

3.3.1. Stage 1: Low-Temperature Pressing

Initially, after the powder material had been prepared and placed it into the die set, it was distributed loosely inside the die set cavity. During this time, the powder system has a weak conductivity. Then, during the preheating process the powder was heated using electric current in a vacuum chamber (4.6×10^{-1} Torr) from a room temperature up to usually 200 to 400 °C. The electric current mainly passes through the die set and heat was primarily produced on them. As the process was going on, the heat was transferred to the powder, and its temperature was rising. Based on the observation, the relative density of the sample formed reached averagely about 80% under the electric, thermal and pressure field at the end of this stage. During this time, the conductivity of the powder system became much more efficient compared to the starting time. After that, the electric current will mainly pass through the powder system and the Joule heat will be generated due to the contact resistance of the powder among itself which causes the increased temperature of a compact sample. In this process also, it combusts any air that was trapped inside the die set that would interfere with the proper bonding between powder particles. At the same time, the pressure forced on the die and punch along with the electric current significantly enhances the solid diffusion of particles which can lead to the perfect dispersion of powders [119]. Besides providing Joule heat for a compact, the electric field is also accelerating the diffusion of atoms among the powder particle compact. The observed current's influence on the atoms of particles mass transport which can be caused by one of the several essential effects including flux (electromigration), an increase in point defect concentration, or a reduction in mobility activation energy for defects [120]. Munir [121], suggested that the effect of an electric field was reliant on its strength and the value of the effective charge of the diffusion atoms. Based

on his results, it was clarified concerning electromigration, where the field modifies the diffusion flux equation by a field related term, which was expressed by the equation **(3.3-2)**.

$$J_i = \frac{D_i X_i}{RT}\left(RT\frac{\partial \ln X_i}{\partial x} + Fz_i^* E\right)$$

(3.3-2)

Symbols in equation (3.3-2):

J_i - Flux of atoms of species i.

D_i - Diffusion coefficient of atoms of species i.

X_i - Concentration of atoms of species i.

F - Faraday constant.

z_i^* - Effective charge of diffusion atom.

E - Electric field.

R - Gas constant.

T - Temperature.

x - Coordinate along which diffusion is taking place.

3.3.2. Stage 2: High-Temperature Pressing

Based on an end point of the stage one, the temperature continues to rise upon the setting sintering temperature while the pressure on the punches was maintained. The stress which was transmitted to the low-density porous body and the small contact area between particles is much higher compared to the macroscopic applied stress. In addition to that, the plastic deformation ability for the powder materials at high temperature was one of the excellent properties for this process. According to Quach et al. [120], besides the sintering stress, applied pressure also provided additional driving force where the function of applied stress was expressed as equation **(3.3-3)**. It represents that, at a given temperature, the densification was higher when a larger pressure was applied.

$$\frac{d\rho}{(1-\rho)dt} = B(g\frac{\gamma}{x} + P)$$

(3.3-3)

Symbols in equation (3.3-3):

ρ - Fractional density.

B - Parameter that includes the diffusion coefficient (of the slowest species) and temperature.

g - Geometric constant.

γ - Surface energy.

x - Parameter representing a size scale which is related to particle size.

t -   Time.

P -   Effective pressure.

During the stage two, where the temperature starts to rise from the preheating temperature (200 to 400 °C) to the sintering temperature (900 to 1,150 °C), the powder was deformed and broken down under the effect of an external pressure field at elevated temperature. Due to this process, the loaded particle of powder materials then move towards each other [122]. Plastic deformation, crushing, breakage and others shaping of the partially dense network of particles powder happen as a result of action from an external pressure which is continually forcing particles to touch each other during the sintering process. The heating rate also influences the electric current passing through the sample during the sintering process which can be described as following equation **(3.3-4)** and **(3.3-5)** [123].

$$\frac{I}{A} = \sqrt{\frac{\rho \cdot C}{\sigma} \cdot \frac{dT}{dt}} \tag{3.3-4}$$

Hence,

$$E = \frac{U}{L} = \sqrt{\rho C \sigma \cdot \frac{dT}{dt}} \tag{3.3-5}$$

Symbols in equation (3.3-4) and (3.3-5):

I -   Electric current. $\dfrac{dT}{dt}$ -   Present heating rate.

A -   Surface area of a compact. L -   Length of the compact.

ρ -   Density of a compact. U -   Voltage applied to the compact.

C -   Heat capacity of a compact. E -   Electric field.

σ -   Electrical resistivity of a compact.

While the heat flux described as follows in equation **(3.3-6).**

$$q = \frac{Q}{At} = \rho C L \frac{dT}{dt} \tag{3.3-6}$$

47

q - Heat flux density.

Based on equation **(3.3-5)** and **(3.3-6)**, it represents that both heat flux density (q) and electric field (E) will be increased with the increase of the heating rate which indicates that the current passing through the particles during the temperature rise was greater than in the heat of the preservation process. More interface areas will be formed in stage two compared to stage one as the sintering progresses. Due to the high-density current produced during the temperature increasing period, this would generate a significant amount of heat at the interface which helps to continue the plastic deformation and shaping of the particle powder materials. As this process is going on, the interface areas between particles are getting bigger while the resistance of the particle will be smaller which gives advantages towards densification of the compact which can be enhanced greatly, nevertheless, at the end of this stage two, the powder system was still not fully dense [124].

3.3.3. Stage 3: Sintering with Pressing

During the stage three, while maintaining the applied pressure towards the die set, the sintering temperature (900 to 1,150 °C) will be constants for some short period (2 to 10 s). Significant heating was generated towards the interface particles, where the melting point of fine powder particles was likely to be achieved at these interfaces, this causes the generation of a liquid phase at local areas. When the liquid phase was formed, it would lead to the welding of the contact surface between particles [125]. In the meantime, with the help of the applied constant pressure to the compact, the liquid phase fills into the nearby pores due to the viscous flow and capillary force which results in the disappearance of the interface between particles and fast densification of the compact [126]. Murray et al. [127], also stated that the densification rate under the condition of an external pressure field can be expressed as equation **(3.3-7)**.

$$\left(\frac{d\rho}{dt}\right)_{p>0} = \frac{3}{2} \cdot \frac{\gamma}{nr_1} \cdot \left(1 + p\frac{r_1}{2\gamma}\right)(1-\rho)\left[1 - \frac{\sqrt{2}\tau_c r_1}{2\gamma\left(1 + p\frac{r_1}{2\gamma}\right)} \cdot \ln\frac{1}{(1-\rho)}\right] \quad \textbf{(3.3-7)}$$

Symbols in equation (3.3-7):

$\dfrac{d\rho}{dt}$ -   Densification rate. ρ -   Relative density of sintering sample.

γ -   Surface tension of materials. τ_c -   Yield stress of material.

n -   Viscosity of materials. p -   External pressure applied.

r_1 -   Radius of closed gap.

This was also supported by Wakai and Shinoda [122], who stated that by applying the stress concept during the sintering process gives the relation between the total energy and pore volume to be changed. During the condition of grains in the perfect sink for vacancies, two particles will approach each other where they are driven by the force that was obtained by adding the stress over the boundary area and the surface tension along the circumference. Therefore, when the pore volume decreases, the porous material also will shrink and as a result the total energy also will be decreased which helps the process of densification.

3.3.4. Stage 4: Post-Sintering Cooling

The final stage of the process was the cooling period where the electric current is switched off after completion of stage three. During this time, the compacts were cooled down to room temperature in the sintering chamber.

3.4. Summary of the Chapter

The conventional sintering processes takes a long time to be completed due to the densification process which involves a coarsening or neck growth which was a critical mechanism needed to achieve the densification of samples where it was caused by surface diffusion or evaporation/condensation. Although several researchers have made developments using the spark plasma sintering process, the total time needed to achieve higher densification of the samples still takes a long time. This is due to the spark plasma sintering depending on gaps between the particles to simulate the spark discharge that has been made by the pulse current. Therefore the applied pressure cannot be too high which would close the gap and cause the spark to disappear. By using the parameters of the process such as low sintering temperature and short sintering time they also effectively inhibit

the grain growth and permit the formation of materials with density and fine crystalline structure. Thus, using a higher heating rate in the electrical-field activated sintering and forming process could be a major characteristic where it contributes to speeding up the process to a few minutes to be completed. Therefore, taking the consideration as stated above, it can be concluded that the densification of the components by using electrical-field activated sintering and forming process can be achieved by the involvement of the particle rearrangement, deformation, breakage and interface disappearance which was different from the conventional sintering process. It could be completed within a short time due to it being a coupled process of the electrical-field which generated the Joule heat and high pressure. There were four stages involved in the densification mechanism of the electrical-field activated sintering and forming process which were low-temperature pressing, high-temperature pressing, sintering with pressing and post-sintering cooling.

Chapter 4: Die Sets Development

4.1. Introduction

The development of the die sets design for the experiment of electrical-field activated sintering and forming process has been described in this chapter which provides a detailed report of its comparison features, die set materials and the powder materials used to be sintered. The die sets were utilised for the experimental purpose to test the parameter that has been set for the experiment of electrical-field activated sintering and forming process using titanium (Ti) and titanium tin alloy (90Ti10Sn) powder material. **Figure 4.1-1** shows the orientation position of the die set in the vacuum chamber when using the Gleeble® 3800 machine. The dimension of the die set needs to fit the puncher tooling perfectly to have a high efficiency of heating and pressure during the process. Two die sets designs had been made for the development of electrical-field activated sintering and forming process tooling. The first and second die sets were named as A and B respectively. As for the die set A, it was used for the initial testing to investigate the efficiency and robustness of the die set towards the applied parameter of the experiment which required a high temperature and pressure. Meanwhile, the die set B has been made based on the improvement and optimisation experiment using die set A for more efficient use in the electrical-field activated sintering process. The output samples that the die sets A and B would produce were a cylindrical shape with the diameter of 4 mm and height of 4 mm.
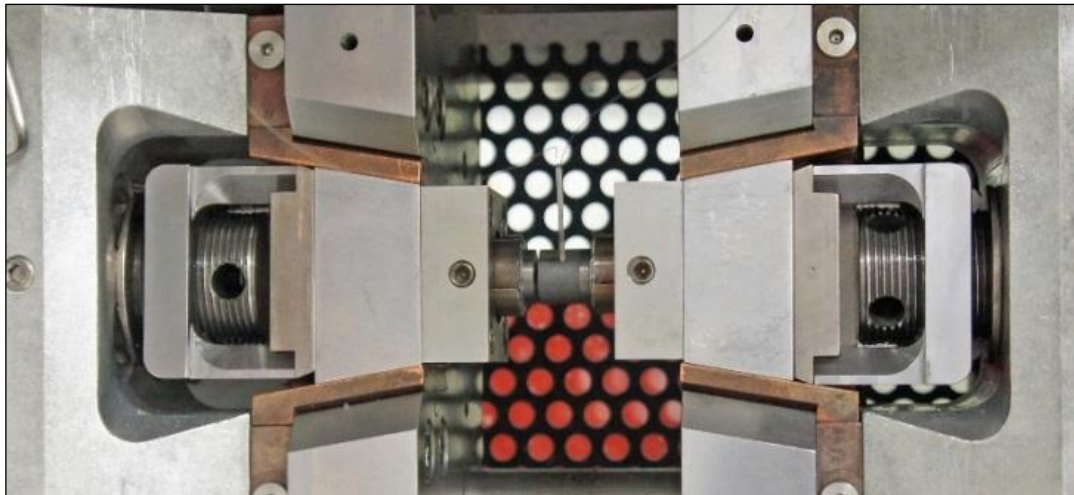
Figure 4.1-1: Orientation position of the die set and thermocouple in the vacuum chamber of Gleeble® 3800 machine.

4.2. Features of the Die Sets

The die set A and B were made to provide a comparison on which die set shows the most robust design during the working environment of the electrical-field activated sintering and forming process. Die set B was the optimised design from die set A. In the die set A, the overall dimension was 16 mm in diameter, 14 mm in die height and 6 mm in the thickness wall of the die set. The punch nose has the diameter and height of four and five millimetres respectively. Meanwhile, for die set B, the overall dimension was 16 mm in diameter, 22 mm in die height and 6 mm in the thickness wall of the die set. The punch nose still has the same diameter as die set A which is four millimetres, but the height of nine millimetres has been added to die set B due to the new large transition. The die sets A and B produced the same cylindrical sample output which has four millimetres in both of diameter and height. The shape design on large transitions at die set B was introduced to reduce the thermal stress concentration in the punch. Another positive contribution towards the punch modification on the die set B was the concentrated heating at the punch nose during the process whereas more uniform temperature distribution occurred in the die's middle section. By using this feature of design in the die set B, it could help to optimise the process of heating, especially for conductor materials.

Based on the observation of the previous research that has been done, it was shown that for temperature measurement during the process, the thermocouple was only attached to the surface body of the die [126], [128]–[133]. Due to the thermocouple only be planted on the surface body of the die during the experiment, the nominal temperature of the sample was slightly lower than the actual temperature inside the sample. Thus there are temperature gradients for the real temperature of the sample. For die set A and B, the placement of the thermocouple has been made by drilling a small hole of cylindrical cavities on the body of die. In the die set A, the size of the hole was 1.6 mm in diameter and 3 mm in depth. Meanwhile, for die set B still have the same diameter as die set A which was 1.6 mm, but the depth has been increased to 4 mm due to the optimisation made from die set A. Due to this improvement, the thermocouple besides being securely located inside the tight cavities, the position of the tip of the thermocouple could get near to the sample's wall. Die sets A and B would have three to four millimetres gap between the sample and die walls respectively.

Therefore, it could help to achieve an accurate temperature reading during the electrical-field activated sintering and forming process compared to the previous research. The shapes and comparison features between die set A and B for the cylindrical sample can be seen in **Figure 4.1-1**.

Table 4.2-1: Comparison of the features between die set A and B for cylindrical sample.

Part	Die Set A	Die Set B
Punches		
Die		

4.3. Material Selection for Die Sets

Based on the previous study by using conventional electroplasticity sintering application, the most popular selected die sets material was graphite, which shows an excellent choice concerning its capability working at high temperatures up to 1,700 °C [134]. It was used to produce the cylindrical samples with dimensions that were in the range of 20 to 42 mm in diameter and 5 to 15 mm in height [101], [105]–[108], [135], [136]. Therefore, the material selection for die sets used in the experiment has been made which consisted of two possible materials which were graphite and tungsten carbide. The selection of graphite was made due to the positive reviews on previous research as has been mentioned before. Tungsten carbide was selected due to the excellent compressive strength compared to other materials which would make the die set more robust when dealing with the high pressure and temperature environment during the electrical-field activated sintering and forming process. In addition to that, besides maximum service temperature (T_{max}) and compressive strength, the thermal

expansion coefficient (TECoE) also has to be taken into consideration. This is because the fraction of a die set material expands per degree of temperature increse during the process need to be small between the value of thermal expansion coefficient for punches, a body of die and powder that has been sintered. **Table 4.3-1** shows the mechanical and thermal properties of the graphite and tungsten carbide materials used. Further details regarding the guidelines on how to choose the suitable combination of die sets with powder being sintered by comparing the compressive strength, thermal expansion coefficient and maximum service temperature of selected materials have been shown in the section below. By using the guidelines, all the possible combinations for the die set with particularly sintered powder can be managed and known whether it is a good combination or not based on the fulfilment of requirement.

Table 4.3-1: Mechanical and thermal properties between graphite(C) and tungsten carbide (WC) materials based on compressive strength, thermal expansion coefficient and maximum service temperature [134].

Materials	Compressive Strength	Thermal Expansion Coefficient	Maximum Service Temperature
	(MPa)	(µstrain/°C)	(°C)
C	43 to 350	0.6 to 4.3	1,300 to 1,700
WC	4,250 to 6,830	4.5 to 7.1	727 to 777

4.3.1. Thermal Expansion Coefficient of the Die and Punches Materials

Based on the **Table 4.3-1**, graphite and tungsten carbide has been selected for two possible used material of the die set. Both of the materials shows a great compressive stress especially tungsten carbide. It was an excellent contribution towards the electrical-field activated sintering and forming process due to the experiment which used the applied pressure in the range of 75 to 125 MPa. After that, the comparison of selected combinations of the die set concerning of the thermal expansion coefficient between the punches and body of die needed to be made as shown in **Table 4.3-2**. It was suggested that the thermal expansion coefficient value for the die must be less than the punches (TECoE die < TECoE punches) when using different materials to prevent the punches from being stuck inside the die during the opening of the punches for the ejection process. This was because when the thermal expansion coefficient of the die is higher than the punches, the fraction of used material in the die tends to expand rapidly per degree of temperature compared to the punches. Due to this,

the nose of the punches would be trapped inside the die and push against the inside die wall. Eventually, the punches would break if excessive force was applied during the opening of the punches. The best condition was to have a similar material for the die and punches to get the same thermal expansion coefficient value for the uniform of heating and cooling during the electrical-field activated sintering and forming process.

Table 4.3-2: Selection combination of the die sets materials of graphite (C) and tungsten carbide (WC) by comparing thermal expansion coefficient among the materials for the punches and body of the die.

Die Materials	Punches Materials	C	WC
	TECoE (µstrain/°C)	0.6 to 4.3	4.5 to 7.1
C	0.6 to 4.3	Acceptable	Acceptable
WC	4.5 to 7.1	Not Acceptable	Acceptable

Based on **Table 4.3-2**, four possible combinations can be made for the material of die and punches. The first option was both of the die and the punches using graphite as its material. It was an acceptable combination due to the value of thermal expansion coefficient being the same. The second choice showed the punches would be utilising the tungsten carbide material. Meanwhile, for the die would use the graphite. The combination was also acceptable due to the range of thermal expansion coefficient of the die (graphite) was less than the punches (tungsten carbide). For the third combination which made the tungsten carbide as the die, and graphite as the punches, were not acceptable due to die (tungsten carbide) thermal expansion coefficient range value exceeding the punches (graphite). Lastly, the fourth combination was when tungsten carbide would be the material for both die and punches. Same effect as the first option would be happen, it was acceptable due to the value of thermal expansion being the same. Therefore, it can be summarised that based on the first selection combination of the die sets only three combinations are chosen as shown in next **Table 4.3-3**.

4.3.2. Thermal Expansion Coefficient of the Die Sets and Sample Materials

The selection of the combination materials for the die set from **Table 4.3-2** has been continued. It has come to the three possible materials for the die set which can be used for electrical-field activated sintering and forming process as shown in **Table 4.3-3**. The same

approach as used in **Table 4.3-2** has been made towards the three materials of the die set and the sample materials which were titanium (Ti) and titanium tin alloy (90Ti10Sn) by comparison of its thermal expansion coefficient value. Besides the criteria that need to be fulfilled in the first selection concerning the temperature related expansion behaviour of materials for the die and the punches, the ability to take out easily the sintered sample from the die during the ejection process also needs to be considered. It was a precautionary step not to use a higher knocking force during the ejection process which would break the die set and sintered samples. Therefore, it was recommended that the thermal expansion coefficient for the die and the punches must be less than the sintered sample material (TECoE punch and die < TECoE sintered sample). The purpose was to prevent the sintered sample from being trapped inside the die due to the materials used by the die and the punch expands with the increasing temperature which would push the wall of the sintered sample to the die and the punches. As a result, it would inhibit the movement of the ejection process.

Table 4.3-3: Selection combination of die sets materials of graphite (C) and tungsten carbide (WC) with powder that need to been sintered which is titanium (Ti) and titanium tin alloy (90Ti10Sn) by comparing on their thermal expansion coefficient.

Combination of Die Set	Die Set		Sample Materials	Ti	90Ti10Sn
	Section	Materials	TECoE (µstrain/°C)	8.5 to 9.3	8.7 to 9.1
First	Punches	C	0.6 to 4.3	Acceptable	Acceptable
	Die	C	0.6 to 4.3	Acceptable	Acceptable
Output Results				**Acceptable**	**Acceptable**
Second	Punches	WC	4.5 to 7.1	Not Acceptable	Not Acceptable
	Die	C	0.6 to 4.3	Acceptable	Acceptable
Output Results				**Poorly Acceptable**	**Poorly Acceptable**
Third	Punches	WC	4.5 to 7.1	Not Acceptable	Not Acceptable
	Die	WC	4.5 to 7.1	Not Acceptable	Not Acceptable
Output Results				**Not Acceptable**	**Not Acceptable**

The output results from **Table 4.3-3** shows that for the first combination of the die set which consists of graphite punches and die with powder that needs to be sintered which was Ti and 90Ti10Sn has no problem and can be accepted. This was due to the thermal expansion coefficient of the punch and die being much less than the sintered sample. For the second

combination of the die set which consists of a graphite die and tungsten carbide punch was poorly accepted when tested with Ti and 90Ti10Sn samples. This is because the comparison range of thermal expansion coefficients of the tungsten carbide was near to the tested sample materials. This would create some difficulties with the opening of the punches which might be tighter due to the sample and punches being expanded towards each other as the temperature increases. Nevertheless, after the punches have been open, the ejection process would have no problem and be easily done due to the graphite die having a lower thermal expansion coefficient compared to the tested material. Lastly for the third combination where all the die and punches were made from tungsten carbide was not accepted due to both of thermal expansion coefficients being nearly in the range of sintered samples. Therefore, only two material combinations of die sets has been forward to the next stage where it compares the maximum heating temperature of the material die sets and sintered materials as shown in **Table 4.3-4**.

4.3.3. Maximum Service Temperature of the Die Sets and Sample Materials

The consideration of maximum service temperature of the material used by die sets towards the sintering heating applied to the sample also needs to be made. It was important to know the highest temperature at which die sets material can be used for an extended period without significant problems such as oxidation, chemical change, excessive creep, loss of strength or other primary property for which the material was usually used. This was to ensure the die set must perform with excellent efficiency even if the higher sintering temperature ($T_{sintering}$) of the sample was used. Hence, it was advised that the maximum service temperature for the materials of the die and the punch must be greater than the temperature of the sintered sample (T_{max} punch and Die > $T_{sintering}$ sample).
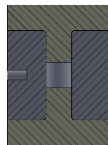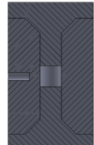
Based on **Table 4.3-4**, for the first combination of the die set by using graphite as the material for the die and the punches was acceptable for both the Ti and 90Ti10Sn samples due to the maximum service temperature for graphite being higher compared to the sintering temperature used by the samples. Meanwhile for the second combination of the die set which used graphite as a material for the die and tungsten carbide for the punch it shows different results. For Ti sample, the combination of the second die set was poorly acceptable due to the

maximum service temperature for the punches which used the tungsten carbide material being less (727 to 777 °C) than the sintering temperature of the Ti sample (700 to 1,100 °C). On the other hand, the graphite die has no problem to be used for the Ti sample. Therefore, it still can be utilised for the low-sintering temperature until to 777 °C during the electrical-field activated sintering and forming process. For the 90Ti10Sn sample, it is still using the same second combination of the die set but as an output result it was not acceptable due to the maximum service temperature of the tungsten carbide punches being much lower (727 to 777 °C) compared to the 90Ti10Sn sintering temperature range (950 to 1,150 °C).

Table 4.3-4: Selection combination of die sets materials of graphite (C) and tungsten carbide (WC) with powder that need to be sintered which is titanium (Ti) and titanium tin alloy (90Ti10Sn) by comparing their maximum service temperature of the die sets and sintering temperature of the powder during the electrical-field activated sintering and forming process.

Combination of Die Set	Die Set		Sample Materials	Ti	90Ti10Sn
	Section	Materials	Max. Service Temp. (°C)	700 to 1100	950 to 1,150
First	Punches	C	1,300 to 1,700	Acceptable	Acceptable
	Die	C	1,300 to 1,700	Acceptable	Acceptable
Output Results				**Acceptable**	**Acceptable**
Second	Punches	WC	727 to 777	Not Acceptable	Not Acceptable
	Die	C	1,300 to 1,700	Acceptable	Acceptable
Output Results				**Poorly Acceptable**	**Not Acceptable**

Table 4.3-5: Classification on the sample dimension produced, the material used, section drawing of the die sets and pictures of the die sets used for electrical-field activated sintering and forming process.

Types	Die Set A	Die Set B
Sample Dimensions	Cylindrical: Ø 4 × 4 mm	Cylindrical: Ø 4 × 4 mm
Materials of Dies	Graphite: Grade: GV	Graphite: Grade: Mersin 2333
Materials of Punches	Tungsten Carbides: Grade: VA80	Graphite: Grade: Mersin 2333
Section of Die Sets		
Picture of Die Sets		

Based on the findings in **Table 4.3-4**, for the electrical-field activated sintering and forming process using the Ti sample, the second die set combination which used tungsten carbide and graphite as a material for the punch and the die respectively has been selected for the design of the die set A. Meanwhile, for the 90Ti10Sn sample used the first combination of die set which used graphite as a material for both die and punches was appointed to optimise the design of the die set B. The selection has been made as the comparison study for the material combination of the die set usage during the experiment. The details regarding classification of the used die sets have been described in **Table 4.3-5**.

4.4. Summary of the Chapter

There were two designs of die sets used for the electrical-field activated sintering and forming process which was named as the die set A and B. Die set B was the optimisation design made from the die set A. Large transitions were introduced for the modification of the die set A to the die set B to reduce the thermal stress concentration in the punches. Another positive contribution towards the punch modification was the concentrated heating at the punch's nose, as more uniform temperature distributions in the middle section of the die occurred which could help to optimise the process of sintering. The final output sample was in the cylindrical shape of four millimetres in diameter and height respectively. The material selection for the die set needs to follow the guidelines on how to choose the suitable combination of die sets with powder being sintered by comparing the compressive strength, thermal expansion coefficient and maximum service temperature of the selected materials. By using the guidelines, all the possible combinations for the die set with sintered powder can be managed and known whether it was a good combination or not based on the fulfilment of the process requirement. The purpose of this guideline was to prevent the punches and the sample becoming trapped inside the die during the ejection process. Besides that, the die set also needs to be robust due to the impact from a higher forming pressure. For die set A, the material of the punch was tungsten carbide (grade: VA 80) meanwhile for the die was used graphite (grade: GV). It was employed in the experiment for the Ti sample. Meanwhile, as for the die set B, all the punches and die were made from graphite (grade: Mersin 2333) and used in the experiment for the 90Ti10Sn sample. The selection has been achieved as the comparison study for the material combination of the die set usage during the experiment.

Chapter 5: Coupled FE Thermal-Electrical Analysis

5.1. Introduction

By using ABAQUS/CAE software (Abaqus version 6.13, Simulia Dassault System) as a tool for FE simulation, the effect of coupled thermal-electrical characteristics of the die sets during the heating and cooling process was examined. The information collected from the FE simulation is useful for the experimental process in order to gain information on how the heating distribution happened to the die sets used in the electrical-field activated sintering and forming process. The initial step of the analysis involved the electrical potential being exposed to the die sets A and B where it was calculated by using electrical boundary conditions. Meanwhile, for step two, transient heat transfer analysis was conducted by the application of Joule heat generation to each finite element under a given thermal boundary condition. The temperature dependency of the electrical conductivity was used for the analysis where the electrical and thermal analyses are fully coupled. Below shows a brief summary of the theoretical background of coupled thermal-electrical analysis [137], [138].

5.2. Theory of Coupled Thermal-Electrical Analysis

The equation of conservation of charge was shown as in the equation **(5.2-1)**.

$$\int_{S} J.n \, dS = \int_{v} r_c \, dV \qquad (5.2\text{-}1)$$

Symbols in equation (5.2-1):

V - Any control volume whose surface was S.

n - Outward normal to S.

J - Electrical current density (current per unit area).

r_c - Internal volumetric current source per unit volume.

By using the definition of an electrical field, Ohm's law can be written as shown in the equation **(5.2-2)**. The constitutive relation was linear where it was assumed that the electrical conductivity was independent of the electrical field.

$$J = \sigma.E = -\sigma.\nabla\phi \qquad (5.2\text{-}2)$$

Symbols in equation (5.2-2):

ϕ - Electrical potential field.

E - Electrical potential.

σ - Electrical conductivity.

Using Ohm's law in the equation **(5.2-2)** in a conservation equation, an electrical equation analysis was obtained in the equation **(5.2-3)**. Joule's law describes the rate of electrical energy, P_{ec}, dissipated by current flowing through a conductor as in the equation **(5.2-4)**.

$$\int \nabla \delta \phi . (\sigma . \nabla \phi) \, dV = \int_v \delta \phi r_c \, dV + \int_s \delta \phi \bar{J} \, ds \qquad \textbf{(5.2-3)}$$

Symbols in equation (5.2-3):

$\bar{J}$ - Electrical current density towards a control volume V $\left(\bar{J} = J.n\right)$.

$$P_{ec} = J.E = (E.\sigma).E \qquad \textbf{(5.2-4)}$$

Symbols in equation (5.2-4):

P_{ec} - The rate of electrical energy.

On the other hand, an equation for conductive thermal analysis was as shown in the equation **(5.2-5)**.

$$\int_v \rho C_v \frac{\partial \theta}{\partial t} \delta \theta \, dV + \int_v \nabla \delta \theta . (k.\nabla \theta) \, dV = \int_v \delta \theta r \, dV + \int_s \delta \theta q \, dS \quad \textbf{(5.2-5)}$$

Symbols in (5.2-5):

θ	-	Temperature.	C_v - Specific heat.
k	-	Thermal conductivity.	q - Heat flux towards a control volume V.
ρ	-	Density.	r - Heat generation density.

5.3. Procedure

In the coupled thermal-electrical analysis, both transient responses have been applied for electrical analysis in step one and thermal analysis in step two where they are sequentially conducted in each time increment. As a result, the temperature at integration points of each of the die sets A and B can be obtained dependent on the step time to complete the process. Concerning sample material used in the simulation, all the die sets A and B used solid titanium material. The simulation analysis was only concentrated on the heating distribution process on the design of die sets A and B. In **Figure 5.3-1** shows the simplified parts used in the Gleeble® 3800 machine for thermal-electrical analysis.
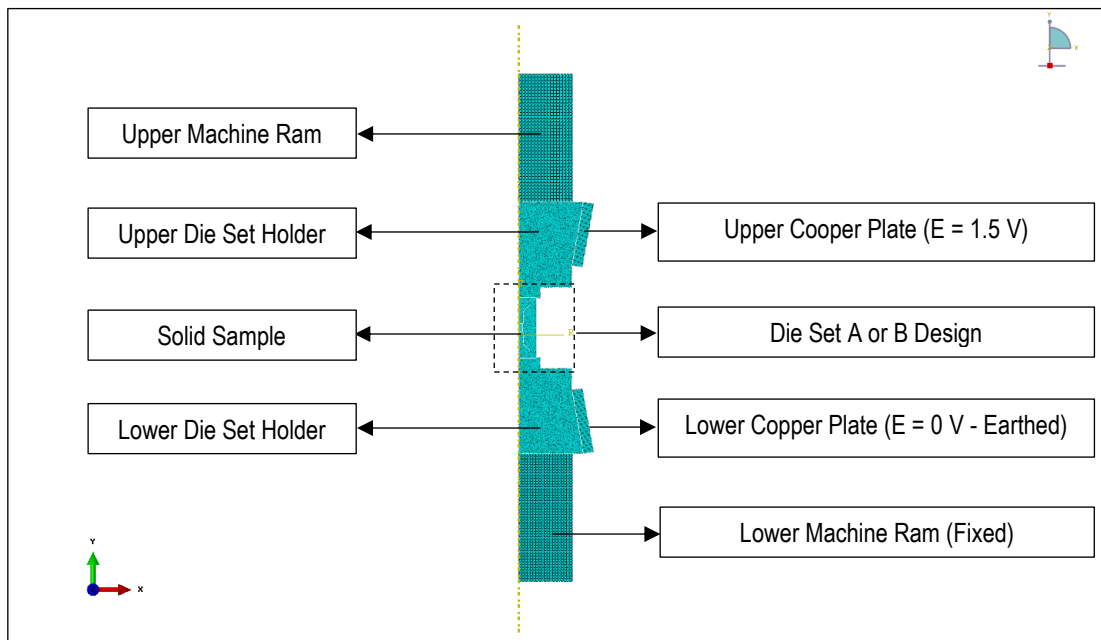
Figure 5.3-1: Simplified parts used in the simulation of coupled thermal-electrical analysis.

In **Table 5.3-1**, shows the physical, thermal and electrical properties of tungsten carbide, graphite, titanium and copper-nickel-silver alloy material used to evaluate the coupled thermal-electrical analysis. Meanwhile, regarding boundary conditions, the electrical potential at the first plate was set to 1.5 V and at the second plate was assumed to be zero because it was electrically grounded as shown in **Figure 5.3-1**. For the first and second machine ram, the displacement for both are assumed to be zero due to the sample titanium being already in the solid condition and the temperature for the cooling condition after the end of step one was set

to 30 °C for both of the machine rams. The emissivity and the film coefficient used were 0.8 and 10 respectively, while the ambient temperature was set to 20 °C. The initial time increment was 1×10^{-5} s and the automatic time increment function provided from Abaqus was used. After the first step of the electrical and thermal analysis, no electrical load exists. Therefore, general transient heat transfer analysis was conducted to save calculation time in step two. As presented in **Table 5.3-2**, the global seed of the part that has been used in the simulation of electrical-heat analysis for meshing is shown. Meanwhile, the thermal electric element type has been assigned for all the parts.

Table 5.3-1: Physical properties of part materials used in the thermal-electrical analysis [123], [134].

Part Name	Materials	Density	Specific Heat	Thermal Conductivity	Electric Conductivity
		(kg/m^3)	(J/kg)	(W/m.K)	(S/m)
Upper and Lower Machine Ram	Tungsten Carbide	15,580	292	88	1×10^6
Upper and Lower Die Set Holder					
Punches of Die Set A					
Die of Die Set A	Graphite	1,860	771	81	9.1×10^6
Die and Punches of Die Set B					
Sample	Titanium	4,530	550	17.15	2.5×10^6
Upper and Lower Copper Plate	Copper-Nickel-Silver Alloy	8,720	383	30	2.63×10^6

Table 5.3-2: Global seeds used for meshing the simulation of thermal-electrical analysis.

Part Name	Global Seed
Upper and Lower Machine Ram	15×10^{-4}
Upper and Lower Die Sets Holder	3×10^{-4}
Upper and Lower Copper Plate	4×10^{-4}
Die and Punches of Die Sets A and B	2.5×10^{-4}
Sample	1×10^{-4}

5.4. Results and Discussion

In the section below shows the results and discussions of coupled thermal-electrical analysis for the design of die set A and B using a solid titanium sample. It consists of two steps which was the electrical and thermal analysis for step one. Meanwhile, in the step two, the heat transfer analysis was conducted.

5.4.1. Die Set A

In **Figure 5.4-1** shows the heating temperature distribution of die set A for step one electrical and thermal analysis and step two for heat transfer analysis after the current switch off. Based on the observation, the tungsten carbide punches of the die set A indicate the highest temperature recorded throughout the entire process with rapid heating at the beginning of the process. It can be supported with the **Figure 5.4-2 (No. 1)** where it shows the contours of the heating temperature starting at the nose of the tungsten carbide punches of the die set A which have the temperature of 93.169 °C at the time of 0.039 s. After that, the temperature continued to rise to given the heat at the core of the titanium samples as presented in the **Figure 5.4-2 (No. 2)** and **(No. 3)** which indicated the temperature had achieved 380.054 °C at the time of 1.403 s and 602.928 °C at the time of 4.415 s respectively. Then, the heating temperature continued to increase steadily until at the end of the proses of step one which indicated the time of 150 s. The heating also fully covered the titanium samples at the temperature of 999.279 °C at the core and 912.903 °C at the surface of the sample. On the other hand, the heating temperature recorded for tungsten carbide punches of the die set A are already achieving the value of 1,096.900 °C at the time of 150 s. For this situation, precautionary steps need to be made due to the maximum service temperature of the tungsten carbide being around 727 °C to 777 °C [134]. Therefore, according to **Table 5.4-1**, by only limiting the working temperature of tungsten carbide punches to 706.954 °C, the heating generated for sintering the titanium samples was 602.928 °C for the core and 521.263 °C for the surface with the time of the process being 4.415 s.
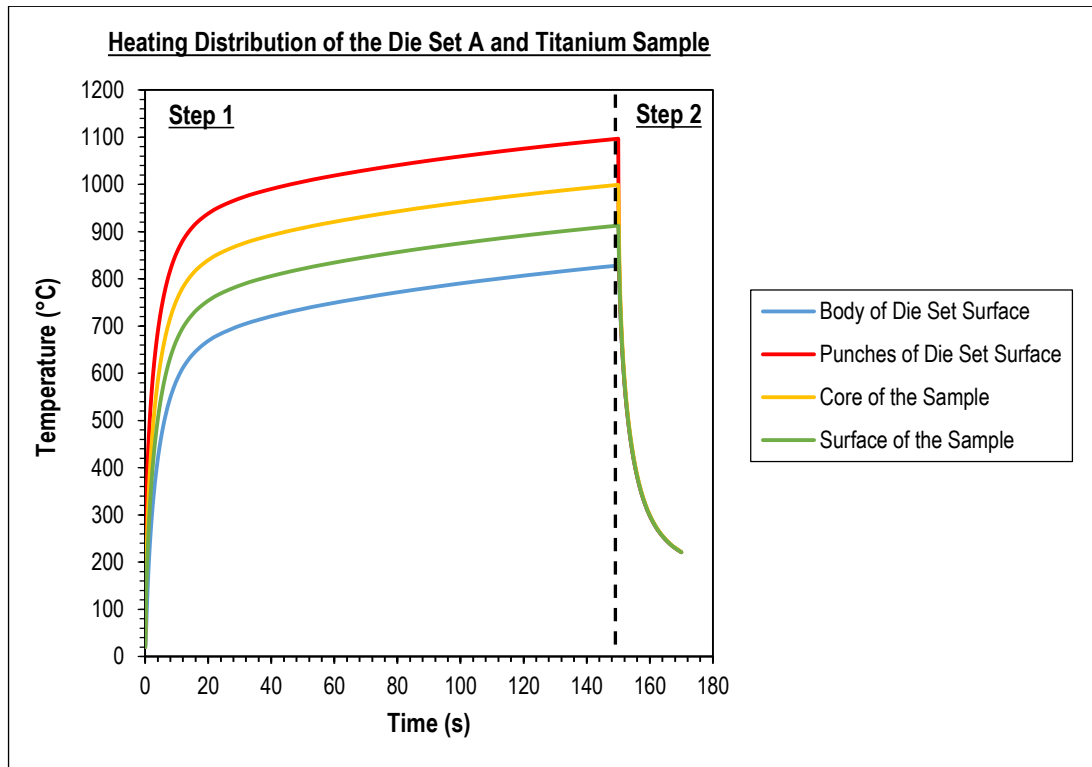
Figure 5.4-1: Heating temperature distribution of the die set A and the titanium sample for step one: electrical and thermal analysis and step two: heat transfer analysis after the current switch off.

Table 5.4-1: Temperature data for contour of the die set A and the titanium sample as presented in **Figure 5.4-2**.

Contour No.	Step Time (s)	Body of Die Set Surface (°C)	Punches of Die Set Surface (°C)	Core of the Samples (°C)	Surface of the Sample (°C)
1	0.039	20.105	93.169	31.033	27.187
2	1.403	225.569	493.545	380.054	306.627
3	4.415	437.006	706.954	602.928	521.263
4	150.000	828.208	1,096.900	999.279	912.903
5	150.085	826.803	963.440	969.541	891.025
6	150.428	771.942	790.411	821.079	787.718
7	152.531	534.920	537.514	546.136	538.243
8	170.010	220.698	220.869	221.399	220.899

During step two of the heat transfer analysis, the rapid cooling of the die set A and titanium samples have occurred. By only consuming 2.531 s, the heating temperature can be dropped on average to 539.203 °C for all the parts of the die set A and the titanium sample. Meanwhile, the heat transfer analysis was stopped at 170.010 s which indicates the

temperature of the die set and the sample recorded averagely 220.966 °C. The temperature data for the contour of the die set A and the titanium sample as presented in **Figure 5.4-2 (No. 1)** to **(No. 8)** can be referred to **Table 5.4-1**.
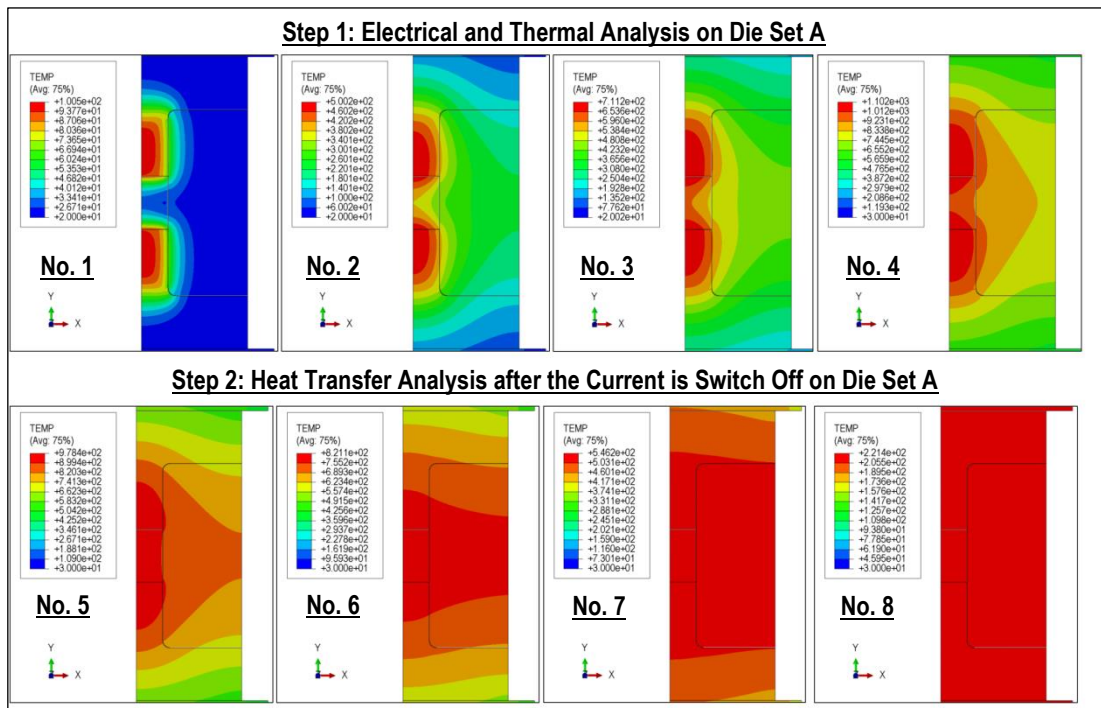
Figure 5.4-2: Contour of the die set A and the titanium sample for heating temperature distribution at integration points of step one and two.

5.4.2. Die Set B

In **Figure 5.4-3**, shows the heating temperature distribution of the die set B with the titanium sample for electrical and thermal analysis in step one and heat transfer analysis on step two. The material used for punches and body of die set B was graphite due to its high efficiency transmitting heating to the samples. Moreover, different from die set A, by using the die set B the heating temperature of the titanium sample at the core and surface graphite punches increases rapidly with the temperature value as presented in **Table 5.4-2**. Therefore, the design of a large transition at the punches of die set B plays a significant role to ensure the high efficiency of the heating during the electrical-field activated sintering and forming process for powder material. It can be seen in **Figure 5.4-4 (No. 1)** to **(No. 4),** the heating started at the tip of the die set B nose and continued to the core of the sample. By increasing the step time to 1.5 s, the heating temperature of the punches of die set B could reach 1,781.43 °C

which was in the range of maximum working temperature for graphite and have recorded the heating temperature at core and surface titanium sample of 1,814.18 °C and 1,249.96 °C respectively. The illustration of its contour can be seen in **Figure 5.4-4 (No. 4)**.
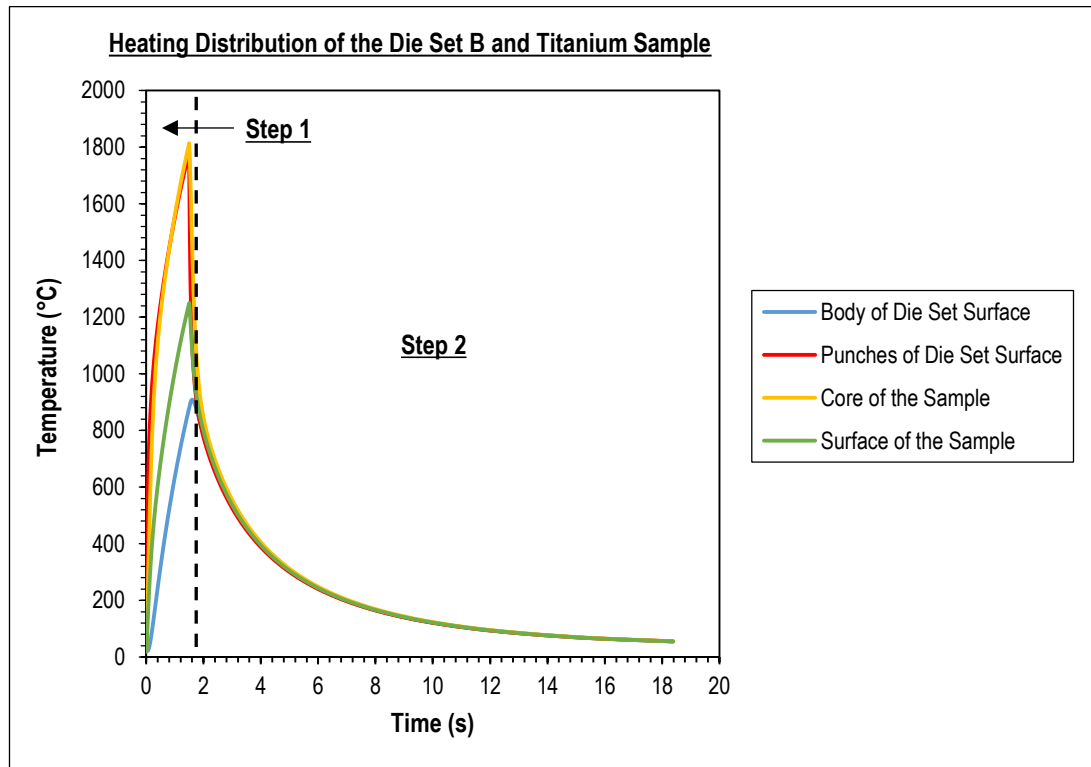
Figure 5.4-3: Heating temperature distribution of die set B and titanium sample for step one: electrical and thermal analysis and step two: heat transfer analysis after the current switch off.

Table 5.4-2: Temperature data for contour of die set B and titanium sample as presented in **Figure 5.4-4**.

Contour No.	Step Time (s)	Body of Die Set Surface (°C)	Punches of Die Set Surface (°C)	Core of the Samples (°C)	Surface of the Sample (°C)
1	0.0016	20.0077	252.2520	72.4356	42.3028
2	0.0654	23.4331	616.5490	264.9520	155.9590
3	0.1543	60.8733	874.5500	623.9510	327.5860
4	1.5000	879.7710	1,781.4300	1,814.1800	1,249.9600
5	1.5962	908.4660	1,124.6200	1,477.8700	1,092.2000
6	1.7674	869.4480	893.537	1,043.9200	914.4260
7	8.5843	150.2230	149.3760	153.3770	150.9260
8	18.3864	55.2520	55.1351	55.7322	55.3644

Meanwhile, after the end of step one, the rapid cooling due to the heat transfer to the die set B and the titanium sample which indicated the total time of 18.3864 s to achieve the average temperature of 55.3709 °C. The illustration of the die set B contour during the start until the end of the process step two can be referred to **Figure 5.4-4 (No. 5)** to **(No.8)**. Temporarily, the temperature data for the contour of die set D and titanium sample as presented in **Figure 5.4-4 (No.1)** to **(No. 8)** can be referred to **Table 5.4-2**.
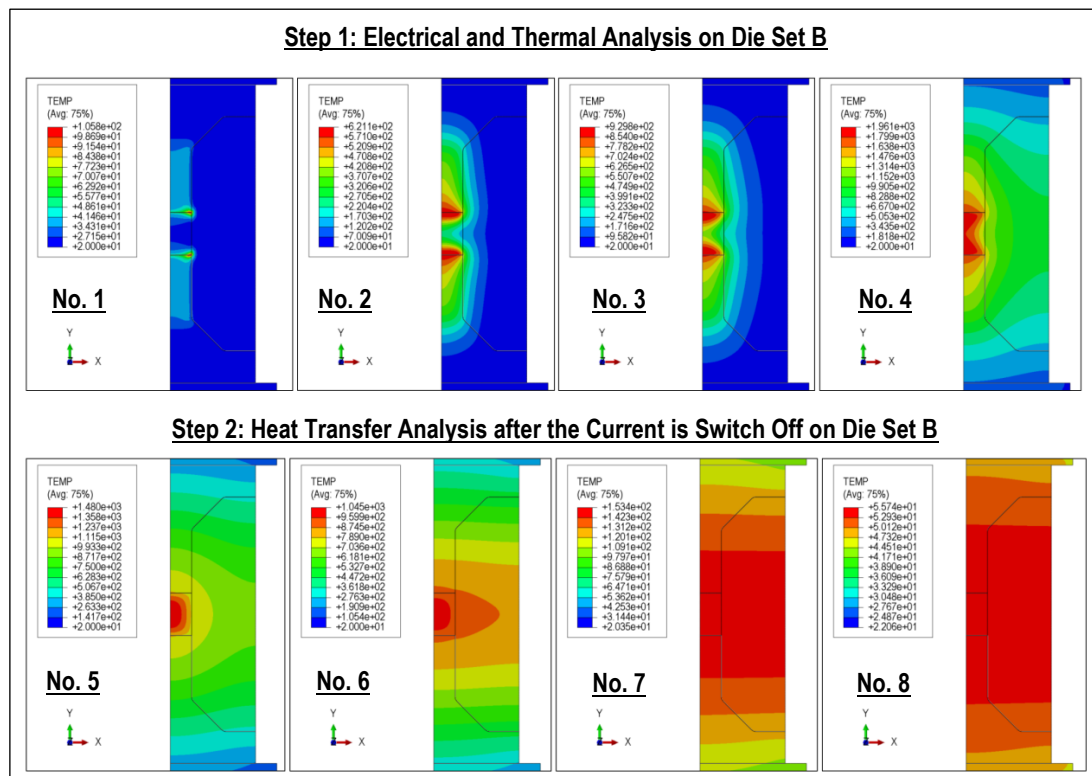
Figure 5.4-4: Contour of die set B and titanium sample for heating temperature distribution at integration points of step one and two.

5.5. Summary of the Chapter

Based on the simulation of the electrical-heat analysis, the observation has been made as presented in **Table 5.5-1**. It can be summarised that the die set B has shown the best result concerning the heating distribution towards its parts compared to the die set A. In step one which was electrical analysis involving the electrical potential, the die set B has shown the most rapid heating temperature distribution compared to the die set A. As presented in **Figure 5.5-1**, punches of the die set B surface and the core of the titanium sample have recorded the

highest temperature reading of 1,781.43 °C and 1,814.18 °C respectively in the step time of 1.5 s.

Table 5.5-1: Comparison of highest temperature data for die sets A and B during step one: electrical and thermal analysis and step two: heat transfer analysis.

Analysis	Die Set	Step Time (s)	Body of Die Set Surface (°C)	Punches of Die Set Surface (°C)	Core of the Samples (°C)	Surface of the Sample (°C)
Step 1	A	150.000	828.208	1,096.900	999.279	912.903
	B	1.5000	879.7710	1,781.4300	1,814.1800	1,249.9600
Step 2	A	170.010	220.698	220.869	221.399	220.899
	B	18.3864	55.2520	55.1351	55.7322	55.3644

Meanwhile, in the step two of the thermal analysis which involved of the transient heat transfers shows that the die set A has the slowest cooling compared to the die set B as presented in **Figure 5.5-2**. Rapid cooling of the die set was needed to shorten the process time which the die set B fulfilled the requirement by achieving the average of 55.370925 °C in just 18.3864 s.
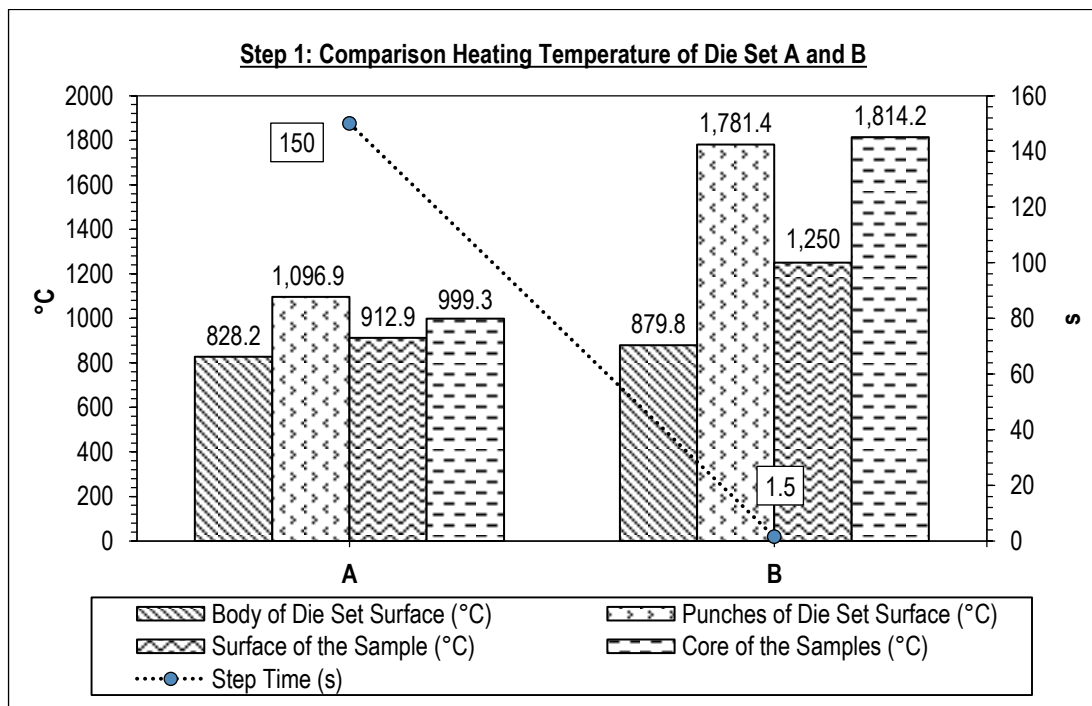
Figure 5.5-1: Comparison heating temperature of die sets A and B for electrical analysis in step one.
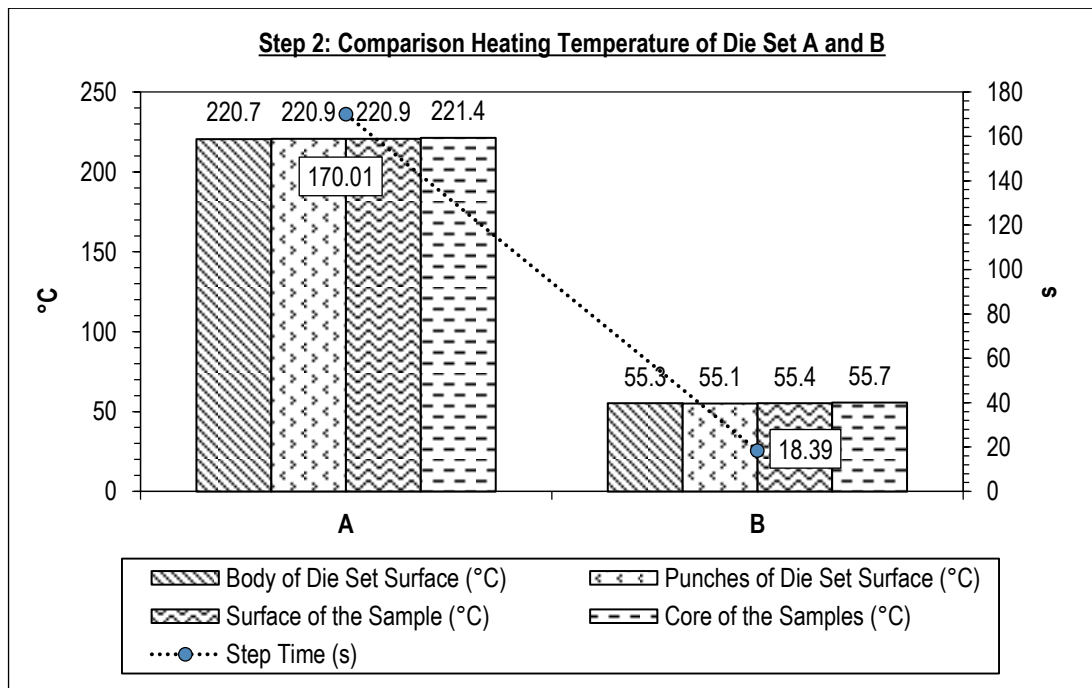
Figure 5.5-2: Comparison heating temperature of die sets A and B for thermal analysis in step two.

Chapter 6: Process Investigation with a Gleeble® 3800 Machine

6.1. Introduction

In the experiment of the electrical-field activated sintering and forming process, two kinds of powders were used as a raw material which were Ti and 90Ti10Sn. The experiment was conducted using a Gleeble® 3800 thermal mechanical machine from Dynamic System Inc. USA. Each of the parameters employed in the experiments, such as pressure, heating temperature, heating rate and holding time was controlled automatically using a computer-controlled system called QuickSim™ software. Regarding electrical-field produced by Gleeble® 3800 machine, it has a high current which was 3,000 to 30,000 A and low voltage which was three to ten voltages. It was also capable of controlling the accuracy of the temperature up to ±3 °C. There were two configurations of die sets used in the experiment which was the previous design of die set A and the new model of die set B. Die set B was the optimised design from die set A. For die set A, the material of the punch was made from tungsten carbide (grade: VA80) and for its die used graphite (grade: GV). Meanwhile, for die set B, both the punches and dies were made from graphite (grade: Mersin 2333). The selection of the graphite material was prepared for the optimisation of die set B by considering that the value of the thermal expansion coefficient of punches and die must be less than the powder material being tested. This was to prevent the punches, die and samples becoming trapped and stuck during the ejection process. In addition to that, by using graphite for the die set material, a higher sintering temperature can be utilised which up to its maximum service temperature around 1,300 to 1,700 °C. Large transitions were introduced for the modification of die set A to die set B in order to reduce the thermal stress concentration in the punches. Another positive contribution towards the punches modification was the concentrated heating at the punch nose of die set B, where more uniform temperature distribution in the middle of the die section occurred which helped to optimise the process of heating. The final output for both of the die set A and B was a cylindrical shape of four millimetres in diameter and height respectively.

After the powder material had been weighed, it was carefully poured into assigned die sets. Then, the die set with the powder material was placed into the chamber of Gleeble® 3800 machine with the thermocouple as in **Figure 3.1-1**. Following this, the die set with the powder material was heated promptly to a certain sintering temperature in the vacuum

atmosphere. The high electrical current was passed through the die set and powder material with simultaneously a certain pressure was applied to the upper and lower of punches. After that, the ejection process has been made to take out the sample from the die set. Then, the samples obtained from the experiments were analysed for their relative density using Sartorius YDK03 apparatus set and the sample's surface microstructure using a scanning electron microscope machine (SEM/EDS – HITACHI SU-6600). In addition to that, a chemical element weight percentage test has been performed at the centre and edge of the sample parts using energy dispersive spectroscopy (EDS) facility. A micro- (ZHVµ Micro Vickers) and nano-hardness (NanoTest Vantage) test were also done at the sintered neck of the sample produced. All the results and discussions regarding the experiment study have been described in detail to obtain conclusive findings of reliability for the overall processes and used die sets for producing an excellent quality of micro-components.

6.2. Equipment and Powder Materials

In this section, the detailed description of used equipment and powder materials in the electrical-field activated sintering and forming process has been made. It consists of the used equipment of Gleeble® 3800 machine, die set A and B, density determination kit from Sartorius YDK03, Tungsten Filament Scanning Electron Microscope (W-SEM) from HITACHI S-3700 (2010), ZHVµ Vickers and NanoTest Vantage System hardness tester. Meanwhile, powder materials used in the experiment consisted of Ti and 90Ti10Sn.

6.2.1. Gleeble® 3800 Machine

Gleeble® 3800 from Dynamic System Inc. USA as shown in **Figure 6.2-1** was designed specially to offer increased capabilities for thermal deformation and was equipped with a heavy-duty mechanical system and high-speed servo valves for the quick response. Gleeble® 3800 was capable of exerting as much as 20 tonnes of static force in compression and up to 10 tonnes of force in tension. Besides that, the stroke displacement rates also can be programmed to be as fast as 2,000 mm/s as mention in **Table 6.2-2**. In addition to that, Gleeble® 3800 systems offer a high-speed thermal system for heating specimens. It has an ability to reproduce the broad range of thermal profiles that materials undergo in actual

processes which were critical to the success of thermal-mechanical testing and physical simulation. Gleeble® 3800 systems have both high heating and cooling rates to accomplish the assigned task. The heating and quenching rate could operate up to 10,000 °C/s respectively as shown in **Table 6.2-1**.

Gleeble® 3800 also has an ability to control the temperature uniformity with the thermal gradients within the test specimen. In this condition, thermal gradients are dependent upon the material, thermal and electrical resistivity, surface-to-volume ratio, specimen length, total cross section, free span and grips. In the experiment of electrical-field activated sintering and forming process, each of the parameters used such as pressure, heating temperature, heating rate and holding time, was controlled automatically using a computer-controlled system called QuickSim™ software. In terms of electrical-field produced by the Gleeble® 3800 machine, it has high current in the range of 3,000~30,000 A with a low voltage which was three and ten voltage. Below in **Table 6.2-1** and **Table 6.2-2** shows the general specification of the thermal and mechanical system for Gleeble® 3800 machine.
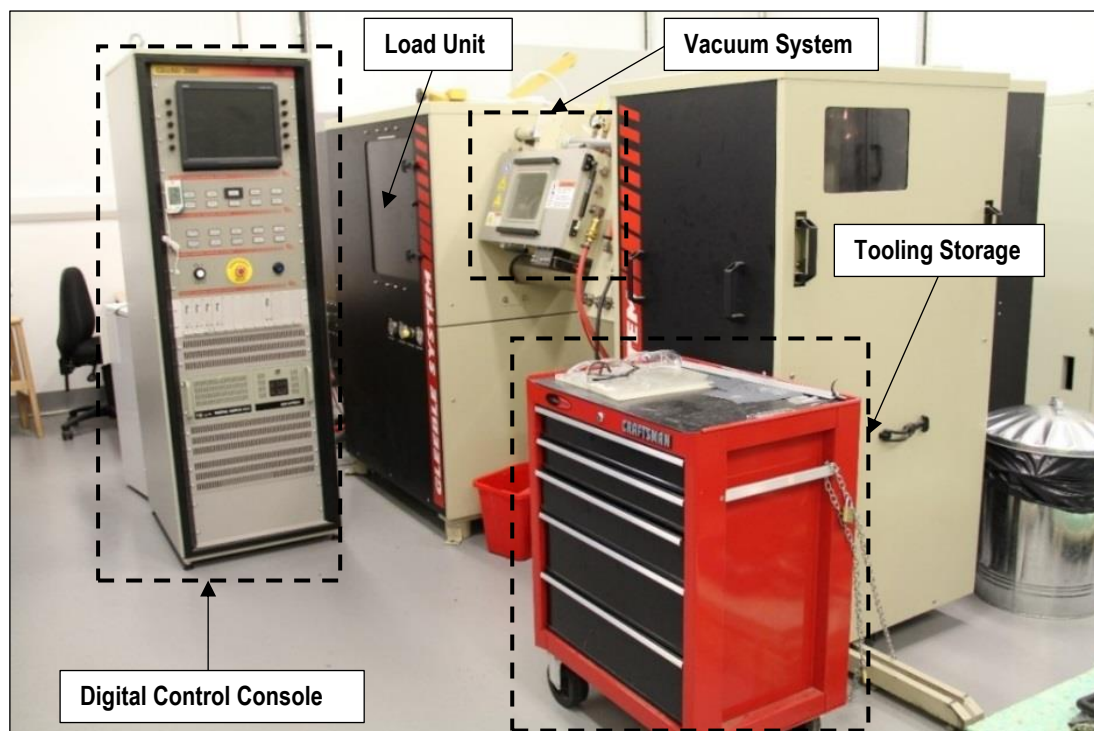
Figure 6.2-1: Gleeble® 3800 machine.

Table 6.2-1: General specification of the thermal system for Gleeble® 3800 machine [123].

Type of Heating System	Direct resistance with closed-loop control.
Temperature Controller	Digital closed-loop control using 16-bit analog-to-digital converter and 16/32-bit digital signal processor.
Temperature Range	Room temperature up to 1700°C based on choice of thermocouples.
Response Rate	10,000°C/s.
Thermocouple Sampling Rate	120 times per second at 60 Hz (100 times per second at 50 Hz).
Resolution	One degree (°C or F).
Maximum Number of Simultaneous Thermal Channels	Four thermocouple channels or three thermocouple channels and one pyrometer channel. (Pyrometer system is optional).
Accuracy of Control	± One degree Celsius (in steady state).
Accuracy of Measurement	± One percent of temperature plus the accuracy of the thermocouple wire (steady state).

Table 6.2-2: General specification of the mechanical systems for Gleeble® 3800 machine [123].

Test Frame	Horizontal type with dual 99 mm diameter columns.
Mechanical System	Closed-loop hydraulic servo control.
Maximum Static Force/Load in Compression	20,000 kg (~ 44,000 lbs.) (196 kN).
Maximum Static Force/Load in Tension	10,000 kg (~ 22,000 lbs.) (98 kN).
Maximum Stroke Rate (No Load)	2,000 mm/s in tension or compression.
Minimum Stroke Rate (Varies with Configuration)	0.001 mm/s in tension or compression.
Maximum Stroke Distance	125 mm.
Maximum Number of Compression Stroke	10 strokes (hits) over 20 mm distance.
Force Measurement Accuracy	± 1.0% of full scale.
Stroke Measurement Accuracy	± 0.5% of full scale.
Force Measurement Resolution	± 1 kg.
Stroke Measurement Resolution	0.002 mm.
C-Strain Measurement Resolution	0.002 mm (Standard).

6.2.2. Relative Density Test

The results obtained from the experiment were analysed for their relative density using density determination kit (Sartorious YDK03). During the testing, the Archimedean principle was applied for determining the density of a sample with Sartorious YDK03 measuring device.

A sample immersed in a liquid was subjected to the force of buoyancy. The value of this force was the same as the weight of the liquid displaced by the volume of the sample. By using hydrostatic balance from a density determination kit (Sartorious YDK03) enables to weight a sample in air as well as in water in order to:

a) Determine the density of a sample if the density of the liquid causing buoyancy was known as presented in equation **(6.2-1)**.

$$\rho = \frac{W(a).\rho(fl)}{W(a) - W(fl)} \tag{6.2-1}$$

Symbols in equation (6.2-1):

ρ	-	Specific gravity of the sample.	$W(a)$	-	Weight of the solid in air.
$\rho(fl)$	-	Density of the liquid.	$W(fl)$	-	Weight of the solid in liquid.

Or

b) Determine the density of liquid if the volume of the immersed sample was known as presented in equation **(6.2-2)**.

$$\rho(fl) = \frac{G}{V} \tag{6.2-2}$$

Symbols in equation (6.2-2):

G - Buoyancy of the immersed sample.

V - Volume of the solid.

The relative density of the sample from experimental electrical-field activated sintering and forming process was collected by making a ratio percentage of the calculated value density of the sample from equation **(6.2-1)** to the reference theoretical density of sample that been tested. In **Figure 6.2-2** shows density determination kit (Sartorious YDK03).

Figure 6.2-2: Density determination kit (Sartorius YDK03) and powder measuring scale (Sartorious Practum).

6.2.3. Scanning Electron Microscope (SEM)

The Tungsten Filament Scanning Electron Microscope (W-SEM) from HITACHI S-3700 (2010) as shown in **Figure 6.2-3** was used to observed imaging microstructures of sample's surface fracture. Using this imaging microstructure, it help to show the deformation and breakage of the powder material particle after the densification mechanism process end during the electrical-field activated sintering and forming process. Other than powder materials form, Tungsten Filament Scanning Electron Microscope (W-SEM) from HITACHI S-3700 (2010) is also suitable for imaging metallic, ceramics, polymers, ceramic matrix composites (CMC), metal matrix composites (MMC), carbon fibre composite (CFC) and fibrous materials.

A chemical element weight percentage test was also performed at the centre and the edge of the sample by using Energy Dispersive Spectroscopy (EDS) facility (Oxford Inca 350 with 80 mm X-Max detector) which was built in W-SEM machine to allowed elemental analyses of materials. This process has been done to monitor the percentage of carbon element that was absent on the inside and the edge of the sample after a cleaning process due to the usage of the graphite die set.
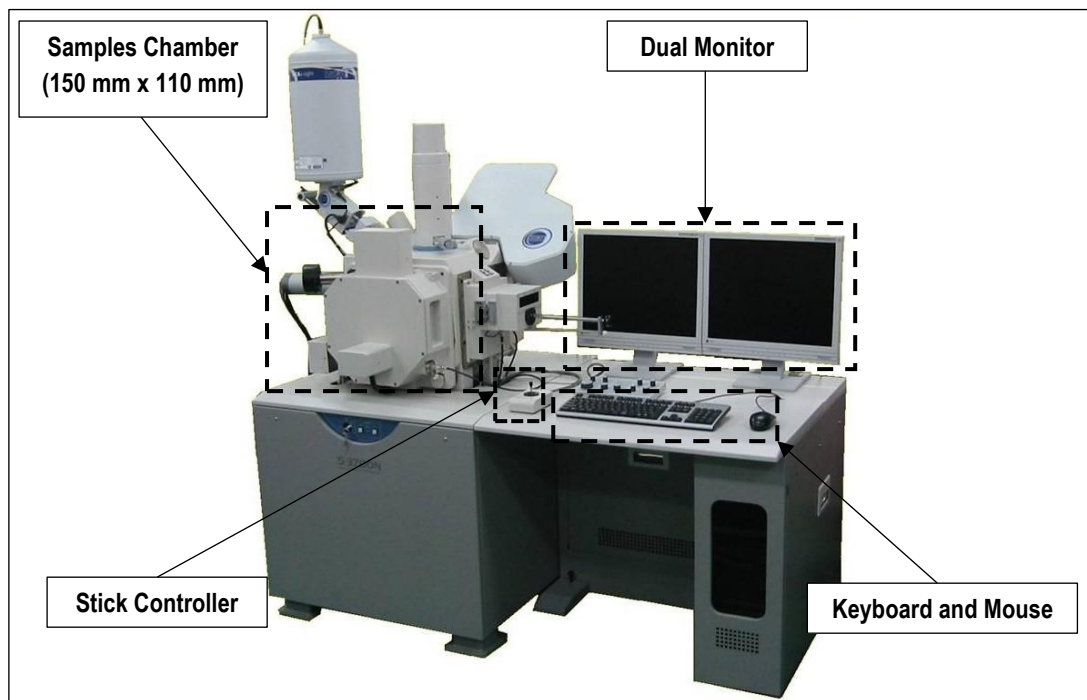
Figure 6.2-3: Tungsten Filament Scanning Electron Microscope (W-SEM) from HITACHI S-3700 (2010).

6.2.4. Surface Hardness Test

There were two surface hardness testing facilities used for analysis of the sample produced by electrical-field activated sintering and forming process which was ZHVμ Micro Vickers and NanoTest Vantage System. The ZHVμ Micro Vickers hardness tester as shown in **Figure 6.2-4** covers Vickers and Knoop hardness test using ISO6507, ISO4545 and ASTM E 384 standard procedure for the load range from HV0.01 to HV2. The hardness tester was provided with an automatic six-position turret for up to two indenters and up to four microscope lenses. A broad practical application range was ensured with the lenses covering the total magnification from 25 × to 1,000 ×. The test cycle was fully automatic and dwell times can be set in the hardness tester device. Load change was also automatic and can be set in the menu software of the tester apparatus. For more sophisticated or automated applications, computer controlled versions are used for semi or fully automatic systems based on the High Definition Software (ZHμ.HD). The advantage of this software was it could create and overview image of the specimen in high resolution to define indentation positions which allow for single or multiple traverses to be configured and carried out accurately on the specimen surface. This method has been applied to determine of micro-hardness value where multiple

indentations have been placed in the vertical and the horizontal line positions from the centre to the edge of the samples.
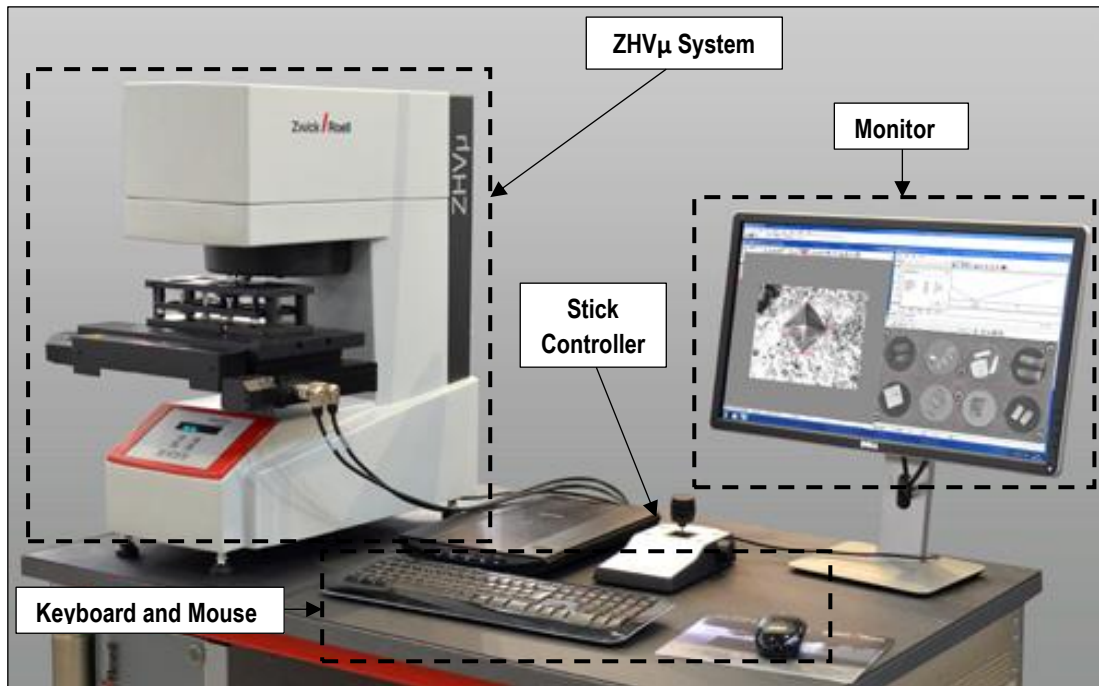
Figure 6.2-4: ZHVµ Vickers hardness tester.
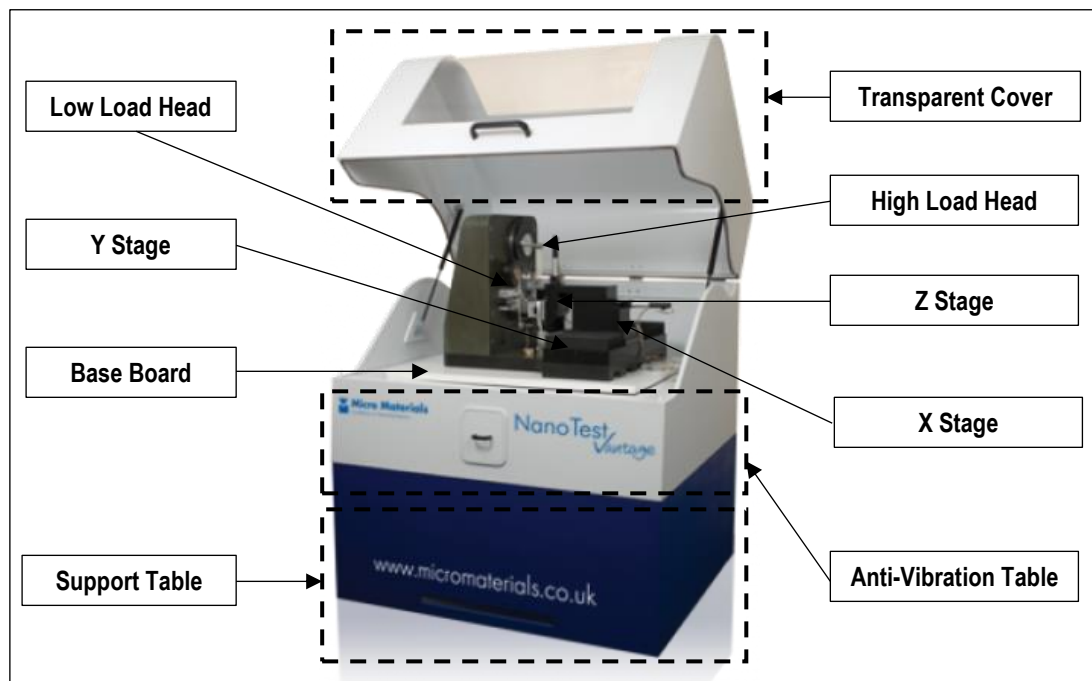
Figure 6.2-5: NanoTest Vantage System.

The nano-hardness test for the electrical-field activated sintering and forming process was also being done by using the NanoTest Vantage system as shown in **Figure 6.2-5** which consists of a variety of nano-mechanical testing methods in one instrument. All relevant requirements for the nano-indentation standard including ISO14577 and ASTM E2546-07 have been fulfilled by NanoTest Vantage. Regarding the operating principle of NanoTest Vantage system for micro-sample, it uses the application of electromagnetic force and capacitive depth measurement to measure the elastic and plastic characteristics of materials at nano-scale. Based on this capability its fits with the micro-sample that has been produced in electrical-field activated sintering and forming process where the interest area that needs to be indented can be targeted.
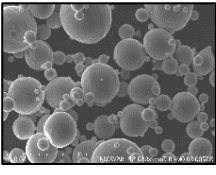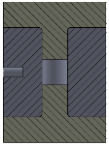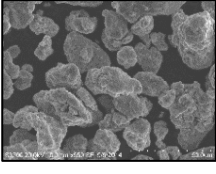
6.2.5. Powder Materials

Table 6.2-3 shows that two kinds of powder were used as raw materials which were Ti and 90Ti10Sn for electrical-field activated sintering and forming process using Gleeble® 3800 machine. For Ti, the average spherical particle size of powder materials was 45 μm. It has a purity of 99.5% Ti and has 4.51 g/cm^3 for theoretical density. Die set A was assign to Ti powder due to the temperature of the sintering process during the experiment was in the range of 700 to 1,100 °C. The die set A still can be utilised in the low-temperature sintering due to the maximum service temperatures of the tungsten carbide punches was in the range of 727 to 777 °C. In addition to that, the selection of the die set A has been made as a comparison study concerning the material combination of the die set usage during the experiment such as the robustness due to applied compressive strength and effect towards the efficiency of the process. The Ti powder material has been developed by Goodfellow Cambridge Ltd. which popular as a provider for the commercial materials.

Meanwhile, for 90Ti10Sn powder material was developed by MBN Nanomateralia. The development of Ti-alpha Sn-stabilized alloys (90Ti10Sn) by High Energy Ball Milling (HEBM) presenting suitable mechanical and physical properties where Tin (Sn) introduction within the hexagonal structure of α-Ti involved a lattice distortion. It was resulting in an increased hardness, achieving a higher stability to oxidation at high temperatures and an expected improved formability. Due to these, it presents an excellent combination of properties like

strength, corrosion resistance, weldability and fabricability, with the additional advantage of being fully heat treatable. Therefore, this material was suitable to be used for in the high-performance mechanical applications. The average particle size of 90Ti10Sn powder materials was 27 µm with the theoretical density of 4.77 g/cm^3. For the experiment of electrical-field activated sintering and forming process, it used die set B due to the sintering temperature of the 90Ti10Sn powder was in the range of 950 to 1,150 °C. The maximum service temperature of graphite was in the range of 1,300 to 1,700 °C which used for die and punches of the die set B. Therefore, it was capable of being used with the assigned sintering temperature.

Table 6.2-3: The classification of the nominal chemistry and physical properties for Ti and 90Ti10Sn powder used in the electrical-field activated sintering and forming process which performed by Gleeble® 3800 machine.

Powder Materials	Nominal Chemistry (wt%)	Average Particles Size (µm)	Theory Density (g/cm^3)	Image of Particles Agglomerates	Die Sets	Section View of the Die Sets
Ti	Ti: 99.5; Others: 0.5	45	4.51		A	
90Ti10Sn	Ti: 90.0; Sn: 10.0	27	4.77		B	

6.3. Parameters of Experiments

In this section, the parameters of the experiments are described that have been used for the electrical-field activated sintering and forming process. The crucial parameters that need to be configured during the experiment were the applied pressure, the second heating temperature for the sintering stage, the heating rate and the holding time of the second heating temperature respectively. All the stated parameters contributed to the densification of the samples. The development of the experiment parameter has been made starting by using the guideline parameters obtained from the literature review of the previous electroplasticity sintering applications such as resistance heating and spark plasma sintering that has been performed concerning titanium and titanium alloy materials before this in the section **2.3.2.**

Application of Electrical-Field Activated on Sintering. In addition to that, the development of the experiment parameter continued with the trials and errors method. It has been implemented to find the most optimum experiment parameter to produce an excellent density of samples with high efficiency of the process.

6.3.1. Titanium (Ti)

As has been mentioned in **Table 2.3-1**, the range of the temperature used during the experiment on previous electroplasticity sintering application was in the range of 600 to 1,300 °C with the sintering time of 20 to 60 minutes and capable of producing the sample with the relative density of 90 to 99%. The heating rate of the process also limited to 25 to 200 °C/min and the pressure that has been applied was in the range of 10 to 100 MPa.

Table 6.3-1: Experiment parameters for Ti powder material performed by Gleeble® 3800 machine for electrical-field activated sintering and forming process.

Parameter No.	Units	Ti-1	Ti-2	Ti-3	Ti-4
Weight Powder	g	0.2267	0.2267	0.2267	0.2267
Pressure	MPa	**75**	**75**	**125**	**125**
Force	kN	0.9	0.9	1.6	1.6
Initial Temp. (Room Temp.)	°C	20	20	20	20
First Heating Rate	°C/s	20	20	20	20
First Heating Temp.	°C	200	200	200	200
First Heating Time	s	9.0	9.0	9.0	9.0
First Holding Time	s	30.0	30.0	30.0	30.0
Second Heating Rate	°C/s	**50**	**50**	**50**	**100**
Second Heating Temp.	°C	**700**	**1,100**	**1,100**	**1,100**
Second Heating Time	s	10.0	18.0	18.0	9.0
Second Holding Time	s	**2.0**	**5.0**	**5.0**	**5.0**
Cooling Rate	°C/s	10	10	10	10
Final Temp. (Room Temp.)	°C	20	20	20	20
Cooling Time	s	68.0	108.0	108.0	108.0
Process Total Time	s	**119.0**	**170.0**	**170.0**	**161.0**

Meanwhile, the information as stated in **Table 2.3-1** was used as a guideline and tested several trials and errors testing in the electrical-field activated sintering and forming process for Ti material, the final parameter has been obtained as presented in **Table 6.3-1** and **Table 6.3-2** which consists of four parameters. For the sintering temperature, it was used in the range of 700 to 1,100 °C and fast heating rate of 50 to 100 °C/s. The short holding time also has been implementing during the sintering process with the duration of two to five seconds. Therefore, it could make the process to finish more quickly with the total time in the range of 119 to 170 s. The pressure that has been applied was in the range of 75 to 125 MPa.

Table 6.3-2: List chart of heating temperature and applied pressure parameters for Ti samples.
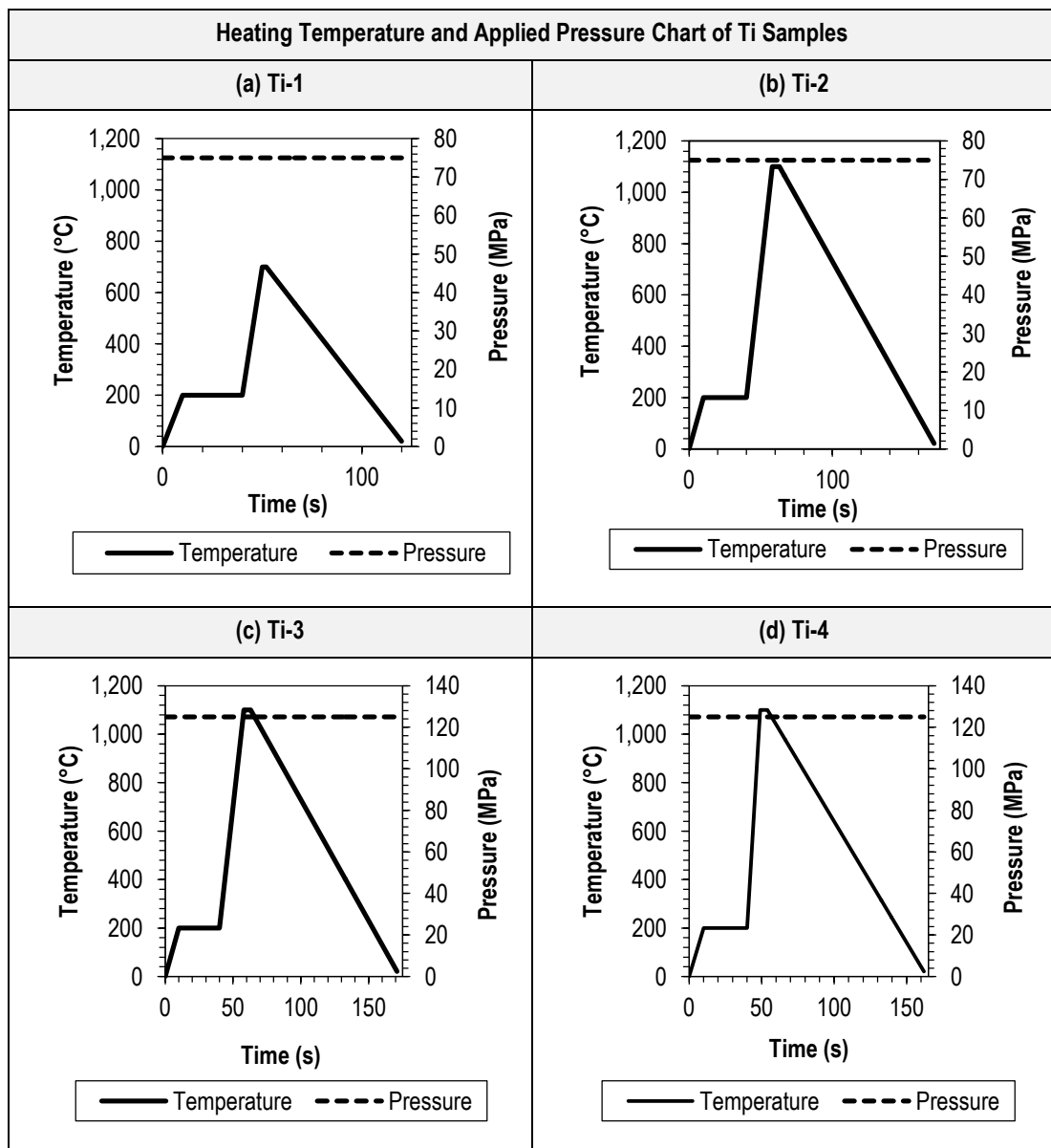
6.3.2. Titanium Tin Alloy (90Ti10Sn)

Based on **Table 2.3-2** which showed the previous electroplasticity sintering application with the temperature used to dense the sample of titanium alloy was between 68 to 83% was in the range of 700 to 1,100 °C and used the slow heating rate of 20 °C/min. The holding time during the sintering was in the range of three to 30 minutes with the applied pressure of 30 to 40 MPa.

Table 6.3-3: Experiment parameters for 90Ti10Sn powder material performed by Gleeble® 3800 machine for the electrical-field activated sintering and forming process.

Parameter No.	Units	90Ti10Sn-1	90Ti10Sn-P2	90Ti10Sn-P3	90Ti10Sn-P4
Weight Powder	g	0.2398	0.2398	0.2398	0.2398
Pressure	MPa	**125**	**125**	**125**	**125**
Force	kN	1.6	1.6	1.6	1.6
Initial Temp. (Room Temp.)	°C	20	20	20	20
First Heating Rate	°C/s	20	20	20	20
First Heating Temp.	°C	200	200	200	200
First Heating Time	s	9.0	9.0	9.0	9.0
First Holding Time	s	30.0	30.0	30.0	30.0
Second Heating Rate	°C/s	**50**	**50**	**50**	**25**
Second Heating Temp.	°C	**950**	**1,050**	**1,150**	**1,150**
Second Heating Time	s	15.0	17.0	19.0	38.0
Second Holding Time	s	**5.0**	**5.0**	**5.0**	**5.0**
Cooling Rate	°C/s	20	20	20	20
Final Temp. (Room Temp.)	°C	20	20	20	20
Cooling Time	s	46.5	51.5	56.5	56.5
Process Total Time	s	**105.5**	**112.5**	**119.5**	**138.5**

Based on the guideline information stated in **Table 2.3-2** and trials and errors testing in the electrical-field activated sintering and forming process by using 90Ti10Sn powder, four final parameters have been achieved as indicated in **Table 6.3-3** and **Table 6.3-4**. It used the heating sintering temperature of 950 to 1150 °C and fast heating rate of 50 °C/s. Constant pressure and holding time during the heating of sintering has been applied with the value of

125 MPa and 5 s respectively. The total time to finish the process of the experiment was in the range of 105.5 to 138.5 s.

Table 6.3-4: List chart of heating temperature and applied pressure parameters for 90Ti10Sn samples.
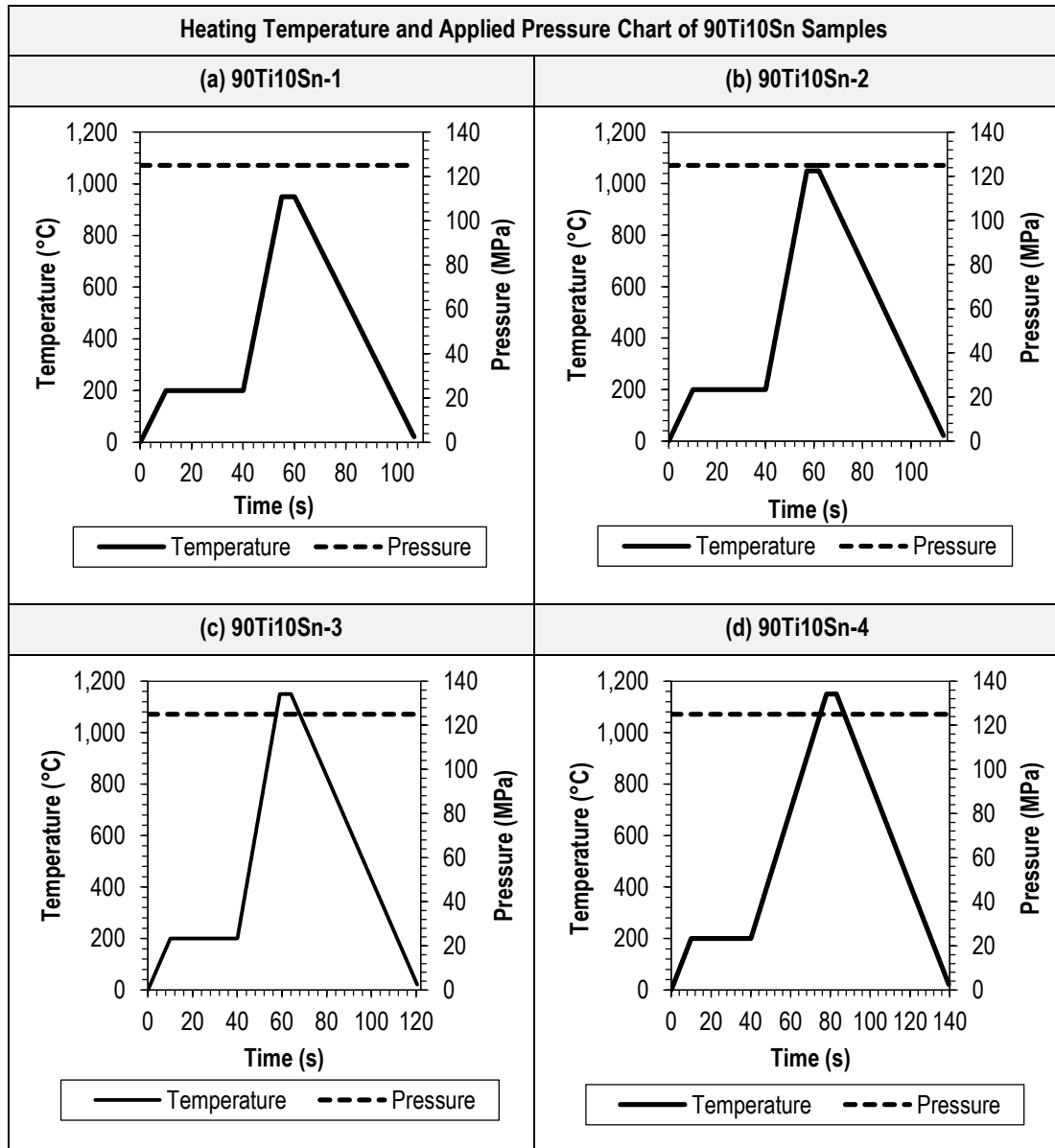
6.4. Procedures of the Experiment

The procedure of the experiment study using Gleeble® 3800 machine was divided into three stages which consisted of the preparation of the powder materials, the preparation of Gleeble® 3800 operating system and the preparation of the ejection process after the electrical-field activated sintering and forming process ended.

6.4.1. Preparation of Powder Materials

The mass of the powder material required during the electrical-field activated sintering and forming process was measured using powder measuring scale (Sartorious Practum) as in **Figure 6.2-2** with the equation **(6.4-1)**. After that, the bottom punch was inserted to one of the holes at the die's body to ensure when the powder was poured it was not leaking. The powder which had already been measured was carefully poured into the die set using the other open hole which not covered by the punch. The upper punch of die set was inserted into the other open holes of the die's body so that it would be fully closed.

$$m = V \times \rho \tag{6.4-1}$$

Symbols in equation (6.4-1):

m - Mass of powder material required during the process (g).

V - Volume of the cavity die set (mm^3).

ρ - Theory skeletal density of powder material required during the process (g/mm^3).

6.4.2. Preparation of Gleeble® 3800 Operating System

The fan of Gleeble® 3800 machine was switched on to make the water cooling at the setting temperature of 17 °C. It needs to wait until the temperature was stable. After the temperature has been achieved to 17 °C, the white start and the blue reset button was pushed to activate the Gleeble® 3800 machine. A small amount of the high-temperature specimen graphite lubricant (Thred Gard) and stickers was put at both the punches of the Gleeble® 3800 machine as in **Figure 6.4-1**. The die set with powder material was located in the vacuum chamber and aligned with the punches of Gleeble® 3800 machine as shown in **Figure 3.1-1** and **Figure 3.1-2**. The run and mechanical button were pressed. After that, the displacement button was slowly tweaked to move the punches of Gleeble® 3800 to touch and hold the die set inside the chamber. The pressure applied at this time must be zero. The measurement of the heating temperature during the experiment process has been made by using the thermocouple Omega Type K – TFAL-010 (Alumel) and TFCY-010 (Chromel) which was inserted into the centre hole of the die set and attached the other end of thermocouple wire to the C-Strain connection of Gleeble® 3800 machine. After that, the door of the vacuum

chamber was closed. The safety door button was made sure to turns green which indicate the door was securely closed. The air inside the chamber was eliminated by shutting down the lever air intake. The vacuum on button was pressed to start the process of taking out the air from the chamber. The excellent vacuum reading for the chamber was 4.5×10^{-1} Torr.
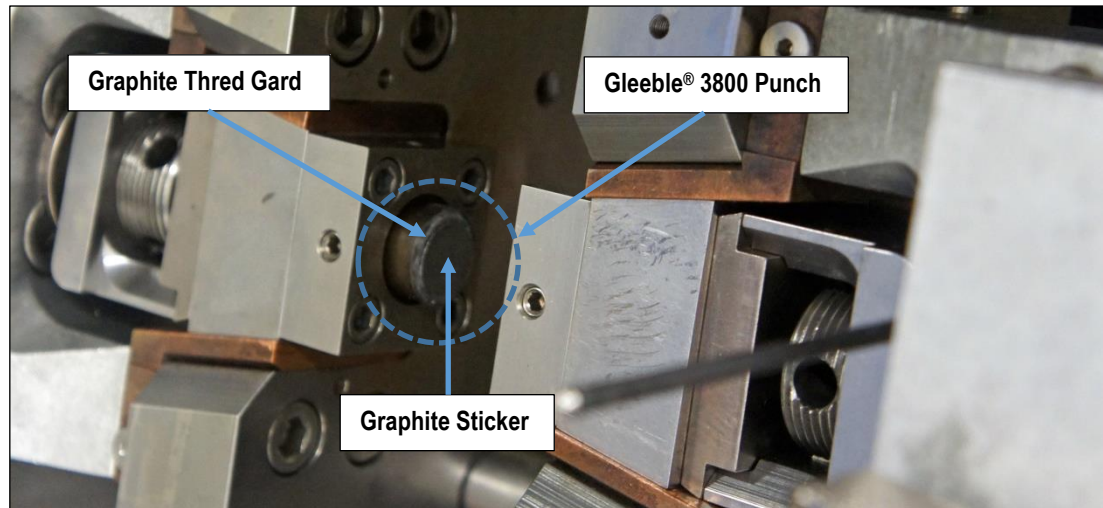
Figure 6.4-1: Small amount of the high-temperature specimen graphite lubricant (Thred Gard) and stickers was put at both the punches of the Gleeble® 3800 machine.

Then, all the parameters of the experiment were input using QuickSim™ software. The process of electrical-field activated sintering and forming process was started. As for safety reason, the emergency stop button was ready to be pressed if something unpredictable happens during the experiment process. Safety eye protection also must be wearing during the course due to excessive bright light produced by the heating process of the die set. After the experimental process had finished, the vacuum chamber was made sure to achieve the temperature of cooling 200 °C before the chamber door was open. It was done to reduce the oxidation towards the die set and powder inside. After the temperature has achieved to 200 °C, the vacuum off button was pressed with the air intake lever was open to allowed air inside the vacuum chamber. The release door button was pressed and vacuum chamber door was opened. The run and mechanical button were pressed. The die set was carefully taken out from the chamber by tweak the displacement button very slowly to release the die set. The punchers of the Gleeble® 3800 machine were cleaned and the process starts again until finished. After all the experiment was finished, switch off the white start, water cooling and fan switch button.

6.4.3. Preparation for the Ejection

After the die set has been taken out from the chamber, the die set was cooled until to the room temperature. The upper and lower punches were carefully opened using a hand. After that, the die set was placed above the die ring and using ejector and hammer, the sample inside the die set was carefully knocked. This action was made to prevent the sample from damaged. The contamination of carbon from the punches and inside wall graphite die set will stick to the surface of the sample. To remove the contamination carbon, the sand paper was used from rough to fine grade (grade: 800, 1,200 and 2,000) to clean the contamination. After that, the clean sample was put to the label plastic bag for the analysis process.

6.5. Results and Discussions

The results and discussion from the electrical-field activated sintering and forming process of Ti and 90Ti10Sn samples using Gleeble® 3800 machine has been made as below.

6.5.1. Samples Dimensions and Weights Measurements

Table 6.5-1 and **Table 6.5-3**, show the results for dimensions and weights measurements of the samples Ti and 90Ti10Sn respectively. In this tables also described the conditions of existing gap after the experiment finished between upper and lower punches with the die whether it was fully closed or not as presented in **Figure 6.5-1**. It was an ideal condition to have a fully closed die set during the experiment due to the current could pass through the overall die set and heat produced more efficiently to densify the powder. It could speed up the die set heating compared if it has a gap where the current flow only could pass through the nose tips of the punches and towards the powder materials. As a result, the efficiency of the heating process would be lower. In addition to that, the sample size also could be made more precise to the design sample which was four millimetres in diameter and height respectively. Therefore, the die set heating distribution during the experiment process has been observed to identify the performance of die set design. Moreover, the output of the actual sample size, the sample weight for before and after the cleaning process due to the sticking carbon and the differentiation of it have been measured and calculated respectively

for each of the Ti and 90Ti10Sn sample as presented in **Table 6.5-1** and **Table 6.5-3** respectively.
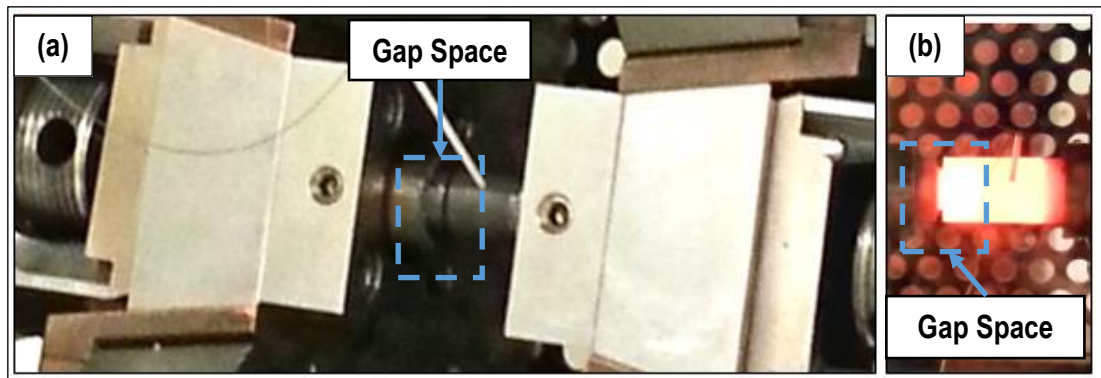
Figure 6.5-1: (a) Before experiment and **(b)** during experiment for the condition gap between upper and lower punches towards the die during the electrical-field activated sintering and forming process (area mark in blue colour). This condition was not an optimum for the die set to be operating during the experiment process.

6.5.1.1. Titanium (Ti)

Table 6.5-1 shows the detailed result of the dimensions and weights measurements of Ti samples using the die set A for the electrical-field activated sintering and forming process. Concerning the existing gap between upper and lower punch towards the die for samples Ti-1 and Ti-2 have shown there was a gap after the process end. Meanwhile, for the sample Ti-3 and Ti-4 has shown there was no gap. It was due to the increasing applied pressure and heating temperature towards samples Ti-3 and Ti-4 which help the die set A fully closed after the experiment ends.

As a result illustrate in **Figure 6.5-2**, for the samples Ti-3 and Ti-4, it demonstrated a better compaction and improved current flow throughout the die set which therefore made an excellent dimension of the final samples. Besides that, if the die set is fully closed during the experiment, it also helps to increase the density of the samples. For sample Ti-3 and Ti-4, it produced the diameter dimension of 3.98 and 3.99 mm respectively. Meanwhile, for the height of the sample Ti-3 and Ti-4, it recorded the reading of 4.02 and 4.01 mm for each. Compare to the samples Ti-1 and Ti-2 the diameter dimension was reported to have 3.97 mm for both with an increasing height of 4.11 and 4.10 mm respectively. The growing height of the sample was a cause of the existing gap between the punch and the die after the process end and as a

result the samples Ti-1 and Ti-2 was not fully compacted. Therefore, the die set heating efficiency and the condition where it was fully closed during the experiment was a crucial factor to be considered to have a better sample results.

Table 6.5-1: Results of the dimensions and weight measurements for Ti samples using the die set A for the electrical -field activated sintering and forming process which performed by Gleeble® 3800 machine.

Parameters and Results	Units	Ti-1	Ti-2	Ti-3	Ti-4
Pressure	MPa	75	75	125	125
Second Heating Rate	°C/s	50	50	50	100
Second Heating Temp.	°C	700	1,100	1,100	1,100
Second Holding Time	s	2.0	5.0	5.0	5.0
Process Total Time	s	119.0	170.0	170.0	161.0
Gap Between Punches and Die		Yes	Yes	No	No
Die Set Heating Temp. Distribution		Uniform	Uniform	Uniform	Uniform
Diameter of the Sample (Ø: 4.00)	mm	3.97	3.97	3.98	3.99
Height of the Sample (H: 4.00)	mm	4.11	4.10	4.02	4.01
Sample Weight Before Cleaning (BC)	g	0.2132	0.2175	0.2064	0.2142
Sample Weight After Cleaning (AC)	g	0.2118	0.2144	0.2048	0.2121
Different Sample Weight (BC-AC)	g	0.0014	0.0031	0.0016	0.0021

Regarding the die set heating distribution during the process, for the titanium sample using the die set A, it shows the heating distribution was uniform for each of the samples. It indicates a good signal for the overall heating of the die set during the electrical-field activated sintering and forming process. The percentage of differentiation sample weight before and after the cleaning process was in the range of 0.657 to 1.425% which indicates the amount of carbon sticking to the samples were very low. Below in **Figure 6.5-3** shows the visual of Ti samples after the ejection process from the die set A and **Table 6.5-2** shows after the cleaning process of edge-burr and carbon.
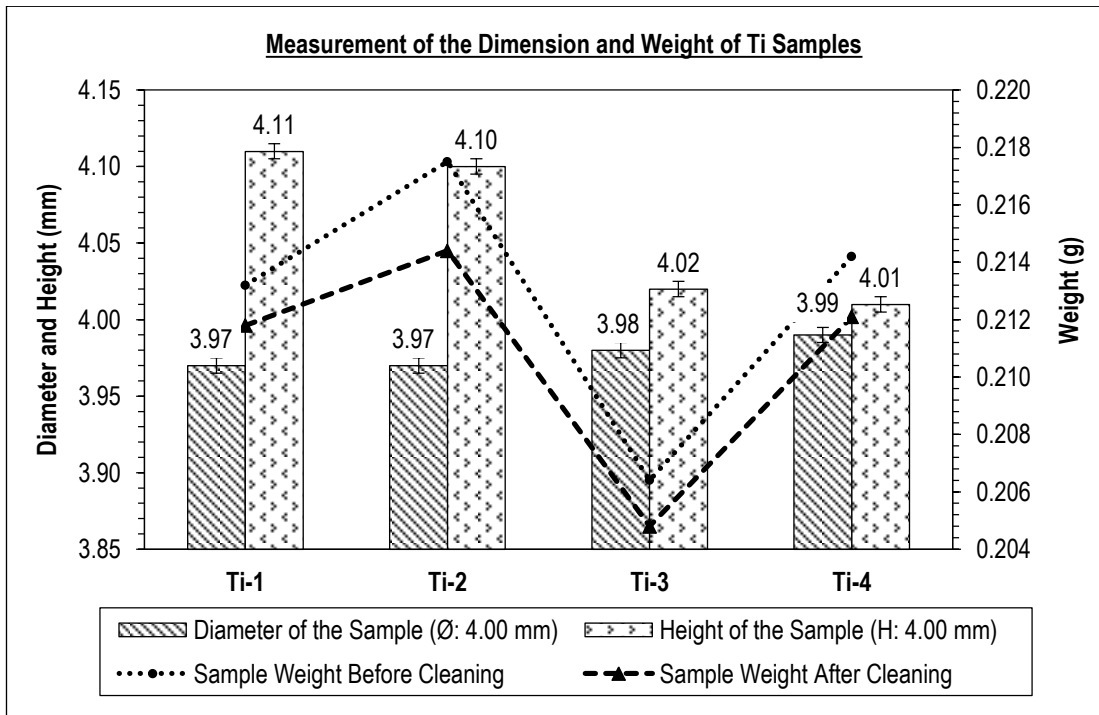
Figure 6.5-2: Measurement of the dimension and weight of Ti samples using die set A performed by Gleeble® 3800 machine for the electrical-field activated sintering and forming process.
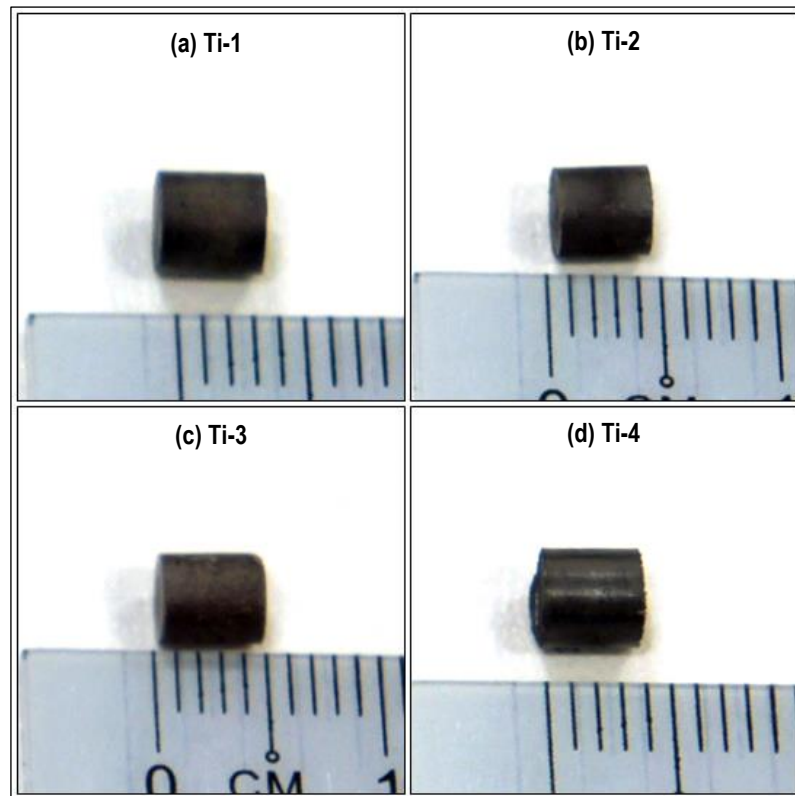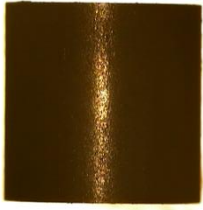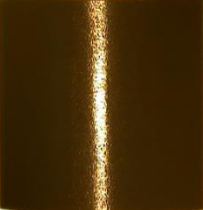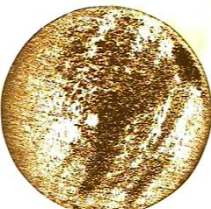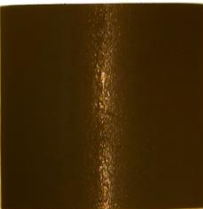
Figure 6.5-3: Ti samples after the ejection process.

Table 6.5-2: Ti samples before and after the cleaning process of edge-burr and carbon.

Samples	Before Cleaning		After Cleaning	
	Top	Side	Top	Side
Ti-1				
Ti-2				
Ti-3				
Ti-4				

6.5.1.2. Titanium Tin Alloy (90Ti10Sn)

Based on **Table 6.5-3**, it shows the details result of the dimensions and weights measurements of 90Ti10Sn samples using the new improvement of die set B for the electrical-field activated sintering and forming process. It has been tested to validate the efficiency of the die set design optimisation. Regarding the gap between upper and lower punches with the die, it shows there was no gap for all the samples after the process end. Due to this, the dimension of the 90Ti10Sn samples shows better results compare to the Ti samples which used the die set A for the experiment. The diameter for the 90Ti10Sn samples one to four recorded the reading of 3.98, 3.97, 3.98 and 3.99 mm respectively. Meanwhile, for the height of the 90Ti10Sn samples one and two, it recorded the same value of 4.03 mm. For 90Ti10Sn

samples three to four, the height was 4.02 and 4.01 mm for each. The details of the results also can be seen in **Figure 6.5-4**.

The heating distribution of the die set during the experiment also has been uniform for all the samples. It was a good condition to achieve higher relative densification and obtain excellent dimensional between the samples. The percentage of differentiation sample weight before and after the cleaning process was in the range of 0.496% to 0.952%. This showing that, even by using all the part in the new improvement design of die set with graphite for the punches and the die, the contaminate of carbon sticking to the samples was still low compared to the results if using the die set A. Below in **Figure 6.5-5** shows the visual of 90Ti10Sn samples after the ejection process from the die set B and **Table 6.5-4** shows after the cleaning process of edge-burr and carbon happen.

Table 6.5-3: Results of the dimensions and weight measurements for 90Ti10Sn samples using the die set B for the electrical -field activated sintering and forming process which performed by Gleeble® 3800 machine.

Parameters and Results	Units	90Ti10Sn-1	90Ti10Sn-2	90Ti10Sn-3	90Ti10Sn-4
Pressure	MPa	125	125	125	125
Second Heating Rate	°C/s	50	50	50	25
Second Heating Temp.	°C	950	1,050	1,150	1,150
Second Holding Time	s	5.0	5.0	5.0	5.0
Process Total Time	s	105.5	112.5	119.5	138.5
Gap Between Punches and Die		No	No	No	No
Die Set Heating Temp. Distribution		Uniform	Uniform	Uniform	Uniform
Diameter of the Sample (Ø: 4.00)	mm	3.98	3.97	3.98	3.99
Height of the Sample (H: 4.00)	mm	4.03	4.03	4.02	4.01
Sample Weight Before Cleaning (BC)	g	0.2377	0.2411	0.2421	0.2416
Sample Weight After Cleaning (AC)	g	0.2362	0.2395	0.2409	0.2393
Different Sample Weight (BC-AC)	g	0.0015	0.0016	0.0012	0.0023
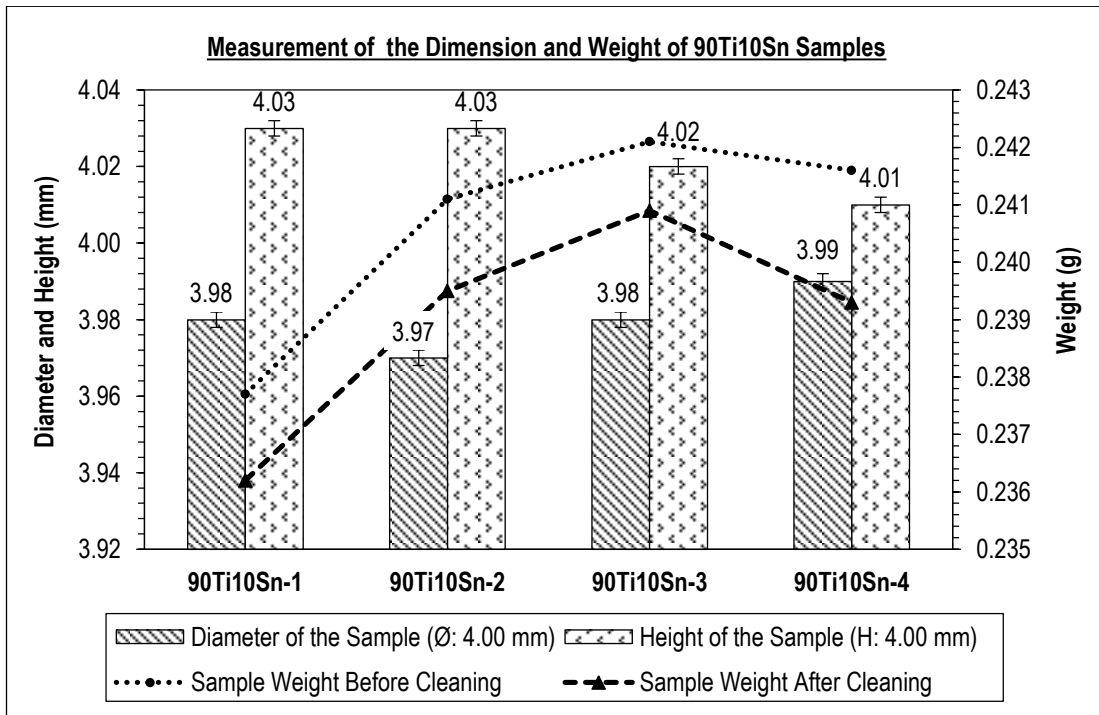
Figure 6.5-4: Measurement of the dimension and weight of 90Ti10Sn samples using die set B performed by Gleeble® 3800 machine for the electrical-field activated sintering and forming process.
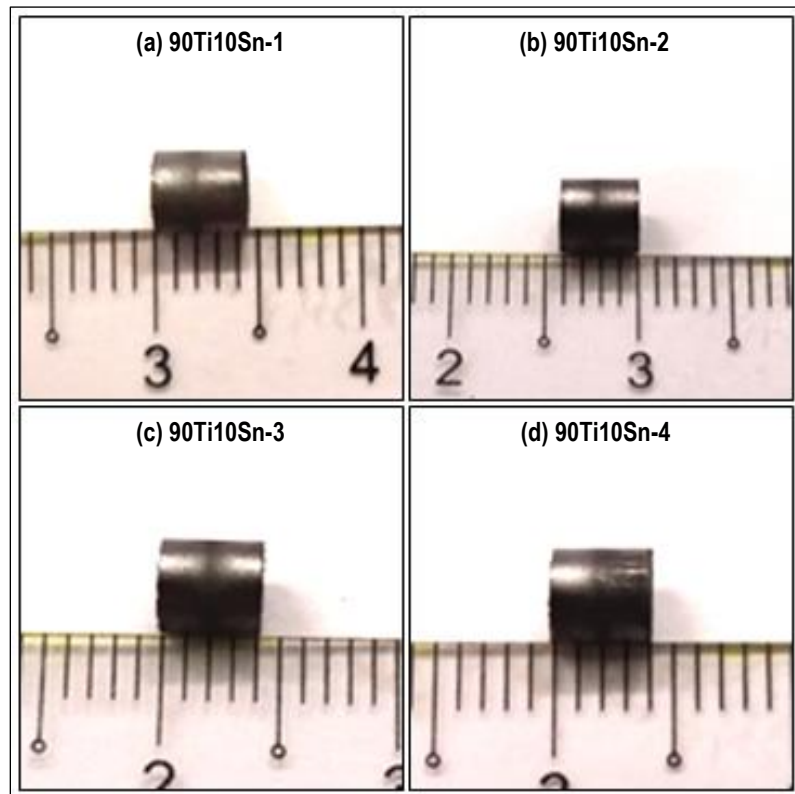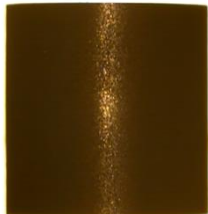
Figure 6.5-5: 90Ti10Sn samples after the ejection process.

Table 6.5-4: 90Ti10Sn samples before and after cleaning process of edge-burr and carbon.

Samples	Before Burr Cleaning		After Burr Cleaning	
	Top	Side	Top	Side
90Ti10Sn-1				
90Ti10Sn-2				
90Ti10Sn-3				
90Ti10Sn-4				

6.5.2. Samples Relative Density

This section describes the results and discussion for the relative density of Ti and 90Ti10Sn samples based on the parameters that have been assigned as shown in **Table 6.5-5** and **Table 6.5-8** respectively.

6.5.2.1. Titanium (Ti)

Based on the data from **Table 6.5-5** and the illustration bar graph on **Figure 6.5-6** shows the incremental value of the relative density directly proportional to the applied pressure, second heating rate, second heating temperature and second holding time for the Ti samples.

The relative density for Ti samples was recorded 92.24% for Ti-1, 95.57% for Ti-2, 96.23% for Ti-3 and 98.55% for Ti-4. For Ti-1 and Ti-2 samples, all the main parameters such as applied pressure and the second heating rate were the same which indicate the reading of 75 MPa and 50 °C/s individually. By increasing the second heating temperature and second holding time from 700 to 1,100 °C and two to five seconds for Ti-1 and Ti-2 samples respectively, the relative increment density of 3.33% can be achieved. The total time needed for Ti-1 and Ti-2 samples to complete the process was 119 s and 170 s for each. Despite the fact that the die set A heating temperature distribution for Ti-1 and Ti-2 samples was uniform during the experiment by using Gleeble® 3800 machine for electrical-field activated sintering and forming process, there was a gap exists between the punches and the die. The densification of Ti-1 and Ti-2 samples could achieve higher if the punches of the die set A was fully closed at the end of the process.

Table 6.5-5: Results of the relative densities of Ti samples using the die set A for the electrical-field activated sintering and forming process which performed by Gleeble® 3800 machine.

Parameters and Results	Units	Ti-1	Ti-2	Ti-3	Ti-4
Pressure	MPa	75	75	125	125
Second Heating Rate	°C/s	50	50	50	100
Second Heating Temp.	°C	700	1,100	1,100	1,100
Second Holding Time	s	2.0	5.0	5.0	5.0
Process Total Time	s	119.0	170.0	170.0	161.0
Gap Between Punches and Die		Yes	Yes	No	No
Die Set Heating Temp. Distribution		Uniform	Uniform	Uniform	Uniform
Relative Density	%	92.24	95.57	96.23	98.55

Based on the observation of **Table 6.5-6** and **Table 6.5-7**, it shows the shrinkage of stroke punches of Gleeble® 3800 machine throughout the process. During the first heating stage for Ti-1 and Ti-2 samples which in the durations of nine seconds, the reduction of stroke punches of Gleeble® 3800 machine to compressed the samples was in the range of 0.00076 to -0.13897 mm and 0.00050 to -0.18359 mm respectively. After that, for the first holding heating stage which happens in the periods of 30 s, the reductions values of Gleeble® 3800 stroke punches was recorded to -0.40224 mm and -0.42096 mm for each Ti-1 and Ti-2 samples. Averagely the value for the reductions of Gleeble® 3800 stroke punches for the first

stage was similar due to the parameters applied to the Ti-1 and Ti-2 samples were equivalent as stated in **Table 6.3-1**. It used 200 °C for the first heating temperature, 20 °C/s for the first heating rate, 30 s for the first holding temperature durations and 75 MPa for the applied pressure.
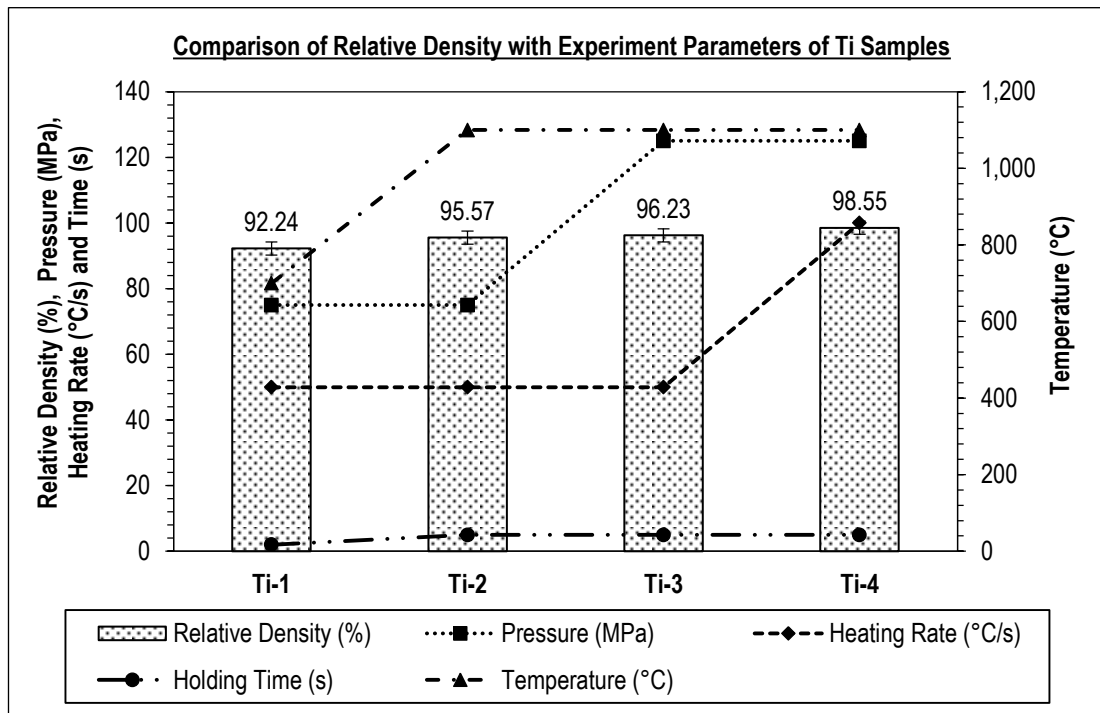
Figure 6.5-6: Comparison of relative density with parameters of experiment for Ti samples.

Differently, during the seconds heating stage of Ti-1 and Ti-2 samples, the reduction of Gleeble® 3800 stroke punches was increased to -0.70504 mm and 1.4816 mm respectively. Ti-2 sample shows the higher in the reduction of stroke due to the second heating temperature stage used was 1,100 °C compared to Ti-1 sample used 700 °C. Therefore, the heating temperature during the sintering stage was essential for the compaction of the Ti samples which leads to the higher relatives density components due to the particles of Ti powder was easy to deform under the high-temperature environment. It was also helped by the longer second holding temperature stage where it indicated the compaction of the samples continued on increased to -0.87206 mm for Ti-1 sample and -1.48030 mm for Ti-2 sample. Ti-2 sample shows the more reductions due to the second holding time used during the experiment was five seconds for 1,100 °C, compared to Ti-1 samples was two seconds for 700 °C. At the end of the cooling stage, the Ti-1 sample indicated the reading of 92.24% for relative density with

the reductions of sample compactions was -1.442 mm. Meanwhile, for the Ti-2 sample shows the higher relative density of 95.57% with more sample compaction reductions of -1.7274 mm compared to Ti-1.

Table 6.5-6: Reduction of Gleeble® 3800 stroke punches during electrical-field activated sintering and forming process for Ti samples.

Time (s)	Reduction of Gleeble® 3800 Stroke Punches (mm)			
	Ti-1	Ti-2	Ti-3	Ti-4
First Heating Stage				
0 to 9	0.00076 to -0.13897	0.00050 to -0.18359	0.00029 to -0.52592	0.00043 to -0.48770
First Holding Heating Stage				
9 to 39	-0.13897 to -0.40224	-0.18359 to -0.42096	-0.52592 to -0.82338	-0.48770 to 0.71492
Second Heating Stage				
39 to 48				-0.71492 to -1.51660
39 to 49	-0.40224 to -0.70504			
39 to 57		-0.42096 to -1.48160	-0.82338 to -1.59940	
Second Holding Heating Stage				
48 to 53				-1.51660 to -1.62700
49 to 51	-0.70504 to -0.87206			
57 to 62		-1.48160 to -1.48030	-1.59940 to -1.56550	
Cooling Stage				
51 to 119	-0.87206 to -1.44200			
53 to 161				-1.62700 to -1.89350
62 to 170		-1.48030 to -1.72740	-1.56550 to -1.84440	

Meanwhile for the comparison of Ti-2 and Ti-3 samples, only applied pressure during the experiment has been changed from 75 to 125 MPa. All the others main parameters have been set to be the same as shown in **Table 6.5-5** and **Figure 6.5-6**. It has been made to test the effect of high applied pressure towards the densification of the Ti samples. By increasing the applied differential pressure of 50 MPa, the relative increment density of 0.66% for the Ti-3 sample has been recorded with the same process total time as Ti-2 sample which was 170 s. In addition to the positive result, the gap between the punches and the die after the electrical-field activated sintering and forming process end for Ti-3 sample also shows the die set A was fully closed. The higher applied pressure on Ti-3 sample helped the die set A to fully close at

the end of the process by breakage and deformed the particles of Ti powder during the high sintering temperature environment of 1,100 °C. The die set heating temperature distribution of Ti-3 sample also was uniform during the process.

Table 6.5-7: The heating temperature and shrinkage of stroke punches of Gleeble® 3800 machine towards compaction of Ti samples as a function of time.
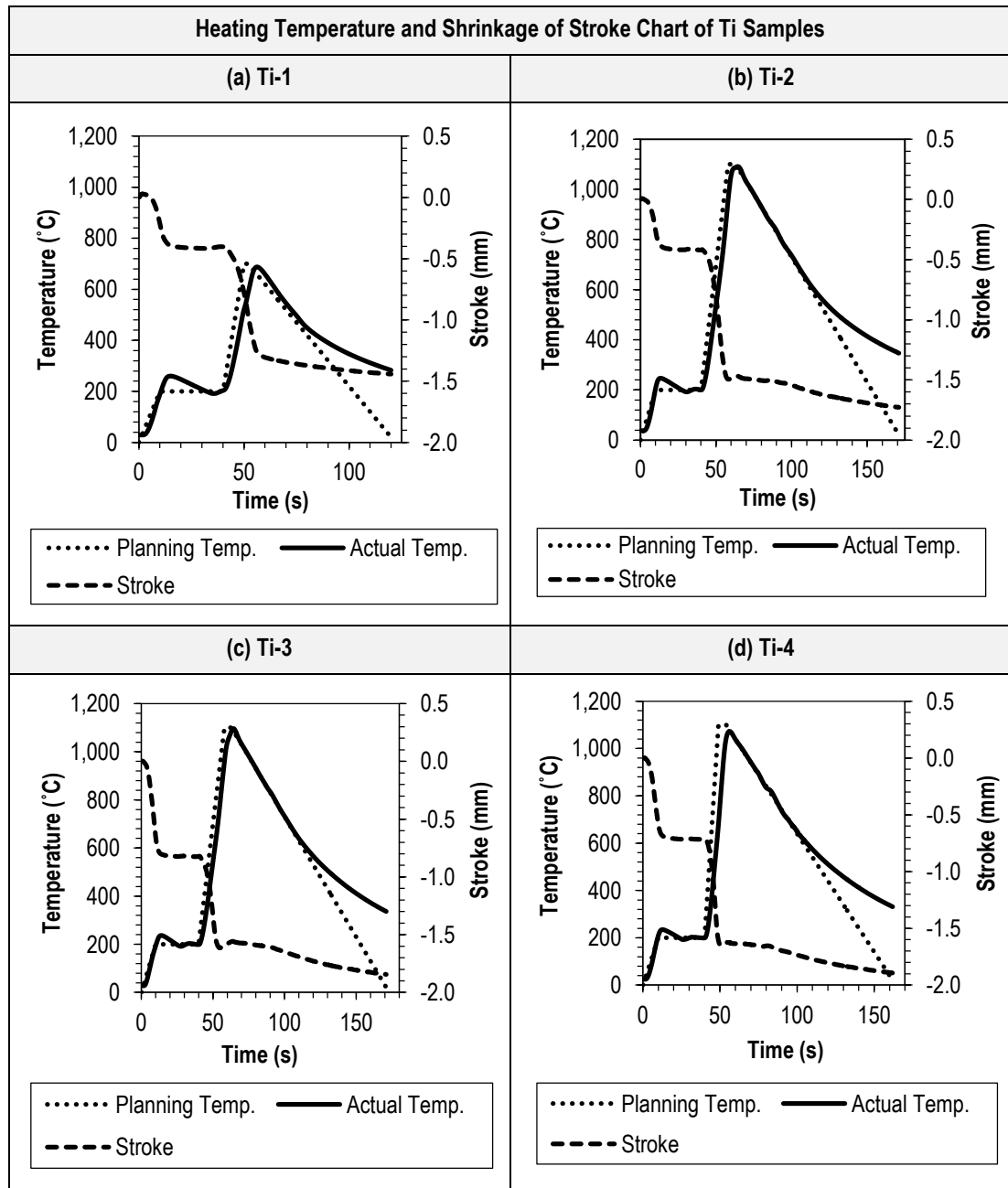
Based on the observation for the shrinkage of Gleeble® 3800 stroke punches throughout the process as presented in **Table 6.5-6** and **Table 6.5-7**, by increasing the applied pressure

in the nine seconds of the first heating stage, the Ti-3 sample has shown to have the compaction reduction of 0.00029 to -0.52592 mm. It indicated the differential compaction reduction was 65.02% compared to the Ti-2 sample which only demonstrates the decrease from 0.00050 to -0.18359 mm. After that, with the applied pressure sustain throughout the process until the cooling stage, the reading for the shrinkage of Gleeble® 3800 stroke punches continued to reduce with the reading of -1.8444 mm for Ti-3 and -1.7274 mm for Ti-2. Based on this finding, Ti-3 shows to have a better relative density of 96.23% compared to Ti-2 which only have 95.57%.

The comparison of the densification samples towards the parameters of experiment continued with the Ti-4 and Ti-3 samples. By using higher second heating rate of 100 °C/s for Ti-4 sample with all the others main parameters remain the same as before, the relative density of its component can be achieved by 98.55% as shown in **Table 6.5-5** and **Figure 6.5-6**. Ti-4 sample shows the most optimum parameter for densification of Ti powder with the electrical-field activated sintering and forming process. In addition to that, the duration of the process was shorter with the process total time of 161 s compared to Ti-3 sample which used 50 °C/s for the second heating rate and as a result the densification of its component was recorded 96.23% with the process total time of 170 s. During the experiment also, the die set temperature distribution for the Ti-4 sample was uniform with the die set A was fully closed at the end of the process. By the effect of the high second heating rate, the compaction of the Ti-4 sample was improved in the second holding heating stage where the reading was shown -1.5166 to -1.627 mm compared to the Ti-3 sample which indicated the reading was -1.5994 to -1.5655 mm as presented in **Table 6.5-6** and **Table 6.5-7**. At the end of the cooling stage, Ti-4 sample has the reading of -1.8935 mm compared to the Ti-3 sample which only can be at -1.8444 mm.

Based on the results findings, it shows that by using electrical-field activated sintering and forming process it has the potential to save the processing time for Ti samples compared to the previous electroplasticity sintering process such as resistance heating and spark plasma sintering which has been described in detail previously in **Table 2.3-1**. Previously for spark plasma sintering, the overall total time required to finish the process was from 20 to 60 minutes and capable of achieved the relative density of samples from 90 to 99% without the

annealing stage. Instead by using electrical-field activated sintering and forming process, the processing times are in the range of 119 to 170 seconds and had achieved the relative density of 92.24 to 98.55 %.

6.5.2.2. Titanium Tin Alloy (90Ti10Sn)

By using the improvement of die set B, the results of relative densification for 90Ti10Sn samples has shown in **Table 6.5-8** and illustration of its comparison bar graph have presented in **Figure 6.5-7**. Based on the observation result, the incremental value of the relative density of 90Ti10Sn samples was directly proportional to the second heating temperature. The increment of 100 °C temperature has made from 90Ti10Sn-1 to 90Ti10Sn-3. As a result, the relative density value for the samples 90Ti10Sn-1, 90Ti10Sn-2 and 90Ti10Sn-3 have indicated the reading of 94.5%, 97.19% and 98.21% with the process total time showed 105.5 s, 112.5 s and 119.5 s respectively. Meanwhile, for the sample 90Ti10Sn-4 the second heating temperature has been remaining the value for 1,150 °C same as sample 90Ti10Sn-3 before, but the second heating rate was reduced to 50% which made it be 25 °C/s. The relative density of the sample 90Ti10Sn-4 was recorded the reading of 98.51% which slightly higher compared to sample 90Ti10Sn-3. Regarding the applied pressure and holding time during the process, the parameters value was all the same throughout the tested 90Ti10Sn samples which were 125 MPa and five seconds for each. By using die set B, all the samples of 90Ti10Sn has shown to have a uniform die set heating temperature distribution during the heating process and all the condition of the die set B was fully closed at the end of the process. Due to this, the dimension of the 90Ti10Sn samples shows better results compare to the Ti samples which used the die set A for the experiment.

Based on **Table 6.5-9** and **Table 6.5-10**, it shows the shrinkage of stroke punches of Gleeble® 3800 machine during the experiment for sample 90Ti10Sn. Averagely the value for the reductions of Gleeble® 3800 stroke punches for the first heating and holding stage was similar due to the applied parameters to the samples of 90Ti10Sn-1 to 90Ti10Sn-4 was the same as stated in **Table 6.3-3**. It used 200 °C for the first heating temperature, 20 °C/s for the first heating rate, 30 s for the first holding temperature and 125 MPa for the applied pressure. Meanwhile, for the second heating and holding stage, the sample 90Ti10Sn-4 shows the

highest reductions of strokes where it indicated the final reading was -3.7426 mm and -3.6899 mm respectively compares to the others tested 90Ti10Sn samples.

Table 6.5-8: Results of the relative densities of 90Ti10Sn samples using the die set B for the electrical-field activated sintering and forming process which performed by Gleeble® 3800 machine.

Parameters and Results	Units	90Ti10Sn-1	90Ti10Sn-2	90Ti10Sn-3	90Ti10Sn-4
Pressure	MPa	125	125	125	125
Second Heating Rate	°C/s	50	50	50	25
Second Heating Temp.	°C	950	1,050	1,150	1,150
Second Holding Time	s	5.0	5.0	5.0	5.0
Process Total Time	s	105.5	112.5	119.5	138.5
Gap Between Punches and Die		No	No	No	No
Die Set Heating Temp. Distribution		Uniform	Uniform	Uniform	Uniform
Relative Density	%	94.50	97.19	98.21	98.51
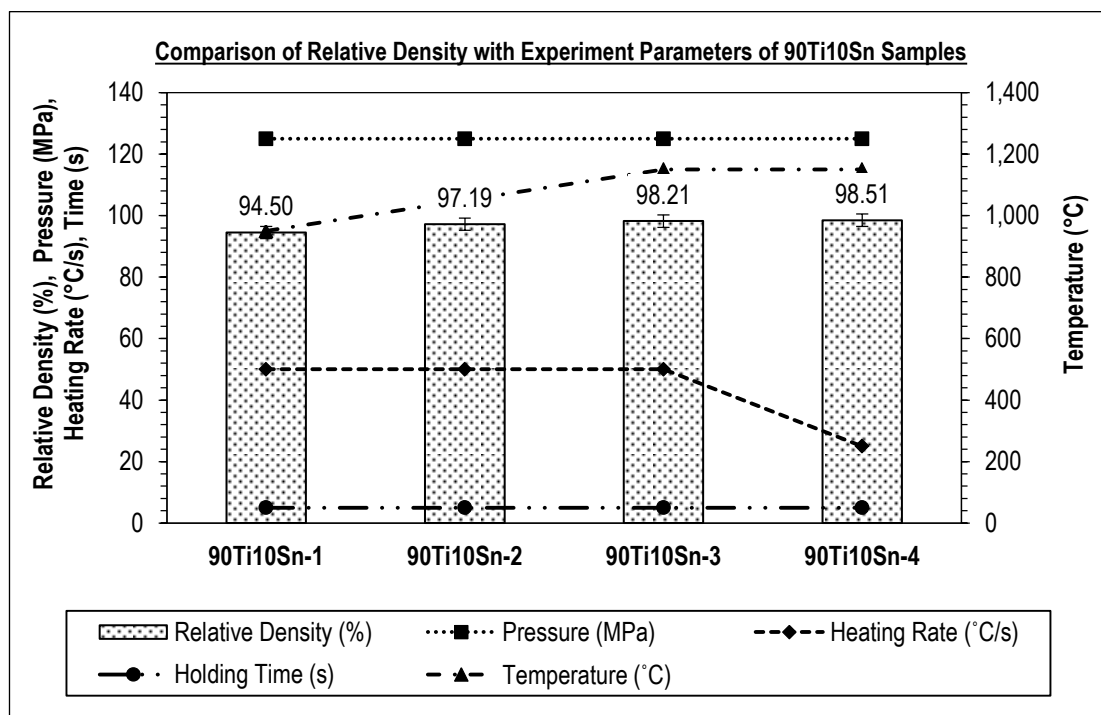
Figure 6.5-7: Comparison of relative density with parameter of experiment for 90Ti10Sn samples.

Therefore, based on this finding it shows that by using slower heating rate during the second stage improved the compaction of the sample 90Ti10Sn-4. It was due to the deformation and breaking of the particles during the formation process for sample 90Ti10Sn-4

can be extended much longer with the help of high temperature and pressure of 1,150 °C and 125 MPa respectively. Thus at the end of cooling stage, 90Ti10Sn-4 once again shows the highest reduction of Gleeble® 3800 stroke punches with the reading of -3.93780 mm. Based on this result, it made the most optimum parameter that can be used during the electrical-field activated sintering and forming process and achieved the relative density of 98.51% with the process total time was 138.5 s.

Table 6.5-9: Reduction of Gleeble® 3800 stroke punches during electrical-field activated sintering and forming process for 90Ti10Sn samples.

Time (s)	Reduction of Gleeble® 3800 Stroke Punches (mm)			
	90Ti10Sn-P1	90Ti10Sn-P2	90Ti10Sn-P3	90Ti10Sn-P3
First Heating Stage				
0 to 9	0.04455 to -0.81284	0.041951 to -0.67252	0.039137 to -0.95853	0.041438 to -1.04150
First Holding Heating Stage				
9 to 39	-0.81284 to -1.80670	-0.67252 to -1.46920	-0.95853 to -2.01780	-1.04150 to -1.94910
Second Heating Stage				
39 to 54	-1.80670 to -3.18700			
39 to 56		-1.46920 to -3.09980		
39 to 58			-2.01780 to -3.62900	
39 to 77				-1.94910 to -3.74260
Second Holding Heating Stage				
54 to 59	-3.18700 to -3.46130			
56 to 61		-3.09980 to -3.26840		
58 to 63			-3.62900 to -3.50920	
77 to 82				-3.74260 to -3.68990
Cooling Stage				
59 to 105.5	-3.46130 to -3.58220			
61 to 112.5		-3.26840 to -3.41610		
63 to 119.5			-3.50920 to -3.71750	
82 to 138.5				-3.68990 to -3.93780

Even with the slower heating rate during the electrical-field activated sintering and forming for sample 90Ti10Sn-4, it still the fastest processing time compared to the previous electroplasticity sintering process as stated in **Table 2.3-2**. By using spark plasma sintering

105

process, the previous sintering process time needed was in the range of three to 30 minutes to achieve the sample relative densification of 68 to 83%. In addition to that, the annealing process needs to be done to the sample about 24 to 40 hours at 1000 °C and 750 °C temperature respectively before or after the sintering process.

Table 6.5-10: The heating temperature and shrinkage of stroke punches of Gleeble® 3800 machine towards compaction of 90Ti10Sn samples as a function of time.

Heating Temperature and Shrinkage of Stroke Chart of 90Ti10Sn Samples	
(a) 90Ti10Sn-1	(b) 90Ti10Sn-2
(c) 90Ti10Sn-3	(d) 90Ti10Sn-4
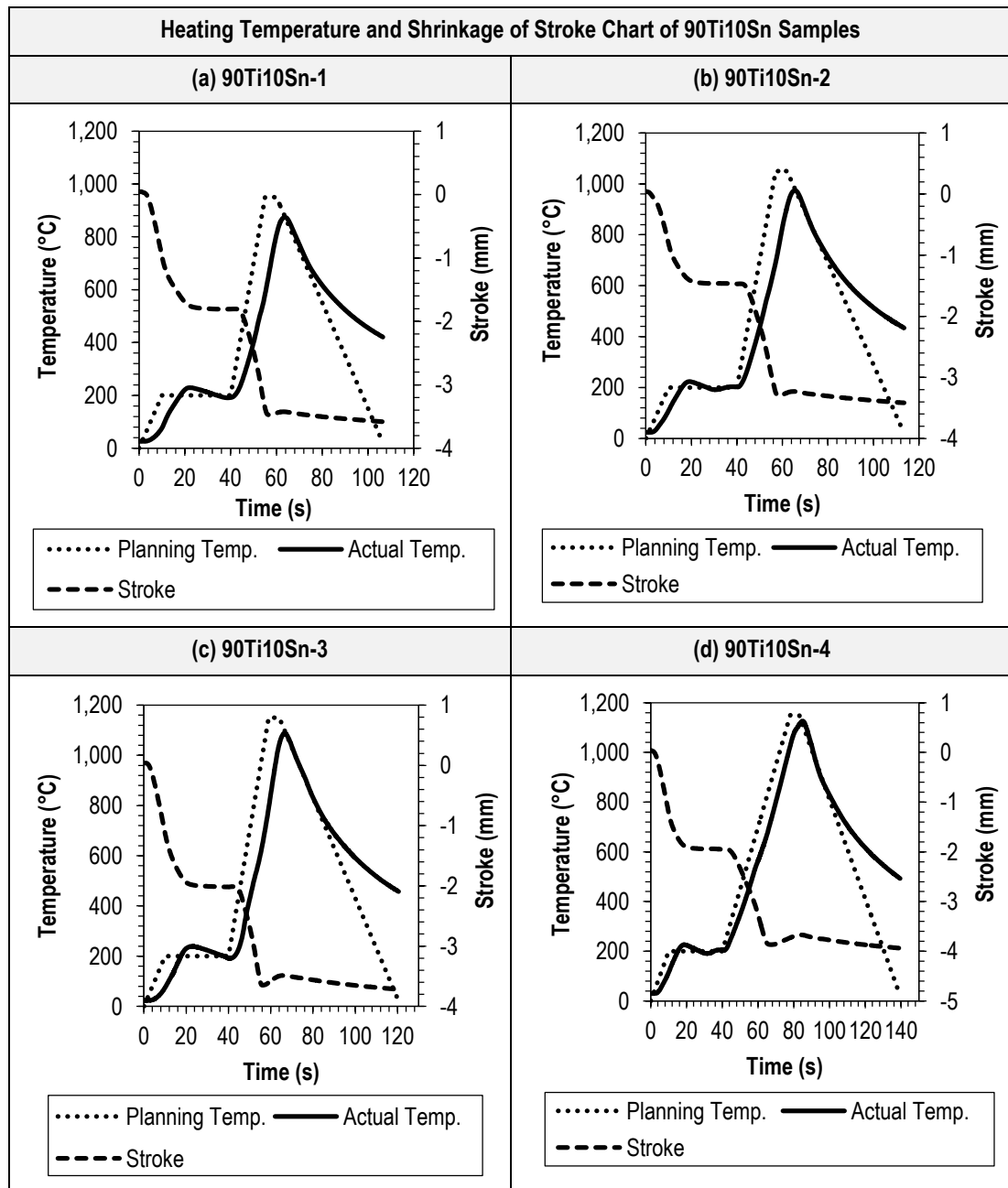
6.5.3. Samples Microstructures

The description of the microstructures particles and chemical element weight percentage of carbon (wt%) has been discussed for samples Ti and 90Ti10Sn. In addition to that, the performance of the assigned die sets A and B also has been compared concerning of its efficiency to withstand the electrical-field activated sintering and forming process.

6.5.3.1. Titanium (Ti)

In **Table 6.5-11** and **Table 6.5-12**, shows the comparison of SEM micrograph for the position at the centre and the edge of Ti samples respectively. Sample Ti-1 shows the most porous of particles densification at the micrograph scale among the others samples at the position of centre and edge where it shows the particle breakage and deformation during the applied constant pressure and high temperature. Moreover, on the sample Ti-1 also shows that the small particles break away from the massive particles which constrained it from moving. This process also occurs in the other samples of which indicated an increase of contact areas as the densification value increased. The pores of the particles melting were reduced as it continued to the samples Ti-2 and Ti-3 at the positions of centre and edge. It was due to the incremental of applied pressure from 75 to 125 MPa and heating temperature from 700 to 1,100 °C. The additional action of the applied pressure also helps the deformation and crushing of Ti particles which can contribute to forcing the Ti particles to touch each other's during the strengthened sintering process until the pores become smaller and disappears.

Meanwhile, for sample Ti-4 shows almost there was no pore existing particularly at the centre of the sample and indicate a small amount of pores exist at the edge of the sample. It was due to the area of electrical heating during the process more concentrated at the centre of the punch nose the die set A. Based on this finding, the modification of the upper and lower punches for the die set A was needed to improve this condition for more uniform densification particles at the centre and edge. Therefore, the optimisation of new die set B has been introduced and shows a better result for the densification of 90Ti10Sn samples. In addition to that, the condition of the die set A fully closed during the process also contributed to the

achievement of no pores at the centre for the sample Ti-4 due to the more current could pass through the overall die set and heat produced more efficiently.

Table 6.5-11: Comparison of SEM micrograph at centre position Ti sample (Magnification: 1.40 k SE).

Centre Position of SEM Micrograph Ti Samples (Magnification: 1.40 k SE)	
(a) Ti-1: 92.24%	**(b) Ti-2: 95.57%**
Particles breakage and deform	Pores reduces size / Particles melting
(c) Ti-3: 96.23%	**(d) Ti-4: 98.55%**
Pores reduces size / Particles melting	Disappearance of particles boundary

Regarding the presence of carbon element at the centre and edge of Ti samples shows the small amount of carbon contaminate was in the range of 2.54 to 3.64 wt% for the centre position and 3.07 to 4.82 wt% for the edge location of the samples as shown in **Table 6.5-13** and **Figure 6.5-8**. It has been caused by a drawback when using graphite die where carbon element at the die's wall can be mixed into the solidified Ti sample during the high temperature of the sintering process. Based on this disadvantage, it was hard to achieve the sample that was purely free from contamination such as carbon especially on the sample surfaces when a graphite die set was used.

Table 6.5-12: Comparison of SEM micrograph at edge position Ti sample (Magnification: 1.40 k SE).

Edge Position of SEM Micrograph Ti Samples (Magnification: 1.40 k SE)	
(a) Ti-1: 92.24%	**(b) Ti-2: 95.57%**
(c) Ti-3: 96.23%	**(d) Ti-4: 98.55%**
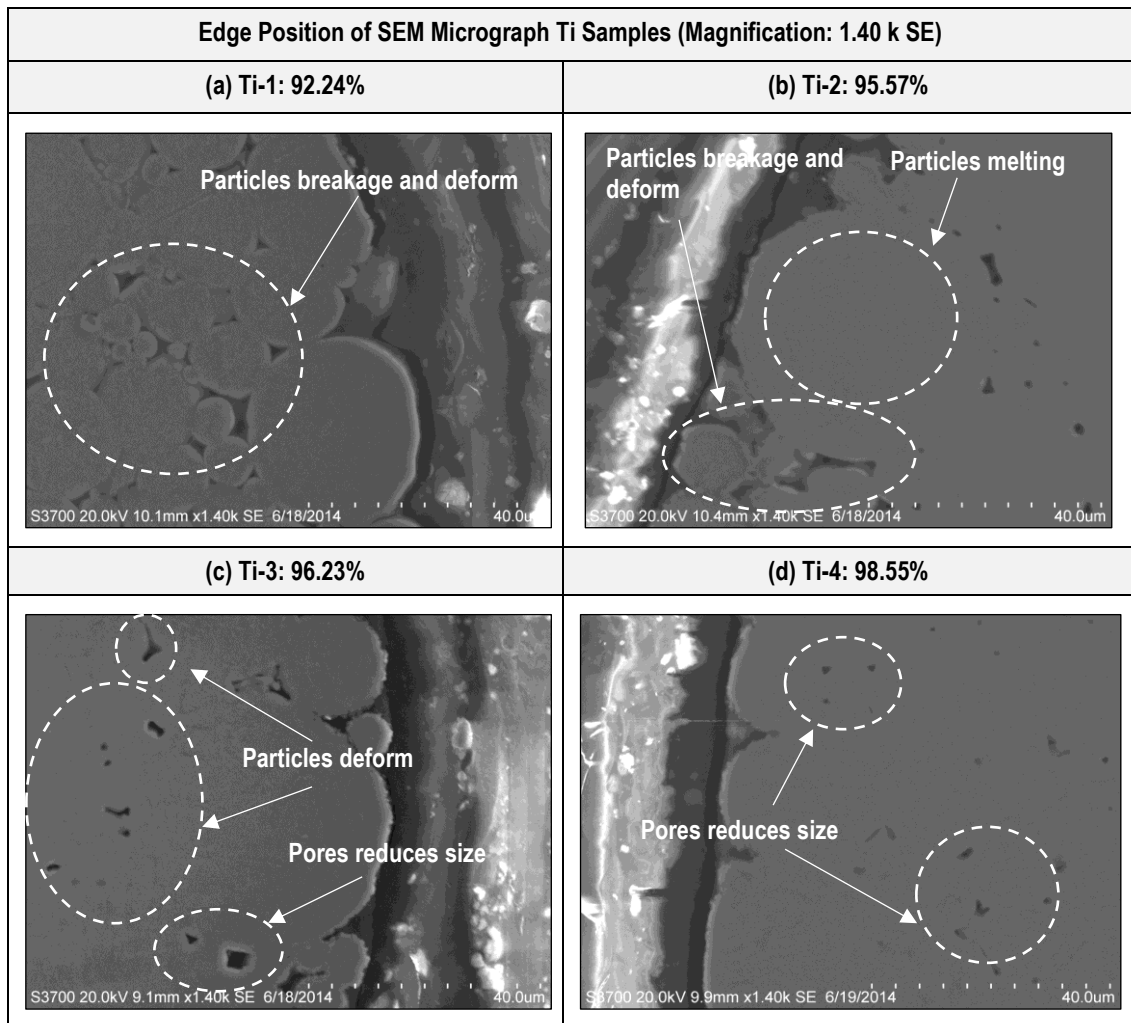
Table 6.5-13: Chemical element weight percentage of carbon (wt%) at the positions centre and edge of Ti samples.

Positions of Inspections	Units	Ti-1	Ti-2	Ti-3	Ti-4
Centre of the Samples	**wt.%**	3.12	2.54	3.64	3.18
Edge of the Samples	**wt.%**	4.82	3.93	4.73	3.07

Nevertheless, the graphite material has a higher maximum service temperature and lower thermal expansion coefficient among the others materials as mention before which was an advantage to be used as the die set for electrical-field activated sintering and forming process. Based on this experiment which used the die set A for Ti samples it shows that die set A can only be used on average up to six times due to the tendency of jammed and sticking

between punches and die at the high temperature caused by different thermal expansion and retractions as explained in section **4.3 Material Selection for Die Sets**.

Comparison of Chemical Element Weight Percentage of Carbon for Ti Samples
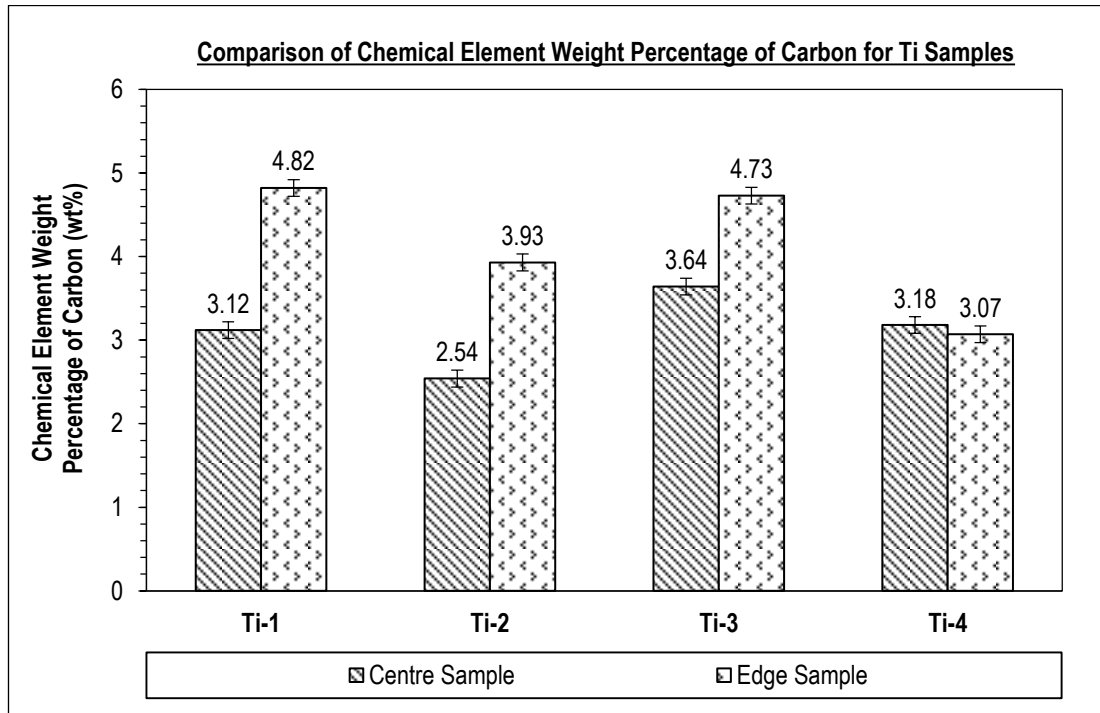
Figure 6.5-8: Comparison of chemical element weight percentage of carbon (wt%) located at centre and edge of Ti samples.

6.5.3.2. Titanium Tin Alloy (90Ti10Sn)

In **Table 6.5-14** and **Table 6.5-15** shows the comparison of SEM micrograph at the centre and the edge of 90Ti10Sn sample. Based on the observation, the pores of the sample decreased as the heating temperature raise which accompanies the densification of sample 90Ti10Sn-1 to 90Ti10Sn-4. The deformation and breakage of the particles play the significant contribution to the densification of the components. In addition to that, there are no coarsening of grains accompanies the process of part densification. By using the die set B, it shows the improvement of the densification of the particles where the pores reduces more efficiently at the centre and edge of the 90Ti10Sn samples. All the sample 90Ti10Sn which formed by using die set B during the experiment was fully closed and have a uniform heating temperature distribution throughout the entire process. In addition to that, there were no

issues found during the ejection of the samples when using die set B, and it could repeatedly be used for electrical-field activated sintering and forming process.

Table 6.5-14: Comparison of SEM micrograph at centre position 90Ti10Sn sample (Magnification: 1.40 k SE).
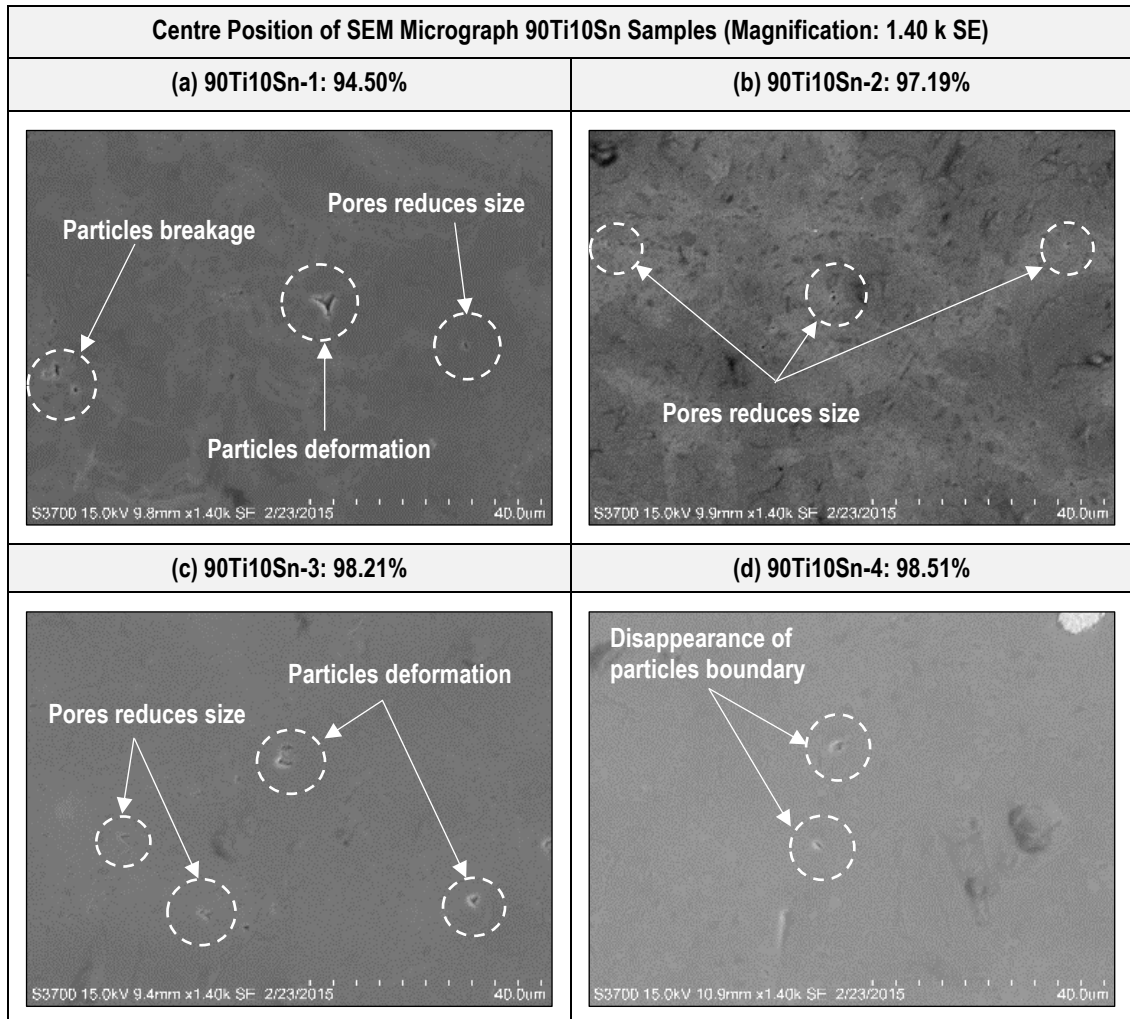
Nevertheless, there were several limitations when using the die set made fully of graphite. Concerning the durability, based on the observation the crucial feature that was the easiest to be broken was the punch nose due to many cycles of the process. The robustness to impact from the higher forming pressure on the graphite die set was a key weakness due to low mechanical strength at the elevated temperature during the forming and sintering process. In addition to that, it also needed to be cleaned after being used several times due to the used powder material melting and may become stuck onto the punches and die surface.

Table 6.5-15: Comparison of SEM micrograph at edge position 90Ti10Sn sample (Magnification: 1.40 k SE).

Edge Position of SEM Micrograph 90Ti10Sn Samples (Magnification: 1.40 k SE)	
(a) 90Ti10Sn-1: 94.50%	**(b) 90Ti10Sn-2: 97.19%**
(c) 90Ti10Sn-3: 98.21%	**(d) 90Ti10Sn-4: 98.51%**
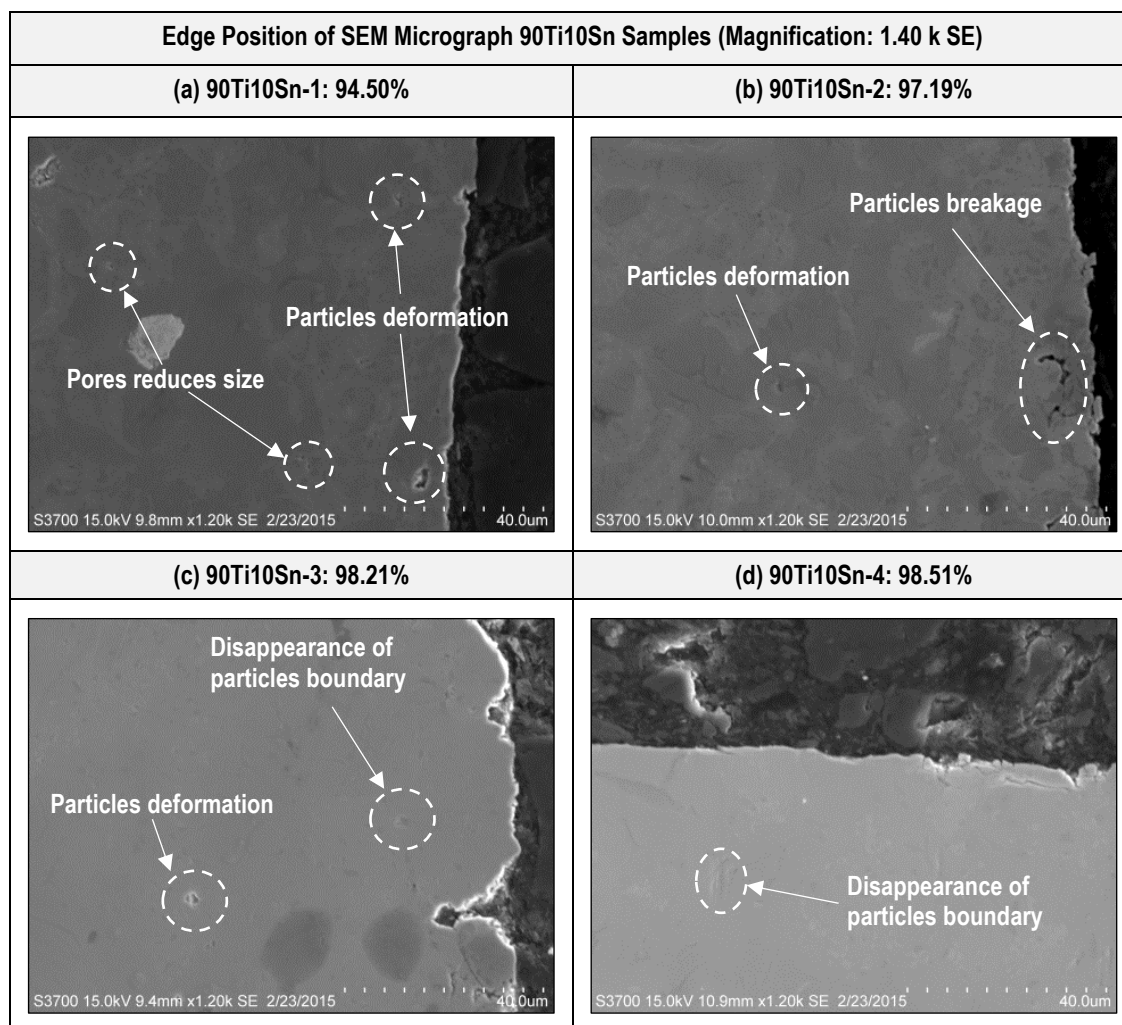
Table 6.5-16: Chemical element weight percentage of carbon (wt%) at the positions centre and edge of 90Ti10Sn samples.

Positions of Inspections	Units	90Ti10Sn-1	90Ti10Sn-2	90Ti10Sn-3	90Ti10Sn-4
Centre of the Samples	**wt.%**	2.57	2.71	2.58	2.70
Edge of the Samples	**wt.%**	2.72	2.87	2.80	2.75

Concerning the chemical element weight percentage carbon of 90Ti10Sn samples also shows in **Table 6.5-16** and **Figure 6.5-9**. The range was indicated of 2.58 to 2.71 wt% for the centre position and 2.72 to 2.87 wt% for the edge location. The results regarding the contamination of carbon element for 90Ti10Sn samples was better compared to Ti samples as stated in **Table 6.5-13**.
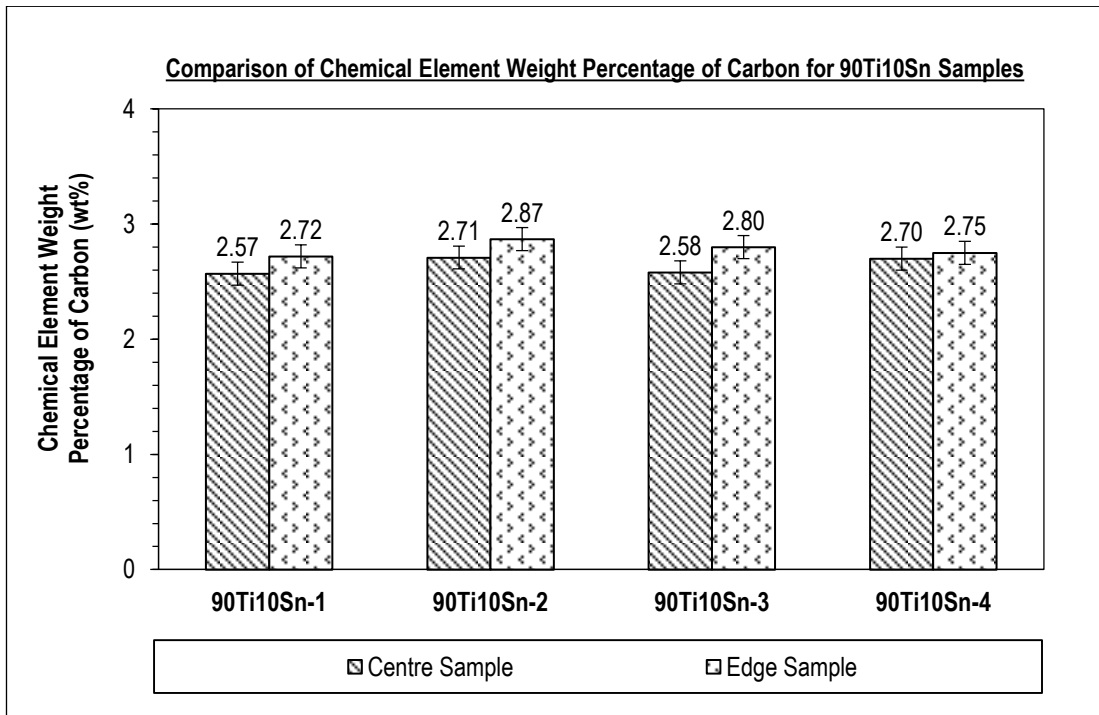
Figure 6.5-9: Comparison of chemical element weight percentage of carbon (wt%) located at centre and edge of 90Ti10Sn samples.

6.5.4. Samples Hardness

Based on the best relative density samples of Ti and 90Ti10Sn, it has been chosen to conduct the samples hardness test. The initial micro-hardness test has been carried out to Ti samples, and further investigation has been performed by using nano-hardness test for samples Ti and 90Ti10Sn.

6.5.4.1. Titanium (Ti)

Sample Ti-4 has been chosen for the micro- and nano-hardness test due to its relative densification was the higher compare to the others Ti samples. As in **Figure 6.5-10**, it shows the position of micro-hardness indentation of Ti-4 samples by using ZHVµ Micro Vickers hardness tester. Seven indentations have been made for the horizontal and vertical at the surface and half of the full height Ti-4 sample which was two millimetres. The position for tag number one was nearer to the edge of the sample Ti-4, meanwhile as the value of tag for indentation increasing to seven it was nearer to the centre of the samples Ti-4. The micro-

113

hardness force used was 1,000 gf with the dwell time of five seconds for both surface and inside indentation of sample Ti-4. The detailed data for each indentation can be found at **Table 6.5-17**.
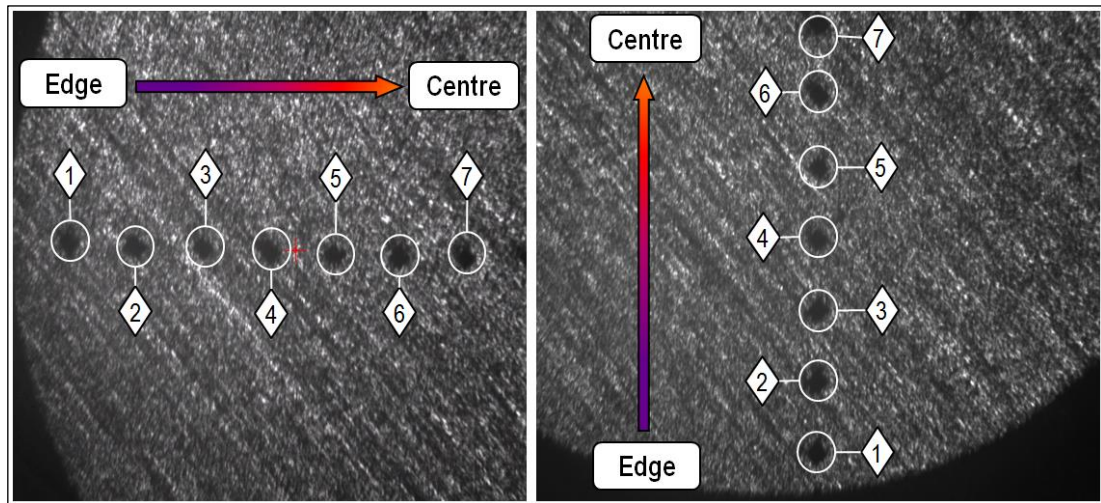
Figure 6.5-10: Position of micro-hardness indentation of Ti-4 sample by using ZHVμ Micro Vickers hardness tester.

Table 6.5-17: Micro-hardness test (HV) data for surface and inside (half of the full height sample: 2.00 mm) microstructure of Ti-4 sample.

Indentation No.	Surface Ti-4 Sample (HV)				Inside Ti-4 Sample (HV)			
	Horizontal	Vertical	Average	Standard Deviation	Horizontal	Vertical	Average	Standard Deviation
1	202	208	205.0	± 3.0	199	204	201.5	± 2.5
2	211	208	209.5	± 1.5	205	211	208.0	± 3.0
3	211	219	215.0	± 4.0	199	207	203.0	± 4.0
4	207	262	234.5	± 27.5	208	206	207.0	± 1.0
5	212	247	229.5	± 17.5	199	200	199.5	± 0.5
6	230	212	221.0	± 9.0	198	204	201.0	± 3.0
7	248	238	243.0	± 5.0	204	206	205.0	± 1.0

Based on the illustrated bar chart in **Figure 6.5-11**, it shows that the micro-hardness value at the surface of sample Ti-4 was increasing from the average value of 205 HV for indentation one (edge) to 243 HV for indentation seven (centre). The difference of the micro-hardness value was influenced by the weight percentage of contamination carbon element

existing at the centre and edge of surface sample Ti-4. According to Ogden and Jaffee [139] which has been made a research regarding the hardness of unalloyed titanium and Chu et al. [140] by using Ti-13Cr stated that the value of hardness was increased as the weight percentage of carbon element increased. Therefore, it supported the statement as mention in **Table 6.5-13** where it showed the value of the weight percentage of carbon element at the centre was 3.18 wt% for sample Ti-4 was higher compared to the edge which was 3.07 wt%.
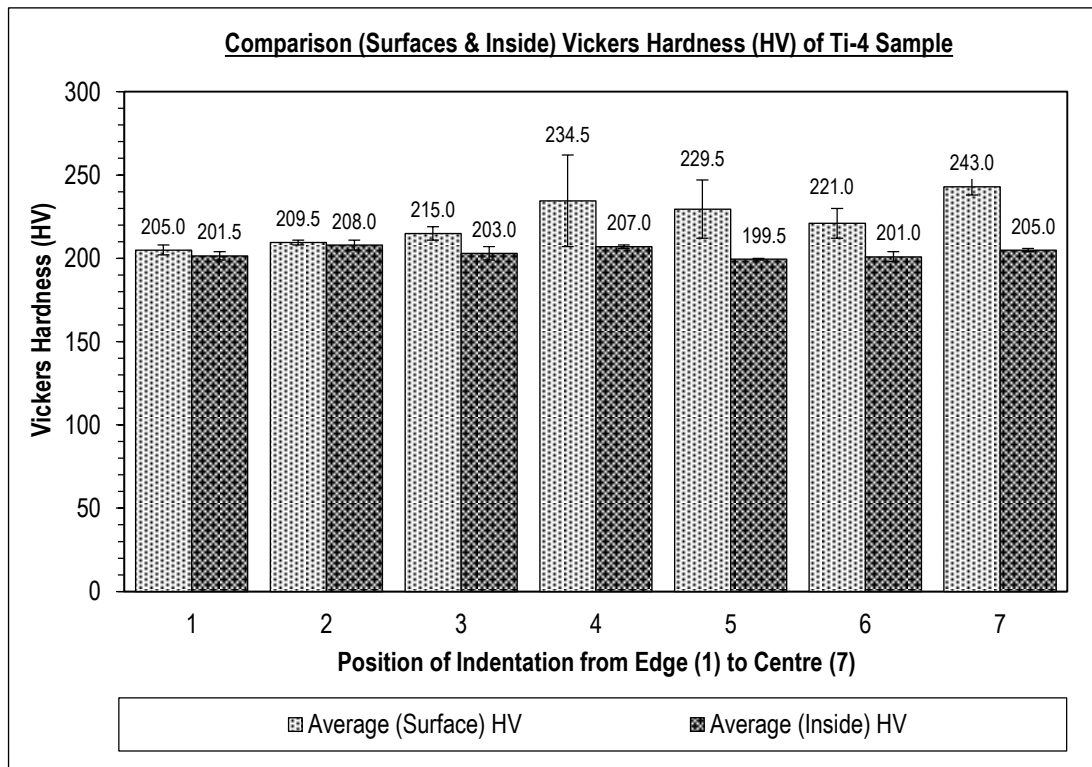
Figure 6.5-11: Comparison micro-hardness test value (HV) for surface and inside (half of the full height sample: 2.00 mm) microstructure of Ti-4 sample.

The extensive analysis also has been made where the sample Ti-4 has been polished until half of the full sample height which made the sample Ti-4 height becomes two millimetres to eliminate the carbon contamination. By using the same position as shown in **Figure 6.5-10**, seven indentations of hardness sample has been made. Based on the detail data provided in **Table 6.5-17** and bar chart in **Figure 6.5-11**, it shows the micro-hardness value for inside the sample Ti-4 to be more consistent with the value of 201.5 HV to 205 HV for the indentation one (edge) to seven (centre) respectively.
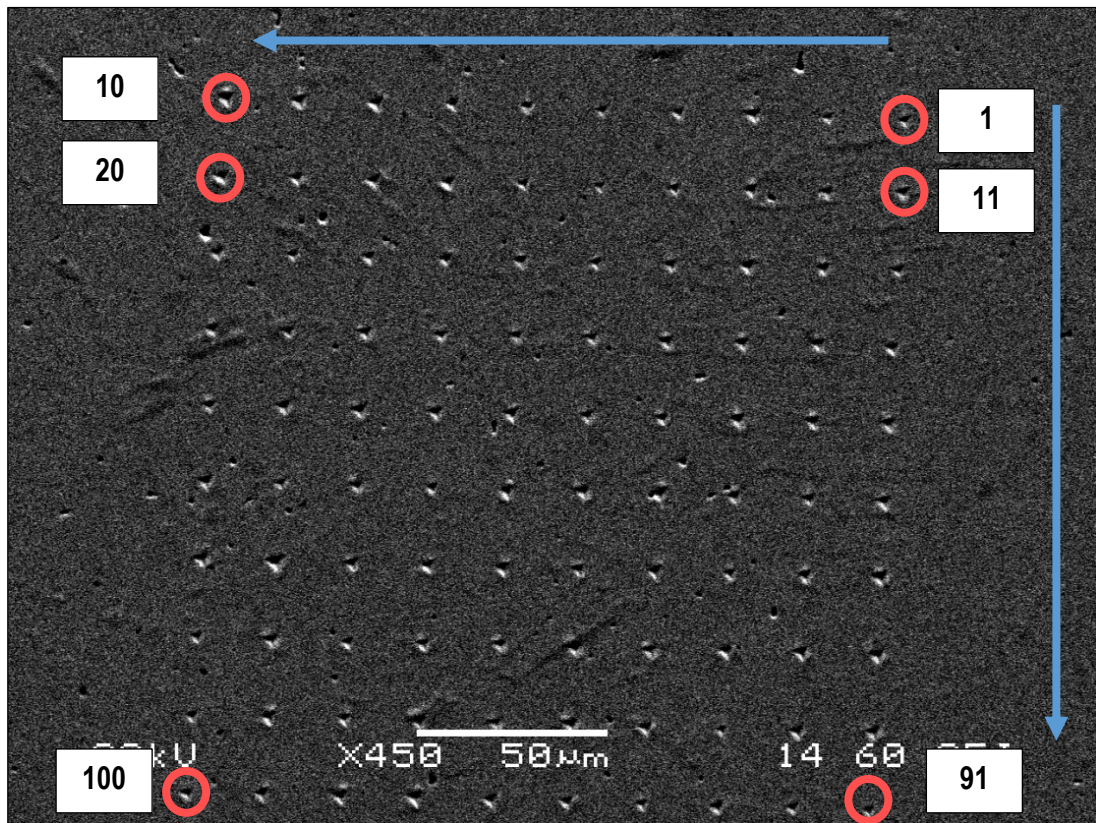
Figure 6.5-12: Position of nano-hardness indentation of Ti-4 sample by using NanoTest Vantage hardness tester.

Table 6.5-18: Average value for nano-hardness test for Ti-4 by using NanoTest Vantage hardness tester.

Results	Units	Means	Errors
Max Depth	nm	523.2280	42.3289
Plastic Depth	nm	486.34690	44.51551
Maximum Load	mN	20.02	0.00
Hardness	GPa	**2.914900**	**0.485036**
Reduced Young Modulus, Er	GPa	**132.6744**	**5.5850**
Elastic Recovery Parameter, ERP		0.076875	0.011983
Contact Compliance	nm/mN	2.456280	0.171244
Plastic Work	nJ	3.493967	0.330311
Elastic Work	nJ	0.583074	0.032564
Fit MSE		0.005174	0.001477

By using the NanoTest Vantage hardness system, 100 indentations have been made as in **Figure 6.5-12** for the analysis of nano-hardness test on sample Ti-4. Based on the

consistency of the micro-hardness test reading at the inside of the sample Ti-4 before this, the nano-indentations of the sample Ti-4 also have been made in the same condition. As a result in **Table 6.5-18** shows the average value for 100 indentations of nano-hardness that has been made which indicated the reading for the nano-hardness value was 2.9149 GPa and the reduced Young Modulus (Er) was 132.6744 GPa. Meanwhile, in **Figure 6.5-13** also shows the distribution of nano-hardness and reduced young modulus (Er) value for sample Ti-4.
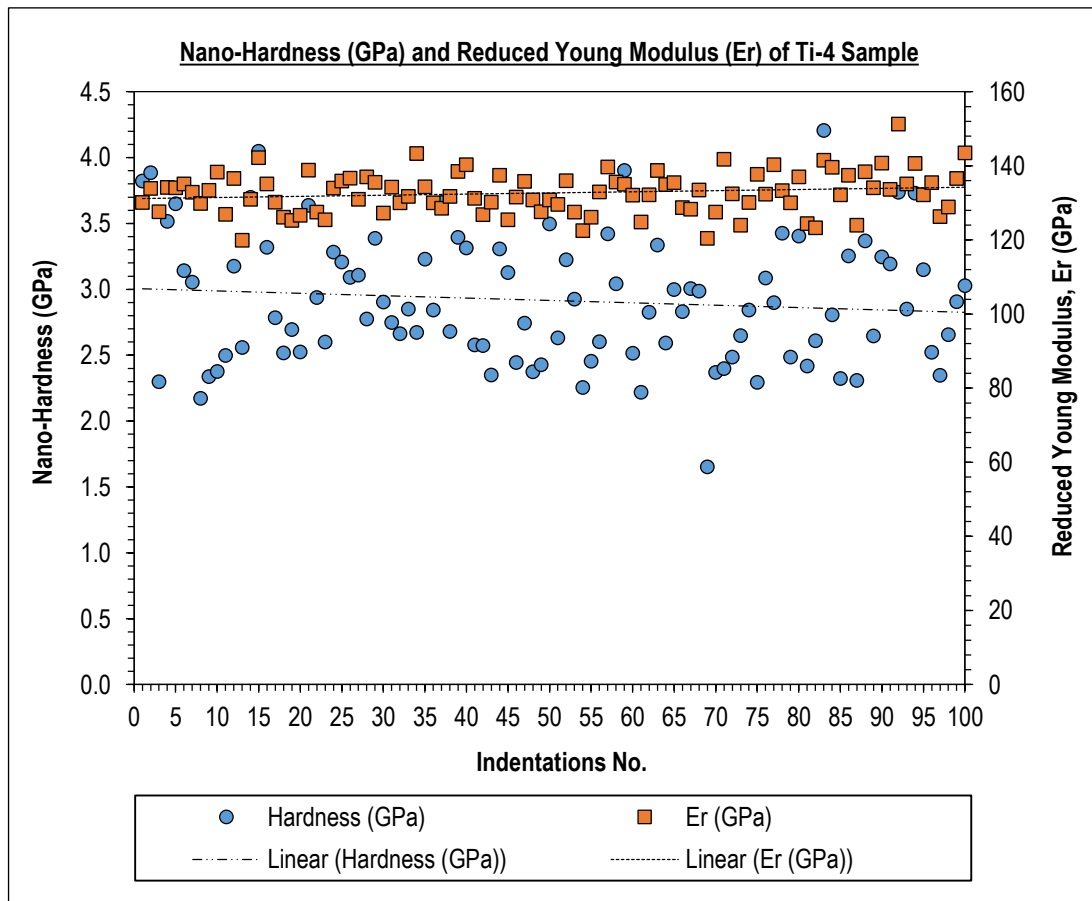
Figure 6.5-13: Distribution of nano-hardness and reduced Young Modulus (Er) value for Ti-4.

6.5.4.2. Titanium Tin Alloy (90Ti10Sn)

The nano-hardness test has been done at the sample 90Ti10Sn-4 by using NanoTest Vantage hardness tester as shown in **Figure 6.5-14** due to its higher relative densification recorded which was 98.51%. Meanwhile, in **Table 6.5-19** shows the average value for 100 indentations of nano-hardness that has been made which indicated the reading for the nano-hardness and reduced Young Modulus (Er) value was 5.637277 GPa and 113.1747 GPa

respectively. In **Table 6.5-15** also shows the distribution of nano-hardness and reduced Young's modulus (Er) value for the sample 90Ti10Sn-4.
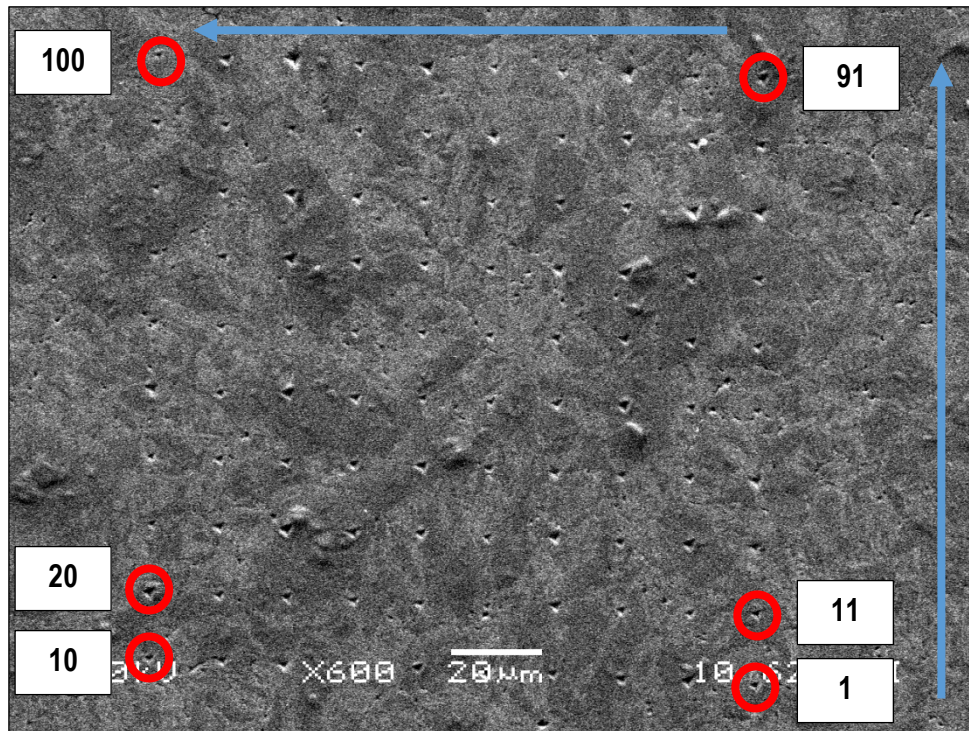
Figure 6.5-14: Position of nano-hardness indentation of 90Ti10Sn-4 sample by using NanoTest Vantage hardness tester.

Table 6.5-19: Average value for nano-hardness test for 90Ti10Sn-4 by using NanoTest Vantage hardness tester.

Results	Units	Means	Errors
Max Depth	nm	406.3308	63.5915
Plastic Depth	nm	344.65590	60.28239
Maximum Load	mN	20.02	0.00
Hardness	GPa	**5.637277**	**1.452738**
Reduced Young Modulus, Er	GPa	**113.1747**	**21.7738**
Elastic Recovery Parameter, ERP		0.183057	0.040490
Contact Compliance	nm/mN	4.107555	0.817621
Plastic Work	nJ	2.216614	0.531322
Elastic Work	nJ	0.968589	0.216421
Fit MSE		0.002170	0.001004
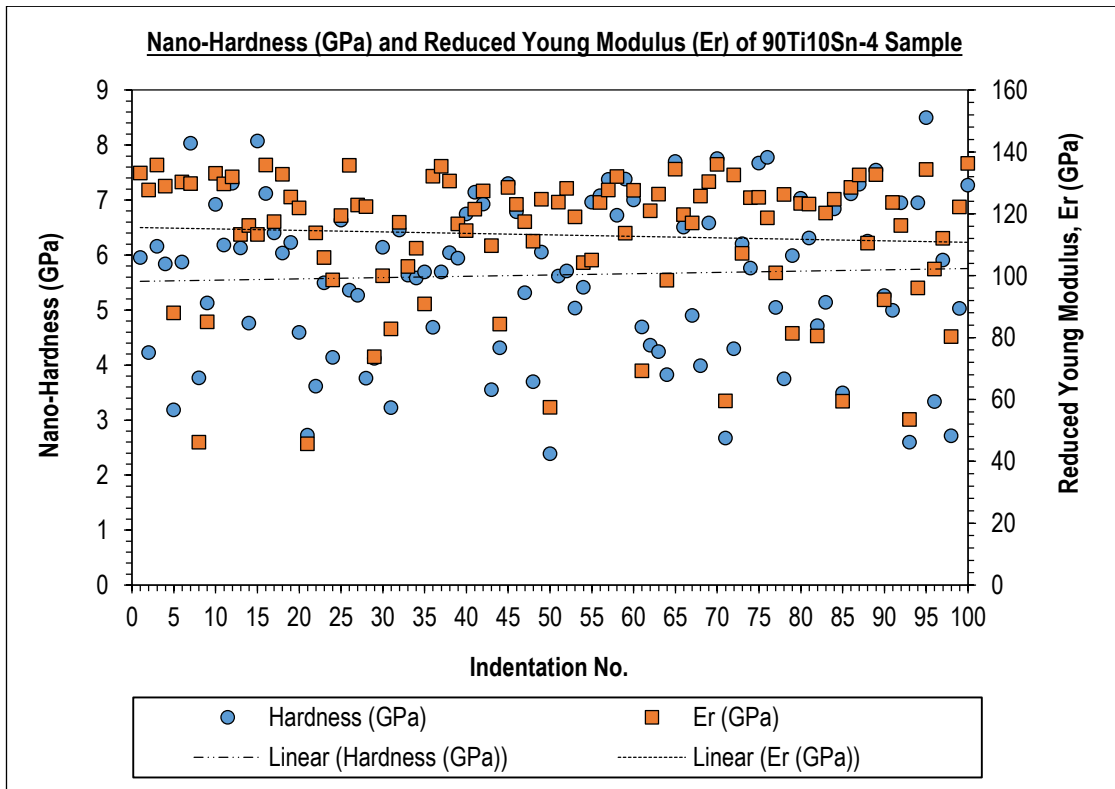
Figure 6.5-15: Distribution of nano-hardness and reduced Young Modulus (Er) value for 90Ti10Sn-4.

6.6. Summary of the Chapter

Based on the work that has been made in this chapter, it can be summarised that the efficiency of the used die set during the electrical-field activated sintering and forming process plays a significant contribution towards the sample size and its densification. It was an ideal condition to have a fully closed die set during the experiment so that the current could pass through the overall die set and produce heat more efficiently. It could speed up the die set heating compared to if it has a gap where the current flow only could pass through the nose tips of the punches and towards the powder materials. As a result, the efficiency of the heating process would be lower. In addition to that, the sample size also could be more precise to the design sample which was four millimetres in diameter and height respectively. For example, the sample Ti-3 and Ti-4 shows a better dimensional measurement compared to the others Ti sample as stated in **Table 6.5-1** by using the die set A. Meanwhile, by using the optimised die set B, all the 90Ti10Sn samples shows the better dimension reading due to the die set B was fully closed at end of the experiment as shown in **Table 6.5-3**.

Concerning the densification of the Ti and 90Ti10Sn samples during electrical-field activated sintering and forming process, it shows that Ti-4 and 90Ti10Sn-4 have the highest relative densification of 98.55% and 98.51% compared to the others Ti and 90Ti10Sn samples with the process total time of 161 s and 138.5 s respectively. By using this efficiency process, it has the potential to save time compared to the conventional electroplasticity sintering process. For the Ti-4 sample, it was used the optimum parameters of 125 MPa for the applied pressure, 1,100 °C for the second heating temperature, 100 °C/s for the second heating rate and five seconds for the second holding time. Meanwhile, for the 90Ti01Sn-4 sample, it was used the optimum parameters of 125 MPa for the applied pressure, 1,150 °C for the second heating temperature and 25 °C/s for the second heating rate and five seconds for the second holding time. All the others parameters of the first heating stage process parameters for the Ti-4 and 90Ti10Sn-4 samples was the same which was 200 °C for the first heating, 20 °C/s for the second heating rate and 30 s for the first holding temperature. The cooling rate for the Ti-4 used 10 °C/s and 90Ti10Sn-4 used 20 °C/s. By using high heating temperature, heating rate, holding time and applied constant pressure during the electrical-field activated sintering and forming process, it helps the deformation and breaking of the particles during the formation process for Ti and 90Ti10Sn samples. It differed from the conventional powder sintering process methods, where neck and grain growth are critical mechanisms needed to achieve the densification.

Regarding the presence of carbon element at the centre and edge of Ti and 90Ti10Sn samples, it shows a small amount of carbon contamination. For Ti samples, it indicates the reading was in the range of 2.54 to 3.64 wt% for the centre and 3.07 to 4.82 wt% for the edge location. Meanwhile, for 90Ti10Sn samples, it showed the reading was in the range of 2.58 to 2.71 wt% for the centre and 2.72 to 2.87 wt% for the edge location. It was due to the drawback when using graphite material for punches or die where the carbon can be mixed into solidified sample during the high-temperature sintering process. Furthermore, based on the highest densification of Ti and 90Ti10Sn samples, it has been chosen for testing of micro- and nano-hardness. Micro-hardness tests have been made for sample Ti-4. It indicated the average reading of 205 to 243 HV at the surface and 199.5 to 208 HV at the inside of the sample Ti-4. For nano-hardness testing, Ti-4 and 90Ti10Sn-4 have been applied with 100 indentations which show the hardness value of 2.9149 GPa and 5.637277 GPa value respectively.

Chapter 7: Open-Air Sintering with a Projection Welding Machine

7.1. Introduction

Based on the experiments that have been made using the Gleeble® 3800 machine and after obtaining the guideline values of the optimum parameters to produced high densification components, experiments have been performed using Projection Welding machine in the open-air environment for the electrical-field activated sintering and forming process. The purpose of adopting the Projection Welding machine in this process was to deliver the same capabilities as the Gleeble® 3800 machine which will be used more practically in the factory rather than the Gleeble® 3800 machine which more suitable for experimental purposes. In addition to that, it was a further study comparison of densification samples for the vacuum and open-air working environment. In **Figure 7.1-1** shows the stock Projection Welding machine before the modification of the die set holder and the insertion of a neoprene rubber sheet for the excessive pressure absorption. In **Table 7.1-1** shows the details regarding technical specifications for type 100 of Projection Welding machine used in the open-air electrical-field activated sintering and forming process. Meanwhile, for the input parameters of the process, the Projection Welding machine used the micro-processor of the Resistance Welding Controller (Model: BF 550).
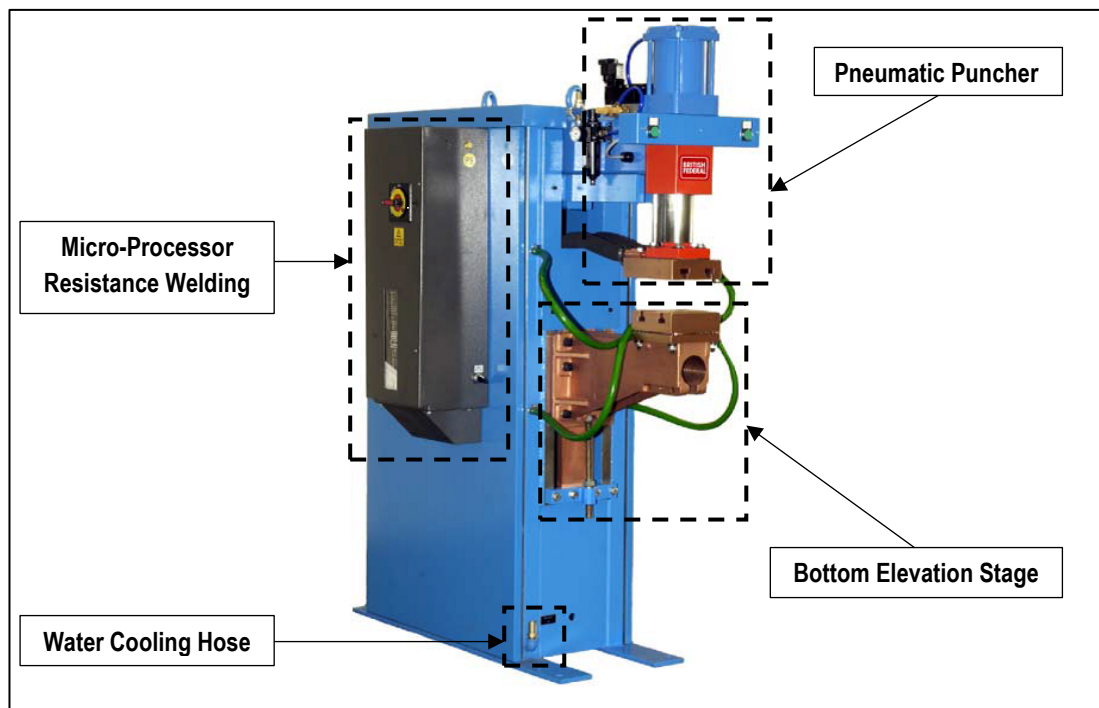
Figure 7.1-1: Stock Projection Welding machine.

Table 7.1-1: Technical specifications for type 100 of Projection Welding machine.

Technical Specifications	Units	Values
Continuous power at 100% duty cycle	kVA	70
Max short circuit power	kVA	330
Max welding power	kVA	350
Nominal power at 50% duty cycle	kVA	100
Nominal supply voltage	V	415
Continuous primary current at 100% duty cycle	A	170
Supply frequency	Hz	50
Supply phase	-	2
Supply capacity	kVA	200
HRC fuse size to BS88	A	200
Feed cable c.s.a up to 30m long	mm^2	70
Maximum short circuit primary current	A	800
Maximum short circuit secondary current	A	37,000
Maximum welding current	A	29,000
Duty cycle for maximum welding	%	7.1
Continuous secondary current at 100% duty cycle	A	7,299
Number of taps	-	3
Secondary open circuit volts	V	9.9
Weld cylinder diameter	mm	125
Weld force min/max with a 1.5/5.5 bar supply	kN	1.8/6.7
Weld force min/max with a 20/80 psi supply	lbf	400/1,500
Weld cylinder stroke max	mm	76
Air pressure normal	bar	5.5
Air pressure maximum operating	bar	7
Air connection/hose size	mm	12/10
Cooling water minimum operating pressure	bar	3
Cooling water consumption	lit/min	20
Cooling water maximum inlet temperature	°C	30
Cooling water connection/hose size	mm	12/19
Machine weight	kg	570
Machine size	mm	590W × 1,285D × 1,685H

7.2. Tooling for Projection Welding Machine

Two modifications have been introduced for the development of Projection Welding machine tooling which was die set holder and the installation of neoprene rubber pad for the excessive applied pressure absorption. The purpose of the die set holder for the Projection Welding machine as illustrated in **Figure 7.2-1** and **Figure 7.2-2** was made to hold the used die set during the open-air electrical-field activated sintering and forming process more securely without any slip. It was because, during the experiment process, the used die set must be position vertically to be compressed by the upper and lower punches of the Projection Welding machine which at the same time the electricity current flow also would be applied. Due to this matter, it would be dangerous if the used die set was not securely located without die set holder because the temperature involved in this process was very high which was reached to 1,300 °C. Meanwhile, for the development of excessive pressure absorption, the modification at the Projection Welding machine's puncher has been made by adding five neoprene rubber pad due to the pneumatic pressure system used in Projection Welding machine cannot be stop when it was not reached the maximum stroke and it cannot automatic adjust for a certain pressure as used in the hydraulic system for Gleeble® 3800 machine. Therefore, the padding for the applied pressure must be implementing in the improvement system of Projection Welding machine. In **Table 7.2-1** and **Table 7.2-2** shows the summary of the parts used for the die set holder for Projection Welding machine and neoprene rubber pad.

(a) Die Set Holder with Neoprene Rubber Pad   (b) Die Set Holder
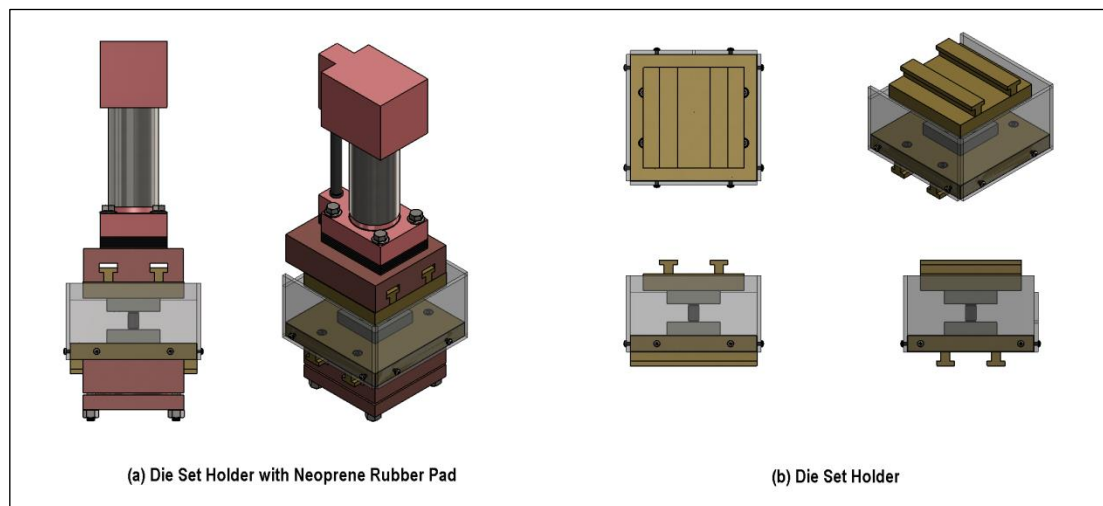
Figure 7.2-1: Die set holder with neoprene rubber pad.

Based on the observation after the installation of neoprene rubber pad for the absorption of excessive applied pressure by the Projection Welding machine, it was shown that the percentage of force was reduced about 49.46 to 72.03% depending on the air supply given as presented in **Table 7.3-1**. The average of reduction force before and after the installation of neoprene rubber pad was 1389.38 N and the average percentage was 57.87% which indicates a high absorption of force was been made. It was important to protect the graphite die set from breaks or defects by the excessive applied constant pressure because the graphite die set has a weakness where it has a low mechanical strength at the elevated temperature during the electrical-field activated sintering and forming process. Besides that, due to the high temperature heating involved in the electrical-field activated sintering and forming process, expansion of the die set and sample occurred. Therefore, it would be beneficial to have an absorption mechanism to allow an extra small space for the expansion to be released. It was different with Gleeble® 3800 machine due to it has an automatic adjustment for the expansion to be taking place while maintaining the applied pressure that has been assigned during the input parameter of the experiment. In **Figure 7.2-3** shows the comparison between the stock machine and after the complete installation of the tooling and neoprene rubber pad for Projection Welding machine.

ITEM NO.	PART NUMBER	MATERIAL	QTY.
1	Bottom Plate	Brass	1
2	Bottom Tool Guide	Brass	2
3	Bottom Die Set Plate	Tungsten Carbide	1
4	Die	Graphite Mersin 2333	1
5	Above Punch Die	Graphite Mersin 2333	1
6	Lower Punch Die	Graphite Mersin 2333	1
7	Above Die Set Plate	Tungsten Carbide	1
8	Above Plate	Brass	1
9	Above Tool Guide	Brass	1
10	B18.3.1M - 8 x 1.25 x 30 Hex SHCS -- 30SHX	Stainless Steel	8
11	B18.3.1M - 6 x 1.0 x 25 Hex SHCS -- 25SHX	Stainless Steel	8
12	Side Guard	Clear Polycarbonate	2
13	Front Guard	Clear Polycarbonate	1
14	B18.6.7M - M5 x 0.8 x 25 Type I Cross Recessed PHMS -- 25S	Steel	8
15	Back Guard	Clear Polycarbonate	1

Figure 7.2-2: Details part of die set holder.

Table 7.2-1: Summary of die set holder tooling.
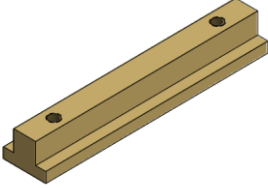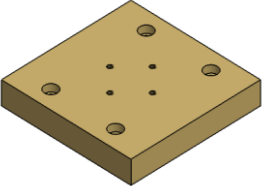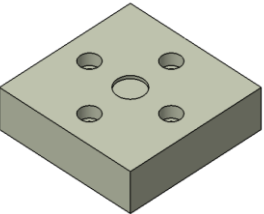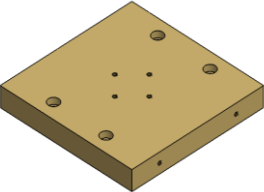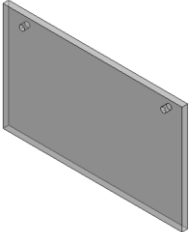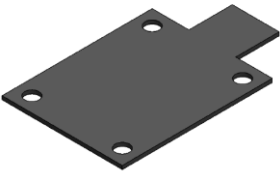
Design of Parts	Descriptions	
	Name	Above and Bottom Tool Guide.
	Material	Brass.
	Quantity	Four units.
	Note	It was inserted to the Above and Bottom Elevation Plate of Projection Welding machine and was tightens with stainless steel hexagon socket screw M8 × 30 mm.
	Name	Above Plate.
	Material	Brass.
	Quantity	One unit.
	Note	It was pair with Bottom Tool Guide and was tightens with stainless steel hexagon socket screw M8 × 30 mm. At the middle of the Above Plate, the Above Die Set Plate will be located and locked with stainless steel hexagon socket screw M6 × 25 mm.
	Name	Above and Bottom Die Set Plate.
	Material	Tungsten carbide.
	Quantity	Two units.
	Note	The dies set would be positions in the middle cup with the depth of 1.5 mm. The Above and Bottom Die Set Plate mount together to Above and Bottom Plate with stainless steel hexagon socket screw M6 × 25 mm.
	Name	Bottom Plate.
	Material	Brass.
	Quantity	One unit.
	Note	It was pair with Bottom Tool Guide and was tightens with stainless steel hexagon screw M8 × 30 mm. At the middle of the Bottom Plate, the Bottom Die Set Plate will be located and locked with stainless steel hexagon socket screw M6 × 25 mm. At the perimeter side of it, there was a hole for mounting clear polycarbonate Guard with steel screw M5 × 25 mm.
	Name	Front, Side and Back Guard.
	Material	Clear polycarbonate.
	Quantity	Four units.
	Note	It was mounting to the Bottom Plate with steel screw M5 × 25 mm. The purpose of it was to protect the user from spark which might be occurred during the open-air electrical-field activated sintering and forming process.

Table 7.2-2: Summary of Neoprene Rubber Pad.

Design of Part	Description	
	Name	Rubber Pad.
	Material	Neoprene.
	Quantity	Five units.
	Note	It was mounting to the puncher of Projection Welding machine. The purpose of it was to absorb the excessive applied pressure during the process. Each of the neoprene rubber pads has the thickness of three millimetres which made the total height for five units be 15 mm.
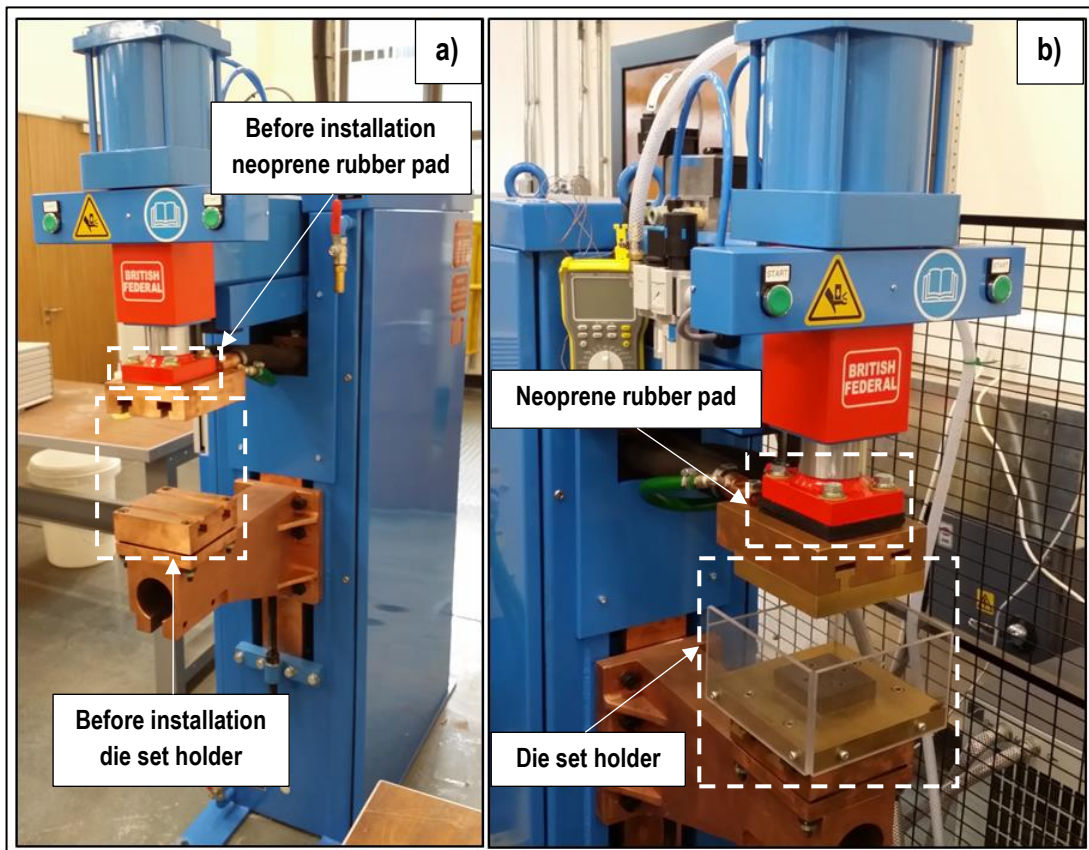
Figure 7.2-3: Comparison between **(a)** stock Projection Welding machine and **(b)** after complete installation of the tooling for Projection Welding machine.

7.3. Force Management

Meanwhile, regarding the force management for Projection Welding machine, there were two steps on how to accomplish this situation for the pneumatic puncher system. It has been done to maintain the applied force needed in the experiment of open-air electrical-field

activated sintering and forming process. The first step was to increase the air supply of the Projection Welding machine to the appropriate force needed as desired based on the references in **Table 7.3-1**. If it was still not enough applied force required, the second step could be done by manually lifting up of small gap towards the bottom elevation stage as illustrated in **Figure 7.3-1** of the Projection Welding machine so that the range space between punches and die set would be smaller and the Projection Welding machine's puncher would compress more.

Table 7.3-1: Percentage of differentiate force before and after installation of neoprene rubber pad at Projection Welding machine.

Air Supply	Before Rubber Sheet	After Rubber Sheet	Different Force Before – After Installation	
Bar (10^5 Pa)	Force (N)	Force (N)	Force (N)	Percentage (%)
2.6	1738	486	1252	72.03
2.8	1903	581	1322	69.48
3.0	1961	680	1281	65.32
3.2	2047	742	1305	63.75
3.4	2151	826	1325	61.60
3.6	2248	898	1350	60.05
3.8	2329	981	1348	57.88
4.0	2442	1076	1366	55.94
4.2	2526	1125	1401	55.46
4.4	2622	1162	1460	55.68
4.6	2712	1255	1457	53.72
4.8	2744	1308	1436	52.33
5.0	2849	1382	1467	51.49
5.2	2906	1411	1495	51.45
5.4	2967	1477	1490	50.22
5.5	2982	1507	1475	49.46
Average			1389.38	57.87

Typically, the force needed for the electrical-field activated sintering and forming experiment by using Gleeble® 3800 machine was in the range of 900 to 1,600 N for the material Ti and 90Ti10Sn to achieve the samples densification above 92%. Therefore, by the application of the neoprene rubber pads after the reduction of excessive applied force, the

existing force was still in the range needed in the experiment which indicated the reading of 486 to 1,507 N as shown in **Table 7.3-1**. In **Figure 7.3-2** and **Figure 7.3-3** below also showed the comparison force measurement graph before and after the installation neoprene rubber pad.

Figure 7.3-1: Stock Projection Welding machine measurements and name of the section parts.

Figure 7.3-2: Graph of force measurement for Projection Welding machine before installation of neoprene rubber pad.

129

Figure 7.3-3: Graph of force measurement for Projection Welding machine after installation of neoprene rubber pad.

7.4. Heating Control

Regarding the heating control on the process parameter with the Projection Welding machine, several repetitions of the heating process have been done by using die set B without powder as illustrated in **Figure 7.4-1**. Meanwhile, in **Figure 7.4-2** shows the schematic drawing of the Projection Welding machine tooling and current flows with applied pressure during the open-air electrical-field activated sintering and forming process. The setting force for the heating control experiment was set to 3.6 bar (898 N) which has been measured before this at **Table 7.3-1**. Therefore, by using die set B, the applied pressure value for 3.6 bar (898 N) was 71.46 MPa. The pulsation for the heating control process was set from one to nine pulses to shows the variants of the total process time which significantly influences the heating temperature of the process. The percentage of used current of 2.00 to 6.00 kA also has been limited to 10 to 20% which already gives the range of the temperature needed in the experiment. The detail regarding achieved temperature has been described in **Figure 7.4-4**, **Figure 7.4-5** and **Figure 7.4-6**. Meanwhile for the others parameters used in the heating control process was shown below in **Table 7.4-1** which is the same for all the used current.
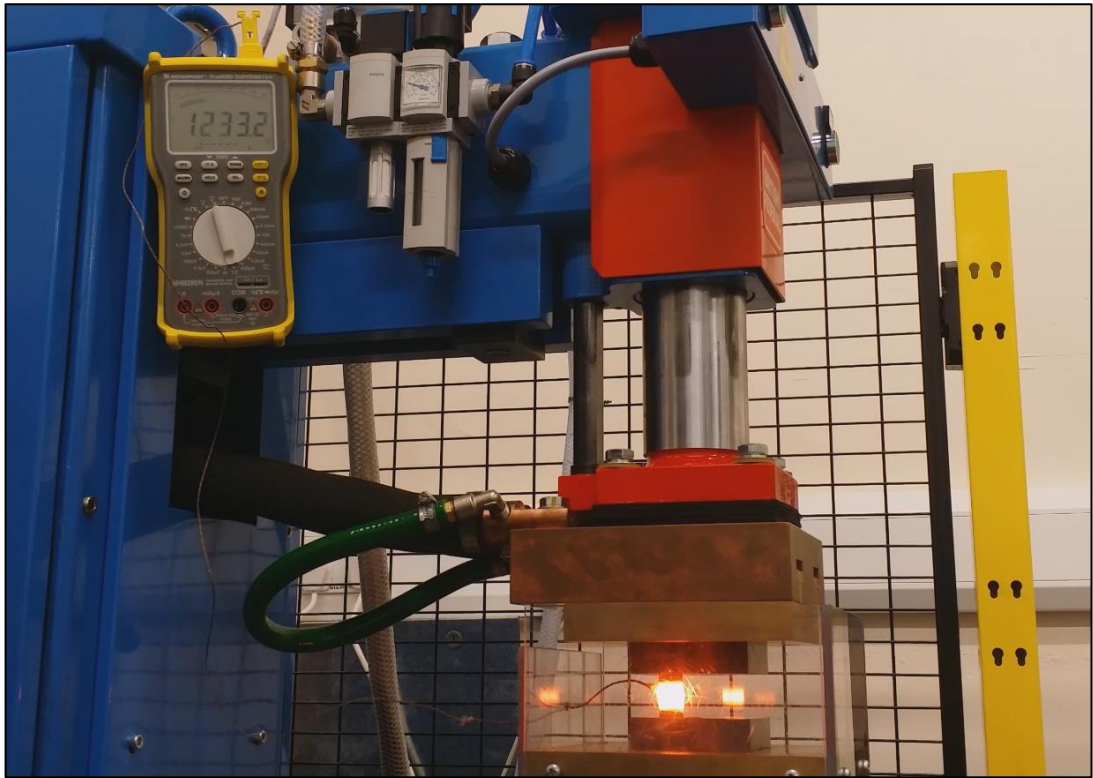
Figure 7.4-1: Die set with powder material during the open-air electrical-field activated sintering and forming experiment using Projection Welding machine.
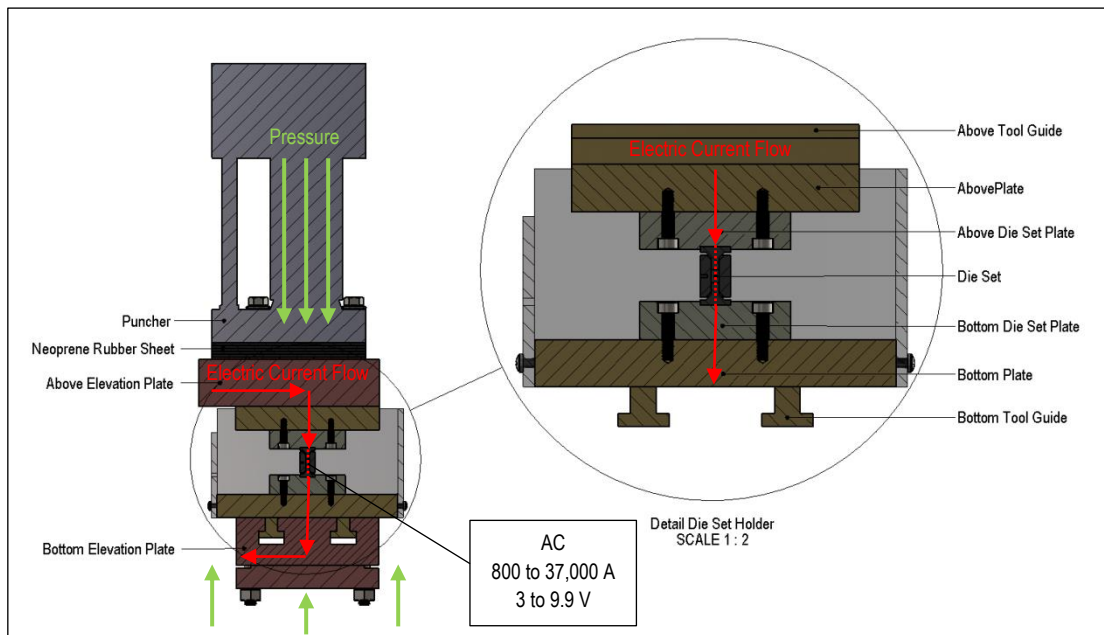
Figure 7.4-2: Schematic drawing of the Projection Welding machine tooling and current flows (red arrows) during the open-air electrical-field activated sintering and forming process.

Table 7.4-1: Constant parameter of heating control process for 2.00 kA, 4.00 kA and 6.00 kA with the range of pulsation from one to nine pulses.

Constant Parameter	Symbol	Value	
		Cycle Units	SI Units
Force	F		898 N
Pressure	P		71.46 MPa
Pre-squeeze time	PSQ	250 Cycle	5 s
Squeeze time	SQ	250 Cycle	5 s
Up slope time	U1	30 Cycle	0.6 s
First weld time	W1	99 Cycle	1.98 s
First cool time	CL1	99 Cycle	1.98 s
Second weld time	W2	99 Cycle	1.98 s
Second cool time	CL2	99 Cycle	1.98 s
Down slope time	DS	30 Cycle	0.6 s
Hold time	HT	250 Cycle	5 s
Off time	OFF	250 Cycle	5 s

7.4.1. Sequence of the Machine Control
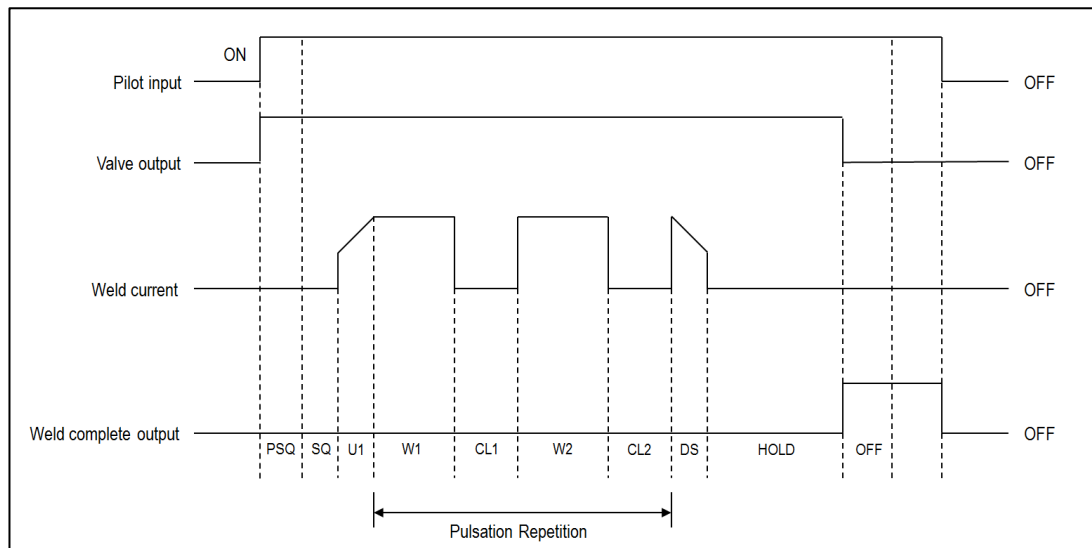
Figure 7.4-3: Basic sequence operation of Projection Welding machine.

Based on **Figure 7.4-3**, this shows the basic sequence of operation of the Projection Welding machine. In this diagram, it only demonstrates the case study for one pulsation

repetitions. The parameters such as first weld time, first cool time, second weld time and second cool time were prepared for the set number of pulsation repetitions which in this heating control process has been applied from one to nine pulses. Below was the detailed descriptions of the parameters that have been used in the heating control process and experiment of open-air electrical-field activated sintering and forming process with the Projection Welding machine.

a) Pre-Squeeze Time (PSQ) – [0 to 250 Cycles]

During this time interval, the electrodes move into contact with the parts to be heated. Pressure built during this period and maintained through the heating sequence until the hold period ends. The process for pre-squeeze time can be set from zero to 250 cycles or which can be stated as from zero to five seconds.

b) Squeeze Time (SQ) – [1 to 250 Cycles]

As the electrode pressure was built up and stabilised, the electrodes fully come into contact with the die set. Therefore, squeeze time was provided for this purposed. The process for squeeze time can be configured from one to 250 cycles or which can be stated as from 0.02 to five seconds.

c) Up-Slope Time (U1) – [0 to 30 Cycles]

In the heat interval of heating sequences, the weld current may be programmed to rise (increase gradually) over a number of up-slope cycles from 10% of the value to the full value of first heat current. The time for up-slope time can be set from zero to 30 cycles or which can be stated as from zero to 0.6 s.

d) First Weld Time (W1) and Second Weld Time (W2) – [0 to 99 Cycles]

The number of cycles for which the actual heating current flows can be programmed for each heating time interval where it could be from zero to 99 cycles or which can be stated as from zero to 1.98 s.

e) First Weld Current and Second Weld Current (I1 and I2) – [2 to 60 kA]

The current for first and second heating can be set from two to 60 kA. The primary current was measured for each cycle. Based on this data, the firing angle was adjusted to get the required weld current.

f) Percentage of First and Second Heat (H1 and H2) – [0 to 99%]

The current was set as a percentage of maximum heat which was from zero to 99%. Maximum current depends on the capacity of the first weld current that has been set.

g) First and Second Cool Time (CL1) – [0 to 99 Cycles]

Current does not flow during this interval and allow the electrode and welding transformer to cool before the next heating sequences apply and the electrodes remain in contact with the die set. The time for first and second cool time can be adjusted from zero to 99 cycles which also can be stated from zero to 1.98 s.

h) Down Slope (DS) – [0 to 30 Cycles]

In the heat interval of heating sequences, the weld current may be programmed to decrease gradually over a number of down slope cycles from 10% of the value to the full value of second heat current. The time for up-slope time can be set from zero to 30 cycles or which can be stated as from zero to 0.6 s.

i) Hold Time (HOLD) – [0 to 250 Cycles]

Heating sequences end with hold period, where the weld was allowed to cool under the electrode pressure. Electrode pressure created at the pre-squeeze period was released at the end of the hold time. The process for hold time can be set from zero to 250 cycles or which can be states as from zero to five seconds.

j) Pulsation (PS) – [1 to 9 Times]

The pulsation time indicates that the number of occasions for the first weld time, first cool time, second weld time and second cool time would repeat which from one to nine times in the same heating sequences.

7.4.2. Energy Required for Heating the Die Set and the Sample Material

By assuming the whole die set and material are heated up to the same temperature, a simplified calculation of the energy and power required for heating the die set and sample material are being made as below. Based on equation **(7.4-1)**, the amount of the heat needed to raise the temperature can be calculated.

$$Q = C_p . m . dT \qquad \text{(7.4-1)}$$

Symbols in equation (7.4-1):

| Q | - | Amount of heat required. | m | - | Mass of heated part. |
| C_p | - | Specific heat of heated part. | dT | - | Temperature different. |

Based on the equation **(7.4-1)**, therefore for the total amount of heat required to raise the desired temperature for the die set and the sample are stated as on the equation **(7.4-2)**.

$$Q = \left[(C_{P1} . m_{Die\ Set}) + (C_{p2} . m_{Sample}) \right] . dT \qquad \text{(7.4-2)}$$

C_{P1} - Specific heat for material of die set used. | $m_{Die\ Set}$ - Mass of die set.

C_{P2} - Specific heat for material of sample used. | m_{Sample} - Mass of sample.

Hence, if the amount of heat required (Q) rising to the certain temperature was fully consumed, the amount of heat (Q) calculated was equal to energy (E) employed as stated in equation **(7.4-3)**.

$$Q = E \qquad\qquad\text{(7.4-3)}$$

Thus, the power (P) required to raise the die set and sample at the specified time and specific temperature can be calculated as in equation **(7.4-4)**.

$$P = \frac{E}{T} \qquad\qquad\text{(7.4-4)}$$

Symbols in equation (7.4-3) and (7.4-4):

P - Power required raising the die set and sample to specific temperature and time.

E - Energy required for heating the die set and sample material.

T - Process time duration.

Due to the limitations of controlling the parameters in the Projection Welding machine, where it only can be set the time and current of the process, the comparison of power value can be made to find the proper power adjustment to match the power needed in the experiment as calculated in equation **(7.4-4)**.

Based on **Table 7.1-1**, the continuous power at 100% duty cycle for Projection Welding machine was 70,000 VA or 70,000 W. Meanwhile, the range of first and second weld current was in between 2,000 to 60,000 A and for the percentage of first and second was in between zero to 99% as presented in the section **7.4.1 Sequence of the Machine Control**.

The actual current used during the first or second weld current at the specific percentage of the heat of experiment with Projection Welding machine was as in equation **(7.4-5)**.

$$I_{Actual} = I.H \qquad\qquad (7.4\text{-}5)$$

Symbols in equation (7.4-5):

I_{Actual} -   Actual current used during the experiment with Projection Welding machine.

I -   First or second weld current.

H -   Percentage of first or second heat.

After that, the ratio of the actual current during the experiment with the maximum of weld current which was 60,000 A used in the Projection Welding machine was determined as in the equation **(7.4-6)**.

$$R = \frac{I_{Actual}}{I_{Maximum}} \qquad\qquad (7.4\text{-}6)$$

Symbols in equation (7.4-6):

R -   Ratio of the actual current during the experiment with the maximum of weld current.

$I_{Maximum}$ -   Maximum weld current for Projection Welding machine.

Therefore, the power used based on the ratio of actual current during the experiment was calculated as the equation **(7.4-7)**.

$$P_{Used} = P_C.R \qquad\qquad (7.4\text{-}7)$$

Symbols in equation (7.4-7):

P_{Used} -   Power used based on ratio of actual current during the experiment.

P_C -   Continuous power at 100% of duty cycle for Projection Welding machine.

Compare the value of used power (P_{Used}) in the Projection Welding machine as in the equation **(7.4-7)** to power (P) required raising the die set and sample at the specified time and specific temperature as in the equation **(7.4-4)**. Therefore, to match the power needed as in the equation **(7.4-4)**, the input of weld current which is in the range of 2.00 to 60.00 kA and the percentage of heat which is in the range of zero to 99% can be adjusted accordingly.

Nevertheless, these descriptions of energy required for heating the die set and sample materials are an estimation and assuming the whole die set and material are heated up to the same temperature. However, in the real environment process of open-air electrical-field activated sintering and forming using Projection Welding machine, usually it requires more weld current and percentage of heat due to the heat transfer at the tooling and sample material.

7.4.3. Reference Heating Temperatures

In this section, it describes the reference of heating data temperature for the die set B without powder material using the Projection Welding machine for the open-air electrical-field activated sintering and forming process as shown in **Table 7.4-2**. It was because the Projection Welding machine cannot directly set the desired temperature required in the experiment. Therefore, with this data, it can be used as a guideline to establish the parameter of the experiment when using Projection Welding machine. In this reference, die set B has been chosen because it shows the best quality and efficiency compared to the die set A. The reference heating data temperature for die set B also used the weld current of 2.00 kA, 4.00 kA and 6.00 kA. Meanwhile for the percentage heat current from 10 to 20% and pulsation from one to nine pulses to shows the range of temperature can be achievable with the combination of the above stated parameter. The detail description of each heating current has been described at **7.4.3.1 Heating Current: 2.00 kA**, **7.4.3.2 Heating Current: 4.00 kA** and **7.4.3.3 Heating Current: 6.00 kA** as below. It focuses on the duration of the pulsation which influences the length of the process. Meanwhile, for the percentage of heat, it influences the outcome of the temperature used in the experiment process.

Table 7.4-2: Data for the heating temperature of the Projection Welding machine by usage of the die set B without powder material in the open-air electric-field activated sintering and forming process.

Current			2.00 kA	4.00 kA	6.00 kA
Heat (%)	Pulsation	Time (s)	Temperature (°C)		
10	1	29.12	88.2	106.2	107.2
	2	37.04	144.8	92.6	70.7
	3	44.96	161.7	137.1	148.1
	4	52.88	171.2	160.0	163.9
	5	60.80	155.2	170.8	182.2
	6	68.72	157.1	178.6	196.4
	7	76.64	171.1	179.3	209.6
	8	84.56	199.9	174.7	222.4
	9	92.48	198.5	167.7	223.9
12	1	29.12	126.4	111.3	48.6
	2	37.04	116.8	112.0	152.8
	3	44.96	182.2	136.4	190.3
	4	52.88	222.1	147.7	222.0
	5	60.80	233.2	166.5	242.5
	6	68.72	269.7	170.2	261.5
	7	76.64	199.1	175.0	271.5
	8	84.56	264.8	244.7	285.5
	9	92.48	253.0	269.1	282.2
14	1	29.12	98.5	117.9	56.6
	2	37.04	111.9	206.7	124.1
	3	44.96	175.3	244.3	149.9
	4	52.88	136.9	270.2	166.8
	5	60.80	145.6	296.2	286.3
	6	68.72	156.5	300.2	313.8
	7	76.64	200.4	309.6	334.5
	8	84.56	267.5	317.7	337.5
	9	92.48	256.9	319.0	349.0

Table 7.4-2 (Continued): Data for the heating temperature of the Projection Welding machine by usage of the die set B without powder material in the open-air electric-field activated sintering and forming process.

Current			2.00 kA	4.00 kA	6.00 kA
Heat (%)	Pulsation	Time (s)	Temperature (°C)		
16	1	29.12	102.3	135.2	65.5
	2	37.04	186.5	235.5	240.4
	3	44.96	233.6	277.4	299.6
	4	52.88	271.3	316.9	359.5
	5	60.80	306.2	353.7	386.0
	6	68.72	348.3	390.8	434.3
	7	76.64	368.5	419.5	467.6
	8	84.56	410.6	513.9	481.5
	9	92.48	452.3	550.4	501.0
18	1	29.12	125.4	163.2	76.6
	2	37.04	333.0	236.4	351.2
	3	44.96	402.7	284.1	436.7
	4	52.88	455.4	336.5	513.2
	5	60.80	505.2	387.7	579.8
	6	68.72	428.4	406.4	628.1
	7	76.64	556.3	496.3	671.8
	8	84.56	628.6	483.5	711.6
	9	92.48	512.4	519.6	619.3
20	1	29.12	153.0	176.2	84.5
	2	37.04	344.5	308.5	193.7
	3	44.96	462.2	376.4	252.5
	4	52.88	539.4	614.9	467.6
	5	60.80	654.5	622.5	850.1
	6	68.72	733.0	669.6	1,038.4
	7	76.64	805.5	664.7	1,126.4
	8	84.56	911.7	931.3	1,129.0
	9	92.48	963.1	1,054.9	1,257.2

7.4.3.1. Heating Current: 2.00 kA

By using the weld current of 2.00 kA, the graph in **Figure 7.4-4** shows that to achieve the heating temperature of 963.1 °C which was the highest temperature in this weld current, it required nine pulsations which made total time would be 92.48 s. Meanwhile, for the percentage of heat, it needs to be set to 20%. For the experiment open-air electrical-field activated sintering and forming process by using 90Ti10Sn materials, this was not an optimum parameter which can be used due to it requiring the temperature of 1,150 °C to achieve the densification sample above 98% based on the experiment done on the Gleeble® 3800 machine.

Current : 2.00 kA - Heating Temperature and Time Vesus of Pulsation

	PS: 1	PS: 2	PS: 3	PS: 4	PS: 5	PS: 6	PS: 7	PS: 8	PS: 9
H1 & H2 = 10%	88.2	144.8	161.7	171.2	155.2	157.1	171.1	199.9	198.5
H1 & H2 = 12%	126.4	116.8	182.2	222.1	233.2	269.7	199.1	264.8	253.0
H1 & H2 = 14%	98.5	111.9	175.3	136.9	145.6	156.5	200.4	267.5	256.9
H1 & H2 = 16%	102.3	186.5	233.6	271.3	306.2	348.3	368.5	410.6	452.3
H1 & H2 = 18%	125.4	333.0	402.7	455.4	505.2	428.4	556.3	628.6	512.4
H1 & H2 = 20%	153.0	344.5	462.2	539.4	654.5	733.0	805.5	911.7	963.1
Process Time	29.12	37.04	44.96	52.88	60.80	68.72	76.64	84.56	92.48

Figure 7.4-4: Graph of heating temperature and time versus the pulsation process of Projection Welding machine for current 2.00 kA.

7.4.3.2. Heating Current: 4.00 kA

Meanwhile, by using weld current 4.00 kA, the percentage of heat 20% and nine pulsations, the heating temperature can be achieved to 1,054.9 °C as presented in **Figure 7.4-5**. The total time for the heating process was 92.48 s. Therefore, it would be beneficial to

use this guideline for the experiment parameter tested with 90Ti10Sn material when using the Projection Welding machine. Nevertheless, this heating data has been used of the die set B without the powder material. Thus it might require a slight increment of the percentage of heat during the experiment due to the energy required to heat up the powder material. It is also shown that, from the pulsations four to nine by using the percentage of heat 20%, the heating temperature rapidly increasing compared to the others percentages of heat by its pulsations group. It indicated the reading of temperature from 614.9 to 1054.9 °C respectively which was on average double the amount of heat produced by using the percentage of heat 18% during the process of open-air electrical-field activated sintering using die set B without powder material.

Current : 4.00 kA - Heating Temperature and Time Vesus of Pulsation

	PS: 1	PS: 2	PS: 3	PS: 4	PS: 5	PS: 6	PS: 7	PS: 8	PS: 9
H1 & H2 = 10%	106.2	92.6	137.1	160.0	170.8	178.6	179.3	174.7	167.7
H1 & H2 = 12%	111.3	112.0	136.4	147.7	166.5	170.2	175.0	244.7	269.1
H1 & H2 = 14%	117.9	206.7	244.3	270.2	296.2	300.2	309.6	317.7	319.0
H1 & H2 = 16%	135.2	235.5	277.4	316.9	353.7	390.8	419.5	513.9	550.4
H1 & H2 = 18%	163.2	236.4	284.1	336.5	387.7	406.4	496.3	483.5	519.6
H1 & H2 = 20%	176.2	308.5	376.4	614.9	622.5	669.6	664.7	931.3	1,054.9
Process Time	29.12	37.04	44.96	52.88	60.80	68.72	76.64	84.56	92.48

Figure 7.4-5: Graph of heating temperature and time versus the pulsation process of Projection Welding machine for current 4.00 kA.

7.4.3.3. Heating Current: 6.00 kA

The last heating temperature observation was set to weld current 6.00 kA. The highest temperature that can be achieved during the testing of heating temperature of die set B without powder material was 1,257.2 °C with the percentage of heat 20% and nine pulsations

as presented in **Figure 7.4-6**. Hence, it could be used for the heating of the die set B with the 90Ti10Sn material due it requiring the increment of the percentage of heat to get the higher temperature for heating up the powder material. The rapid incrementing of heating temperature was occurring at the pulsation of five to nine which by using the percentage of heat 20%. It indicated the reading of temperature from 850.1 to 1257.2 °C respectively. Based on this observation, for the setting of the experiment parameters of 90Ti10Sn powder, all the pulsations would be set to nine pulsations with first and second weld current has been set to 20% for each. It was due to the performance of heating temperature obtained during the process being in the range of temperature needed in the open-air electrical-field activated sintering and forming process as stated earlier.

Current: 6.00 kA - Heating Temperature and Time Vesus of Pulsation

	PS: 1	PS: 2	PS: 3	PS: 4	PS: 5	PS: 6	PS: 7	PS: 8	PS: 9
H1 & H2 = 10%	107.2	70.7	148.1	163.9	182.2	196.4	209.6	222.4	223.9
H1 & H2 = 12%	48.6	152.8	190.3	222.0	242.5	261.5	271.5	285.5	282.2
H1 & H2 = 14%	56.6	124.1	149.9	166.8	286.3	313.8	334.5	337.5	349.0
H1 & H2 = 16%	65.5	240.4	299.6	359.5	386.0	434.3	467.6	481.5	501.0
H1 & H2 = 18%	76.6	351.2	436.7	513.2	579.8	628.1	671.8	711.6	619.3
H1 & H2 = 20%	84.5	193.7	252.5	467.6	850.1	1,038.4	1,126.4	1,129.0	1,257.2
Total Process Time	29.12	37.04	44.96	52.88	60.80	68.72	76.64	84.56	92.48

Figure 7.4-6: Graph of heating temperature and time versus the pulsation process of Projection Welding machine for current 6.00 kA.
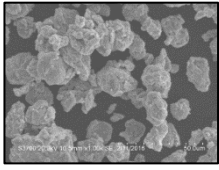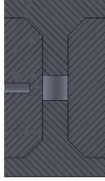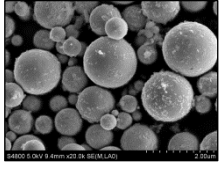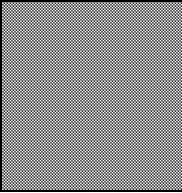
7.5. Procedures of Experiment

The procedure of the experiment using the Projection Welding machine was divided into three stages. The preparation of the powder materials and the ejection process after the open-air electrical-field activated sintering and forming process was the same as used in the

143

procedure of experiment Gleeble® 3800 machine before this which has been explained in section **6.4.1 Preparation of Powder Materials** and **6.4.3 Preparation for the Ejection** respectively. The only difference of procedure of the experiment was the preparation of the Projection Welding machine operating system which has been described in the section **7.5.1 Preparation of Projection Welding Operating System** below.

As described in **Table 7.5-1**, 90Ti10Sn and Cu powder has been chosen for the open-air electrical-field activated sintering and forming process. For 90Ti10Sn powder, it consists of average particles size of 27 μm with theoretical density of 4.76 g/cm^3. Based on the high-efficiency performance of die set B during the experiment with the Gleeble® 3800 machine, it has been chosen for this experiment using the Projection Welding machine. Meanwhile, Cu powder has been selected for the experiment using the domed hollow cylinder and the turbine die set block due to the lower heating temperature required for the experiment which was in the range of 500 to 700 °C. In addition to that, the material used for the die set block for holding the graphite die set was made from stainless steel (AISI 316 L) where it has a melting point in the range of 1380 to 1400 °C. Therefore, the precautionary step was made where not to test the powder material which required the higher temperature than melting point of stainless steel which in this case Cu powder was suitable to be selected. As for Cu powder, it consists of 50 μm for the average particles size and has the theory density of 8.96 g/cm^3. The section view of the stainless steel block and graphite die set for the experiment using Cu powder cannot be illustrated due to the confidentiality of the design which related to the Micro-FAST Project.

Table 7.5-1: The classification of the nominal chemistry and physical properties for 90Ti10Sn and Cu powder used in the open-air electrical-field activated sintering and forming process which performed by Projection Welding machine.

Powder Materials	Nominal Chemistry (wt%)	Average Particles Size (µm)	Theory Density (g/cm³)	SEM Image of Particles Agglomerates	Die Sets	Section View of the Die Set
90Ti10Sn	Ti: 90.0; Sn: 10.0	27	4.76		B	
Cu	Cu: 99.0; Others: 1.0	50	8.96		DHC	
					TR	

7.5.1. Preparation of Projection Welding Operating System

The electricity for the main power of the Projection Welding machine and air for the pneumatic system was turned on. The 'on' button at the Projection Welding machine was twisted to operate the machine. The upper electrode of Projection Welding machine was position at the end of its stroke by releasing the air from the above air cylinder puncher. The position of the die set was carefully made an adjustment based on the limit stroke of the upper electrode of Projection Welding machine to ensure the die set was fully closed by the end of the process as shown in **Figure 7.4-1** and **Figure 7.4-2**. The thermocouple of Omega Dual Type K was inserted into the centre hole of the die set to measure the heating temperature. After that, the air cylinder was closed in order to let the upper electrode of the Projection Welding machine back to its original position. The clear polycarbonate for the front, side and back guard was installed before the process began for the safety reason in the case of the die set was broken during the process due to the excessive applied pressure. All the parameters of the experiment have been input by using advanced micro-processor weld controller BF-550. The cooling system of compact 3000/5000 air blast water cooler was turned on before the process began. The experiment of open-air electrical-field activated sintering and forming process was started by pressing two on button with both hands. As for the safety reason, the emergency off button was ready to be twisted if something unpredictable happens during the process. Safety eye protection also must be wearing during the course due to excessive bright

light produced by the heating process of the die set. After the process end, the die set was taken out for the ejection process. The cooling system of compact 3000/5000 air blast water cooler was turned off after the process end. The die set holder at the puncher of Projection Welding machine was cleaned and start the process again until the experiment finished. After all the experiment was finished, the Projection Welding machine main power of electricity, air supply and compact 3000/5000 air blast water cooler was switched off.

7.6. Results and Discussions

The results and discussion from the open-air electrical-filed activated sintering and forming process of 90Ti10Sn and Cu sample using Projection Welding machine have been made as below.

7.6.1. Titanium Tin Alloy (90Ti10Sn)

Based on the detail parameters in **Table 7.6-1**, there were four samples of 90Ti10Sn that have been made by the open-air electrical-field activated sintering and forming process using the Projection Welding machine. In this experiment, the die set B has been used due to the excellent quality, efficiency and good samples produced which has been shown before by using the Gleeble® 3800 machine for 90Ti10Sn samples. Therefore, by using the reference heating data temperature for the die set B tested in the Projection Welding machine which has been described before this in **Table 7.4-2**, several first and second weld currents have been tested which are in the range of 2.00 to 5.00 kA on 90Ti10Sn samples using the Projection Welding machine. It was because the Projection Welding machine cannot directly set the desired temperature required in the experiment. Therefore, with this data, it can be used as a guideline to establish the parameters of the experiment. Meanwhile for others parameters such as applied pressure, first and second heat and pulsation of the process have been set the same for all the 90Ti10Sn samples which were 71.46 MPa, 20% and nine pulsations respectively.

Table 7.6-1: Parameter of experiments titanium tin alloy (90Ti10Sn) cylinder design samples for open-air electrical-field activated sintering and forming process.

Parameters of Experiments	Units	90Ti10Sn-A	90Ti10Sn-B	90Ti10Sn-C	90Ti10Sn-D
Theory Powder Weight	g	0.2393	0.2393	0.2393	0.2393
Actual Powder Weight	g	0.1722	0.1722	0.1722	0.1722
Pressure	MPa	71.46	71.46	71.46	71.46
Force	N	898	898	898	898
Highest Temperature Recorded	°C	922.5	961.3	1,339.8	1,354.1
Pre-Squeeze Time (PSQ)	s	5	5	5	5
Squeeze Time (SQ)	s	5	5	5	5
First Up Slope Time (U1)	s	0.6	0.6	0.6	0.6
First Weld Time (W1)	s	1.98	1.98	1.98	1.98
First Weld Current (I1)	kA	**3.00**	**4.00**	**4.50**	**5.00**
First Heat (H1)	%	20	20	20	20
First Cool Time (CL1)	s	1.98	1.98	1.98	1.98
Second Weld Time (W2)	s	1.98	1.98	1.98	1.98
Second Weld Current (I2)	kA	**3.00**	**4.00**	**4.50**	**5.00**
Second Heat (H2)	%	20	20	20	20
Second Cool Time (CL2)	s	1.98	1.98	1.98	1.98
Pulsation (PS)	Times	9	9	9	9
Down Slope Time (DS)	s	0.6	0.6	0.6	0.6
Hold Time (Hold)	s	5	5	5	5
Off Time (Off)	s	5	5	5	5
Total Time	s	92.48	92.48	92.48	92.48

Nevertheless, some adjustment of the parameters needs to be made where the total weight of the powder that is required to be inserted into the die set B has been reduced to 0.1722 g from 0.2393 g due to the punches and die needing to be gradually closing during the process when using the Projection Welding machine. It required to be fully closed at the end of the experiment to achieve a high efficiency of heating and capable producing an excellent quality of samples which has been proven before this with the experiment using the Gleeble® 3800 machine. This also prevented the die set B from being broken due to the higher compaction of less heated 90Ti10Sn material in the early stage during the open-air electrical-field activated sintering and forming process. It was due to the pneumatic cylinder puncher of

the Projection Welding machine travelling downwards to its final stroke when the experiment process began. During that time, if the theoretical weight of 90Ti10Sn material (0.2393 g) inserted into the die set B was not be fully heated by electrical-field, the condition of die set B would not fully closed. Hence, the 90Ti10Sn material has not enough energy and time to start the sintering and forming which at the same time the high pressure has been applied to the die set B and eventually would break it during the process. Therefore, the safety gap for upper and lower punches to the die after the pouring of 90Ti10Sn material (0.1722 g) needs to be in the range of 1.50 to 2.00 mm to overcome the problem and succeeded produced the samples.

In **Table 7.6-2**, it shows the detail and comparison results of the measurement, chemical element weight percentage of carbon and relative densities of 90Ti10Sn cylinder samples for the open-air electrical-field activated sintering and forming processes. Regarding the performance of the die set B, the heating temperature distribution was uniform and there was no gap between the punches and die after the precautionary step has been taken as explained before this for all the 90Ti10Sn samples. Meanwhile, as the first (W1) and second (W2) weld current value increased the relative density value for the 90Ti10Sn samples also increased which can be seen in **Figure 7.6-1**. It was due to the higher temperature produced as the first and second weld was applied which contributes to the higher densifications of the samples as shown in **Figure 7.6-2**. The comparison measurement of the dimension and weight as well as chemical element weight percentage of carbon (wt%) among 90Ti10Sn samples can be seen in **Figure 7.6-3** and **Figure 7.6-4** respectively.

Table 7.6-2: Result of measurement, chemical element weight percentage of carbon and relative densities of 90Ti10Sn cylinder design samples for open-air electrical-field activated sintering and forming process.

Results of Experiments	Units	90Ti10Sn-A	90Ti10Sn-B	90Ti10Sn-C	90Ti10Sn-D
Gap Between Punches and Die		No	No	No	No
Die Set Heat Temp. Distribution		Uniform	Uniform	Uniform	Uniform
Diameter of the Sample (Ø: 4.00)	mm	4.00	4.03	4.00	3.84
Height of the Sample (H: 4.00)	mm	4.22	4.20	4.10	4.12
Sample Weight Before Cleaning (BC)	g	0.1716	0.1698	0.1705	0.1698
Sample Weight After Cleaning (AC)	g	0.1541	0.1610	0.1673	0.1624
Different Sample Weight (BC – AC)	g	0.0175	0.0088	0.0032	0.0074
Sample Density	g/cm^3	3.531	3.566	3.765	3.783
Carbon Element at Centre Sample	wt%	3.53	4.49	3.48	4.27
Carbon Element at Edge Sample	wt%	5.50	5.72	8.00	7.52
Relative Density	%	**74.18**	**74.92**	**79.10**	**79.47**
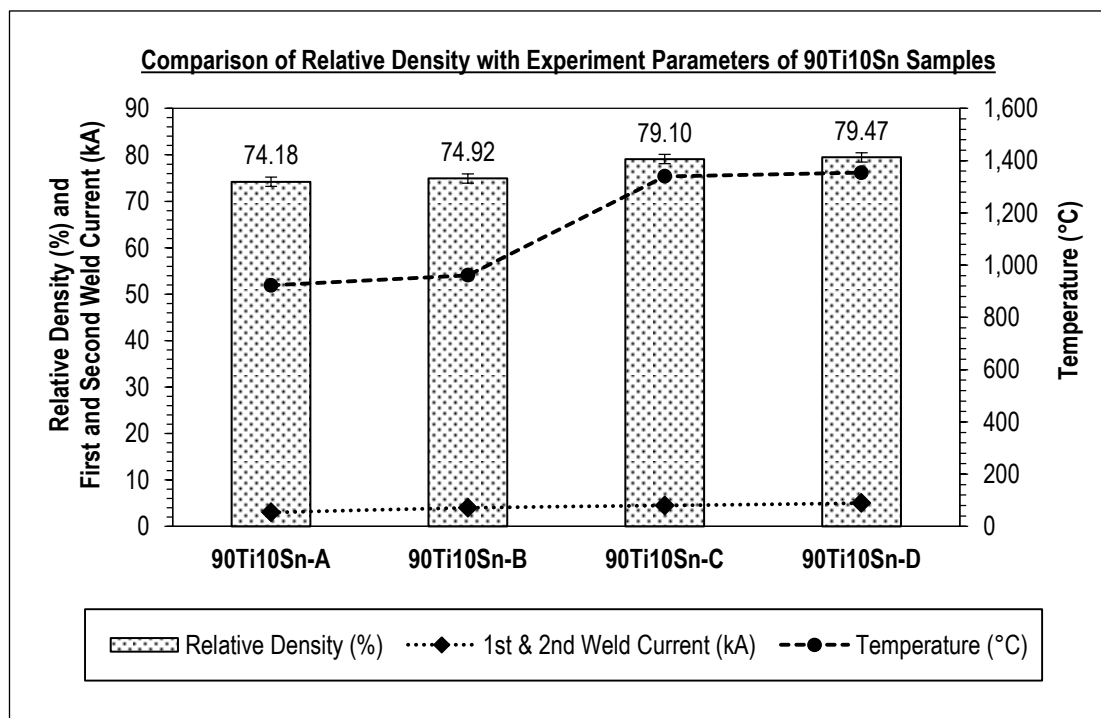
Figure 7.6-1: Comparison of relative density of 90Ti10Sn samples with the input of weld current and the heating temperature generated. All the others parameters are the same as presented in **Table 7.6-1**.
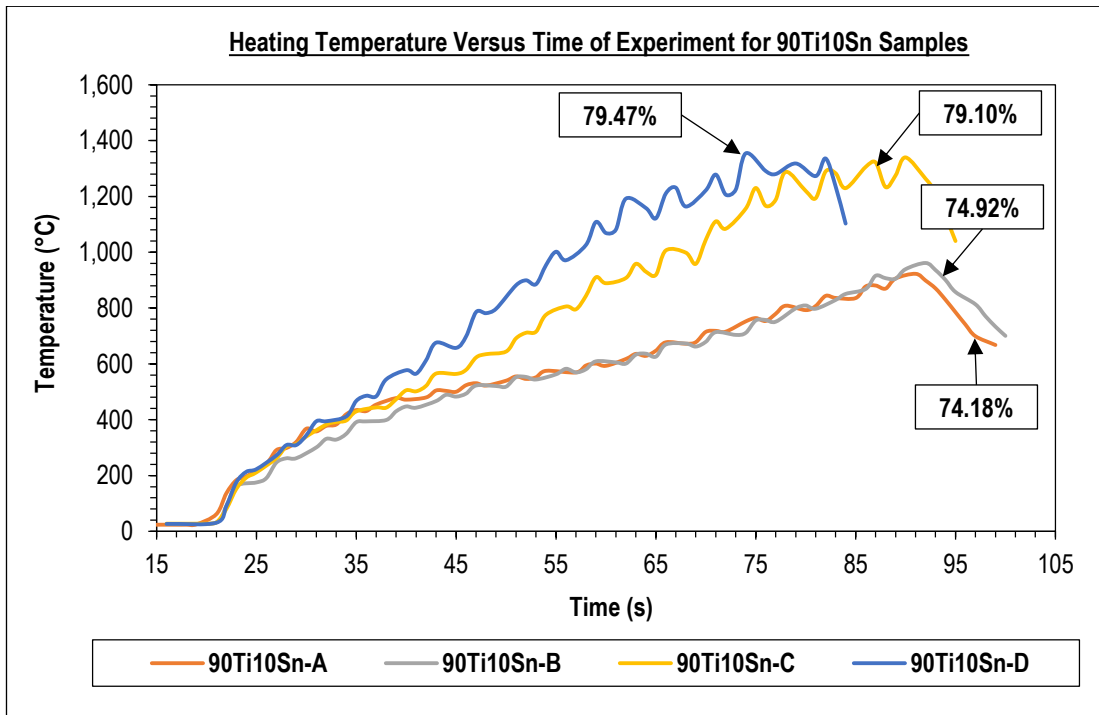
Figure 7.6-2: Heating temperature against time for densification of 90Ti10Sn samples.
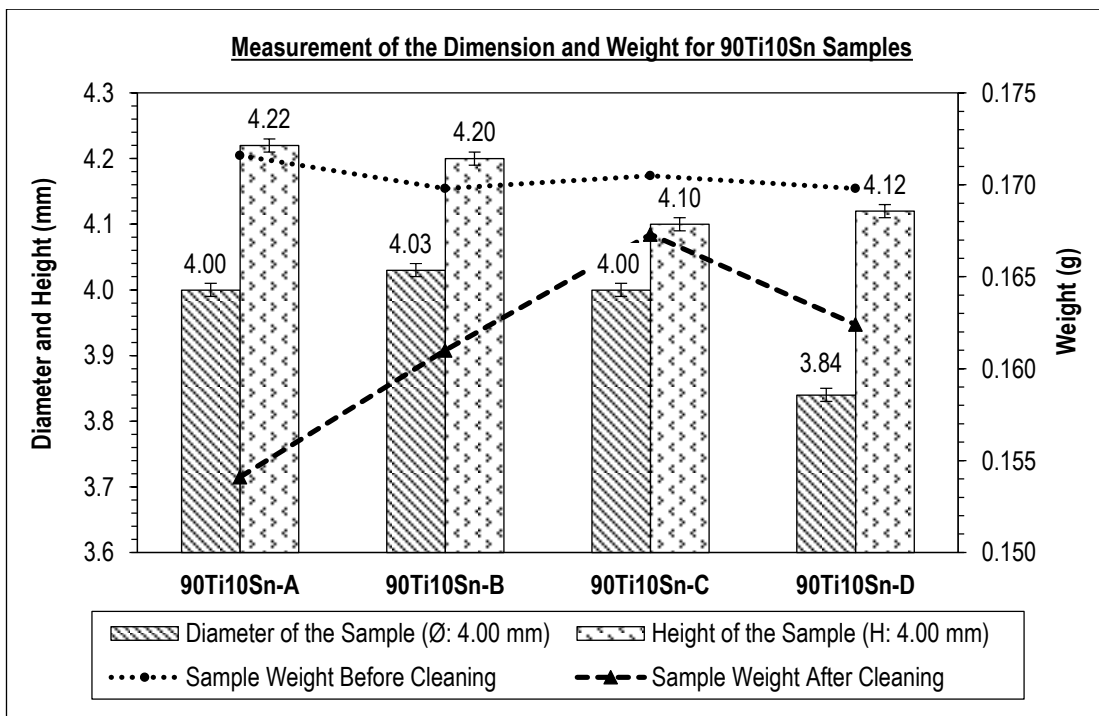
Figure 7.6-3: Measurement of the dimension and weight of 90Ti10Sn samples using die set B performed by Projection Welding machine for the open-air electrical-field activated sintering and forming process.
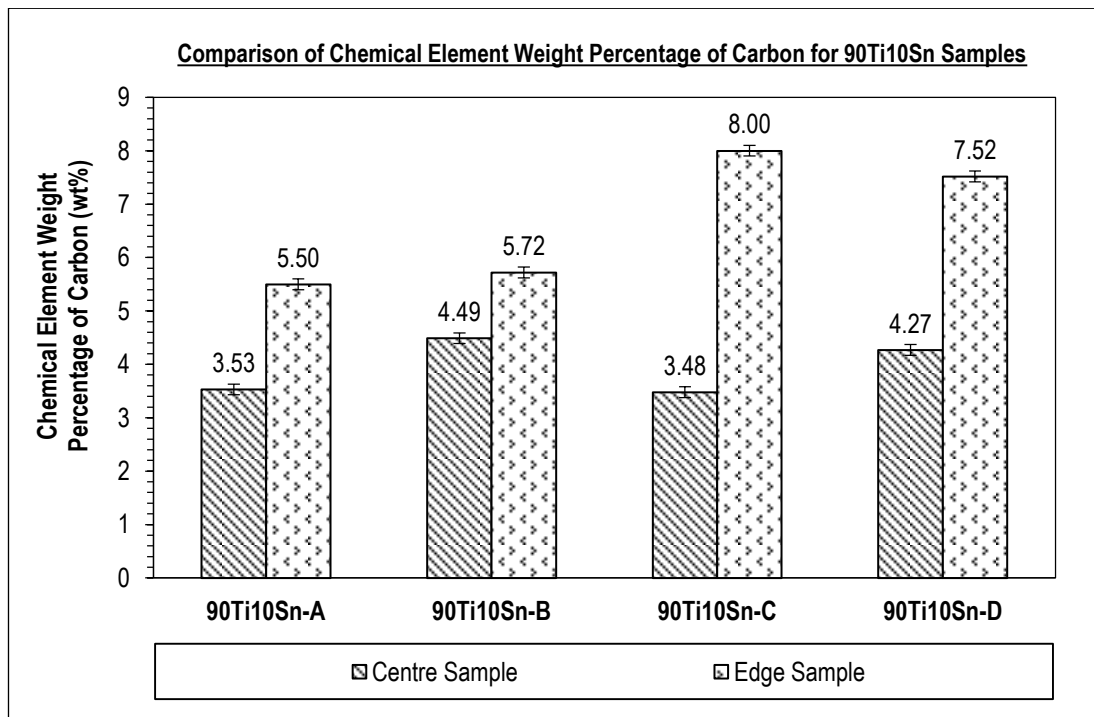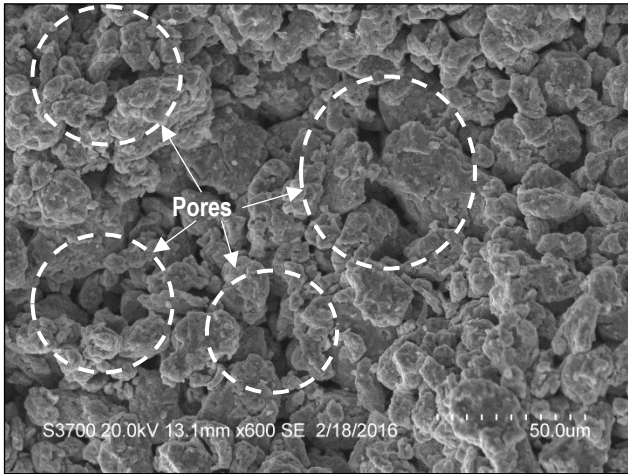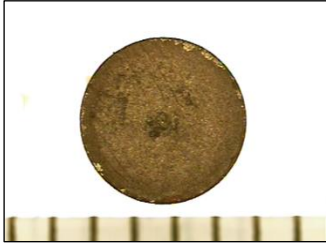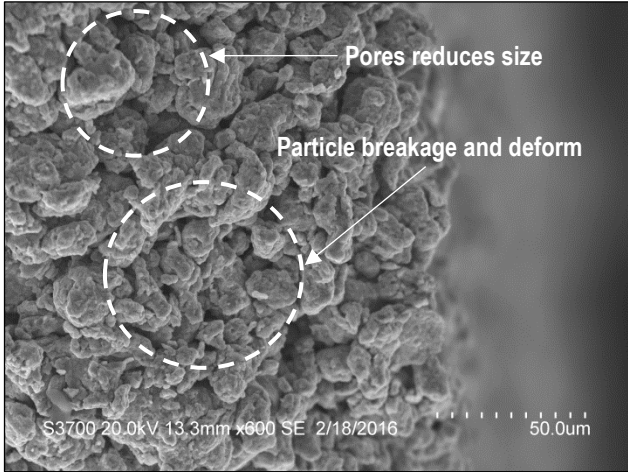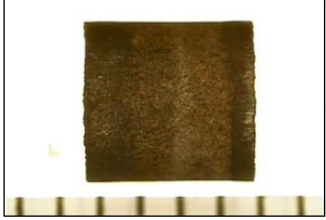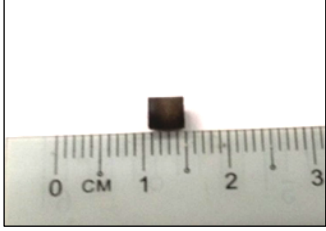
Figure 7.6-4: Comparison of chemical element weight percentage of carbon (wt%) located at centre and edge of 90Ti10Sn samples by using with open-air electrical-field activated sintering and forming process.

7.6.1.1. Cylindrical Sample 90Ti10Sn-A

Based on **Table 7.6-1**, it shows that by using the first and the second weld current of 3.00 kA, the first and the second heat current of 20% and nine pulsations, the highest temperature for the open-air electrical-field activated sintering and forming process of 90Ti10Sn material can be achieved was 922.5 °C. The reading temperature was in the range of the data for heating temperature in **Table 7.4-2** that has been made with the die set B without powder material which indicated the reading between 963.1 °C and 1,054.9 °C by using 2.00 kA and 4.00 kA respectively. The total time to completed the process with achieving the 74.18% relative density of the sample 90Ti10Sn-A was 92.48 s. In **Table 7.6-3**, it shows the SEM micrograph at the centre and edge of cylindrical sample 90Ti10Sn-A (Magnification: 600 SE) along with sample pictures before the cleaning process at the positions top and side. The sample 90Ti10Sn-A has been fractured at half of its height without polishing to identify more clearly the pores at the densified particles that have been sintered and forming during the process.

Table 7.6-3: (a) SEM micrograph at the centre and edge of cylindrical sample 90Ti10Sn-A (Magnification: 600 SE) **(b)** Sample 90Ti10Sn-A pictures at the top and side.

Cylindrical Sample 90Ti10Sn-A – Relative Density: 74.18%		
(a) SEM Micrograph at Centre and Edge Sample		**(b) Top and Side Sample**
Centre		
Edge		

In the SEM micrograph at the centre and the edge of sample 90Ti10Sn-A, it shows the visual of pores reducing the sizes and the particles breakage with deforming at the end of open-air electrical-field activated sintering and forming process. There was inadequate densification occurred which is associated with the lower temperature obtained plus the shorter process time as presented in **Figure 7.6-2** compared to the experiments that have been done by using Gleeble® 3800 machine before. Regarding the measurement of the sample 90Ti10Sn-A, based on the data provided in **Table 7.6-2**, it shows the diameter of the sample was 4.00 mm which was exactly the same as measurement for the design sample. Meanwhile, for the height of the sample it recorded the reading of 4.22 mm even though the condition of the die set B was fully closed at the end of the process. It was due to less applied

pressure with cause by a small gap between the puncher of Projection Welding machine and the die set B. The percentage of different sample weight before and after the cleaning process was 10.198%. Meanwhile, the presence of carbon element at the centre and edge was 3.53 wt% and 5.50 wt% respectively as illustrate in **Figure 7.4-6**.

7.6.1.2. Cylindrical Sample 90Ti10Sn-B

The further analysis has been made for the sample 90Ti10Sn-B by increasing the first and the second weld to 4.00 kA. Meanwhile, for the first and the second heat with the pulsation was maintained the same as sample 90Ti10Sn-A which were 20% and nine times as presented in **Table 7.6-1** respectively. Nevertheless, the sample 90Ti10Sn-B only recorded a small incremental difference of the highest temperature compared to sample 90Ti10Sn-A which from 922.5 to 961.3 °C. Therefore, it influences the sample densification result which indicated the value of 74.92% as shown in **Table 7.6-2** with the same total time of 92.48 s as before. Similar with the justification results of sample 90Ti10Sn-A, it was only capable to achieved a slight improvement of densification due to there was deficient of heating temperature gained during the experiment with a shorter processing time compared to the experiment by using the Gleeble® 3800 machine. The heating temperature against the time for sample 90Ti10Sn-B can be seen in **Figure 7.6-2** which follows the same trends of heating for sample 90Ti10Sn-A.

Based on **Table 7.6-4**, it shows the SEM micrograph at the centre and the edge of cylindrical sample 90Ti10Sn-B. In the centre position of sample 90Ti10Sn-B, there were more pores occurred compared to the edge of its sample which shows a better densification of particles powder. It was due to the particles of 90Ti10Sn powder receiving more heating current at the wall of the die compared to the punches of the die set B to deform the particles. The arrangement of the particles powder was loose inside the die set B due to the reducing weight of powder material to overcome the problem of broken die set during the start process of the experiment which has been stated before this. Therefore, based on this situation, the flow of the current was not able to generate the heat efficiently through the powder material. Alternately the current needs to flow within the body of the die set B during the experiment which caused the die set to have a high temperature at its wall compared to its punches.

As for the measurement of the dimension of the sample 90Ti10Sn-B, it indicated the reading of 4.03 mm for the diameter and 4.20 mm in height. The measurement for the height for the sample 90Ti10Sn-B was higher than 4.00 mm as in the design measurement due to the same cause as the sample 90Ti10Sn-A before this where less pressure has been applied due to the small gap between the puncher of the Projection Welding machine and the die set B. The bottom elevation stage for the Projection Welding machine encounters the slight movement downward when the pneumatic puncher is applied to the die set B. The percentage of different sample weights before and after the cleaning process was 5.183%. Meanwhile, the presence of carbon element at the centre and edge was 4.49 wt% and 5.72 wt% respectively as presented in **Figure 7.6-4**.

Table 7.6-4: (a) SEM micrograph at the centre and edge of cylindrical sample 90Ti10Sn-B (Magnification: 600 SE) **(b)** Sample 90Ti10Sn-B pictures at the top and side.
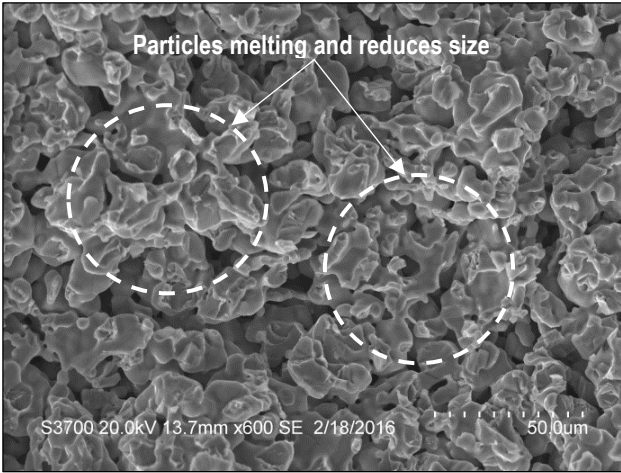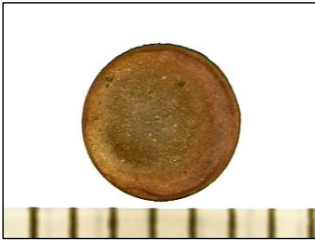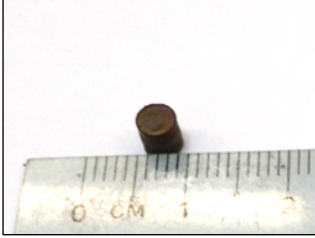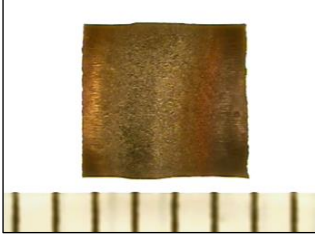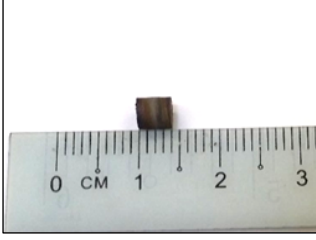
7.6.1.3. Cylindrical Sample 90Ti10Sn-C

Based on the problem that has been faced with the sample 90Ti10Sn-A and 90Ti10Sn-B with the small gap between puncher of Projection Welding machine with the die set B, the bottom elevation stage of the machine has been carefully raised up to ensure there was sufficient contact between the machine's puncher and the die set for the sample 90Ti10Sn-C. In addition to that, by increasing the weld current from 4.00 kA for the sample 90Ti10Sn-B to 4.50 kA for the sample 90Ti10Sn-C while maintaining the first and second heat for 20% with nine pulsations, the heating temperature was also rising from 961.3 to 1,339.8 °C respectively as shown in **Table 7.6-2** and **Figure 7.6-1**. As for the result densification of the sample 90Ti10Sn-C, it shows the growing different of 4.18% from the sample 90Ti10Sn-B which made it to achieved 79.10% of relative density with the total time of 92.48 s. Although the higher temperature has been reached to 1,339.8 °C as illustrated in **Figure 7.6-2** for the sample 90Ti10Sn-C due to the sufficient contact that has been made, there was still less relative densification has been obtained. It was due to the reducing powder material that has been made before the experiment started to save the die set B from being broken which has been explained before this. Therefore, due to the shortage of the volume for the sample 90Ti10Sn-C, this made less densification to the formed sample associated with the Projection Welding puncher which cannot press sufficiently towards the powder during the open-air electrical-field activated sintering and forming process.
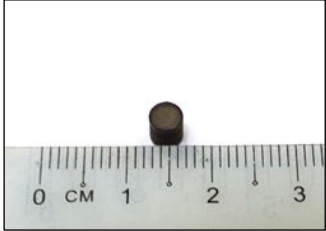
Regarding the measurement of the dimension of the sample 90Ti10Sn-C it shows the improvement concerning the height compared to the previous sample 90Ti10Sn-A and 90Ti10Sn-B which indicated the reading from 4.22 mm and 4.20 mm respectively to 4.10 mm as presented in **Figure 7.6-3**. It was showing the positive influences based on the action of slightly increasing the bottom elevation stage of Projection Welding machine to ensure the die set B was made a full contact with machine's puncher. Meanwhile, the diameter of the sample 90Ti10Sn-C shows the same as reading for the design sample which was 4.00 mm. Based on the reading of chemical element weight percentage of carbon for the sample 90Ti10Sn-C as illustrated in **Figure 7.6-4**, it shows the higher value at the edge of the sample which was 8.00 wt% compared to the centre with the reading value of 3.48 wt%. Apparently, it has occurred to all the samples of 90Ti10Sn material during the experiment due to the body of the die set was

burnt at the high temperature compare to punchers of the die set B. It has been caused by the current needs to flows within the body of the die set B which eventually caused its wall to have a higher temperature compared to the other parts. Therefore, during the forming and breakage of the particles, the burnt carbon has been mixed at the edge of the sample compared to the centre part. In **Table 7.6-5**, it shows the SEM micrograph at the centre and edge of the sample 90Ti10Sn-C which displays visually the particles deformed and reduced the pores size which was better compared to the previous samples of 90Ti10Sn-A and 90Ti10Sn-B. Nevertheless, based on the pictures at top and side of the sample 90Ti10Sn-C, it shows the particles have the better densification at the middle section of the sample compared to the top and bottom sides.

Table 7.6-5: (a) SEM micrograph at the centre and edge of cylindrical sample 90Ti10Sn-C (Magnification: 600 SE) **(b)** Sample 90Ti10Sn-C pictures at the top and side.

Cylindrical Sample 90Ti10Sn-C – Relative Density: 79.10%		
(a) SEM Micrograph at Centre and Edge Sample		**(b) Top and Side Sample**
Centre	Particles melting and reduces size S3700 20.0kV 13.7mm x600 SE 2/18/2016 50.0um	
Edge	Particles breakage and deform S3700 20.0kV 13.9mm x600 SE 2/18/2016 50.0um	
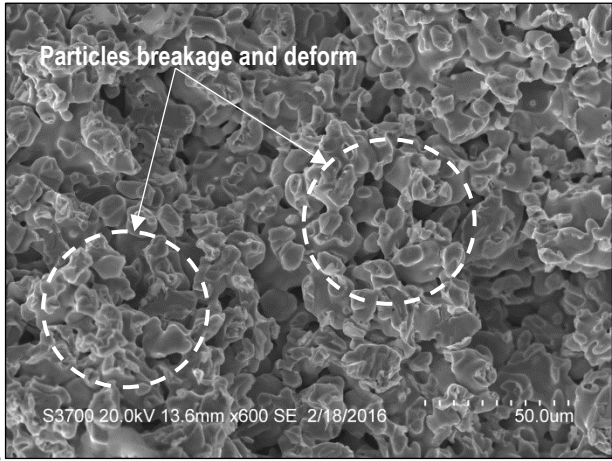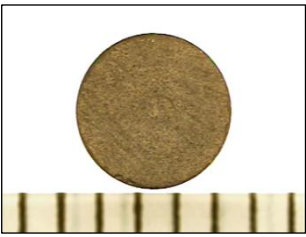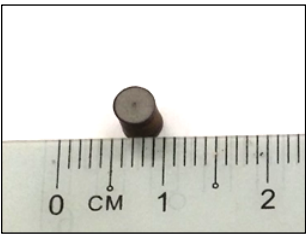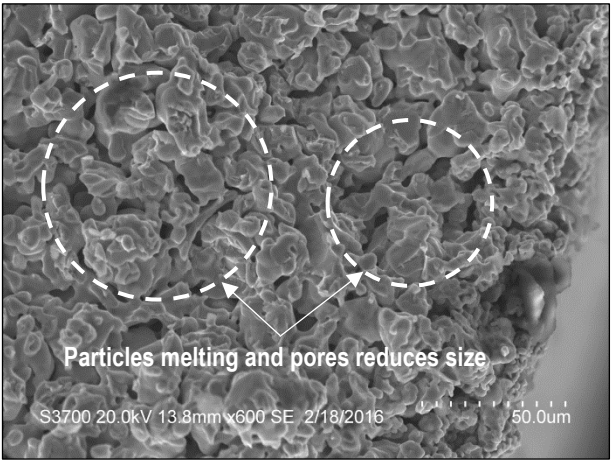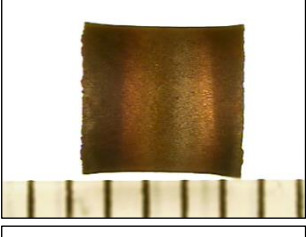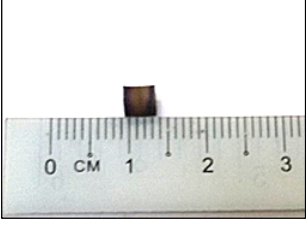
7.6.1.4. Cylindrical Sample 90Ti10Sn-D

In the next experiment conducted for the sample 90Ti10Sn-D, the first and the second weld current continued to increase for 5.00 kA. Meanwhile, for the other parameters such as the first and the second heat along with the pulsations are maintained to 20% and nine times respectively during the open-air electrical-field activated sintering and forming process as stated in **Table 7.6-1**. Alongside with that, the bottom elevation stage of Projection Welding machine also has been carefully raised up same as the procedure that has been done to the sample 90Ti10Sn-C. It was to ensure the sufficient contact between the machine's puncher and the die set B to obtain the sample that has the right dimensions in height and capable to produce the higher temperature during the process. Based on the observation, by using those setting parameters, the heating temperature for the sample 90Ti10Sn-D indicated the reading of 1,354.1 °C which shows a slight increment of the temperature and similar heating graph trends as the sample 90Ti10Sn-C before this which has been illustrated in **Figure 7.6-2**. The relative density result for the sample 90Ti10Sn-D achieved 79.47% with the total time of 92.48 s which indicated the increasing value of 0.37% compared to 90Ti10Sn-C as presented in **Figure 7.6-1**.

Concerning the measurement of the sample 90Ti10Sn-D, it shows the similar results as the sample 90Ti10Sn-C where it indicated the reading of 3.84 mm and 4.12 mm for the diameter and the height of the sample as illustrated in **Figure 7.6-3**. Again it shows the consistency of positive influences based on the action of slightly increasing the bottom stage of Projection Welding machine to ensure the contact between the machine's puncher and the used die set during the experiment. The proportion of different sample weight before and after the cleaning process was 4.358%. Meanwhile, regarding the chemical element weight percentage of carbon, it shows a higher value at the edge of the sample 90Ti10Sn-D which was 7.52 wt% compared to the centre of its sample which was 4.27 wt% as demonstrated in **Figure 7.6-4**. It was the same cause that happened at the sample 90Ti10Sn-C before this where the current heat needs to flow within the body of the die set B which eventually burnt the die and the carbon mixed with the particles at the edge of the sample 90Ti10Sn-D during the densification process. In **Table 7.6-6**, it shows the SEM micrograph at the centre and edge of the sample 90Ti10Sn-D, where it indicated the densification of the sample achieved by the

particles breakage and plastic deformation. Nevertheless, same as a result in the 90Ti10Sn-C, based on the appearance of the sample 90Ti10Sn-D, at the position of top and bottom it shows the densification more efficient at the middle of the sample.

Table 7.6-6: (a) SEM micrograph at the centre and edge of cylindrical sample 90Ti10Sn-D (Magnification: 600 SE) **(b)** Sample 90Ti10Sn-D pictures at the top and side.

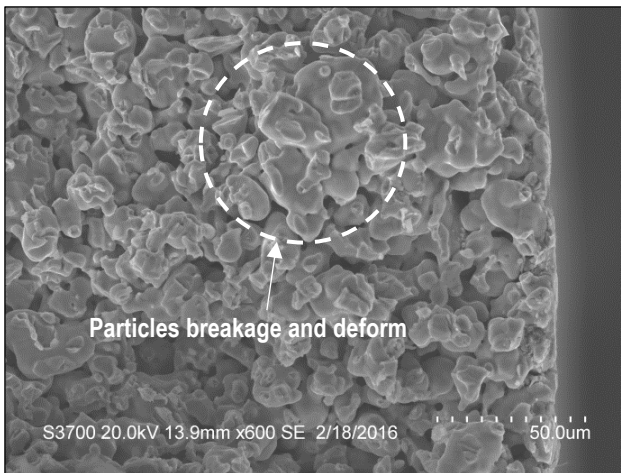| Cylindrical Sample 90Ti10Sn-D – Relative Density: 79.47%		
(a) SEM Micrograph at Centre and Edge Sample		**(b) Top and Side Sample**
Centre	Particles breakage and deform S3700 20.0kV 13.6mm x600 SE 2/18/2016 50.0um	
Edge	Particles melting and pores reduces size S3700 20.0kV 13.8mm x600 SE 2/18/2016 50.0um	

Therefore, based on these findings, the improvement of the process needs to be done in the future by using repetition of the open-air electrical-field activated sintering and forming process and constantly checking the contact between the machine's puncher and the die set for each time the process that has been performed to successfully produced higher densification parts compared to 90Ti10Sn samples. In the further experiment of the intricate design of Cu samples, repetition of heating process, multiple rising up the bottom elevation

stage of Projection Welding machine and adding force only test on the samples after the open-air electrical-field activated sintering and forming process ended has been introduced which showed a positive results on the densification of formed samples. There were two designs of samples that have been tested which were the domed hollow cylinder and the turbine samples. The detail regarding information can be referred to section **7.6.2 Copper (Cu).**

7.6.2. Copper (Cu)

In the development of the intricate design of the copper samples, it has been divided into two forms of samples which were the domed hollow cylinder and the turbine shape. The copper material has been selected due to the lower heating temperature required for the open-air electrical-field activated sintering and forming process which was in the range of 500 to 900 °C. In addition to that, by using the maximum temperature of 900 °C for Cu samples during the previous research electroplasticity sintering of plasma pressure compaction (P^2C) as shown in **Table 2.3-3**, it indicated the densification of Cu samples between 90.43 to 99.00%. The selection of the copper material for this further experiment also was due to the material of the die set block for holding the graphite (grade: Mersin 2333) die set was made from stainless steel (AISI 316 L) as pictured in **Figure 7.6-5** where the melting point of it was in the range of 1,380 to 1,400 °C [134]. Therefore, the precaution step was made where not to run the process on the Cu powder higher than the melting point of stainless steel die set block.

Regarding the detail design of the tooling for the domed hollow cylinder and the turbine die set, it was not described in this thesis due to the confidentialities documentations of the Micro-FAST project. In **Figure 7.6-6**, it shows the position of the die set block for the domed hollow cylinder and the turbine samples inserted at the area of the open-air electrical-field activated sintering and forming process at the Projection Welding Machine. The difference between the previous approaches made on the sample 90Ti10Sn-A to 90Ti10Sn-D by using the die set B compared to the current method was the implementation of the repetition of the heating process, the multiple force test and the various elevations of the Projection Welding machine of the bottom stage. It has been done to maintain the surface contact between machine pneumatic system puncher to stainless steel of the die set block with the aims to

assure the current can flow through the graphite punches and Cu powder particles to generated the heat more efficiently. In addition to that, by using repetition of heating process on the Cu samples, it has sufficient time to make excellent densified components compared to the sample 90Ti10Sn-A to 90Ti10Sn-D before this where it only had the allocation time of 92.48 s for each process.
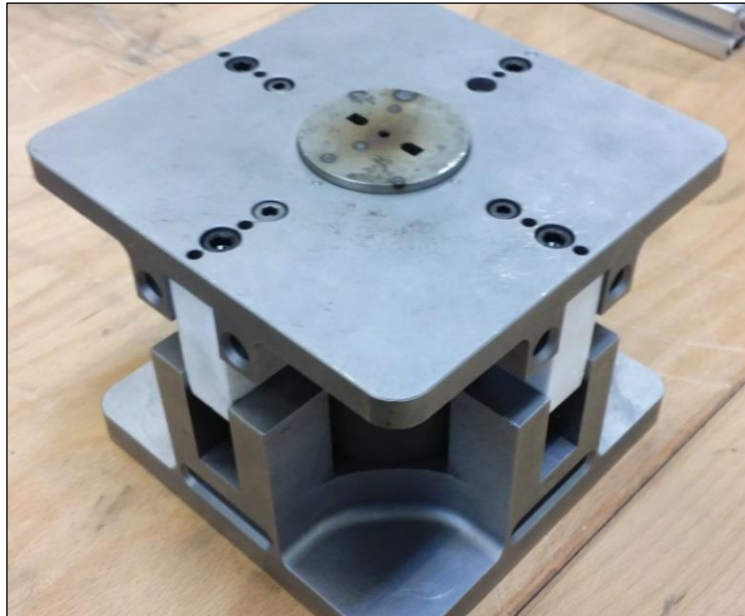
Figure 7.6-5: Stainless steel (AISI 316 L) die set block used for the forming of the domed hollow cylinder and the turbine samples.

Figure 7.6-6: Position of the die set block for the domed hollow cylinder and the turbine sample at Projection Welding machine.

7.6.2.1. Domed Hollow Cylinder Samples

The picture of the domed hollow cylinder graphite die set and stainless steel die set block can be referred to **Figure 7.6-7** where it shows in the condition of the open position before the pouring process of the Cu powder into the graphite die set has been done. The ceramic guide has been used to reduce the current flow from heated the die set block to the minimum heating temperature as possible without exceeding the maximum melting temperature of its material. Instead, by using the design of ceramic guide, the current flow would directly heat the Cu powder particles through the graphite die set and as a result, increased the efficiency of the process. It was also applied to the die set block for the turbine samples.
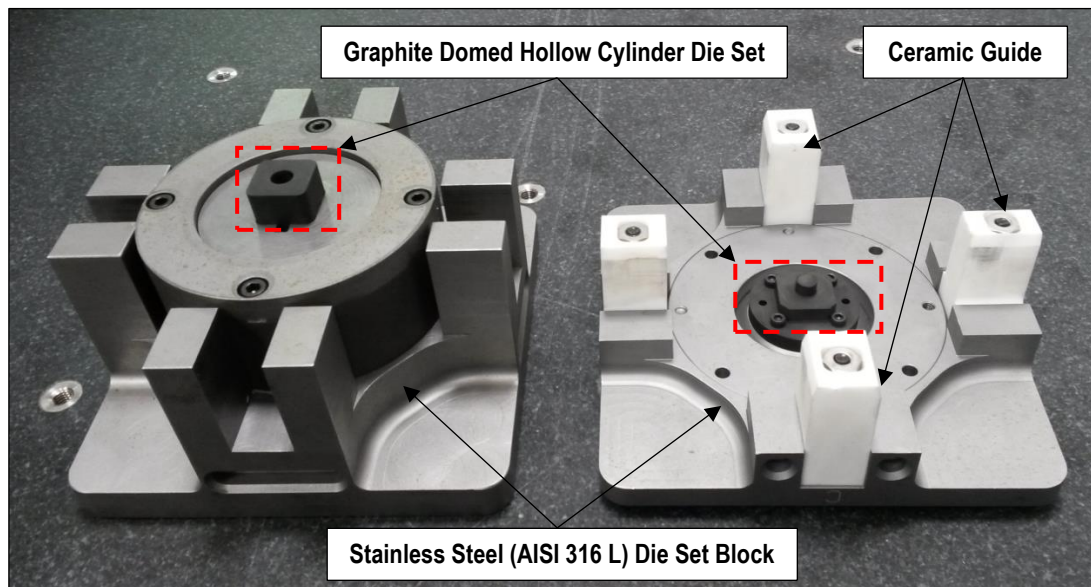
Figure 7.6-7: Open view of the die set block and the graphite die set for the forming of the domed hollow cylinder samples.

In this experiment, there were two samples of the domed hollow cylinder that have been tested in the open-air electrical-field activated sintering and forming process using the Projection Welding machine. The name for the components was DHC-1 and DCH-2. The detail regarding the parameters of the experiment and the output results can be referred to **Table 7.6-7** and **Table 7.6-8** respectively. Based on the improvement towards the procedures of the experiment which has been stated before, DHC-2 shows the highest relative density of 93.23% compared to the sample DHC-1 which only recorded the result of 78.93%.

Table 7.6-7: Detail parameters of the experiment for the forming of the Cu domed hollow cylinder sample.

Parameter of Experiments	Units	DHC-1	DHC-2
Weight Powder	g	**1.2194**	**1.0036**
Force	N	1,076	1,076
Total Elevation of Bottom Stage	Stage	3rd	3rd
Total Repetition of Heating	Times	3	3
Total Repetition of Force Test (No Heating)	Times	**0**	**3**
Highest Temperature Recorded	°C	513.7	933.0
Pre-Squeeze Time (PSQ)	s	5	5
Squeeze Time (SQ)	s	5	5
First Up Slope Time (U1)	s	0.6	0.6
First Weld Time (W1)	s	1.98	1.98
First Weld Current (I1)	kA	3.00	3.00
First Heat (H1)	%	25	25
First Cool Time (CL1)	s	1.98	1.98
Second Weld Time (W2)	s	1.98	1.98
Second Current (I2)	kA	3.00	3.00
Second Heat (H2)	%	30	30
Second Cool Time (CL2)	s	1.98	1.98
Pulsation (PS)	Times	27	27
Down Slope Time (DS)	s	0.6	0.6
Hold Time (Hold)	s	5	5
Off Time (Off)	s	5	5
Total Time Per Repetition for 9 Pulsations	s	92.48	92.48
Total Time	s	277.44	554.88

Table 7.6-8: Results of the experiment for the forming of the Cu domed hollow cylinder samples.

Results of Experiments	Units	DHC-1	DHC-2
Die Set Heating Temp. Distribution		Uniform	Uniform
Gap Between Punches and Die		Yes	No
Sample Weight	g	1.2005	0.9938
Sample Density	g/cm³	7.072	8.353
Relative Density	%	**78.93**	**93.23**

7.6.2.1.1. Domed Hollow Cylinder Sample DHC-1

Based on **Table 7.6-9**, it shows the additional detail parameters of the data information for the sample DHC-1. By using 3.00 kA for both the first and the second weld current, 25% and 30% for the first and the second heat percentage respectively and nine pulsations for each of the heating repetitions, three highest temperatures of the process have been collected in the range of 380.2 to 513.7 °C. It also has been helped with the three for both repetitions of the heating process and the elevations of the Projection Welding machine bottom stage. The sample DHC-1 has achieved the relative density of 78.93% with the total time of 277.44 s. Meanwhile, concerning the die set heating temperature distribution, the results show that it was uniform throughout the process of the heating.

Table 7.6-9: Detail parameters data of the highest temperature recorded based on the first and the second weld current, the first and the second percentage of heat and the pulsations for sample DHC-1. The descriptions times of repetition for heating, force test and elevation bottom stage of the Projection Welding machine also have been described.

Additional Parameters of the Data Information for Sample DHC-1							
1st & 2nd Weld Current: 3.00 kA	**Pulsations**	**1st Heat (H1)**	**2nd Heat (H2)**	**Highest Temp.**	**Repetition of Heating**	**Repetition of Force Test**	**Elevation of Bottom Stage**
		(%)	**(%)**	**(°C)**	**(Times)**	**(Times)**	
	9	25	30	380.2	1	0	1st
				412.7	1	0	2nd
				513.7	1	0	3rd
Total					**3**	**0**	**3rd**

Nevertheless, there was a slight gap between the graphite punches and the die after the experiment ended on the third repetition of heating and elevations of the bottom stage of the Projection Welding machine sequentially which indicates the sample DHC-1 was not formed into the design shape as required. Therefore, based on this finding, it was a reason why the sample DHC-1 could not achieve a higher relative density. Differently with the position of the stainless steel die set block, it made a full contact with the Projection Welding machine's puncher at the end of the process. In **Figure 7.6-8**, shows the heating temperature against the time for the sample DHC-1. It presented the consistencies of incrementing the heating

temperature as the three elevations of the bottom stage took place. In **Figure 7.6-9**, it shows the pictures of the sample DHC-1 at the position of top and side.
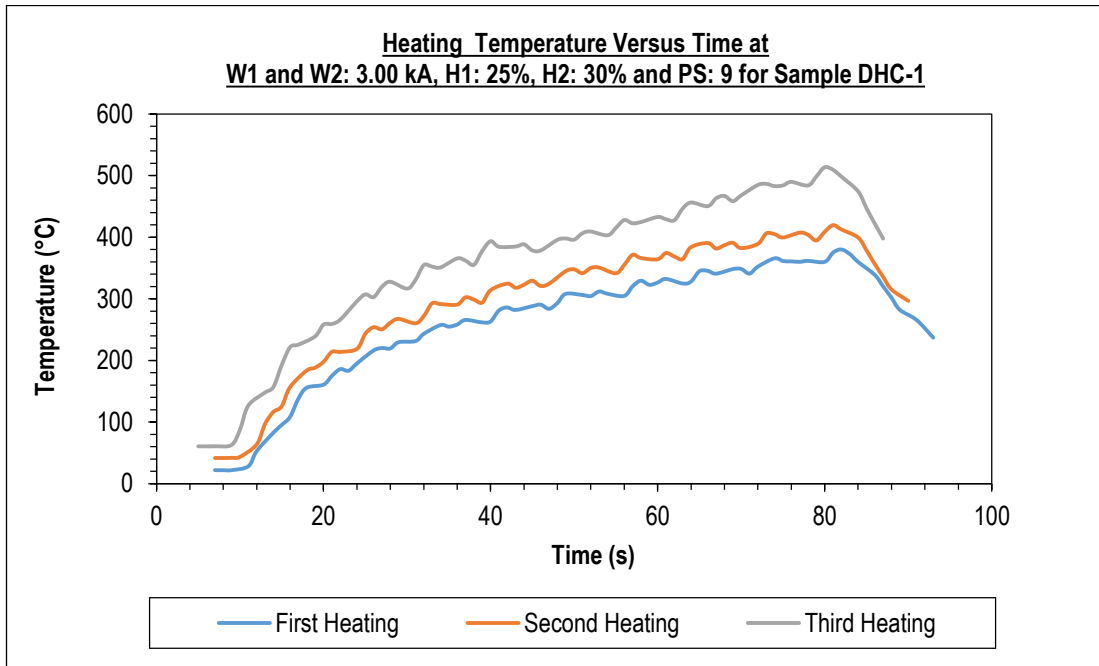
Figure 7.6-8: Heating temperature against time for the sample DHC-1 at 3.00 kA for first and second weld current, 25% for first heat, 30% for second heat and nine pulsations.
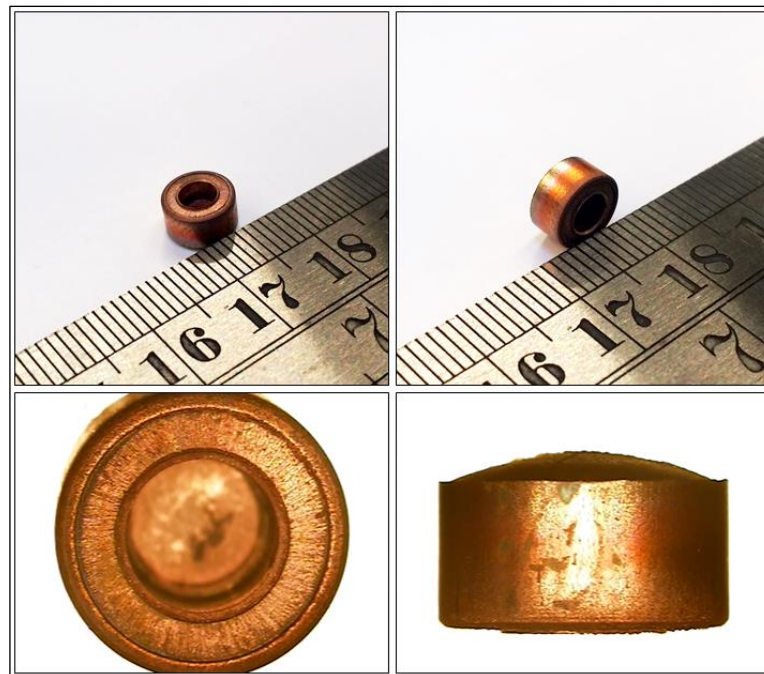
Figure 7.6-9: Sample DHC-1 pictures at top and side position.

7.6.2.1.2. Domed Hollow Cylinder Sample DHC-2

The density of the domed hollow cylinder sample can be improved by taking into consideration these two steps. Meanwhile, all the other parameters remained the same as described for the sample DHC-1. The first improvement steps which were added the repetitions of the force test only without the heating towards the densified sample DHC-2 after the repetitions of the heating end at the first and third elevation of the bottom stage of the Projection Welding machine as shown in **Table 7.6-10**. The total repetitions required for the force test to be made for the sample DHC-2 was three times which has been done twice at the first heating and only one time at the third heating. Besides that, for the second steps, the weight of the Cu powder was reduced from 1.2194 g for the sample DHC-1 to 1.0036 g for the formation of the sample DHC-2. It has been made to ensure the gap between the graphite punch and the die was fully closed at the end of the process. Therefore, based on the optimisation parameter that has been made, the sample DHC-2 has recorded the relative density of 93.23% with the total time of 544.88 s. It can be considered as a good densification result due to its complex feature of the sample compared to the previous electroplasticity sintering process as presented in **Table 2.3-3** where all the parts are simple cylindrical but the processing time consumed around three to five minutes to achieved the samples densification of 90.43 to 99%.

Table 7.6-10: Detail parameters data of the highest temperature recorded based on the first and the second weld current, the first and the second percentage of heat and the pulsations for sample DHC-2. The descriptions times of repetition for heating, force test and elevation bottom stage of the Projection Welding machine also have been described.

1st & 2nd Weld Current: 3.00 kA	Additional Parameters of the Data Information for Sample DHC-2						
	Pulsations	1st Heat (H1)	2nd Heat (H2)	Highest Temp.	Repetition of Heating	Repetition of Force Test	Elevation of Bottom Stage
		(%)	(%)	(°C)	(Times)	(Times)	
	9	25	30	654.4	1	2	1st
				912.0	1	0	2nd
				933.0	1	1	3rd
Total					3	3	3rd

Based on this finding, it showed that by using the repetition of the force test only without the heating during the open-air electrical-field activated sintering and forming process by using the Projection Welding machine, also helps to contribute the higher efficiency process to form a higher densification of the sample. In addition to that, the die set heating temperature distribution was uniform through the process of heating. In **Figure 7.6-10**, it shows the graph for the heating temperature against the time for the sample DHC-2 for each repetition of heating which shows the range of maximum temperature could be achieved from 654.4 °C to 933.0 °C. The differentiation between temperatures values for the sample DHC-2 compared to the sample DHC-1 happens even if the same heating parameter was used due to the elevations of the bottom stage for the sample DHC-2 has been made higher until the surface of the stainless steel die set block was tightly touching the surface of the machine's puncher for each of the repetitions of the heating. As a result illustrated in **Figure 7.6-10**, the heating temperature for the second and the third repetition of the process for the sample DHC-2 achieved higher heating temperature with the rapid looping compared to the sample DHC-1. In **Figure 7.6-11**, it shows the pictures of the sample DHC-2 at the position of top and side.
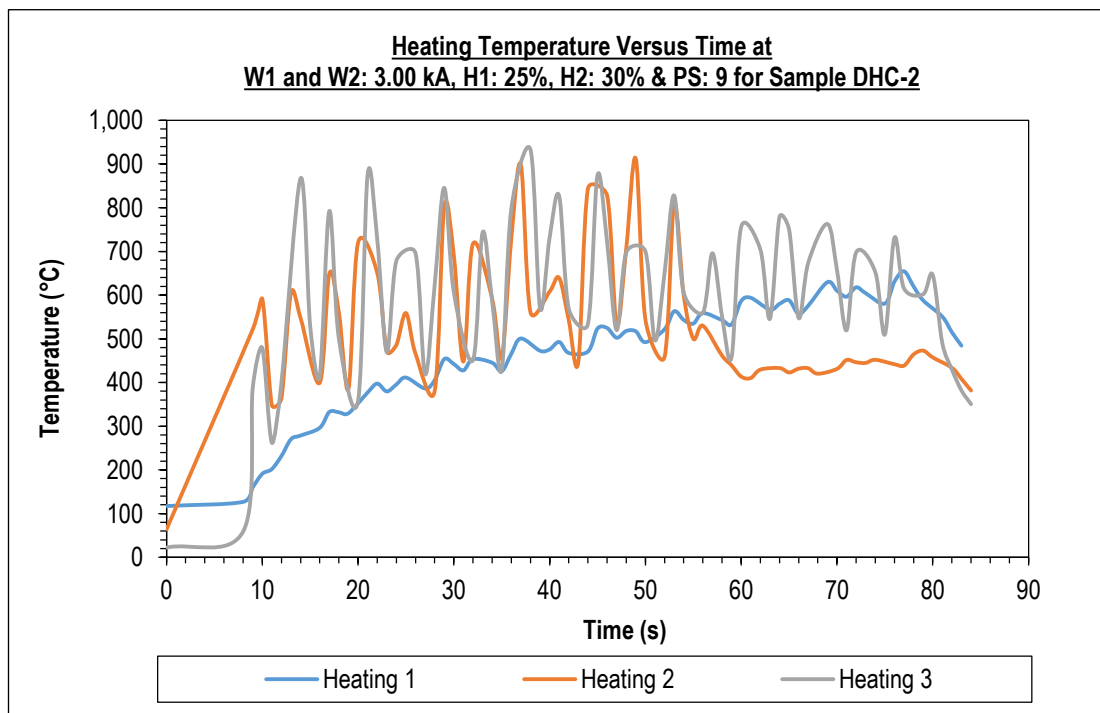
Figure 7.6-10: Heating temperature against time for the sample DHC-2 at 3.00 kA for first and second weld current, 25% for first heat, 30% for second heat and 9 pulsations.
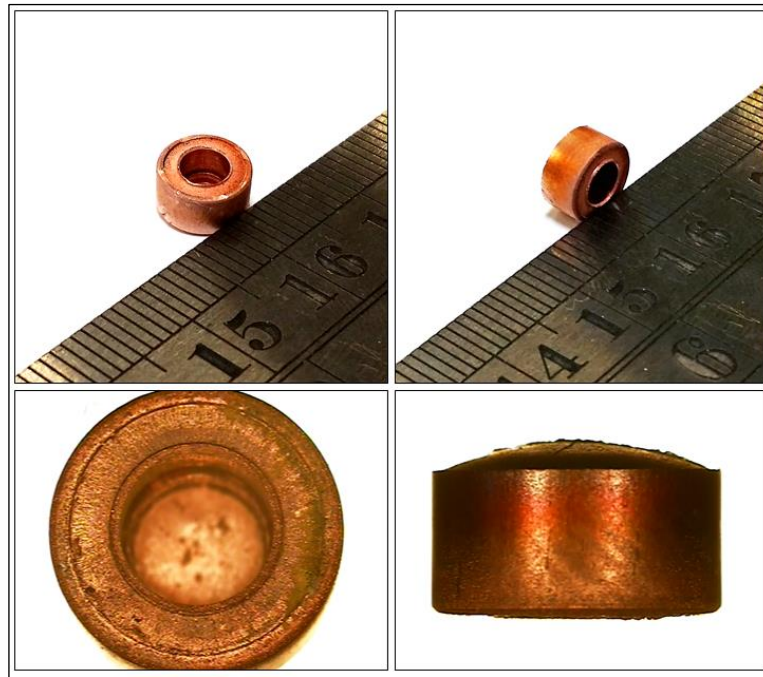
Figure 7.6-11: DHC-2 sample pictures at top and side position.

7.6.2.2. Turbine Samples

The turbine sample was a more complex component than has previously been experimented on with the open-air electrical-field activated sintering and forming process by using the Projection Welding machine. In **Figure 7.6-12**, it shows the condition of the open position for the graphite turbine die set along with the stainless steel die set block before the pouring of the Cu powder. Meanwhile, in **Figure 7.6-13**, it shows after the pouring process of the Cu powder inserted into the graphite turbine die set. In this experiment, two turbine samples have been made in the open-air electrical-field activated sintering and forming process using the Projection Welding machine. The name for the components was TR-1 and TR-2. The detail regarding the parameters of the experiment and the output results can be referred to **Table 7.6-11** and **Table 7.6-12** respectively. Based on the results, it shows that the sample TR-2 has the highest relative density of 88.08% compared to the sample TR-1 which only recorded the result of 66.91%. The reason why the turbine sample cannot achieved a higher densification as the domed hollow cylinder sample DHC-2 were due to the turbine die set was not fully closed between the graphite punches and the die for both of the turbine samples TR-1 and TR-2 as presented in the **Table 7.6-12**.
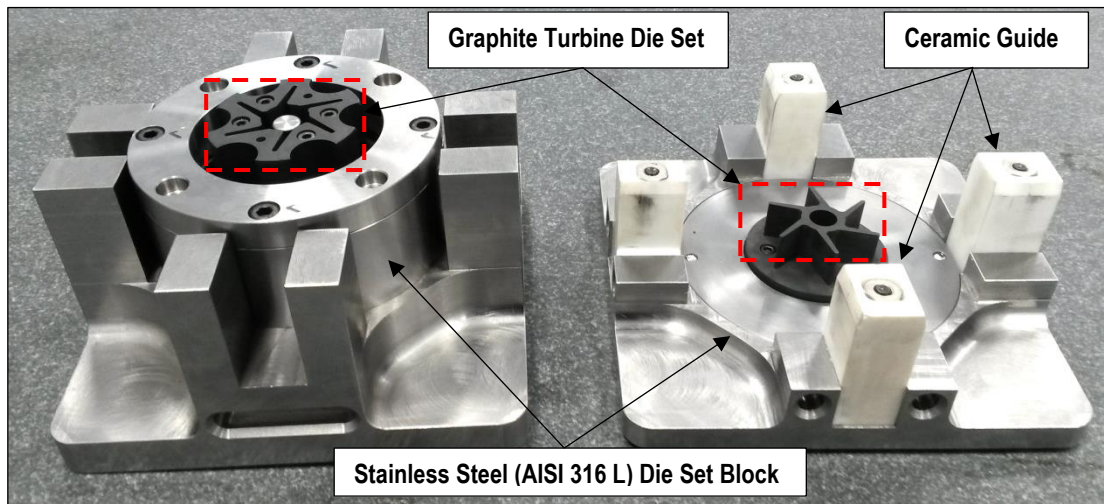
Figure 7.6-12: Open view of the die set for the forming of the turbine sample.
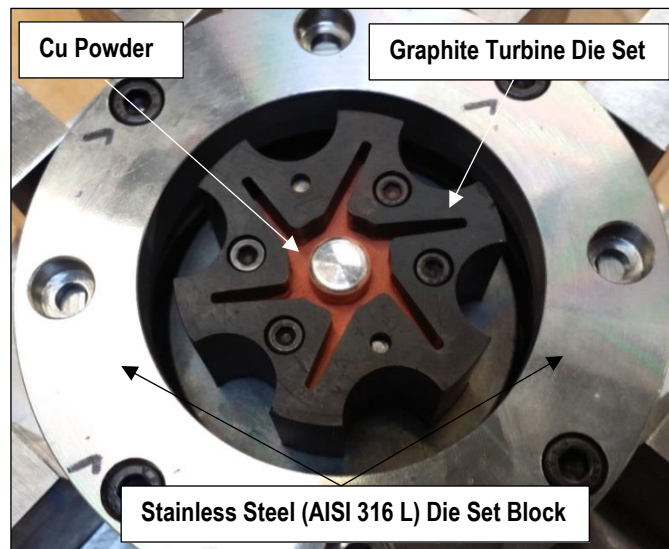
Figure 7.6-13: Cu powder filled in to the turbine die set.

The action of the further elevation for the bottom stage at the Projection Welding machine cannot be made much higher because if the excessive contacts between the stainless steel die set block with the machine's puncher happens, it will break the graphite turbine die set on the inside. It was because the Cu powders that needed to be sintered in the turbine samples was much larger in weight compared to the domed hollow cylinder components. It would take more times for the Cu powder to fully heat in the graphite turbine die set as the final stroke position of the Projection Welding machine pneumatic puncher taking place. Therefore, a precautionary step needs to be taken by not setting the machine's puncher too tight towards the stainless steel die set block with the graphite turbine die set inside. The improvement of

168

the pressure system in the Projection Welding machine needs to be taken for the future research by replacing the pneumatic system to the hydraulic operation. It can be controlled more efficiently by automatically adjusting with more or less travel of the stroke machine's puncher based on the input pressure parameter inserted before the experiment was conducted to produce the force needed during the conditions of the powder particles when they were not fully heated and after they were heated.

Table 7.6-11: Detail parameters of experiment for the forming of the Cu turbine samples.

Parameter of Experiments	Units	TR-1	TR-2
Weight Powder	g	25.0000	20.7077
Force	N	1,076	1,507
Total Elevation of Bottom Stage	Stage	11th	5th
Total Repetition of Heating	Times	12	8
Total Repetition of Force Test (No Heating)	Times	3	4
Highest Temperature Recorded	°C	507.4	537.1
Pre-Squeeze Time (PSQ)	s	5	5
Squeeze Time (SQ)	s	5	5
First Up Slope Time (U1)	s	0.6	0.6
First Weld Time (W1)	s	1.98	1.98
First Weld Current (I1)	kA	3.00	3.00
First Heat (H1)	%	10 to 35	30 to 32
First Cool Time (CL1)	s	1.98	1.98
Second Weld Time (W2)	s	1.98	1.98
Second Current (I2)	kA	3.00	3.00
Second Heat (H2)	%	10 to 35	30 to 32
Second Cool Time (CL2)	s	1.98	1.98
Pulsation (PS)	Times	96	68
Down Slope Time (DS)	s	0.6	0.6
Hold Time (Hold)	s	5	5
Off Time (Off)	s	5	5
Total Time Per Repetition for 5 Pulsations	s	60.80	60.80
Total Time Per Repetition for 9 Pulsations	s	92.48	92.48
Total Time	s	1,014.72	708.16

Table 7.6-12: Results of the experiment for the forming of the Cu turbine samples.

Results of Experiments	Units	TR-1	TR-2
Die Set Heating Temp. Distribution		Uniform	Uniform
Gap Between Punch and Die		Yes	Yes
Sample Weight	g	24.9727	20.6852
Sample Density	g/cm³	5.995	7.892
Relative Density	%	66.91	88.08

7.6.2.2.1. Turbine Sample TR-1

Based on **Table 7.6-13**, it shows the additional detail parameter of the data information for the sample TR-1 which achieved the relative densification of 66.91% with the total time of 1,014.72 s. Based on the experiment using the turbine samples, the optimisation parameter was needed to be obtained as the guideline for the formation of the turbine samples. Therefore, the first and the second percentage of heat, the pulsations, repetition of the heating, the force test and elevation of the bottom stage Projection Welding machine were tested to find the best setting input parameter to obtain the heating temperature around 500 °C. The heating temperature for the turbine samples was limited to around 500 °C due to a precautionary step not to burn the stainless steel die set block even though the ceramic guide has been installed to reduce the current flows from heating it.

Nevertheless, all the parameters for the first and second weld current during the experiment were set to be 3.00 kA. Meanwhile, there were two pulsations used in the experiment of five and nine times. The initial pulsation used nine times with the first and the second heat percentage start from 10 to 25% which obtained the heating temperature from 42.9 to 131.0 °C. During this period only twice the elevation of the bottom stage at the Projection Welding machine has been made alongside with four repetitions of the heating process without the repetitions of the force test. After that, due to the heating temperature having a slow increment, the first and the second percentage of heat was increased to 30% but the pulsation was reduced to five times and as a result it indicated the maximum reading of heating temperature was 151.7 °C. It has been made twice for the repetition of heating and elevation of the bottom stage of the machine. At this point still no repetition of force test has

170

been done due to the value of the maximum heating temperature obtained being low for the formation of the Cu powder particles.

Table 7.6-13: Detail parameters data of the highest temperature recorded based on the first and the second weld current, the first and the second percentage of heat and the pulsations for sample TR-1. The description times of repetition for heating, force test and elevation bottom stage of the Projection Welding machine also have been described.

Additional Parameters of the Data Information for Sample TR-1						
1st & 2nd Weld Current: 3.00 kA	Pulsations	1st & 2nd Heat (H1 & H2)	Highest Temp.	Repetition of Heating	Repetition of Force Test	Elevation of Bottom Stage
		(%)	(°C)	(Times)	(Times)	
	5	30	151.7	2	0	3rd, 4th
		35	408.5	1	0	7th
	9	10	42.9	1	0	1st
		15	66.0	1	0	2nd
		20	93.4	1	0	2nd
		25	131.0	1	0	2nd
		30	350.7	4	0	5th, 6th, 7th
		35	507.4	1	3	7th, 8th, 9th, 10th, 11th
Total				12	3	11th

Then, by using the same parameter of the first and the second heat as five pulsations before, instead, this time the pulsations were increased to nine where it indicated the maximum reading for heating temperature of 350.7 °C. It has been done four times on the repetition of heating and three times of elevation of the bottom stage of the machine. By this moment, it was started showing a better heating temperature with the given input parameter. Due to that, a slightly more incremental for the first and the second heat percentage have been set to 35% with five pulsations. Based on the result, it shows the value of 408.5 °C which is a positive outcome towards the heating temperature of the process. Lastly, by using the same for the first and the second percentage of heat 35%, one repetition of the heating, three repetition of the force test and four new elevations of the bottom stage from previous, the maximum heating temperature can be achieved to 507.4 °C.
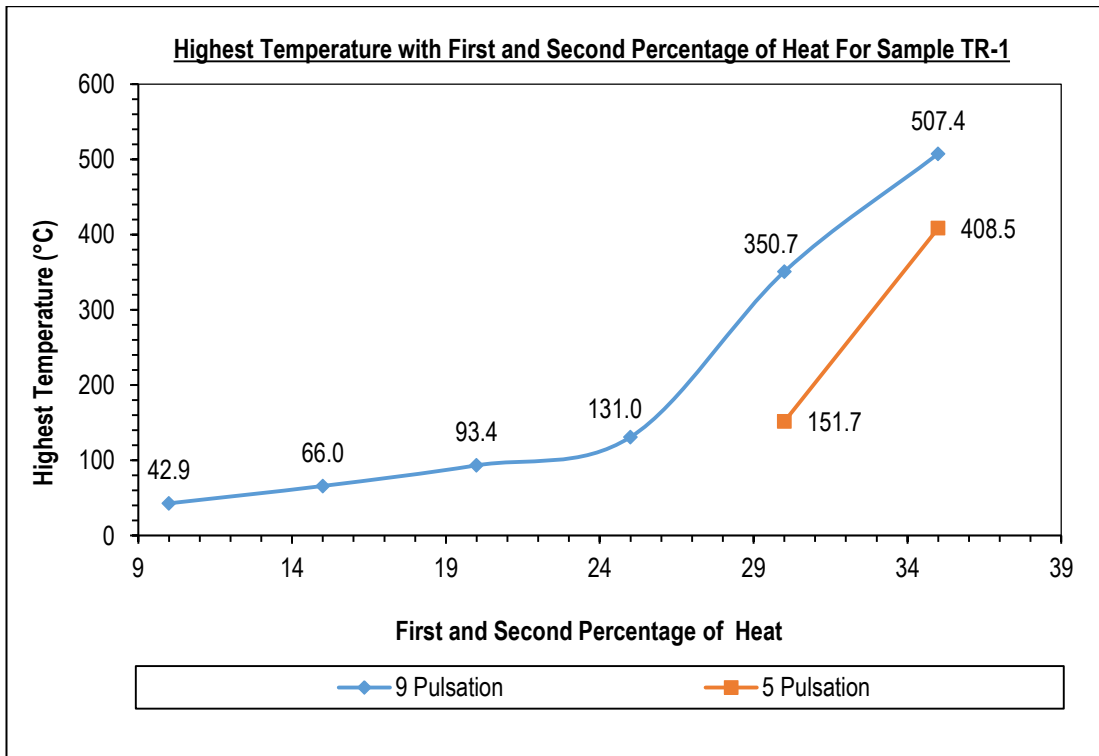
Figure 7.6-14: Highest temperature with the first and the second percentage of heat for the sample TR-1.
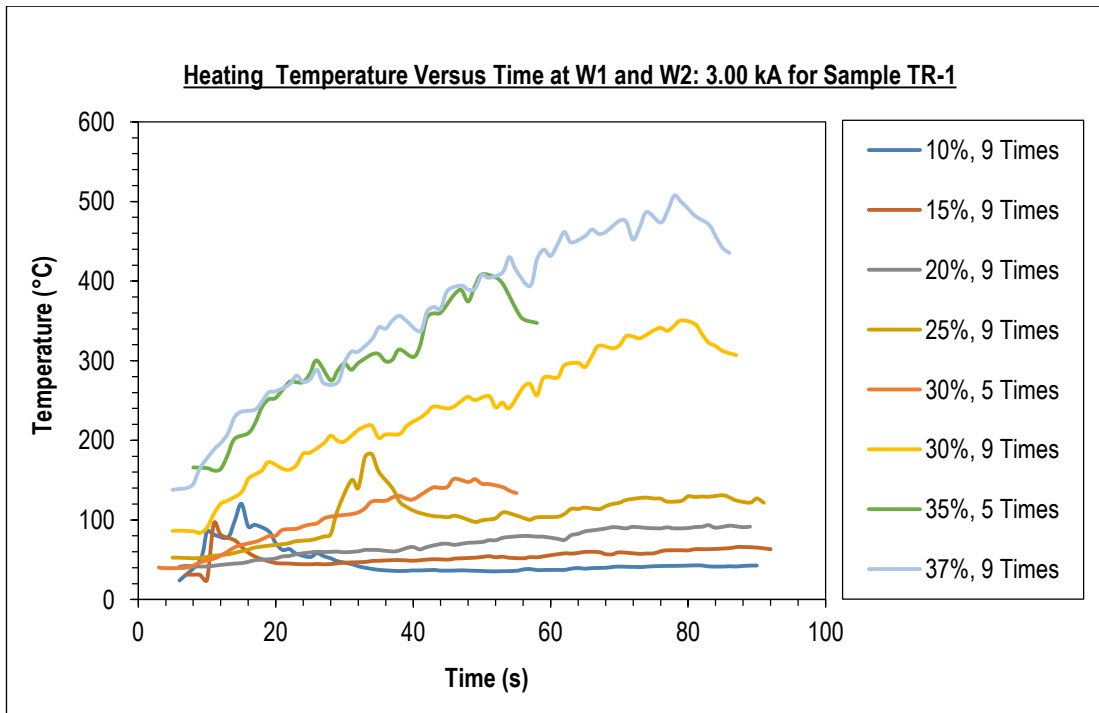
Figure 7.6-15: Heating temperature against time for the sample TR-1 at 3.00 kA for first and second weld current with the pulsations of the process.

172

In **Figure 7.6-14**, it shows the graph of the highest temperature obtained with the first and the second percentage of heat by using five and nine pulsations for the sample TR-1. Meanwhile, the graph of the heating temperature against time for sample TR-1 at 3.00 kA has been shown in **Figure 7.6-15** where it indicated by using first and second heat percentage from 10 to 37% with five to nine pulsations, the heating temperature can achieved the maximum temperature from 42.9 to 507.4 °C. The results were also helped by the repetitions of the heating, the force test and elevation of the bottom stage of the Projection Welding machine which has been described before this. The pictures of the sample TR-1 at the position of the top and the bottom can be referred to **Figure 7.6-16**.

Figure 7.6-16: TR-1 sample pictures at top and side positions.

7.6.2.2.2. Turbine Sample TR-2

Based on the trial and error methods done towards the sample TR-1 to find the optimum parameter for the process, the improvement needs to be made for the next experiment for the sample TR-2 by starting the first and the second heat from 30% to be capable of producing a higher relative density sample compared to sample TR-1. Besides that, the Cu powder weight

also has been reduced from 25.0000 to 20.7077 g. Meanwhile, the force for the experiment sample TR-2 has been increased from 1,076 to 1,507 N. All the other parameters remain the same as presented in **Table 7.6-11** along with the first and the second weld current recorded the reading of 3.00 kA as shown in **Table 7.6-14**.

Table 7.6-14: Detail parameters data of the highest temperature recorded based on the first and the second weld current, the first and the second percentage of heat and the pulsations for sample TR-2. The description times of repetition for heating, force test and elevation bottom stage of the Projection Welding machine also have been described.

Additional Parameter of the Data Information for Sample TR-2						
1st & 2nd Weld Current: 3.00 kA	Pulsations	1st & 2nd Heat (H1 & H2)	Highest Temp.	Repetition of Heating	Repetition of Force Test	Elevation of Bottom Stage
		(%)	(°C)	(Times)	(Times)	
	5	30	298.9	1	0	1st
	9	30	521.8	6	4	1st, 2nd, 3rd, 4th, 5th
		32	537.1	1	0	5th
Total				8	4	5th
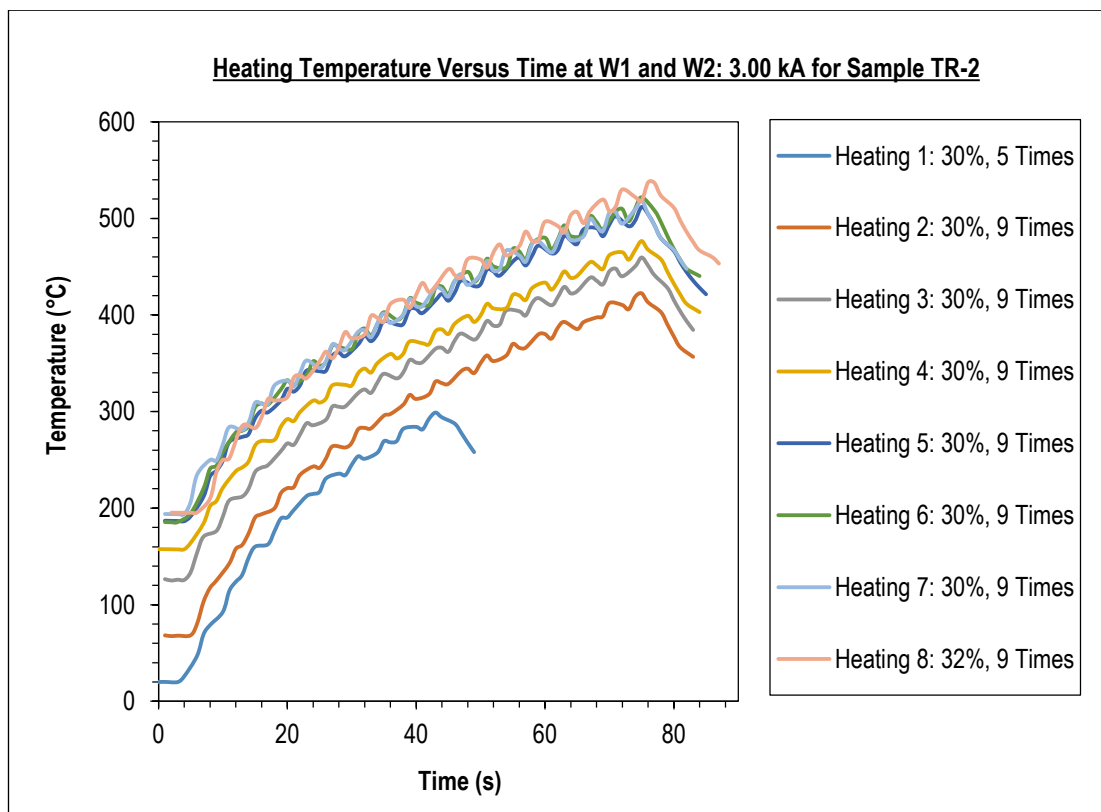
Figure 7.6-17: Heating temperature against time for the sample TR-2 at 3.00 kA for the first and second weld current with the pulsations of the process.

The experiment starts with five pulsations alongside the first and the second percentage of heat has been set to 30% which indicated the maximum heating temperature reading could be achieved to 298.9 °C. After that, the pulsations of the process have been increased to nine times with the same for the first and the second heat percentage of 30%. Regarding the repetition of the heating for the process, it has been done for six times. In addition to that, for the repetition of the force test and the elevation of the bottom stage at the Projection welding machine, it has been completed for four times which made the maximum heating temperature reading achieved to 521.8 °C. It showed positive results concerning the gain in heating temperature around 500 °C by using the nine pulsations with the 30% for the first and second heat. Nevertheless, it still required the additional steps such as the repetition of heating and the force test along with elevations of the bottom stage of the Projection welding machine. Therefore, by increasing the first and second heat percentage to 32% with the same elevation of the bottom stage of the Projection Welding machine as before, without any additional repetition of heating and force test it successfully to reach the maximum temperature of 537.1 °C.
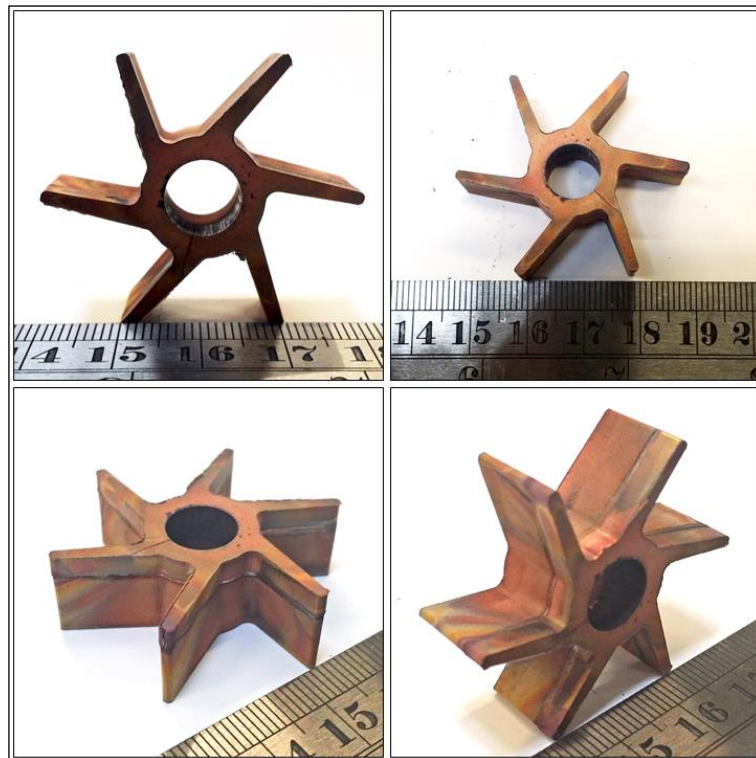
Figure 7.6-18: TR-2 sample pictures at top and side position.

As the result of the relative density of the sample TR-2, it recorded the reading of 88.08% with the total process time of 708.16 s which is 30.21% much faster compared to the sample TR-1 before this. The higher force used in the experiment which was 1,507 N compared to 1,076 N for the sample TR-1 also contributed to the densification of the sample TR-2. Based on the graph of the heating temperature against the time for the sample TR-2 at 3.00 kA which has been shown in **Figure 7.6-17**, it indicated the consistency of the maximum heating temperature based on the increment of the pulsations and the first and the second heat percentage of the process. The pictures of the sample TR-2 at the position of the top and the bottom can be referred to **Figure 7.6-18**.

7.7. Summary of the Chapter

The aims for the development of the Projection Welding machine towards the open-air electrical-field activated sintering and forming process have been made to deliver the same capabilities as the Gleeble® 3800 machine. The Projection Welding machine would be used more practically in the factory rather than the Gleeble® 3800 machine that is more suitable for the experimental purposes. Nevertheless, there is additional tooling, modifications along with the trial and error experiments needed to obtain the optimised parameters towards the usage of the Projection Welding machine. The development works have been done for the die set holder, the force management and the heating control which emphasises the energy required for the heating of the die set and the sample material. Based on the work that has been done in this chapter for the open-air electrical-field activated sintering and forming process by using the Projection Welding machine, it has been successful producing the multiple shapes of the sample such as cylindrical, domed hollow cylinder and turbine.

For the cylindrical sample that has been done for the 90Ti10Sn powder, it shows that 79.47% of relative density can be achieved for the sample 90Ti10Sn-D during the experiment as shown in **Table 7.6-2**. The densification of the cylinder sample 90Ti10Sn-D was not high compared to the results obtained during the experiment using the Gleeble® 3800 machine due to the process time to complete was shorter compared to the samples obtained by the process of the Gleeble® 3800 machine. It was because of the limitation of the pulsations heating in the Projection Welding machine which was limited to a maximum of nine times. By using only nine

times for the pulsations, it indicated the process total time of 92.48 s for each repetition of the heating process compared to 138.5 s which has been used for the experiment using Gleeble® 3800 machine to obtain the relative density of 98.51% for the sample 90Ti10Sn-4 as presented in **Table 6.5-8**. Nevertheless, the result obtained from the sample 90Ti10Sn-D was better if compared to the previous one of the electroplasticity sintering process such as spark plasma sintering as shown in **Table 2.3-2**, where it required 30 minutes to complete the process with the temperature of 1,100 °C to achieve the relative densification of 83% for the titanium alloy sample.

Therefore, the repetition of the heating process needs to be made to overcome the shortage time during the open-air electrical-field activated sintering and forming process by using the Projection Welding machine. Meanwhile, for the force test has been made to add more pressure towards the compaction of the sample after the heating process ends. In addition to that, the contact between the machine's puncher and the die set for each time of the process need to be continuously checked by carefully bringing up slightly higher the elevation of the bottom stage of the Projection Welding machine to successfully produce a better densification of parts. Based on the improvement towards the procedures of the experiment which has been stated before, the domed hollow cylinder sample DHC-2 by using the Cu powder has been tested and shows the highest relative density of 93.23% with the total time of 554.88 s as presented in **Table 7.6-7** and **Table 7.6-8**. It can be considered as a good densification result due to the complex feature of the sample compared to the previous electroplasticity sintering process as presented in **Table 2.3-3**, where all the parts are simple cylindrical but the processing time consumed around three to five minutes to achieve the samples densification of 90.43 to 99%.

After that, further experiments on the more complex shapes have been made by the turbine samples. Based on the results, it shows that the turbine sample TR-2 have the highest relative density of 88.08% with the total process time of 702.16 s as shown in **Table 7.6-11** and **Table 7.6-12**. The reason why the turbine sample TR-2 cannot achieve a higher densification as the domed hollow cylinder sample DHC-2 was due to the turbine die set was not fully closed between the graphite punches and the die. The action of the further elevation for the bottom stage at the Projection Welding machine for the sample TR-2 cannot be made

much higher to force the gap closed. If excessive contact between the stainless steel die set block and the machine's puncher happens, it will break the graphite turbine die set on the inside. It can be explained by the Cu powders that needed to be sintered in the turbine samples was much larger in weight compared to the domed hollow cylinder components. Thus, it would take more time for the Cu powder to fully generate heat in the graphite turbine die set as the final stroke position of the Projection Welding machine pneumatic puncher takes placed.

Therefore, the improvement of the pressure system in the Projection Welding machine needs to be adopted for the future research to successfully produce the higher relative density sample by replacing the pneumatic system with the hydraulic operation. It can be controlled more efficiently by automatically adjusting with more or less travel of the stroke machine's puncher based on the input pressure parameter inserted before the experiment is conducted to produce the force needed during the conditions when the powder particles were not fully heated and after they were heated.

Chapter 8: Conclusions and Recommendations for Future Work

8.1. Conclusions

Based on the research of the electrical-field activated sintering and forming process, improvements have been shown concerning the shortening of the process time for the manufacture of micro-components with a variety of powder material. In the conventional powder sintering method, neck and grain growth is an important mechanism to achieve the densification of the sample. Thus, this is the reason why the conventional powder sintering takes a long time to become completed due to the grain growth which was caused by coarsening associated with the surface diffusion or evaporation/condensation at high-temperature. In addition to that, compared to the spark plasma sintering process, it was not depended on the spark discharge to create the heating but using the electrical-field current and assisted by the high pressurisation where the mechanical plastic deformation, breakage and interface melting of the particles make a significant contributor to the densification of the samples produced. It was essential for the particle changing process to be present to achieve satisfactory and quick densification of the micro-parts beside the Joule heat inducing the plasticity. There was also no plasma occurring in the powder system due to the low voltage applied and rapid contacts established by the high pressure which made it would not be possible to simulate electrodischarge during a rapidly compacted powder system. Meanwhile, for the spark plasma sintering process, it required gaps between the particles, to simulated the spark discharge which as a result the pressure that needs to be applied cannot be too high to prevent the sparks from disappearing. The main difference between electrical-field activated sintering and forming process with the spark plasma sintering process was the better efficiency of the current flow to heat the particles of the powder, the high heating rate during the experiment to speed up the process, pressure dependent on the densification of the samples along with the simplified process setup and control. The detail regarding the stage of the densification mechanism for the electrical-field activated sintering and forming process can be referred to section **3.3 Densification Mechanism** which consists of the four stages period which are low-temperature pressing, high-temperature pressing, sintering with pressing and post-sintering cooling.

Hence, by taking consideration of the overview on the previous research compared to the research concept process which combines the micro-forming technology and the fast powder

sintering with applying the external electrical-field currents alongside the high applied pressure simultaneously towards the die set and material particles of the samples, this offers some potential as shown below compared to the existing conventional processes.

1) Fast sintering process;
2) Short manufacturing cycles;
3) No green compacts and argon gas needed;
4) Easy to control the microstructure of the part formed;
5) Options to use different metal powders and other materials combinations;
6) Potential for forming structurally and functionally graded parts;
7) Potential to form the bulk component with nano-structured materials;
8) Feasibility of the forming for micro-components with high strength materials;
9) Feasibility to form the 3D micro-parts with the dedicated micro-tool design and control;
10) Reducing the influences from the size-effect issues in the micro-forming process.

The main techniques used to overcome the typical barriers to the proposed process at the micro-scale for the electrical-field activated sintering and forming process were listed as below. This also indicates the gaps which differentiate the proposed process with the conventional methods currently employed.

a) Directly feeding the loose powders into the die set without the need to prepare a green compact and hence, small size components could be made based on the design of the die set used.

b) Directly forming the samples using the shaping of the die set without the need to use the lubricants. This is due to not needing to prepare the green compacts which are required in the conventional powder metallurgy process to help compaction in the mixing stage and reduce the friction.

c) Combining the micro-forming with the fast powder sintering to enable the formation of the complex shapes/features at the micro-sale, assisted by using the large current density to

enable the higher rate of electrical plasticity at the shorter time to achieve the significant plastic flow for attaining complex shapes of the samples produced.

8.2. Contributions to Knowledge

Table 8.2-1 shows the summary of the contributions to knowledge from the previous chapters of the research that has been conducted. All the aims and objectives as stated in section **1.2 Aims and Objectives** of the research have been achieved based on the process investigations, experiments and analyses that have been made.

Table 8.2-1: The summary of the contributions to knowledge based on the previous chapters by research electrical-field activated sintering and forming process of micro-components.

Chapter 1: Introduction	
Objectives	• Understand the research overview, motivation and contribution of the thesis.
Key Findings	• Overview of the research background and problems, aims and objectives, research methodology and thesis structures.
Chapter 2: Literature Review	
Objectives	• Identify the key problem and development issues facing the micro-manufacturing process and concentrates on the micro-forming technique focusing on the size effects issues. • One of the objectives of this research project was to eliminate the size effect problems in the manufacturing process by producing net shape samples which can offer a higher production rate and save cost. • Apprehend on the overview of the powder metallurgy process which is more focused on previous electroplasticity sintering process specifically towards the material titanium, titanium alloy and copper. • Identified for the improvement and the guidelines to develop the experiment parameters and proposed the die set designs.
Key Findings	• Micro-forming was one of the popular micro-manufacturing processes known that could satisfy the demand of the mass production along with enhancing the product performance with minimal waste to satisfy the constant demand by customers as well as manufactures that are relying more on smaller products with various applications. However, it was not an easy task to achieve the desired shape of a product. It was because the intricate details of some products required the use of the specific process to obtain the accuracy in shape and dimensions on the final product. • Other than that, the issues and challenges to manufacturing the micro-product need to be handle specifically such as in the factor that was negligible during the conventional process, unwanted external forces during the experiment to obtain the precise

	positioning, significant characteristic of the volume production, tooling dimension, commercial sensor dimension and performance, grade tolerance and surface quality specification, limitation on the shape of the micro-product and the material capability itself. The details regarding the explanations on these factors can be referred to section **2.1.1 Challenges to Manufacture Micro-Products.**
	• It can be summarised that the manufacture of a micro-product is still a challenging task which needs some improvement to be made due to the lack of sufficient standards, design/ manufacturing rules and understanding of the manufacturing itself.
	• Based on the application of electroplasticity process as explained in section **2.3 Electroplasticity** and **2.3.1 Research Based on Electroplasticity**, it can be considered as a promising new technique with high efficiency and low consumption of energy. It was suitable for the materials that are hard to be formed or less formable metal, especially for the bulk-form of micro-components. It can be explained due to the grain size effect as the Hall-Petch law stated that the finer grains of the material, the higher strength of the material would be. The details regarding size effects can be referred to section **2.1.4 Size Effects in Micro-Forming Processes.**
	• The application of the electroplasticity also can be seen have been utilised in the sintering technology which shows a significant potential to produce the micro-component by using powder as a raw material. Nevertheless, there were significant challenges to manufactured micro-parts to fulfil the requirement of the process which can complete in the short time but still achieved the higher relative densification of the samples as below. The detail description regarding the topic can be referred to **2.3.2 Application of Electrical-Field Activated on** Sintering. ▪ According to the reviews it has been shown that even though several researchers have made developments to the process using mainly spark plasma sintering process with titanium materials, the total time to achieved samples densification above 90% was approximately in the range of 20 to 60 minutes. ▪ In addition to that, some of the operations used in the titanium alloy materials need to have an annealing process done to the samples for about 24 to 40 hours at 1,000 °C and 750 °C respectively before or after the sintering process. ▪ Most of the components that have been produced were in the cylindrical shape which had the overall sizes in the range of five to 42 mm in diameter and five to 15 mm in thickness. ▪ The material for the die set was mainly graphite due to the maximum service heating temperature in the range of 1,300 to 1,700 °C.
	• Therefore, the electrical-field activated sintering and forming process has been developed to save time compared to the conventional electroplasticity sintering process. The concept comprises applying external electrical-field currents alongside the high applied pressure simultaneously to the die set and material particles of the samples.
Chapter 3: Process Concept of Electrical-Field Activated Sintering and Forming	
Objectives	• Explained the densification mechanism of the electrical-field activated sintering and

	forming process.
	• Comparisons between the research process with spark plasma sintering regarding the mechanism densification of the part formed and common parameters used.
Key Findings	• There were four stages involved in the densification mechanism of the electrical-field activated sintering and forming process which can be classified as low-temperature pressing, high-temperature pressing, sintering with pressing and post-sintering cooling. The details regarding the topic can be viewed on section **3.3.1 Stage 1: Low-Temperature Pressing** to **3.3.4 Stage 4: Post-Sintering Cooling**.
	• Although several researchers have made developments to the process using spark plasma sintering process, it still required a longer time to achieve the higher relative densification of samples. It was due to the spark plasma sintering depended on the gaps between the particles to simulated spark discharge that has been made by the pulse current. Therefore, if the application of pressure was too high, it would cause the disappearance of spark.
	• By using the parameters of the process such as low sintering and short sintering time also, efficiently inhibit the grain growth and permit the formation of material with density and fine crystalline structures. Thus, by using higher heating rate in the research process, it could be a major characteristic where it contributes to speed up the process to few minutes to be completed.
	• Therefore, it can be concluded that, the densification of the components by using electrical-field activated sintering and forming process can be archived by the involvement of the particle rearrangement, deformation, breakage and interface disappearance which was different from the conventional sintering process. It could be completed within a short time due to it being a continuously coupled process of the electrical-field which generated the Joule heat and high pressure.
Chapter 4: Die Sets Development	
Objectives	• Development of the die set for the experiment used in the facility of the Gleeble® 3800 and Projection Welding machine.
	• Consideration of the tool geometric design and the selection of the material used by the die set.
Key Findings	• There were two designs of the die sets that has been made for the electrical-field activated sintering and forming process which named as the die set A and B. The die set B was the optimisation design made from the die set A. The final output sample was in the cylindrical shape of four millimetres in diameter and height respectively.
	▪ Large transitions were introduced for the modification of the die set A to the die set B to reduce the thermal stress concentration in the punches.
	▪ Another positive contribution towards the punch modification was the positive effect of the concentrated heating at the punch nose, as more uniform temperature distributions in the middle section of the die occurred which could help to optimise the process of sintering.

	•	The material selection for the die set needed to follow the guidelines by comparing the compressive strength, thermal expansion coefficient and maximum service temperature of the selected material as discussed in section **4.3.1 Thermal Expansion Coefficient of the Die and Punches Materials** to **4.3.3 Maximum Service Temperature of the Die Sets and Sample Materials**. The purpose of this guideline was to hinder the punches and the sample from becoming trapped inside the die during the ejection process. In addition to that, by using the guidelines, all the possible combination for the die set with particularly sintered powder can be managed and known whether it was a good combination or not based on the fulfilment of the requirement of the process.
Chapter 5: Coupled FE Thermal-Electrical Analysis		
Objectives	•	Investigate the effect of the heating distributions applied to the die sets A and B during the electrical-field activated sintering and forming process by using the ABAQUS/CAE software as a tool for the coupled FE thermal-electrical analysis.
Key Findings	•	Based on the simulation of the electrical-heat analysis, it can be summarised that the die set B has shown the best result concerning the heating distribution towards its parts compared to the die set A. In step one which was an electrical analysis involving the electrical potential, the die set B has shown the most rapid heating distribution temperature compared to the die set A. The punches of the die set B surface and the core of the titanium sample has recorded the highest temperature reading of 1,781.43 °C and 1,814.18 °C for each in the step time of 1.5 s compared with the die set A where it recorded the value of 1,096.9 °C and 999.279 °C respectively with the step time of 150 s. It was proven for the modification of the punches for the die set B made a positive impact towards the heating tooling as describe in **Chapter 4: Die Sets Development.**
	•	Meanwhile, in step two of the thermal analysis which involved the transient heat transfers this shows that the die set A has the slowest cooling compared to the die set B. Rapid cooling of the die set was needed to shorten the process time which the die set B fulfilled the requirement by achieving the average of 55.370925 °C in just 18.3864 s compared to die set A which required 170.01 s to achieved the average declined temperature of 220.96625 °C. It was due to the die set B being made fully of the graphite (grade: Mersin 2333) material meanwhile for the die set A it has the combinations of the tungsten carbide (grade: VA 80) material for the punches and the graphite (grade: GV) material for its die. Therefore, for the die set that has utilised the graphite material, has a greater thermal conductivity which measures how well a material transfer the heat of 80 to 240 W/m.°C compared to tungsten carbide which has the value of 28 to 88 W/m.°C.
Chapter 6: Process Investigation with a Gleeble® 3800 Machine		
Objectives	•	Experimental study on the electrical-field activated sintering and forming process with a Gleeble® 3800 machine on the material of titanium (Ti) and titanium tin alloy (90Ti10Sn) alongside die set A and B.
	•	The samples obtained from the experiments were being analysed and discussed in detail to achieved conclusive results and findings of reliability of the overall process and the die sets for producing an excellent quality of the micro-products with high process efficiency.
Key Findings	•	The efficiency of the used die set during the electrical-field activated sintering and forming process provides significant contributions towards the sample size and its densification. It was an ideal condition to have a fully closed die set during the experiment as the current could pass through the die set and heat produced more efficiently. It could speed up the

die set heating compared if it has a gap where the current flow only could pass through the nose tips of the punches and towards the powder materials. As a result, the efficiency of the heating process would be lower. In addition to that, the sample size also could be more precise to the design sample which was four millimetres in diameter and height respectively.

- The sample Ti-3 and Ti-4 with the condition of fully closed die set A shows a better dimension measurement compared to the sample Ti-1 and Ti-2 where the die set A has a gap between punches and die at the end of the experiment as stated in **Table 6.5-1**.

- By using the optimised die set B, all the 90Ti10Sn samples shows the better dimensional reading due to die set B was fully closed at the end of the experiment as shown in **Table 6.5-3**.

- The die set B geometry design has shown the higher durability and the efficiency of transferring the heating to produce the samples and there were no issues during the ejection process of the samples. Moreover, the die set B can be used repeatedly in the cycle process compared to die set A during actual experiment.

- Concerning the densification of the samples, it shows that Ti-4 and 90Ti10Sn-4 have the highest relative densification of 98.55% and 98.51% compared to the others Ti and 90Ti10Sn samples with the process total time of 161 s and 138.5 s respectively. By using this efficiency process, it has the potential to save time compared to the conventional electroplasticity sintering process.

  - For the Ti-4 sample, it was used the optimum parameters of 125 MPa for the applied pressure, 1,100 °C for the second heating temperature, 100 °C/s for the second heating rate and five seconds for the second holding time.

  - Meanwhile, for the 90Ti01Sn-4 sample, it used the optimum parameters of 125 MPa for the applied pressure, 1,150 °C for the second heating temperature and 25 °C/s for the second heating rate and five seconds for the second holding time.

  - All the others parameters of the first heating stage process parameters for the Ti-4 and 90Ti10Sn-4 samples were the same which was 200 °C for the first heating, 20 °C/s for the second heating rate and 30 s for the first holding temperature. The cooling rate for the Ti-4 used 10 °C/s and 90Ti10Sn-4 used 20 °C/s.

- By using a high heating temperature, heating rate, holding time and applied constant pressure during the electrical-field activated sintering and forming process, it helps the deformation and breaking of the particles during the formation process for Ti and 90Ti10Sn samples. It differed from the conventional powder sintering process methods, where neck and grain growth are critical mechanisms needed to achieve the densification.

- Concerning the presence of carbon elements at the centre and edge of Ti and 90Ti10Sn samples, it shows the small amount of carbon contaminated.

  - For Ti samples, it indicates the reading was in the range of 2.54 to 3.64 wt% for the

	centre and 3.07 to 4.82 wt% for the edge location.
	▪ Meanwhile, for 90Ti10Sn samples, it showed the reading was in the range of 2.58 to 2.71 wt% for the centre and 2.72 to 2.87 wt% for the edge location.
	▪ This was due to the drawback of using graphite material for punches or die where the carbon can be mixed into the solidified sample during the high-temperature sintering process.
	• Furthermore, based on the highest densification of Ti and 90Ti10Sn samples, it has been chosen for testing of micro- and nano-hardness. Micro-hardness test has been made for sample Ti-4. It indicated the average reading of 205 to 243 HV at the surface and 199.5 to 208 HV at the inside of the sample Ti-4. For nano-hardness testing, Ti-4 and 90Ti10Sn-4 have been applied with 100 indentations which show the hardness value of 2.9149 GPa and 5.637277 GPa value respectively.
Chapter 7: Open-Air Sintering with a Projection Welding Machine	
Objectives	• Investigate the open-air electrical-field activated sintering and forming process with the application of the Projection Welding machine. It was a further comparison study for the vacuum environment which used the Gleeble® 3800 machine.
	• Besides the cylinder shape of the 90Ti10Sn micro-components, there were two others samples shape made by the Cu powder that have been produced using the Micro-FAST project die sets which was named as the domed hollow cylinder and the turbine samples.
Key Findings	• The aims for the development of the Projection Welding machine towards the open-air electrical-field activated sintering and forming process have been made to deliver the same capabilities as the Gleeble® 3800 machine which would be used more practically in the factory rather than the Gleeble® 3800 machine that more suitable for the experimental purposes.
	• Based on the work that has been done in this chapter, it has been successful in producing the multiple shapes of the sample such as cylindrical, domed hollow cylinder and turbine blade.
	▪ For the cylindrical sample that has been done for the 90Ti10Sn powder, it shows that 79.47% of relative density can be achieved for the sample 90Ti10Sn-D during the experiment. The densification of the cylinder sample 90Ti10Sn-D was not high compared to the results obtained during the experiment using the Gleeble® 3800 machine due to the process time to completed was shorter compared to the samples obtained by the vacuum process. It was because of the limitation of the pulsations heating in the Projection Welding machine being limited to a maximum of nine times. By using only nine times for the pulsations, it indicated the process total time of 92.48 s for each repetition of the heating process compared to 138.5 s which has been used for the experiment using Gleeble® 3800 machine to obtained the relative density of 98.51% for the sample 90Ti10Sn-4. Nevertheless, the result obtained from the 90Ti10Sn-D was better when compared to the previous of the electroplasticity sintering process such as spark plasma sintering as shown in **Table 2.3-2**, where it required 30 minutes to complete the process with the temperature of 1,100 °C to achieve the relative densification of 83% for the titanium alloy sample.

	▪ Therefore, the repetition of the heating process needs to be made to overcome the shortage time during the open-air electrical-field activated sintering and forming process by using the Projection Welding machine. Meanwhile, for the force test only has been made to add more pressure towards the compaction of the sample after the heating process ends. In addition to that, the contact between the machine's puncher and the die set for each time of the process need to be continuously checked by carefully bringing up slightly higher the elevation of the bottom stage of the Projection Welding machine to successfully produce a better densification parts. ▪ Based on the improvement towards the procedures of the experiment which has been stated before, the domed hollow cylinder sample DHC-2 by using the Cu powder has been tested and shows the highest relative density of 93.23% with the total time of 554.88 s. It can be considered as a good densification result due to its complex feature of the sample compared to the previous electroplasticity sintering process as presented in **Table 2.3-3**, where all the parts are simple cylindrical but the processing time consumed around three to five minutes to achieve the samples densification of 90.43 to 99%. ▪ After that, further experiments on more complex shapes have been made by working on the turbine samples. Based on the results, it shows that the turbine sample TR-2 have the highest relative density of 88.08% with the total process time of 702.16 s. The reason why the turbine sample TR-2 cannot achieve a higher densification as the domed hollow cylinder sample DHC-2 was due to the turbine die set was not fully closed between the graphite punches and the die. The action of the further elevation for the bottom stage at the Projection Welding machine for the sample TR-2 cannot be made much higher to force the gap closed. It was due to if excessive contact between the stainless steel die set block and the machine puncher happens, it will break the graphite turbine die set on the inside. It can be explained by the Cu powders that needed to be sintered in the turbine samples being much larger in weight compared to the domed hollow cylinder components. Thus, it would take more time for the Cu powder to fully generate heat in the graphite turbine die set as the final stroke position of the Projection Welding machine pneumatic puncher was taking placed.
Chapter 8: Conclusions and Recommendations for Future Work
Objectives	• The conclusions from the whole of the development work conducted and the suggestions for the recommendations for the future work on the development of electrical-field activated sintering and forming process has been provided.
Key Findings	• A summary of the development research work towards the electrical-field activated sintering and forming process has been presented in detail. It has covered the introduction of the research, literature reviews of the previous study, process concept of the research, die sets development, coupled FE thermal-electrical analysis on the development of the die set, process investigation with the Gleeble® 3800 machine and the open-air sintering with the Projection Welding machine. Considerations for future work that may assist in further the development of the research were also given.

8.3. Recommendations for Future Work

The recommendations for future works on this research have been described as below.

1) Utilise other alternative thermocouples for the measurement of the temperature where it can work at the highest temperature above 1,400 °C during the electrical-field activated sintering and forming process. This was suitable for the experiment which used the powder material of ceramic and nitrides powder where it needs the temperature of the process to be above 1,300 °C to achieve the excellent result of the relative density samples.

2) An extensive development work on the Projection Welding machine needs to be done regarding producing the control of the induced heat during the experiment. The usage of the additional control panel where the parameters of the experiment could be directly input into the machine system as applied in the Gleeble® 3800 machine would be helpful towards the efficiency of the process for the heating temperature that needs to be achieved.

3) In addition to that for the force management of the Projection Welding machine, this can be made by replacing the pneumatic system with a hydraulic system. It can be controlled more efficiently by automatically adjusting with more or less travel of the stroke machine's puncher. This is based on the input pressure parameter inserted before the experiment is conducted to produce the force needed during the condition of the powder particles both being not fully heated and after they are heated. It has been done to eliminate the possibility of breaking the die set due to excessive applied pressure and to secure satisfactory compaction towards the sintered samples.

4) Due to the fact that the samples produced are small, new mechanical testing methods/devices on the micro-samples are needed as the current option is designed to be more reliable for macro-size components. Also new standards of the procedure for testing also need to be established.

5) Regarding the presence of the carbon element at the centre and edge of the samples can be test and exam by using Wavelength-Dispersive X-Ray Spectroscopy (WDXS or WDS) compare to Energy-Dispersive X-Ray Spectroscopy (EDS) in order to get the accurate results for the value of the chemical element weight percentage of sample's carbon composition.

References

[1]   "Semiconductor Equipment Sales Forecast: $37 Billion in 2015 and $38 Billion in 2016," *SEMI Organization*, 2015. [Online]. Available: http://www.semi.org/en/node/60181. [Accessed: 29-Sep-2016].

[2]   C. K. Malek and V. Saile, "Applications of LIGA technology to precision manufacturing of high-aspect-ratio micro-components and -systems: a review," *Microelectronics J.*, vol. 35, no. 2, pp. 131–143, Feb. 2004.

[3]   S. Y. Liang, "Mechanical machining and metrology at micro/nano scale," in *Proc. of SPIE - The International Society for Optical Engineering, Third International Symposium on Precision Mechanical Measurements*, 2006, vol. 6280, pp. 628002– 628008.

[4]   Y. Qin, "Overview of Micro-Manufacturing," in *Micro-Manufacturing Engineering and Technology*, Elsevier Inc., 2010, pp. 1–23.

[5]   Y. Qin, A. Brockett, Y. Ma, A. Razali, J. Zhao, C. Harrison, W. Pan, X. Dai, and D. Loziak, "Micro-manufacturing: research, technology outcomes and development issues," *Int. J. Adv. Manuf. Technol.*, vol. 47, no. 9–12, pp. 821–837, 2010.

[6]   R. Ruprecht, T. Benzler, T. Hanemann, K. Müller, J. Konys, V. Piotter, G. Schanz, L. Schmidt, A. Thies, H. Wöllmer, and J. Haußelt, "Various replication techniques for manufacturing three-dimensional metal microstructures," *Microsyst. Technol.*, vol. 4, no. 1, pp. 28–31, 1997.

[7]   S. C. H. Thian, Y. Tang, J. Y. H. Fuh, Y. S. Wong, L. Lu, and H. T. Loh, "Micro-rapid-prototyping via multi-layered photo-lithography," *Int. J. Adv. Manuf. Technol.*, vol. 29, no. 9–10, pp. 1026–1032, 2006.

[8]   Y. Qin, "Micro-forming and miniature manufacturing systems — development needs and perspectives," *J. Mater. Process. Technol.*, vol. 177, no. 1–3, pp. 8–18, Jul. 2006.

[9]   A. Hannewald, "Micro-screws from the rotary press," *Umformtechnik*, vol. 2, pp. 28–29, 2002.

[10]   F. Vollertsen, Z. Hu, H. S. Niehoff, and C. Theiler, "State of the art in micro forming and

investigations into micro deep drawing," *J. Mater. Process. Technol.*, vol. 151, no. 1–3, pp. 70–79, Sep. 2004.

[11]   U. Engel and E. Egerer, "Basic Research on Cold and Warm Forging of Microparts," *Key Eng. Mater.*, vol. 233–236, pp. 449–456, 2003.

[12]   M. Geiger, M. Kleiner, R. Eckstein, N. Tiesler, and U. Engel, "Microforming," *CIRP Ann. - Manuf. Technol.*, vol. 50, no. 2, pp. 445–462, Jan. 2001.

[13]   R. W. Armstrong, "On size effects in polycrystal plasticity," *J. Mech. Phys. Solids*, vol. 9, no. 3, pp. 196–199, Jul. 1961.

[14]   N. Tiesler and U. Engel, "Microforming - effects of miniaturisation," in *Proceedings of 8th International Conference on Metal Forming*, 2000, pp. 355–360.

[15]   E. Uhlmann, G. Spur, N. A. Daus, and U. Doll, "Application of µ-EDM in the machining of micro structured forming tools," *Tech. Pap. - Soc. Manuf. Eng. AD*, no. 285, pp. 1–11, 1999.

[16]   E. Uhlmann, S. Piltz, and U. Doll, "Machining of micro/miniature dies and moulds by electrical discharge machining—Recent development," *J. Mater. Process. Technol.*, vol. 167, no. 2–3, pp. 488–493, Aug. 2005.

[17]   R. Orrù, R. Licheri, A. M. Locci, A. Cincotti, and G. Cao, "Consolidation/synthesis of materials by electric current activated/assisted sintering," *Mater. Sci. Eng. R Reports*, vol. 63, no. 4–6, pp. 127–287, 2009.

[18]   F. F. Lange, "Densification of powder compacts: An unfinished story," *J. Eur. Ceram. Soc.*, vol. 28, no. 7, pp. 1509–1516, Jan. 2008.

[19]   M. Zadra, F. Casari, L. Girardini, and A. Molinari, "Spark plasma sintering of pure aluminium powder: mechanical properties and fracture analysis," *Powder Metall.*, vol. 50, no. 1, pp. 40–45, 2007.

[20]   N. P. Mahalik, "Introduction," in *Micromanufacturing and Nanotechnology*, Berlin/Heidelberg: Springer-Verlag, 2006, pp. 1–468.

[21]   J. Jeswiet, M. Geiger, U. Engel, M. Kleiner, M. Schikorra, J. Duflou, R. Neugebauer, P. Bariani, and S. Bruschi, "Metal forming progress since 2000," *CIRP J. Manuf. Sci. Technol.*, vol. 1, no. 1, pp. 2–17, 2008.

[22] J. Jeswiet and M. Hauschild, "EcoDesign and future environmental impacts," *Mater. Des.*, vol. 26, no. 7, pp. 629–634, Jan. 2005.

[23] S. S. Dimov, E. B. J. P. Brousseau, R. Minev, and S. Bigot, "Micro- and nano-manufacturing: Challenges and opportunities," *J. Mech. Eng. Sci.*, vol. 226, pp. 3–15, 2011.

[24] U. Engel and R. Eckstein, "Microforming—from basic research to its realization," *J. Mater. Process. Technol.*, vol. 125–126, pp. 35–44, Sep. 2002.

[25] M. Koç and T. Özel, "Fundamentals of Micro-Manufacturing," in *Micro-Manufacturing: Design and Manufacturing of Micro-Products*, John Wiley & Sons, Inc., 2011, pp. 1–23.

[26] H. Ike and M. Plancak, "Coining process as a means of controlling surface microgeometry," *J. Mater. Process. Technol.*, vol. 80–81, pp. 101–107, Aug. 1998.

[27] Y. Saotome and H. Iwazaki, "Superplastic backward microextrusion of microparts for micro-electro-mechanical systems," *J. Mater. Process. Technol.*, vol. 119, no. 1–3, pp. 307–311, Dec. 2001.

[28] A. R. Razali, "High-precision, high speed strip feeding in micro-forming," University of Strathclyde, 2010.

[29] A. R. Razali and Y. Qin, "A review on micro-manufacturing, micro-forming and their key issues," *Procedia Eng.*, vol. 53, pp. 665–672, 2013.

[30] P. Rougeot, S. Regnier, and N. Chaillet, "Forces analysis for micro-manipulation," *2005 Int. Symp. Comput. Intell. Robot. Autom.*, pp. 105–110, 2005.

[31] F. Arai, D. Ando, T. Fukuda, Y. Nonoda, and T. Oota, "Micro manipulation based on micro physics-strategy based onattractive force reduction and stress measurement," *Proc. 1995 IEEE/RSJ Int. Conf. Intell. Robot. Syst. Hum. Robot Interact. Coop. Robot.*, vol. 2, pp. 236–241, 1995.

[32] F. Arai and T. Fukuda, "A new pick up and release method by heating for micromanipulation," *Proc. IEEE Tenth Annu. Int. Work. Micro Electro Mech. Syst. An Investig. Micro Struct. Sensors, Actuators, Mach. Robot.*, no. i, pp. 1–6, 1997.

[33] R. S. Fearing, "Survey of sticking effects for micro parts handling," *Proc. 1995 IEEE/RSJ Int. Conf. Intell. Robot. Syst. Hum. Robot Interact. Coop. Robot.*, vol. 2,

1995.

[34] J. T. Feddema, P. Xavier, and R. Brown, "Micro-assembly planning with van der Waals force," *Proc. 1999 IEEE Int. Symp. Assem. Task Plan. (Cat. No.99TH8470)*, no. July, pp. 32–38, 1999.

[35] J. Tomas, "Adhesion of ultrafine particles—A micromechanical approach," *Chem. Eng. Sci.*, vol. 62, no. 7, pp. 1997–2010, Apr. 2007.

[36] R. B. Aronson, "The New World of Micromanufacturing," *Manuf. Eng.*, vol. 140, p. 4, 2003.

[37] R. B. Aronson, "Micromanufacturing is growing," *Manuf. Eng.*, vol. 132, p. 4, 2004.

[38] Y. Kibe, Y. Okada, and K. Mitsui, "Machining accuracy for shearing process of thin-sheet metals—Development of initial tool position adjustment system," *Int. J. Mach. Tools Manuf.*, vol. 47, no. 11, pp. 1728–1737, 2007.

[39] B.-Y. Joo, S.-H. Rhim, and S.-I. Oh, "Micro-hole fabrication by mechanical punching process," *J. Mater. Process. Technol.*, vol. 170, no. 3, pp. 593–601, Dec. 2005.

[40] G.-L. Chern and Y. Chuang, "Study on vibration-EDM and mass punching of micro-holes," *J. Mater. Process. Technol.*, vol. 180, no. 1–3, pp. 151–160, Dec. 2006.

[41] Y. Okazaki, N. Mishima, and K. Ashida, "Microfactory—Concept, History, and Developments," *J. Manuf. Sci. Eng.*, vol. 126, no. 4, p. 837, 2004.

[42] L. Alting, F. Kimura, H. N. Hansen, and G. Bissacco, "Micro engineering," *CIRP Ann. - Manuf. Technol.*, vol. 52, no. 2, 2003.

[43] B. Nau, A. Roderburg, and F. Klocke, "Ramp-up of hybrid manufacturing technologies," *CIRP J. Manuf. Sci. Technol.*, vol. 4, no. 3, pp. 313–316, Jan. 2011.

[44] D. F. Heaney, "Mass production of micro-components utilising lithographic tooling and injection molding technologies," in *Proceedings of 1st International Conference on Micro-Manufacturing*, 2006, pp. 280–283.

[45] J. A. Palmer, J. D. Williams, T. Lemp, T. M. Lehecka, F. Medina, and R. B. Wicker, "Advancing three-dimensional MEMS by complimentary laser micro manufacturing," in *Proceedings SPIE 6109, Micromachining and Microfabrication Process Technology XI, 61090A*, 2006, vol. 6109, p. 61090A–61090A–8.

[46]   a. Sharon,   a. Bilsing, G. Lewis, and X. Z. X. Zhang, "Manufacturing of 3D microstructures using novel UPSAMS process (ultra precision manufacturing of self-assembled micro systems)," *Sixt. Annu. Int. Conf. Micro Electro Mech. Syst. 2003. MEMS-03 Kyoto. IEEE*, pp. 542–545, 2003.

[47]   W. Pfleging, W. Bernauer, T. Hanemann, and M. Torge, "Rapid fabrication of microcomponents - UV-laser assisted prototyping, laser micro-machining of mold inserts and replication via photomolding," *Microsyst. Technol.*, vol. 9, no. 1–2, pp. 67–74, 2003.

[48]   C. L. Kuo, J. D. Huang, and H. Y. Liang, "Fabrication of 3D Metal Microstructures Using a Hybrid Process of Micro-EDM and Laser Assembly," *Int. J. Adv. Manuf. Technol.*, vol. 21, no. 10–11, pp. 796–800, 2003.

[49]   J.-W. Chen and J. M. Zybko, "Diode laser bonding of planar microfluidic devices, MOEMS, bioMEMS, diagnostic chips, and microarrays," in *Proceedings SPIE 5718, Microfluidics, BioMEMS, and Medical Microsystems III*, 2005, vol. 5718, pp. 92–98.

[50]   A. J. Krejcie, S. G. Kapoor, and R. E. DeVor, "A hybrid process for manufacturing surgical-grade knife blade cutting edges from bulk metallic glass," *J. Manuf. Process.*, vol. 14, no. 1, pp. 26–34, Jan. 2012.

[51]   S. H. Ahn, D. M. Chun, and C. S. Kim, "Nanoscale hybrid manufacturing process by nano particle deposition system (NPDS) and focused ion beam (FIB)," *CIRP Ann. - Manuf. Technol.*, vol. 60, no. 1, pp. 583–586, 2011.

[52]   B. X. Jia, Z. L. Wang, F. Q. Hu, X. H. Li, and W. S. Zhao, "Research on Multifunctional Micro Machining Equipment," *Mater. Sci. Forum*, vol. 471–472, pp. 37–42, 2004.

[53]   L. B. Zhou, Y. Yaguchi, T. Fujii, J. Shimizu, and H. Eda, "Development of a Multifunctional Micro-Machining System and its Applications," *Key Eng. Mater.*, vol. 238–239, pp. 3–8, 2003.

[54]   Y.-S. Liao, S.-T. Chen, and C.-S. Lin, "Development of A Multi-function High Precision Tabletop CNC Machine for Making Micro Parts (Advanced machine tool)," *Proc. Int. Conf. Lead. Edge Manuf. 21st century LEM21*, vol. 2005, no. 2, pp. 485–490, Oct. 2005.

[55]   M. Rahman, H. S. Lim, K. S. Neo, A. Senthil Kumar, Y. S. Wong, and X. P. Li, "Tool-

based nanofinishing and micromachining," *J. Mater. Process. Technol.*, vol. 185, no. 1–3, pp. 2–16, Apr. 2007.

[56] Y. B. Bang, K. M. Lee, and S. Oh, "5-Axis Micro Milling Machine for Machining Micro Parts," *Int. J. Adv. Manuf. Technol.*, vol. 25, no. 9–10, pp. 888–894, 2005.

[57] M. Arentoft and N. A. Paldan, "Production equipment for manufacturing of micro metal components," in *Proceedings of the 9th International ESAFORM Conference on Material Forming*, 2006, pp. 579–582.

[58] Y. Qin, Y. Ma, C. Harrison, A. Brockett, M. Zhou, J. Zhao, F. Law, A. Razali, R. Smith, and J. Eguia, "Development of a new machine system for the forming of micro-sheet-products," *Int. J. Mater. Form.*, vol. 1, no. 1, pp. 475–478, 2008.

[59] C. Hartl, J. Lungershausen, J. Equia, L. Uriate, and P. Lopes Garcia, "Micro hydroforming process and machine system for miniature/micro products," in *Proceedings of International Conference 7th Euspen, Bremen 2*, 2007, pp. 69–72.

[60] G.-Y. Kim, J. Ni, and M. Koç, "Modeling of the Size Effects on the Behavior of Metals in Microscale Deformation Processes," *J. Manuf. Sci. Eng.*, vol. 129, no. 3, p. 470, 2007.

[61] W. Sylwestrowicz and E. O. Hall, "The Deformation and Ageing of Mild Steel," *Proc. Phys. Soc. Sect. B*, vol. 64, no. 9, pp. 747–753, 2002.

[62] N. J. Petch, "The Cleavage Strength of Polycrystals," *J. Iron Steel Inst.*, vol. 174, pp. 25–28, 1953.

[63] M. Koç and S. Mahabunphachai, "Feasibility investigations on a novel micro-manufacturing process for fabrication of fuel cell bipolar plates: Internal pressure-assisted embossing of micro-channels with in-die mechanical bonding," *J. Power Sources*, vol. 172, no. 2, pp. 725–733, Oct. 2007.

[64] N. Hansen, "The effect of grain size and strain on the tensile flow stress of aluminium at room temperature," *Acta Metall.*, vol. 25, no. 8, pp. 863–869, Aug. 1977.

[65] L. V. Raulea, A. M. Goijaerts, L. E. Govaert, and F. P. T. Baaijens, "Size effects in the processing of thin metal sheets," *J. Mater. Process. Technol.*, vol. 115, no. 1, pp. 44–48, Aug. 2001.

[66] J. . Michel and P. Picart, "Size effects on the constitutive behaviour for brass in sheet

metal forming," *J. Mater. Process. Technol.*, vol. 141, no. 3, pp. 439–446, Nov. 2003.

[67] T. A. Kals and R. Eckstein, "Miniaturization in sheet metal working," *J. Mater. Process. Technol.*, vol. 103, no. 1, pp. 95–101, Jun. 2000.

[68] S. Miyazaki, H. Fujita, and H. Hiraoka, "Effect of specimen size on the flow stress of rod specimens of polycrystalline Cu-Al alloy," *Scr. Metall.*, vol. 13, no. 6, pp. 447–449, Jun. 1979.

[69] R. M. Onyancha and B. L. Kinsey, "Investigation of Size Effects on Process Models for Plane Strain Microbending," in *ASME 2006 International Manufacturing Science and Engineering Conference, Manufacturing Science and Engineering, Parts A and B, Ypsilanti, Michigan, USA*, 2006, pp. 257–266.

[70] J. T. Black and R. A. Kohser, "Powder Metallurgy," in *DeGarmo's Materials and Processes in Manufacturing*, Wiley, 2011, p. 461.

[71] R. K. Raiput, "Powder Metallurgy," in *A Textbook of Manufacturing Technology: Manufacturing Process*, Laxmi Publications (P) LTD, 2007, pp. 219–220.

[72] J. W. Newkirk and S. N. Thakur, "Heat Treatment of Powder Metallurgy Steel Components," in *Steel Heat Treatment*, CRC Press, 2006, pp. 741–786.

[73] "Powder Metallurgy - Conventional Processing," *European Powder Metallurgy Association (EPMA)*. [Online]. Available: http://www.epma.com/powder-metallurgy-conventional-processing. [Accessed: 04-Oct-2016].

[74] E. P De Garmo, J. T Black, and R. A Kohser, "Powder Metallurgy," in *DeGarmo's Materials and Processing in Manufacturing*, 11th ed., Hoboken, NJ : John Wiley & Sons, 2013, pp. 481–506.

[75] The European Powder Metallurgy Association, "Powder Metallurgy - Sintering Temperatures for Some Common Metals," *The European Powder Metallurgy Association*, 2013. [Online]. Available: http://www.azom.com/article.aspx?ArticleID=1727. [Accessed: 18-Sep-2015].

[76] O. A. Troitskii, "Electromechanical Effect in Metals," *ZhETF Pis ma Redaktsiiu*, vol. 10, pp. 18–22, 1969.

[77] G. Tang, J. Zhang, M. Zheng, J. Zhang, W. Fang, and Q. Li, "Experimental study of

electroplastic effect on stainless steel wire 304L," *Mater. Sci. Eng. A*, vol. 281, no. 1–2, pp. 263–267, Apr. 2000.

[78] G. Tang, M. Zheng, Y. Zhu, J. Zhang, W. Fang, and Q. Li, "The application of the electro-plastic technique in the cold-drawing of steel wires," *J. Mater. Process. Technol.*, vol. 84, no. 1–3, pp. 268–270, Dec. 1998.

[79] M. S. Siopis, "Investigation of electrical-assisted forming at the microscale," University of New Hampshire, Ann Arbor, 2009.

[80] J. Mai, L. Peng, X. Lai, and Z. Lin, "Electrical-assisted embossing process for fabrication of micro-channels on 316L stainless steel plate," *J. Mater. Process. Technol.*, vol. 213, no. 2, pp. 314–321, Feb. 2013.

[81] C. Ross and J. T. Roth, "The Effects of DC Current on the Tensile Properties of Metals," in *ASME 2005 International Mechanical Engineering Congress and Exposition Materials*, 2005, pp. 363–372.

[82] R. E. Reed-Hill, *Physical Metallurgy Principles*, 2nd Ed. PWS Kent, 1973.

[83] T. a. Perkins, T. J. Kronenberger, and J. T. Roth, "Metallic Forging Using Electrical Flow as an Alternative to Warm/Hot Working," *J. Manuf. Sci. Eng.*, vol. 129, no. 1, p. 84, 2007.

[84] L. Yao, C. Hong, G. Yunqou, and H. Xinbin, "Effect of Electric Current Pulse On Superplastic of Aluminum Alloy 7475," *Trans. Nonferrous Met. Soc. China*, vol. 6, no. 1, pp. 77–80, 1996.

[85] O. A. Troitskii, "Anisotropy of the Effect of Electron-Beam and α-Irradiation on the Deformation Process of Zinc Single Crystals in the Brittle State," *Akad. Nauk SSSR 148*, pp. 332–334, 1963.

[86] H. Conrad, "Electroplasticity in metals and ceramics," *Mater. Sci. Eng. A*, vol. 287, no. 2, pp. 276–287, Aug. 2000.

[87] G. Tang, J. Zhang, Y. Yan, H. Zhou, and W. Fang, "The engineering application of the electroplastic effect in the cold-drawing of stainless steel wire," *J. Mater. Process. Technol.*, vol. 137, no. 1–3, pp. 96–99, Jun. 2003.

[88] C. D. Ross, D. B. Irvin, and J. T. Roth, "Manufacturing Aspects Relating to the Effects

of Direct Current on the Tensile Properties of Metals," *J. Eng. Mater. Technol.*, vol. 129, no. 2, p. 342, 2007.

[89]   J. S. Andrawes, T. J. Kronenberger, T. a. Perkins, J. T. Roth, and R. L. Warley, "Effects of DC Current on the Mechanical Behavior of AlMg1SiCu," *Mater. Manuf. Process.*, vol. 22, no. 1, pp. 91–101, 2007.

[90]   J. T. Roth, I. Loker, D. Mauck, M. Warner, S. F. Golovashchenko, and A. Krause, "Enhanced Formability of 5754 Aluminum Sheet Metal Using Electric Pulsing," in *Society of Manufacturing Engineers (Technical Papers)*, 2008, pp. 405–412.

[91]   V. V. Stolyarov, "Deformability and nanostructuring of TiNi shape-memory alloys during electroplastic rolling," *Mater. Sci. Eng. A*, vol. 503, no. 1–2, pp. 18–20, Mar. 2009.

[92]   M. S. Siopis and B. L. Kinsey, "Experimental Investigation of Grain and Specimen Size Effects During Electrical-Assisted Forming," *J. Manuf. Sci. Eng.*, vol. 132, no. 2, p. 21004, 2010.

[93]   Y. Lu, T. Qu, P. Zeng, L. Lei, G. Fang, and J. Sun, "The influence of electroplastic rolling on the mechanical deformation and phase evolution of Bi-2223/Ag tapes," *J. Mater. Sci.*, vol. 45, no. 13, pp. 3514–3519, 2010.

[94]   S. Maki, Y. Harada, K. Mori, and H. Makino, "Application of resistance heating technique to mushy state forming of aluminium alloy," *J. Mater. Process. Technol.*, vol. 125–126, pp. 477–482, Sep. 2002.

[95]   K. Mori, S. Maki, and Y. Tanaka, "Warm and Hot Stamping of Ultra High Tensile Strength Steel Sheets Using Resistance Heating," *CIRP Ann. - Manuf. Technol.*, vol. 54, no. 1, pp. 209–212, Jan. 2005.

[96]   K. Mori, S. Saito, and S. Maki, "Warm and hot punching of ultra high strength steel sheet," *CIRP Ann. - Manuf. Technol.*, vol. 57, no. 1, pp. 321–324, 2008.

[97]   J. Yanagimoto and R. Izumi, "Continuous electric resistance heating—Hot forming system for high-alloy metals with poor workability," *J. Mater. Process. Technol.*, vol. 209, no. 6, pp. 3060–3068, Mar. 2009.

[98]   C. M. Dzialo, M. S. Siopis, B. L. Kinsey, and K. J. Weinmann, "Effect of current density and zinc content during electrical-assisted forming of copper alloys," *CIRP Ann. -*

Manuf. Technol., vol. 59, no. 1, pp. 299–302, 2010.

[99]   K. Mori and Y. Okuda, "Tailor die quenching in hot stamping for producing ultra-high strength steel formed parts having strength distribution," *CIRP Ann. - Manuf. Technol.*, vol. 59, no. 1, pp. 291–294, 2010.

[100]   K. Mori, T. Maeno, and Y. Fukui, "Spline forming of ultra-high strength gear drum using resistance heating of side wall of cup," *CIRP Ann. - Manuf. Technol.*, vol. 60, no. 1, pp. 299–302, 2011.

[101]   M. Eriksson, Z. Shen, and M. Nygren, "Fast densification and deformation of titanium powder," *Powder Metall.*, vol. 48, no. 3, pp. 231–236, 2005.

[102]   R. Chaudhari and R. Bauri, "Microstructure and Mechanical Properties of Titanium Processed by Spark Plasma Sintering (SPS)," *Metallogr. Microstruct. Anal.*, vol. 3, no. 1, pp. 30–35, 2014.

[103]   K. Asaoka and M. Kon, "Sintered porous titanium and titanium alloys as advanced biomaterials," *Thermec 2003 Processing and Manufacturing of Advanced Materials*, vol. 426–432, no. 4. Department of Dental Engineering, School of Dentistry, University of Tokushima, 3 Kuramoto-cho, Tokushima 770-8504, Japan, pp. 3079–3084, 2003.

[104]   J. Onagawa, T. Goto, O. Ise, N. Ishii, T. Horikawa, and K. Sawada, "Corrosion Resistance of Titanium-Platinum Alloy Prepared by Spark Plasma Sintering," *Mater. Trans. JIM*, vol. 37, no. 11, pp. 1699–1703, 1996.

[105]   Y. F. Yang, H. Imai, K. Kondoh, and M. Qian, "Comparison of spark plasma sintering of elemental and master alloy powder mixes and prealloyed Ti-6Al-4V powder," *Int. J. Powder Metall.*, vol. 50, no. 1, pp. 41–47, 2014.

[106]   S. . Wang, L. . Chen, Y. . Kang, M. Niino, and T. Hirai, "Effect of plasma activated sintering (PAS) parameters on densification of copper powder," *Mater. Res. Bull.*, vol. 35, no. 4, pp. 619–628, 2000.

[107]   T. S. Srivatsan, B. G. Ravi, A. S. Naruka, L. Riester, S. Yoo, and T. S. Sudarshan, "Microstructure and hardness of copper powder consolidated by plasma pressure compaction," *J. Mater. Eng. Perform.*, vol. 10, no. 4, pp. 449–455, 2001.

[108]   T. S. Srivatsan, B. G. Ravi, A. S. Naruka, L. Riester, S. Yoo, and T. S. Sudarshan, "A

study of microstructure and hardness of bulk copper sample obtained by consolidating nanocrystalline powders using plasma pressure compaction," *Mater. Sci. Eng. A*, vol. 311, no. 1, pp. 22–27, 2001.

[109] Z. J. Zhou and Y. S. Kwon, "Fabrication of W–Cu composite by resistance sintering under ultra-high pressure," *J. Mater. Process. Technol.*, vol. 168, no. 1, pp. 107–111, 2005.

[110] C. H. Liu and P. W. Kao, "Microstructure and mechanical properties of resistance sintered titanium," *Scr. Metall. Mater.*, vol. 24, no. 12, pp. 2279–2284, Dec. 1990.

[111] M. Zadra, F. Casari, L. Girardini, and A. Molinari, "Microstructure and mechanical properties of cp-titanium produced by spark plasma sintering," *Powder Metall.*, vol. 51, no. 1, pp. 59–65, Mar. 2008.

[112] L. Liu, G. Liu, Y. Xiong, J. Chen, C. Kang, X. Huang, and Y. Tian, "Fabrication of Fresnel zone plates with high aspect ratio by soft X-ray lithography," *Microsyst. Technol.*, vol. 14, no. 9–11, pp. 1251–1255, 2008.

[113] J. R. Serrano and L. M. Phinney, "Displacement and thermal performance of laser-heated asymmetric MEMS actuators," *J. Microelectromechanical Syst.*, vol. 17, no. 1, pp. 166–174, 2008.

[114] K. Feng, M. Hong, Y. Yang, and W. Wang, "Combustion synthesis of VC/Fe composites under the action of an electric field," *Int. J. Refract. Met. Hard Mater.*, vol. 27, no. 5, pp. 852–857, Sep. 2009.

[115] M. Demuynck, J.-P. Erauw, O. Van der Biest, F. Delannay, and F. Cambier, "Densification of alumina by SPS and HP: A comparative study," *J. Eur. Ceram. Soc.*, vol. 32, no. 9, pp. 1957–1964, Jul. 2012.

[116] Z. Shen, M. Johnsson, Z. Zhao, and M. Nygren, "Spark Plasma Sintering of Alumina," *J. Am. Ceram. Soc.*, vol. 85, no. 8, pp. 1921–1927, 2002.

[117] M. P. Harmer and R. J. Brook, "Fast firing-microstructure benefits," *J. Br. Ceram. Soc.*, vol. 80, no. 5, pp. 147–148, 1981.

[118] M. Zulkipli, Y. Qin, K. Huang, H. Hijji, Y. Zhao, and J. Zhao, "Forming of titanium and titanium alloy miniature-cylinders by electrical-field activated powder sintering and

forming," in *4th International Conference on New Forming Technology (ICNFT 2015): MATEC Web of Conferences*, 2015, vol. 21.

[119] M. Karttunen, P. Ruuskanen, and J. Enqvist, "Electrically Conductive Composite Powders and Compounds Produced with Solid State Synthesis," *Mater. Manuf. Process.*, vol. 20, no. 5, pp. 887–892, 2005.

[120] D. V. Quach, H. Avila-Paredes, S. Kim, M. Martin, and Z. A. Munir, "Pressure effects and grain growth kinetics in the consolidation of nanostructured fully stabilized zirconia by pulsed electric current sintering," *Acta Mater.*, vol. 58, no. 15, pp. 5022–5030, Sep. 2010.

[121] Z. A. Munir, "The effect of external electric fields on the nature and properties of materials synthesized by self-propagating combustion," *Mater. Sci. Eng. A*, vol. 287, no. 2, pp. 125–137, Aug. 2000.

[122] F. Wakai and Y. Shinoda, "Anisotropic sintering stress for sintering of particles arranged in orthotropic symmetry," *Acta Mater.*, vol. 57, no. 13, pp. 3955–3964, Aug. 2009.

[123] W. Chen, *Gleeble System and Application*, 1st ed. New York, NY, USA: Gleeble System School, 1998.

[124] F. Li, J. Pan, O. Guillon, and A. Cocks, "Predicting sintering deformation of ceramic film constrained by rigid substrate using anisotropic constitutive law," *Acta Mater.*, vol. 58, no. 18, pp. 5980–5988, Oct. 2010.

[125] N. Beri, S. Maheshwari, C. Sharma, and A. Kumar, "Technological Advancement in Electrical Discharge Machining with Powder Metallurgy Processed Electrodes: A Review," *Mater. Manuf. Process.*, vol. 25, no. 10, pp. 1186–1197, 2010.

[126] D. Lu, Y. Yang, Y. Qin, and G. Yang, "Effect of particle size and sintering temperature on densification during coupled multifield-activated microforming," *J. Mater. Res.*, vol. 27, no. 20, pp. 2579–2586, 2012.

[127] P. Murray, E. P. Rodgers, and A. E. Williams, "Practical and theoretical aspects of the hot pressing of refractory oxides," *Trans. J. Br. Ceram. Soc.*, vol. 53, pp. 474–509, 1954.

[128] K. Huang, Y. Yang, Y. Qin, and G. Yang, "316 L Stainless Steel Powder Densification during the Coupled Multi-Fields Activated Micro-Forming," *Mater. Manuf. Process.*, vol. 28, no. 2, pp. 183–188, Feb. 2013.

[129] K. Huang, Y. Yang, Y. Qin, and G. Yang, "Densification behavior of copper powder during the coupled multi-physics fields-activated microforming," *Int. J. Adv. Manuf. Technol.*, vol. 69, no. 9–12, pp. 2651–2657, Aug. 2013.

[130] J. Liu, Y. Yang, K. Feng, and D. Lu, "Study on the effect of current on reactive sintering of the W–C–Co mixture under an electric field," *J. Alloys Compd.*, vol. 476, no. 1–2, pp. 207–212, May 2009.

[131] A. K. Du, G. Yang, D. Lu, Y. Qin, and Y. Yang, "Densification of MnZn Ferrite Sintered under Multi-Physical Field Coupling," *Appl. Mech. Mater.*, vol. 271–272, pp. 212–217, 2012.

[132] A. Du, Y. Yang, Y. Qin, and G. Yang, "Effects of Heating Rate and Sintering Temperature on 316 L Stainless Steel Powders Sintered Under Multiphysical Field Coupling," *Mater. Manuf. Process.*, vol. 28, no. 1, pp. 66–71, 2012.

[133] D. Lu, Y. Yang, Y. Qin, and G. Yang, "Forming Microgears by Micro-FAST Technology," *J. Microelectromechanical Syst.*, vol. 22, no. 3, pp. 708–715, Jun. 2013.

[134] "CES EduPack 2013 Version 12.2.13," *Granta Design Limited*. 2013.

[135] H. W. Zhang, R. Gopalan, T. Mukai, and K. Hono, "Fabrication of bulk nanocrystalline Fe–C alloy by spark plasma sintering of mechanically milled powder," *Scr. Mater.*, vol. 53, no. 7, pp. 863–868, Oct. 2005.

[136] R. Nicula, F. Turquier, M. Stir, V. Y. Kodash, J. R. Groza, and E. Burkel, "Quasicrystal phase formation in Al–Cu–Fe nanopowders during field-activated sintering (FAST)," *J. Alloys Compd.*, vol. 434–435, pp. 319–323, May 2007.

[137] "Abaqus Theory Manual: 6.7.2 Coupled Thermal-Electrical Analysis," *Dassault System Simulia*. 2010.

[138] T. Ogasawara, Y. Hirano, and A. Yoshimura, "Coupled thermal-electrical analysis for carbon fiber/epoxy composites exposed to simulated lightning current," *Compos. Part A Appl. Sci. Manuf.*, vol. 41, no. 8, pp. 973–981, 2010.

[139] H. R. Ogden and R. I. Jaffee, "The effects of carbon, oxygen and nitrogen on the mechanical properties of titanium and titanium alloys," Titanium Metallurgical Laboratory, Battelle Memorial Institute, Columbus, Ohio, United States, TML-20, 1955.

[140] M. Chu, I. P. Jones, and X. Wu, "Effect of Carbon on Microstructure and Mechanical Properties of a Eutectoid β Titanium Alloy," *J. Mater. Eng. Perform.*, vol. 14, no. 6, pp. 735–740, 2005.